

**MEMBRANE DEFORMATION AND LIPID SIGNALING: FUNCTIONS OF SRGAP
FAMILY PROTEINS AND PI(4,5)P₂**

Jaeda Coutinho-Budd

A dissertation submitted to the faculty of the University of North Carolina at Chapel Hill in
partial fulfillment of the requirements for the degree of Doctor of Philosophy in the
Curriculum in Neurobiology

Chapel Hill
2012

Approved by:

Franck Polleux, Ph.D.

Mark J. Zylka, Ph.D.

Larysa Pevny, Ph.D.

Ken McCarthy, Ph.D.

Mohanish Deshmukh, Ph.D.

© 2012
Jaeda Coutinho-Budd
ALL RIGHTS RESERVED

ABSTRACT

JAEDA COUTINHO-BUDD: Membrane Deformation and Lipid Signaling: Functions of srGAP Family Proteins and PI(4,5)P₂
(Under the direction of Franck Polleux, Ph.D., and Mark Zylka, Ph.D.)

The plasma membrane plays a structural and functional role in the life of a cell. Not only does it aid in encapsulating the intracellular contents to separate one cell from the next, but it also serves as an anchor for the actin cytoskeleton scaffold, as well as a home base for lipids that serve as messengers in a number of downstream signaling pathways. Given the importance of these aspects in cellular regulation, variations in the plasma membrane could lead to vast consequences in cellular function. This work explores plasma membrane alterations in two ways: 1) investigating membrane deformation by the slit-robo GTPase Activating Protein (srGAP) proteins of the Bin/Amphiphysin/Rvs (BAR) superfamily, and 2) reducing the levels of phosphatidylinositol (4-5)-bisphosphate (PI(4,5)P₂) using chemical dimerization. The work presented in this thesis demonstrates that srGAP2 can induce neurite outgrowth and branching, and inhibit migration of cortical pyramidal neurons, through the ability of its N-terminal F-BAR domain to induce filopodia-like protrusions. srGAP2 is more potent at inducing protrusions than srGAP1 or srGAP3 in non-neuronal cells, an activity mimicked by their respective F-BAR domains. This work also explores the ways in which the F-BARs of srGAP proteins vary in their regulation of membrane dynamics. Finally, this work investigates the feasibility of using rapamycin-inducible translocation of the yeast 5-phosphatase to deplete PI(4,5)P₂ *in vivo*.

To Graham and the rest of the Coutinho and the Budd families for your never-ending support. Oh the places we'll go...

ACKNOWLEDGEMENTS

There is not enough space in this thesis to adequately acknowledge all of the people who have helped me along the way, but here is my attempt to make it brief. Thank you to Franck Polleux for inspiring creativity, enthusiasm, and scientific growth, Mark Zylka for providing a scientific home, and the rest of my dissertation committee, Larysa Pevny, Ken McCarthy, and Mohanish Deshmukh, for offering helpful advice and scientific direction. To friends and co-workers who have provided daily support and engaging scientific discussion. Special thanks go to Sabrice Guerrier, my unofficial graduate mentor who pushed me to combine my “gut instinct” with “proper literature searches,” and Meghan Morgan-Smith, without whom this whole experience would have been entirely more miserable. I am grateful for financial support, specifically the predoctoral fellowship provided by the NIH (5F31NS068038), and of course, the support of my family: Graham, Loki, Odin, Josee, Rochelle, Yamara, Piper, Ralph, Lenore, and Laura.

TABLE OF CONTENTS

LIST OF FIGURES.....	xi
LIST OF ABBREVIATIONS.....	xiv
CHAPTER 1: General Introduction.....	1
1.1 Cortical development	1
1.2 Neuronal morphology and neurite outgrowth	2
1.3 BAR SUPERFAMILY: Proteins that coordinate membrane deformation with actin cytoskeleton dynamics.....	4
1.3.1 Bin/Amphiphysin/Rvs domain-containing proteins, the founding Subfamily	4
1.3.2 F-BAR domains, the elongated BAR domain.....	5
1.3.3 Inverse BAR domains form filopodia-like protrusions.....	6
1.4 srGAP family of F-BAR proteins	7
1.5 PI(4,5)P₂-mediated interactions between the plasma membrane and actin cytoskeleton	10
1.6 PI(4,5)P₂ is a critical regulator of cellular function	12
1.6.1 PI(4,5)P ₂ aids in subcellular protein localization	14
1.6.2 PI(4,5)P ₂ acts as a second messenger.....	14
1.6.3 PI(4,5)P ₂ regulates ion channel function.....	15
1.6.3.i PI(4,5)P ₂ regulation of TRPV1	16
1.7 Rapamycin-induced depletion of PI(4,5)P₂.....	18
1.8 Nociceptive neuronal subsets of the dorsal root ganglia	19
1.9 Overview and rationale of aims explored in this thesis	20
1.9.1. Do changes in plasma membrane curvature and its	

neighboring actin cytoskeleton affect cortical neuronal development?.....	21
1.9.2 Are the F-BAR domains of srGAP1, srGAP2, and srGAP3	21
1.9.3 Do alterations in the lipid composition of the plasma membrane regulate cellular function <i>in vivo</i> ?	22
1.10 Figures and legends	23
CHAPTER 2: The F-BAR domain of srGAP2 induces membrane protrusions required for neuronal migration and morphogenesis	30
2.1 INTRODUCTION	30
2.2 RESULTS	32
2.2.1 Expression of srGAP2 in the developing cortex.....	32
2.2.2 Full-Length srGAP2 and its F-BAR domain induce filopodia formation.....	32
2.2.3 The F-BAR domain of srGAP2 deforms membrane like an I-BAR domain.....	34
2.2.4 srGAP2 regulates neurite formation and branching through the ability of its F-BAR domain to form filopodia	35
2.2.5 Reduction of srGAP2 expression promotes neuronal migration	37
2.2.6 The F-BAR domain is necessary and sufficient for srGAP2-mediated inhibition of radial migration.....	38
2.2.7 srGAP2 inhibits migration by increasing leading process dynamics and branching	38
2.2.8 srGAP2 partially requires its RhoGAP and SH3 domains to inhibit migration	40
2.3 DISCUSSION	43
2.3.1 srGAP2 is a novel F-BAR domain-containing protein	43
2.3.2 A role for srGAP2 during neuronal development	44
2.3.3 Regulation of srGAP2: GAP and SH3 domains	45
2.4 EXPERIMENTAL PROCEDURES	46

2.4.1 Animals	46
2.4.2 Protein purification	46
2.4.3 In vitro GAP assay	47
2.4.4 Liposome preparation, liposome tubulation assays, and electron microscopy	47
2.4.5 Ex vivo cortical electroporation and primary cortical neuron cultures	47
2.5 SUPPLEMENTAL EXPERIMENTAL PROCEDURES	48
2.5.1 Sequence alignments.....	48
2.5.2 shRNA design and validation	48
2.5.3 Constructs.....	49
2.5.4 COS7 cell culture, transfections, staining and filopodia measurements	50
2.5.5 <i>Ex vivo</i> cortical electroporation and primary cultures.....	51
2.5.6 Time lapse confocal microscopy of cortical sections.....	51
2.5.7 Dissociated cortical neuron culture.....	52
2.5.8 Quantification of neuron migration and neurite branching.....	52
2.5.9 In situ hybridization	53
2.5.10 Liposome preparation.....	53
2.5.11 Electron microscopy	53
2.6 FIGURES AND LEGENDS	54
CHAPTER 3: The F-BAR domains from srGAP1, srGAP2, and srGAP3 differentially regulate membrane deformation	85
3.1 INTRODUCTION	85
3.2 RESULTS.....	89
3.2.1. The srGAP family of proteins, through their respective F-BAR domains, exhibit different abilities to induce filopodia in non-neuronal cells	89
3.2.2 srGAP proteins can interact through their F-BAR domains	89

3.2.3 The F-BAR domains of different srGAP proteins localize to distinct regions of filopodia	90
3.2.4 Molecular dynamics of the F-BAR Domains of srGAP1-3.....	91
3.2.5 Lipid specificity varies between the F-BARs of srGAP proteins	93
3.2.6 F-BAR(1) constrains cellular protrusions in cortical neurons, whereas F-BAR(2) and F-BAR(3) induce protrusions	95
3.3 DISCUSSION	96
3.4 MATERIALS AND METHODS	101
3.4.1 Plasmid constructs and sequence alignments.....	101
3.4.2 Cell culture	101
3.4.3 Live cell imaging.....	103
3.4.4 Biochemistry	104
3.5 FIGURE LEGENDS.....	106
CHAPTER 4: Rapamycin-induced depletion of PI(4,5)P₂ is effective in cell lines, but not in dorsal root ganglia neurons <i>in vitro</i> or <i>in vivo</i>.....	117
4.1 INTRODUCTION	117
4.2 RESULTS.....	119
4.2.1 Rapamycin-induced dimerization is an effective tool for studying biological processes in cell lines	119
4.2.2 Construction of two mouse lines to study rapamycin-induced PI(4,5)P ₂ depletion in thermal sensitivity <i>in vivo</i>	120
4.2.3 Injection of rapamycin does not induce translocation of Venus-FKBP-Inp54p from the cytoplasm to the plasma membrane in DRG neurons.....	121
4.2.4 Expression of Inp54p in CGRP+ neurons leads to basal depletion of PI(4,5)P ₂ In cultured DRG neurons	122
4.2.5 Expression of Inp54p in CGRP+ neurons does not affect behavior <i>in vivo</i>	124
4.3 DISCUSSION	124

4.4 MATERIALS AND METHODS	128
4.4.1 DNA plasmid constructs	128
4.4.2 Cell culture and live-imaging	128
4.4.3 Generation of FRB ^{PLF} -CFP and Venus-FKBP-Inp54p Knockin Mice.....	129
4.4.4 Neuronal dissociation and imaging.....	130
4.4.5 Immunohistochemistry	131
4.4.6 Drug administration	132
4.4.7 Behavior.....	132
4.5 FIGURES AND LEGENDS.....	133
CHAPTER 5: DISCUSSION	139
5.1 Summary of Findings	139
5.2 srGAP2 in neuronal morphology.....	141
5.2.1 Regulation of srGAP2 autoinhibition.....	142
5.3 Functional Differences Between F-BARs of the srGAP protein family	144
5.4 Challenges to rapamycin-inducible PI(4,5)P₂ depletion <i>in vivo</i>.....	146
5.4.1 Future directions with the current design	146
5.4.1i Behavioral assessment Rosa-FRB ^{PLF} /CGRP-Inp54p double heterozygous mice.....	146
5.4.1ii Stabilization of the FRB ^{PLF} domain might be necessary for sufficient PI(4,5)P ₂ depletion <i>in vivo</i>	148
5.4.1iii The magic ratio problem	149
5.4.1iv Rapamycin-Induced Depletion of PI(4,5)P ₂ with Inp54p Might Not Work in Neurons	150
5.4.2 Alternative design and approach to rapamycin-inducible PI(4,5)P ₂ depletion <i>in vivo</i>	151
REFERENCES	153

LIST OF FIGURES

Figure 1.1 Cortical neuron development in vivo and in vitro.....	23
Figure 1.2 BAR superfamily proteins	24
Figure 1.3 PI(4,5)P ₂ -mediated actin regulation through actin-related proteins	25
Figure 1.4 PI(4,5)P ₂ metabolism.....	26
Figure 1.5 PI(4,5)P ₂ signaling and ion channel regulation.....	27
Figure 1.6 Schematic of rapamycin-induced depletion of PI(4,5)P ₂ from the plasma membrane.....	28
Figure 1.7 Subtypes of nociceptive neurons in the DRG.....	29
Figure 2.1 srGAP2 is expressed in neuronal progenitors and postmitotic neurons and localizes to sites of membrane protrusion	54
Figure 2.2 F-BAR-induced filopodia required F-Actin for their dynamic formation but not for their structural maintenance	56
Figure 2.3 Knockdown of srGAP2 in cortical neurons reduces axonal and dendritic branching	58
Figure 2.4 srGAP2 promotes filopodia formation and neurite outgrowth in an F-BAR-dependent manner.....	60
Figure 2.5 Knockdown of srGAP2 promotes neuronal migration and reduces LP branching	62
Figure 2.6 srGAP2-mediated inhibition of migration requires F-BAR-mediated membrane deformation	64
Figure 2.7 Model for srGAP2-regulated membrane protrusion in neuronal migration	66
Figure 2.S1 srGAP2 induces filopodia formation in a F-BAR-dependent manner in COS7 cells.....	67
Figure 2.S2 Expression of the F-BAR domain of srGAP2 in COS7 cells does not inhibit endocytosis	69
Figure 2.S3 Structural alignment of the predicted F-BAR domain of srGAP2.....	70
Figure 2.S4 Localization of srGAP2-EGFP, F-BAR-EGFP and F-BAR ^{Δ49} -EGFP fusion proteins in COS7 cells and stage 1 E15 cortical neurons	72
Figure 2.S5 Proper expression of srGAP2-EGFP, F-BAR-EGFP and F-BAR ^{Δ49} -EGFP fusion proteins in COS7 cells	73

Figure 2.S6 Control FBP17 F-BAR tubulates liposome.....	74
Figure 2.S7 Neurites induced by different srGAP2 constructs contain microtubules	75
Figure 2.S8 Definition of layers in slices following dorsal electroporation and organotypic culture	76
Figure 2.S9 Expression of srGAP2 in post mitotic neurons inhibits radial migration	77
Figure 2.S10 2.2 kD NeuroD promoter drives gene expression in non-radial glial intermediate progenitors 24 hours after electroporation.....	78
Figure 2.S11 The RhoGAP domain of srGAP2 is specific for Rac1	79
Figure 2.S12 The GAP and SH3 domains participate in srGAP2's ability to promote filopodia formation in neurons.....	80
Figure 2.S13 srGAP2 expressing cells accumulate in stage 2.....	82
Figure 2.S14 The GAP and SH3 domains participate in srGAP2's ability to inhibit migration	83
Figure 3.1 srGAP2 induces significantly more filopodia than srGAP1 or srGAP3.....	106
Figure 3.2 srGAP proteins interact through their F-BAR domains.....	107
Figure 3.3 Synergy between F-BAR domains towards filopodia induction	108
Figure 3.4 The three F-BAR domains of srGAP proteins differ in their subcellular molecular dynamics	109
Figure 3.5 F-BAR(2) binds multiple negatively-charged phospholipids	110
Figure 3.6 F-BAR domains of srGAP proteins differ in their ability to induce filopodia in cortical neurons	111
Figure 3.7 Real-time imaging of membrane and F-Actin dynamics induced by F-BAR domains in cortical neurons.....	112
Figure 3.S1 Conservation and alignments of the srGAP family of proteins	113
Figure 3.S2 The F-Actin network is disrupted after Cytochalasin-D treatment	114
Figure 3.S3 Dose-dependent binding of F-BAR(2) to various phosphoinositides	115
Figure 3.S4 Model of the functional properties of the F-BAR domains of three srGAP family members.....	116

Figure 4.1 Rapamycin-induced translocation effectively allows for PI(4,5)P ₂ reduction in HEK293 cells.....	133
Figure 4.2 Both knockin mouse lines express the correct protein in the appropriate DRG neurons.....	134
Figure 4.3 Rapamycin does not induce translocation in double heterozygotic mice <i>in vivo</i>	135
Figure 4.4 PI(4,5)P ₂ is depleted in CGRP-Inp54p knockin neurons	136
Figure 4.5 PI(4,5)P ₂ add-back does not rescue deficits in calcium signaling in CGRP-Inp54p neurons, most likely due to poor cell health.....	137
Figure 4.6 Expression of Venus-FKBP-Inp54p in heat-sensing CGRP neurons is not sufficient for reduced thermal sensitivity <i>in vivo</i>	138

LIST OF ABBREVIATIONS

- E – embryonic day (post-conception)
- RGC – radial glial cells
- CP - cortical plate
- GTP – guanine triphosphate
- GDP – guanine diphosphate
- GEF – guanine nucleotide exchange factors
- GAP – GTPase activating proteins
- BAR – Bin/Amphiphysin/Rvs
- N-BAR – N-terminal Amphiphathic helix BAR
- FCH – Fer/Fes CIP4 homology
- F-BAR – FCH BAR domain
- I-BAR – inverse BAR
- PI(4,5)P₂ – phosphatidylinositol 4,5-bisphosphate
- CC – coiled coil
- SH3 – Src Homology 3
- FBP17 – forming binding protein 17
- toca-1 – transducer of cdc42 actin assembly 1
- WASP – Wiscott aldrich syndrome protein
- IRSp53 – insulin receptor tyrosine kinase substrate p53
- GFP – green fluorescent protein
- CFP – cyan fluorescent protein
- RFP – red fluorescent protein
- t_{1/2} – half time of fluorescence recovery
- FRAP – fluorescence recovery after photobleaching
- PH – pleckstrin homology

PI – phosphoinositide

PLC – phospholipase C

DAG – diacylglycerol

TRPV1 – transient receptor potential vanilloid 1

GPCR – G protein coupled receptor

FKBP12 – FK506 binding protein 12

FRB – FKBP rapamycin binding

mTOR – mammalian target of rapamycin

Inp54p – Inositol polyphosphate 5-phosphatase 4

rapalog – rapamycin analog

C20-MaRap – carbon 20 methylallylrapamycin

DRG – dorsal root ganglia

CGRP – calcitonin gene related peptide

NGF – nerve growth factor

CHAPTER 1

General Introduction

1.1 Cortical development

Formation of functional neuronal circuits involves the coordinated migration of neurons to their final location, the subsequent generation of a single axon and multiple dendrites and finally the formation of functional synaptic contacts (Barnes and Polleux, 2009). To achieve these complex steps, neurons undergo substantial changes in morphology, involving both cytoskeletal and membrane remodeling (Luo, 2002; Noctor et al., 2004; Oshima et al., 2007). The developing cerebral cortex is a prime example of the intricacy and dynamics of these morphological changes.

The cerebral cortex is a laminar structure, consisting of six layers that can be defined by molecular markers (Molyneaux et al. 2007; Arnold et al., 2008; Gupta et al. 2002). In early murine development, between embryonic day 10 (E10) and E11.5, post-mitotic neurons undergo somal translocation from the ventricular zone to give rise to the preplate, which is then split into the marginal zone and the subplate. Around E12.5, the first projection neurons are born and begin to migrate to the cortical plate (Molyneaux et al., 2007). The cortex forms in an inside-out fashion, so this first wave of migrating neurons will become deep layer VI neurons, with each subsequent layer migrating past its predecessor, until reaching the reelin-producing Cajal-Retzius cells located in the marginal zone (Ogawa et al., 1995). These waves of migration continue throughout embryonic development, culminating around E18 (Gupta et al., 2002; Barnes and Polleux, 2008), and are tightly

regulated in well-defined steps (**Fig. 1.1A**). Cortical neurons, born through asymmetric divisions of radial glial cells (RGC), transition through a multipolar morphology characterized by short, immature neurites that protrude from the cell body to dynamically sense the surrounding environment. These neurons then attach to a RGC, which serves as a scaffold for their migration. At this stage, neurons are characterized by the presence of a single, polarized leading process, and a trailing process at the rear. Recent evidence shows that the trailing process of radially migrating pyramidal neurons extends rapidly to become the axon (Ayala et al., 2007; Luo, 2002). Upon reaching their final destination at the cortical plate (CP), the leading process becomes the apical dendrite and will undergo tremendous branching, and formation of dendritic spines during early postnatal development (Barnes and Polleux, 2009).

1.2 Neuronal morphology and neurite outgrowth

One of the early predominant models used to study neuronal differentiation is based on examining the morphological changes that occur in dissociated neurons *in vitro* (Luo, 2002; Dotti et al., 1988). Dissociated neurons provide the advantage of high-resolution imaging, and the ability to obtain information about cell-autonomous effects of neuronal morphology that is difficult to visualize *in vivo*. Dissociated cortical neurons develop through well-defined stages, from rounded immature neurons with extensive lamellipodia and filopodia (stage 1), to fully mature neurons with dendritic spines (Kwiatkowski et al., 2007; Barnes and Polleux, 2009). Early development of neurons in culture involves three stages, in which neurons progress from a pancake-like morphology in stage 1, to the emergence of immature neurites in stage 2, to stage 3 with its specified axon and dendrites (**Fig. 1.1B**). Neurons can go on to achieve more mature morphologies in culture as well, including the development of dendritic spines, and even the formation of connections between neurons. The majority of the genes known to regulate cortical migration and

morphogenesis rely on the ability to regulate actin and microtubule dynamics (Ayala et al., 2007; Gupta et al., 2002).

The basis of neurite initiation, outgrowth, and branching is rooted in the ability of the cytoskeleton to undergo dynamic changes. Small Rho GTPases, such as RhoA, Rac1, and Cdc42, play an important role in modulating the cytoskeletal transformations that take place during neuronal morphogenesis (Threadgill et al., 1997). These small GTPases switch between an activated state when bound to guanine triphosphate (GTP), and inactivated state when bound to guanine diphosphate (GDP). The GTP-GDP cycle is regulated by and Guanine nucleotide exchange factors (GEFs) to activate the proteins, and GTPase activating proteins (GAPs) to cause inactivation. The classic view of cytoskeletal modulation by these three major GTPases is that Rac1 leads to lamellopodial protrusions through the formation of branched actin networks, Cdc42 regulates filopodia formation by the formation of filamentous actin bundles, and RhoA induces actin depolymerization (Hall, 1994). All three of these GTPases have been shown to be important regulators in cytoskeletal rearrangement during neurite outgrowth (Threadgill et al., 1997; Ng and Luo, 2004).

While several actin structures contribute to the dynamic remodeling of neurites, bundled filamentous actin present in filopodia seems to be particularly important for neurite initiation and branching (Gupta et al., 2002; Gupton and Gertler, 2007; Luo, 2002; Matilla and Lappalainen, 2008; Dent et al., 2007). Two studies from the same lab demonstrated the importance of filopodia in neurite initiation using multiple methods of inhibiting filopodia formation. Dent et al. (2007) found that treatment of cytochalasin D, a toxin that caps actin and potently inhibits actin polymerization, resulted in the depolymerization of the actin cytoskeleton and subsequent lack of bundled actin filaments, leading to an inhibition of neurite initiation. Moreover, this study visualized the emergence of neurites from single filopodia using time-lapse microscopy. Dent et al. (2007) and Kwiatkowski et al. (2007)

further demonstrated the dependence of neurite outgrowth on filopodia using neurons from *mmeevv* mice that lack all three murine actin anti-capper proteins: mammalian enabled (Mena), vasodilator stimulated phosphoprotein (VASP), and Ena-VASP like (EVL). Ena/VASP are potent inducers of filopodia, and their triple knockout in cortical neurons resulted in loss of filopodia and failed neurite initiation, both *in vitro* and *in vivo*. Interestingly, loss of Ena/VASP proteins also resulted in cortical lamination defects (Bear et al., 2002; Goh et al, 2002; Kwiatkowski et al., 2007), suggesting a complex functional relationship between filopodia formation, neurite initiation, and neuronal migration.

1.3 BAR SUPERFAMILY: Proteins that coordinate membrane deformation with actin cytoskeleton dynamics

An emerging field is providing novel insights into a family of proteins that directly bind and deform cellular membranes. In addition to inducing membrane curvature, members of the Bin/Amphiphysin/Rvs (BAR) superfamily of proteins link the membrane to the actin cytoskeleton, either directly (Yamagishi et al., 2004; Lee et al., 2007) or indirectly (Tsujita et al., 2006; Suetsugu et al., 2006; Scita et al., 2008), to become multifaceted regulators of cell morphology and function. However, this interaction is not necessary for cellular membrane deformation, as it has also been shown that membrane deformation induced by these proteins can preclude the emergence of F-actin bundles (Yang et al., 2009).

1.3.1 Bin/Amphiphysin/Rvs domain-containing proteins, the founding subfamily

The Bin Amphiphysin Rvs (BAR) domain superfamily of proteins can be subdivided into three main groups based on protein structure: BAR/N-BARs (**Fig. 1.3A**), F-BARs (**Fig. 1.3B**), and I-BARs (**Fig. 1.3C**) (Frost et al., 2007). The founding subgroup of this family contains the canonical BAR domains, characterized by three antiparallel alpha-helices on each monomer, which form a homodimer with another BAR domain (Peter et al., 2004).

The six alpha-helices, making up the BAR domain homodimer, form a banana-shaped structure with positive amino acids located on the concave surface, allowing the BAR domain to directly bind negatively-charged, PI(4,5)P₂-containing membrane via electrostatic interactions (**Fig. 1.3D**). These dimeric proteins have been shown to oligomerize to invaginate membrane into the cell to create tubular networks (Itoh et al., 2005; Shimada et al., 2007). A specialized subset of the BAR domain, the N-BAR domain, contains an N-terminal amphipathic alpha-helix that directly inserts into the membrane, increasing membrane curvature (Itoh et al., 2006). Many of these BAR and N-BAR proteins, such as amphiphysin and endophilin, have been implicated in membrane deformation relating to synaptic vesicle formation (Di Paolo et al., 2002; Schuske et al., 2003).

1.3.2 F-BAR domains, the elongated BAR domain

The second subfamily is the Fer-CIP4 Homology (FCH) BAR (F-BAR) domain-containing proteins (**Fig. 1.3B**). F-BAR domains are characterized by the presence of an FCH domain followed by a Coiled-coil (CC) domain, which were predicted (based on secondary structure homology) to fold in a similar way to BAR domains (Frost et al., 2007). These F-BAR domains contain five alpha helices, in contrast to the three that comprise a canonical BAR domains. The crystallization of F-BAR dimers demonstrates increased length and more shallow curvature of the banana-shaped F-BAR homodimer, resulting in larger-diameter membrane tubes (**Fig. 1.3D**) (Henne et al., 2007). The ability of many BAR and F-BAR containing proteins to bind dynamin, a GTP-ase with membrane pinching ability, via their SH3 domains, suggest that these proteins function in vivo to regulate endocytosis by deforming membrane inward until it is pinched into a vesicle by dynamin (Takei et al., 1999; Itoh et al., 2005). Surprisingly, F-BAR domains can deform purified lipids in the absence of other proteins. The structural basis for the ability of F-BAR domain to induce membrane tubules has been studied by combining protein structural information

(Shimada et al., 2007) and cryo-electron microscopy (cryo-EM; Frost et al., 2008). These studies reveal that individual F-BAR dimers can bind end-to-end to form long 'string-like' oligomers, which also display a lateral binding interface to form a 'wall-like' structure reminiscent of the structure adopted by septins (reviewed in Kinoshita, 2006). Like the BAR domain proteins, F-BAR domain proteins, Syndapins and FBP17, have been implicated in endocytosis of synaptic vesicles (Qualmann et al., 1999; Koch et al., 2011; Rodal et al., 2008; Wu et al., 2010). Most of these F-BAR proteins have been found to be important in presynaptic vesicle recycling; however, formin binding protein 17 (FBP17/Toca-2), one of the canonical members of this BAR domain subclass, has been shown to play a role in formation of synaptic spines. Wakita et al. (2011) demonstrated that shRNA-mediated knockdown of endogenous FBP17 results in reduced spine density in cultured hippocampal rat neurons. Interestingly, a very similar protein, cdc42-interacting protein 4 (CIP4/Toca-3), has been shown to inhibit neurite formation by inducing lamellipodial protrusions (Saengsawang et al., 2012). Both of these proteins are related to the transducer of cdc42-dependent actin assembly 1 (Toca-1), which has been shown to suppress neurite outgrowth in PC12 cells (Kakimoto et al., 2006), presumably through its membrane-invaginating activity. These conclusions were later complicated when it was shown that Toca-1 induces neurites in N1E115 neuroblastoma cells through its ability to induce filopodia by complex formation with N-WASP (Bu et al., 2009). This Toca-1-induced filopodia formation was blocked with inhibitors of endocytosis, suggesting a complex link between filopodia and endocytosis.

1.3.3 Inverse BAR domains form filopodia-like protrusions

The last class of characterized BAR domains is the inverse BAR (I-BAR) domains (**Fig. 1.3C**). Like BAR domains, I-BAR domains contain three antiparallel alpha helices; however, I-BAR domains are less curved than BAR and F-BAR domains, and have membrane-binding, positive amino acids located on their convex surfaces (**Fig. 1.3D**)

(Millard et al., 2005), hence the name “Inverse-BAR.” Accordingly, in contrast to the canonical BAR and F-BAR domains, I-BAR domains induce filopodia-like membrane protrusions in vivo and in vitro (Millard et al., 2005; Matilla et al., 2007; Saarikangas et al., 2008; Saarikangas et al., 2009), and have actually been shown to inhibit endocytosis (Quinones et al., 2010). The exact structural mechanism underlying I-BAR-induced protrusive activity is currently unknown, but thought to differ from the oligomerization-based tubulation characterizing F-BAR domains (Saarikangas et al., 2009). Although these I-BAR domain-containing proteins have been long thought of as inducers of membrane protrusion, a relatively new I-BAR domain protein, Pinkbar, has been shown to induce the formation of planar membrane structures (Pykäläinen et al., 2011). It is likely that the functions of many of the BAR superfamily proteins will differ from their original functionalities.

1.4 srGAP family of F-BAR proteins

While canonical F-BAR domains of certain family members such as Toca-1, FBP17, and CIP4 are known to invaginate membrane (Itoh and Camilli, 2006), there are known F-BAR proteins that induce filopodia-like membrane protrusions. Proteins such as GAS7 and PSTPIP2 (MAYP) were shown to induce filopodia formation prior to their characterization as F-BAR domain-containing proteins (Chitu et al., 2005; She et al., 2002). The function of approximately 25 predicted F-BAR proteins in the human genome remain to be identified. One such poorly characterized family of F-BAR domain-containing proteins is the slit-robo GTPase Activating Proteins (srGAPs).

srGAP1, srGAP2, and srGAP3 (also called Wave Related Protein, WRP, and Mental disorder related GTPase Activating Protein, or MEGAP) were identified as interactors of Robo, the receptor for the chemorepulsive cue, Slit (Wong et al., 2001). These proteins share a predicted N-terminal F-BAR domain, a central RhoGAP domain, and a C-terminal Src Homology 3 (SH3) domain (**Fig. 1.3B**). RhoGAP domains bind and

inactivate small GTPases by increasing their intrinsically slow rate of GTP hydrolysis (Schutes and Der, 2006). srGAP1 specifically binds and inactivates Cdc42 and RhoA (Wong et al., 2001), while srGAP3 is specific for Rac1 (Soderling et al., 2002). The orthologue to mammalian srGAP proteins in *C. elegans*, SRGP-1, has been shown to regulate cell-cell junctions and engulfment of apoptotic cells through its regulation of Rac1 (Zaidel-Bar et al. 2011; Neukomm et al., 2011). SH3 domains are polyproline-binding motifs that mediate protein-protein interactions. In addition to Robo, the SH3 domain of srGAP2 has been shown to bind to actin-related proteins such as Wiscott-Aldrich Syndrome protein (WASP), WASP interacting protein (WIP), Diaphanous homologous protein 1 (mDia1) (Linkermann et al., 2009), formin-like 1 (FMNL-1, Mason et al., 2011), and Palladin (Okada et al., 2011). The SH3 domain of srGAP3 has been shown to bind the Wasp family member, WAVE-1 (Soderling et al., 2002) and lamellipodin (Endris et al., 2011) to regulate Rac-dependent cellular protrusions.

In Chapter 2, we propose a model of autoinhibition for srGAP2, and hypothesize that the SH3 domain of srGAP2 is the key to unlocking its filopodia-inducing activity. It is possible that SH3 binding to one or more of these proteins releases the autoinhibition, allowing the F-BAR domains to dimerize, and induce protrusions. Subsequent work involving the crystal structure of Syndapin I (Rao et al., 2010) demonstrates that the SH3 domain of Syndapin I directly binds its F-BAR domain, leading to autoinhibition. Furthermore, this autoinhibition can be released by binding of the SH3 domain to dynamin 1. Alternatively, Guo et al. (2010) found that protein arginine methyltransferase 5 (PRMT5) binds srGAP2 in its N-terminus, and methylates arginine 927 in the C-terminus of srGAP2. The authors show that the methylation mutant, srGAP2^{R927A}, fails to undergo dimerization, and does not induce membrane deformation or cell migration. They hypothesize that this methylation is responsible for releasing srGAP2 from its autoinhibited state. It is possible that both mechanisms are at play in the release of srGAP2 autoinhibition.

Like many RhoGAP proteins, the srGAP family members have also been shown to regulate cell morphology and migration (Yang et al., 2006; Soderling et al., 2002; Soderling et al., 2007; Vogt et al., 2007; Endris et al., 2011; Carlson et al., 2011; Zaidel-Bar et al., 2011). Recently, the expression pattern of srGAP1, 2, and 3 was examined throughout the developing central nervous system, although the spatial and temporal patterns differ between the three (Bacon et al., 2009). srGAP2 and srGAP3 are present in the cerebral cortex throughout late embryonic development, suggesting a similar role for these proteins in regulation of morphology and migration of cortical neurons. srGAP1 expression emerges postnatally, suggesting that it has an alternative role in neuronal function. Recent work has revealed the presence of srGAP1 and srGAP3 in large diameter neurons of adult DRG, with almost complete absence of srGAP2 (Chen et al., 2012). Interestingly, only srGAP3 increased in expression after spaired nerve injury, further suggesting separate functions for the three srGAP proteins.

However, until recently (including work in chapters 2 and 3), little was known about the F-BAR domains of these proteins. Work from the Polleux lab (Guerrier et al, 2009; Chapter 2) was the first to identify the F-BAR of srGAP2 as an inducer of outward membrane protrusions. The formation of these filopodia-like protrusions led to decreased cortical migration, and increased neurite formation in dissociated cortical neurons. Subsequently, srGAP3 has also been shown to regulate neuronal protrusions, specifically spine density and shape (Carlson et al., 2011). Loss of srGAP3 reduces the density of spines in hippocampal and cortical neurons, as well as counter-intuitively reducing the number of mature, mushroom-shaped spines. Interestingly, heterozygous loss of srGAP3 increases the number of thin spines. Recent work from the Polleux lab has found similar results regarding the regulation of spine shape with srGAP2. More interestingly, this work shows that a human-specific, duplicated portion of the srGAP2 F-BAR domain (srGAP2^{p12}) can act as a dominant negative, and recapitulate the srGAP2 loss-of-function phenotype

(Charrier et al., In Press); however, in this work both loss of srGAP2 and inhibition by srGAP2^{p12} lead to increased spine density. These neuronal results for srGAP2 and srGAP3 are particularly exciting given that both have been implicated in forms of brain-related disorders. Loss of srGAP3 is known to play a role in 3p deletion syndrome (Endris et al., 2002), a form of mental retardation, and recent work has revealed a role for srGAP2 in early infantile epileptic encephalopathy (Saitou et al., 2011). Although these proteins are quite similar, there are subtle differences in their function, which are explored more thoroughly in Chapter 3; however, it is currently unclear as to whether these differences arise from their interactions with the actin cytoskeleton, the plasma membrane, or both.

1.5 PI(4,5)P₂-mediated interactions between the plasma membrane and actin cytoskeleton

The BAR superfamily proteins are known to bind electrostatically to negatively-charged lipids, such as phosphatidylinositol 4,5-bisphosphate (PI(4,5)P₂) and phosphatidylserine (PS), embedded in the plasma membrane (Takei et al., 1998; Itoh and De Camilli, 2006). Some of these family members not only bind to negatively-charged phospholipids, but have been shown to cluster PI(4,5)P₂ specifically, such as the I-BAR of IRSp53 (Saarikangas et al., 2009). Although IRSp53 can interact with the actin cytoskeleton both directly (Yamagishi et al., 2006) and indirectly (Scita et al., 2008), PI(4,5)P₂ also has been found to interact with actin filaments to modulate cytoskeletal activity through a variety of other actin-associated proteins, such as cofilin (Ojala et al., 2001), vinculin (Huttelmaier et al., 1998), talin (Martel et al., 2001), gelsolin (Yu et al., 1992; Azuma et al., 2000), neuronal Wiskott-Aldrich syndrome protein (N-WASP; Miki et al., 1996), (**Fig 1.3**).

High concentrations of PI(4,5)P₂ often lead to actin polymerization, whereas depolymerization typically occurs in areas of low PI(4,5)P₂. PI(4,5)P₂ binds cofilin to inhibit

its actin-severing activity, thereby blocking actin depolymerization (Ojala et al., 2001). PI(4,5)P₂ also inhibits gelsolin, a capping protein with actin-severing activity. PI(4,5)P first interferes with gelsolin's ability to bind actin, thereby uncapping actin filaments, and secondly inhibits its actin-severing activity (Yu et al., 1992). Binding to PI(4,5)P₂ is able to relieve the autoinhibition of many of these actin-interacting proteins, such as N-WASP, talin, and vinculin. Talin links membrane-bound adhesion proteins like β -1 integrins to the actin cytoskeleton in a PI(4,5)P₂-dependent manner (Martel et al., 2001). The same regulation allows talin to bind vinculin (Gilmore and Burridge, 1996), which also links proteins to actin, as well as binds VASP proteins (Huttelmaier et al. 1998). Upon electrostatic binding to PI(4,5)P₂, N-WASP intermolecular binding is inhibited, opening up the protein and revealing other protein-binding domains (Miki et al., 1996); N-WASP can also be activated by the binding of cdc42 to its cdc42/rac-interactive binding (CRIB) domain (Symons et al., 1996). Once open, the verprolin-homology domain/cofilin-homology domain/and acidic domain (VCA) binds a G-actin monomer and actin-related protein 2/3 (ARP2/3) to induce actin nucleation and the formation of branched actin networks. Activated N-WASP can also bind and insert profilin-actin complexes into actin polymers to enhance actin polymerization. The proline-rich region binds SH3-containing proteins, such as the F-BAR and I-BAR containing proteins Toca-1 (Takano et al., 2008) and IRSp53 (Lim et al., 2008), respectively. Both of these proteins also interact directly with small Rho GTPases, adding more complexity to the relationship between PI(4,5)P₂ and actin-interacting proteins. It is likely that many of the other SH3-containing BAR superfamily proteins could interact with N-WASP as well.

Additionally, one of the major kinase classes responsible for the production of PI(4,5)P₂, PIP5KI, interacts strongly with multiple regulators of the actin cytoskeleton (**Fig 1.3**; see section 1.6 for more information about PI kinases). Activation and localization of PIP5KI proteins is at least partially dependent upon the small GTPases Cdc42 (Weernink

et al., 2004), Rho (Chong et al., 1994), Rac (Halstead et al., 2010), and Arf6 (Honda et al., 1999). Cdc42 has been shown biochemically to stimulate PIP5K-induced production of PI(4,5)P₂ (Weernink et al., 2004); however, to my knowledge no functional analysis of cdc42 and PIP5K has been performed, suggesting a possible indirect activation through another GTPase. PIP5KI α binds Rho in a GTP-dependent manner, and complexes with Rho-dependent seronine-threonine kinase (ROCK) to activating downstream pathways to induce actin stress fiber formation (Yamamoto et al., 2001). Rac1 has been shown to recruit PIP5KI β to the plasma membrane and induce neurite retraction in N1E115 neuroblastoma cells and cerebellar granule neurons (Halstead et al., 2001). The authors identified the rac1-binding residue in PIP5KI β , and mutated the corresponding, highly-conserved glutamate residue in PIP5KI α and PIP5KI γ . All three wildtype isoforms induced neurite retraction in N1E115 cells, however, the glutamate mutations abolished both neurite retraction and membrane-localization in all three isoforms. Another important GTPase is Arf6, which has been shown to recruit PIP5Ks to the plasma membrane and lead to membrane ruffles, actin comet formation, as well as regulate vesicle trafficking (reviewed in Funakoshi et al., 2011).

Clearly PI(4,5)P₂ plays an important role in regulating morphological changes due to membrane deformation and rearrangement of the actin cytoskeleton. Additionally, PI(4,5)P₂ acts as a guidepost for other non-cytoskeletal-related proteins, serves as a second messenger in intracellular signaling pathways, and operates as modulator of ion channel activity. PI(4,5)P₂ is paramount in cellular biology.

1.6 PI(4,5)P₂ is a critical regulator of cellular function

PI(4,5)P₂ is the most abundant phosphoinositide (PI) present in the plasma membrane (reviewed in Saarikangas et al., 2010). There are eight different mammalian PI

species that interconvert through the local positioning of phosphates around the inositol ring of the lipid headgroup. PI(4,5)P₂ can be synthesized through addition of a phosphate to position 5 of the inositol ring of phosphatidylinositol 4-phosphate (PI(4)P) or the position 4 of phosphatidylinositol 5-phosphate (PI(5)P), or the removal of the phosphate at position 3 of phosphatidylinositol 3,4,5-triphosphate (PI(3,4,5)P₃). PI(4,5)P₂ can also be downregulated by the removal of a phosphate from either positions 4 or 5.

Phosphoinositide anabolism and catabolism are regulated by lipid kinases and phosphatases, respectively, which are specific for each phosphate location in the inositol ring (**Fig. 1.4**) (reviewed in Liu and Bankaitis, 2010).

Conversion between PI species is carefully regulated by these kinases and phosphatases in order to maintain the appropriate phospholipid balance necessary for proper cellular function. For example, loss of PIP5K γ , a kinase that converts PI(4)P to PI(4,5)P₂, results in neural tube closure defects (Wang et al., 2007), defects in synaptic transmission through inhibited endocytosis, and eventually perinatal death (Di Paolo et al., 2004). Interestingly, mice lacking synaptojanin, a 5-phosphatase domain-containing protein that reduces PI(4,5)P₂ to PI(4)P, also die just after birth (Kim et al., 2002). Synaptojanin knockout mice have an overabundance of PI(4,5)P₂, leading to poor synaptic transmission due to an accumulation of clathrin coated vesicles in their presynaptic terminals. In contrast, overexpression of synaptojanin, due to trisomy of the synaptojanin 1 gene, has been linked to the cognitive impairments associated with Down's syndrome (Voronov et al., 2008). Loss of a similar protein, the Oculocerebrorenal Lowe syndrome (OCRL) 5-phosphatase, also leads to mental retardation, among other abnormalities such as insufficient kidney absorption and hypotonia (Lowe et al., 1952).

These diseases arising from altered PI(4,5)P₂ regulation suggest that PI(4,5)P₂ is a critical regulator of cellular function *in vivo*; however, both synaptojanin 1 and OCRL act on multiple phosphoinositides, not just PI(4,5)P₂. To deplete PI(4,5)P₂ in experimental

settings, the yeast 5-phosphatase, Inositol polyphosphate 5-phosphatase (Inp54p) is often used given its simple domain structure. Inp54p lacks the additional protein domains commonly found in other 5-phosphatase family members (Stefan et al., 2002), resulting in a constitutively-active 5-phosphatase domain (Várnai et al., 2006; Nebl et al., 2000). Removal of the C-terminal 13 amino acids disrupts the tether to endoplasmic reticulum, resulting in a cytoplasmic 5-phosphatase that is more amenable to manipulation for experimental reduction in PI(4,5)P₂ (Wiradjaja et al., 2000).

1.6.1 PI(4,5)P₂ aids in subcellular protein localization

Many proteins have been identified that contain domains or motifs to specifically target proteins to PI(4,5)P₂ (Heo et al., 2006). This can be visualized using one of these protein domains, the pleckstrin homology (PH) domain of phospholipase C δ 1 (PLC δ 1), which has become a biosensor for PI(4,5)P₂ abundance at the plasma membrane. When high levels of PI(4,5)P₂ are present, fluorescently-tagged versions of this PH domain can be seen at the plasma membrane. When PI(4,5)P₂ levels are low, the domain is found in the cytoplasm. These PI(4,5)P₂-binding domains often occur in cytoplasmic proteins, which are translocated to the plasma membrane upon interaction with PI(4,5)P₂; therefore, the amount of available PI(4,5)P₂ at the membrane regulates the amount of translocation, and ultimately the extent of protein activity at the plasma membrane. Consequently, fluctuations in the amount of PI(4,5)P₂ at the plasma membrane create differential effects in a number of cellular responses due to PI(4,5)P₂-binding, with implications *in vivo* ranging from phototransduction (Huang et al., 2004), to bipolar disorder (Soares et al., 2000; Soares et al., 2001), to regulation of pain sensitivity (Sowa et al., 2010).

1.6.2 PI(4,5)P₂ acts as a second messenger

In addition to its role in regulating the actin cytoskeleton and protein binding, PI(4,5)P₂ can be cleaved by phospholipase C (PLC) into diacylglycerol (DAG) and inositol 1,4,5-triphosphate (IP₃) that act as second messengers in cell signaling cascades (**Fig.**

1.5A) (Berridge et al., 1983). DAG remains at the plasma membrane to activate protein kinase C (PKC), and IP₃ travels to the endoplasmic reticulum to bind IP₃ receptors and stimulate the release of intracellular calcium. Multiple isoforms of PLC exist, and are activated by different stimuli. PLCβ-induced cleavage of PI(4,5)P₂ is predominantly evoked by the activation of Gα_q-coupled G-protein coupled receptors (GPCRs), whereas receptor tyrosine kinase (RTK) activation by nerve growth factor (NGF) leads to PLCγ activity (Rebecchi and Pentylala, 2000). Both of these subtypes respond to high levels of intracellular calcium (Ca²⁺), but the third major class, PLCδ, is the most sensitive to fluctuations in Ca²⁺ levels (Allen et al., 1997). Regardless of the route of activation, all three of these isoforms have the ability to hydrolyze PI(4,5)P₂ and activate downstream signaling.

1.6.3 PI(4,5)P₂ regulates ion channel function

The levels of PI(4,5)P₂ not only regulate protein localization and intracellular signaling cascades, but they can directly affect the function and activity of ion channels. The first reported case of PI(4,5)P₂-dependent ion channel modulation came from Hilgemann and Ball (1996). Using an inside-out membrane patch, the authors found that a sodium-calcium (Na⁺-Ca²⁺) exchanger and ATP-inhibited potassium (K⁺) channel currents decayed over time in these isolated membrane patches; however, currents could be restored with the addition of PI(4,5)P₂ or components that facilitated in PI(4,5)P₂ assembly. Rescue of channel current was blocked with the addition of PLC. In other words, these channels require a basal level of PI(4,5)P₂ in order to function (**Fig. 1.5B**). These findings have since been corroborated with a variety of other Na⁺, K⁺, Ca²⁺, and non-selective cation channels (Suh and Hill, 2005).

PI-binding regions of these ion channels have been identified based on mutagenesis to areas enriched in basic amino acids in inward rectifying K⁺ channels (Lopes et al., 2002), voltage-gated K⁺ channels KCNQ (Zhang et al., 2003), and sensory

transduction channels (Brauchi et al, 2007; Prescott and Julius, 2003; Ufret-Vincenty et al., 2011). These mutations might not be direct PI(4,5)P₂ binding sites; they might instead alter the conformation of the protein so that it can no longer interact with PI(4,5)P₂. Suh and Hille (2008) put forth two models of PI recognition: 1) electrostatic binding of clustered basic residues merely attract the protein to the negatively-charged lipids, and 2) the arrangement of basic charges that come together after protein folding create a precise PI binding pocket. Both of these models could explain PI specificity based on either the spacing of the basic amino acids along the protein sequence, or the arrangement of the basic residues in this binding pocket. However, without a crystal structure, it is difficult to determine the mechanism of interaction. Crystal structures of membrane-bound proteins are difficult to determine, however, one group has recently crystallized the inward rectifying K⁺ channel, Kir2.2, in the presence of short-chain PI(4,5)P₂, and shown a direct interaction of the ion channel and PI(4,5)P₂ (**Fig. 1.5B**). Hansen et al. (2011) found that one PI(4,5)P₂ binds each of the four protein subunits of Kir2.2, between the transmembrane and cytoplasmic domains, inducing a conformational change in the channel that results in increased channel activity. It is possible that a similar mechanism exists for the PI(4,5)P₂ regulation of other ion channels as well.

1.6.3.i PI(4,5)P₂ regulation of TRPV1

One non-selective cation channel that has been shown to interact with PI(4,5)P₂ is the sensory transduction channel, transient receptor potential vanilloid 1 (TRPV1). TRPV1 responds to acid (H⁺), chemical ligands such as capsaicin, and noxious thermal stimuli above 42° C, and TRPV1-null mice show sensory deficits to each of these stimuli (Caterina et al., 2000). The role of PI(4,5)P₂ in TRPV1 activation has been more controversial over the years. The first studies to report its PI(4,5)P₂ dependence suggested that TRPV1 was inhibited by PI(4,5)P₂ (Chuang et al., 2001; Prescott and Julius, 2003); however, it has since come to light that TRPV1 is bi-modally regulated by PI(4,5)P₂ levels (Lukacs et al.,

2007). In the presence of low concentrations of capsaicin (10-100 nM) or subtle changes in temperature, PI(4,5)P₂ depletion increases TRPV1 currents, and production of PI(4,5)P₂ inhibits these currents. The authors also found that this inhibitory effect is most likely not due to PI(4,5)P₂ directly, as similar results were not seen with excised membrane patches, suggesting this inhibition is due to interaction between PI(4,5)P₂ with other cellular proteins. More recently, however, Klein et al. (2008) reported that depletion of PI(4,5)P₂ inhibited TRPV1 activity at both high and low concentrations. Moreover, they report that while PI(4,5)P₂ is not the only PI to activate TRPV1, it is the most physiologically relevant player in both membrane patches and intact cells.

Recently, PI(4,5)P₂ depletion downstream of the G-coupled Adenosine receptor, A₁R, has been shown to reduce thermal sensitivity through TRPV1, and chronic sensitization through pronociceptive GPCRs in mice *in vivo* (Sowa et al., 2010). The authors found that Prostatic Acid Phosphatase (PAP), an ectonucleotidase that reduces adenosine monophosphate (AMP) to adenosine, reduces PI(4,5)P₂ levels through A₁R activation. PAP knockout mice have increased levels of endogenous PI(4,5)P₂, and the authors have previously shown these mice have increased sensitivity to nociceptive stimuli (Zylka et al., 2008). Intrathecal injection of secretory PAP (S-PAP) reduces PI(4,5)P₂ levels, and inhibits both thermal sensation through TRPV1, and thermal and mechanical sensitization due to inflammation and nerve injury in wildtype animals. In contrast, injection of PI(4,5)P₂ intensifies thermal hypersensitivity and mechanical allodynia with nerve injury models and with pronociceptive stimulation. While many of the previously discussed reports have shown that PI(4,5)P₂ is an important modulator of TRPV1, this work demonstrates that PI(4,5)P₂ is necessary for pain sensitization *in vivo*. Moreover, the authors demonstrated a role in both acute and chronic pain models; however, manipulation of PI(4,5)P₂ in this work was still indirect. A specific genetic reduction *in vivo* would be a more direct method to study the role of PI(4,5)P₂ in nociceptive sensitization.

1.7 Rapamycin-induced depletion of PI(4,5)P₂

A variety of methods have been used to reduce PI(4,5)P₂ signaling, such as activation of PLC, application of PI 4-kinase inhibitors, overexpression of PI(4,5)P₂-binding proteins or antibodies, or the expression of PI 5-phosphatases. While these methods are effective, they can have off-target effects, do not always allow for temporal control of manipulation, and are difficult to implement *in vivo*. Recently, two groups simultaneously developed a temporally-controlled method of PI(4,5)P₂ depletion using a chemically-induced dimerization system (Várnai et al., 2006; Suh et al., 2006).

Protein function often relies on the proximity of its effector. In other words, even an active protein is ineffective if it can't reach its target. Nature has developed ways of targeting proteins to their location of interest, either with specific codes like nuclear localization signals embedded within their sequences (Dingwall et al., 1982), or electrostatic binding as discussed for BAR domains and other PI(4,5)P₂-binding proteins. Some proteins have the ability to bind with multiple proteins, but only do so in the presence of certain chemicals. For instance, the immunosuppressant FK506 Binding Protein 12 (FKBP12) binds multiple drugs, two of which are FK506 and rapamycin. When FKBP12 is bound to FK506, it inactivates the phosphatase calcineurin; however, in the presence of rapamycin, FKBP forms a complex with the mammalian target of rapamycin (mTOR) through its FKBP rapamycin binding (FRB) domain (Crabtree and Schreiber, 1996). These FKBP binding interactions subsequently initiate two distinct signaling pathways.

Many groups have taken advantage of the rapamycin-induced dimerization by fusing proteins of interest to the FKBP or FRB domains: after treatment with rapamycin, these protein domains dimerize, transporting any fused proteins with them. Applications for this use range from regulating GPCR signaling (Putyrski et al., 2011) to specifically controlling synaptic transmission (Karpova et al., 2005). Suh et al. (2006) and Várnai et al. (2006) developed this system to inducibly deplete PI(4,5)P₂ by expressing the FRB domain

at the plasma membrane, and an FKBP-fused 5-phosphatase in the cytoplasm. Upon addition of rapamycin, the FKBP-phosphatase fusion translocates to the plasma membrane due to dimerization with the FRB domain. The enhanced proximity of the lipid 5-phosphatase to its target in the plasma membrane allows for the rapid reduction of PI(4,5)P₂ to PI(4)P (**Fig. 1.6**). Overexpression of constitutively active 5-phosphatases causes the loss of membrane-cytoskeletal adhesion, leading to increased membrane blebbing (Raucher et al., 2000), and long-term depletion of PI(4,5)P₂ can lead to activation of the apoptotic cell death pathway (Azuma et al., 2000; Mejillano et al., 2001). This inducible model of PI(4,5)P₂ depletion has the advantage over constitutive expression of 5-phosphatases because it allows for temporal control, and reduces the risk of complications due to overexpression side-effects.

Currently, there are no known methods to deplete PI(4,5)P₂ *in vivo*. Given that the FRB and FKBP components of this system are genetically encoded, it is possible to implement this inducible system *in vivo* with the addition of rapamycin. Natural rapamycin will interact with the endogenous mTOR pathway; however, it is possible to utilize mutated FRB domains that interact with rapamycin analogs (rapalogs; Stankunas et al., 2003; Bayle et al., 2006). These rapalogs do not interact with endogenous mTOR, but still function to induce dimerization between mutated FRB and FKBP. One FRB mutation that seemed promising for use *in vivo* given its interaction with the rapalog, C20-marap, consists of three amino acid mutations: K2095P, T2098L, and W2101F (Bayle et al., 2006). In order to acutely deplete PI(4,5)P₂ to determine its effects on thermal sensitization *in vivo*, this system needs to be targeted to heat-sensing neurons.

1.8 Nociceptive neuronal subsets of the dorsal root ganglia

The sensory neuronal population of dorsal root ganglia (DRG) is heterogeneous, consisting of at least twenty-five different subtypes. Of these, there are approximately

twelve subtypes of nociceptive, or pain-sensing neurons (Neacsu and Flonta, 2006), that can be broken down into two main groups: A δ and C fibers (reviewed in Julius and Bausbam, 2001). A δ fibers are lightly myelinated neurons of medium diameter that respond to mechanical, thermal, and chemical stimuli, with a thermal threshold of ~53°C (type I) and ~43°C (type II). C fibers are small diameter, unmyelinated neurons that sense mechanical, thermal, and chemical stimuli, in addition to innocuous temperature and itch. The thermal threshold of C fibers is approximately 43°C. C fibers can be further broken down into two neuronal subtypes based on their molecular markers and stimuli-evoked response: peptidergic and nonpeptidergic (Cavanaugh et al., 2009). Peptidergic neurons express substance P (SP), the nerve growth factor (NGF) receptor TrkA, as well as calcitonin gene related protein (CGRP), while nonpeptidergic neurons are marked by proteins such as PAP and Mrgprd (**Fig. 1.7**). Cavanaugh et al. (2009) showed that acute ablation of TRPV1-expressing neurons using the TRPV1 ligand, capsaicin, eliminated heat sensitivity within the parameters of the behavioral tests. In contrast, inducible ablation of non-peptidergic neurons using diphtheria toxin (DTX) application to mice expressing the human diphtheria toxin receptor in the Mrgprd locus causes a significant reduction in mechanical sensitivity. As demonstrated by Cavanaugh et al. (2009), these subtypes of nociceptive DRG neurons can be genetically targeted, and the effectiveness of targeting can be verified molecularly or by specific behavioral responses. TRPV1 is expressed in a portion of A δ , peptidergic, and non-peptidergic nociceptive subtypes; however, 50% of CGRP-expressing neurons express TRPV1, making these neurons adequate genetic targets for the manipulation of heat-sensing neurons *in vivo*.

1.9 Overview and rational of aims explored in this thesis

The plasma membrane plays a structural and functional role in the life of a cell. Not only does it aid in encapsulating the intracellular contents to separate one cell from the

next, but it also serves as an anchor for the actin cytoskeleton scaffold, as well as a home base for lipids that serve as messengers in a number of downstream signaling pathways. Given the importance of these aspects in cellular regulation, variations in the plasma membrane could lead to vast consequences in cellular function. **The overall aim of my dissertation was to study how perturbations to the plasma membrane affect cellular responses.**

1.9.1. Do changes in plasma membrane curvature and its neighboring actin cytoskeleton affect cortical neuronal development? Immense morphological changes take place during neuronal development. As neurons mature, the cell must extend multiple neurite that eventually become the axon and dendrites. In order to construct these neuronal processes, the outer membrane and internal components must be constructed, rearranged, and added at a relatively rapid pace compared to a cell at rest; therefore, it is possible that membrane-deforming proteins play a role in the changes occurring during this period of rapid outgrowth. srGAP2 is a member of the BAR superfamily of membrane-deforming proteins; however, it has internal domains that facilitate interaction with both the plasma membrane, the actin cytoskeleton, and other cellular proteins. Previously characterized F-BAR domains had only been shown to regulate membrane invagination and endocytosis. In Chapter 2, I present work demonstrating that the membrane-deforming F-BAR domain of srGAP2 is sufficient to induce filopodia-like protrusions, and subsequently regulate neuronal development *in vitro* and *in vivo*.

1.9.2 Are the F-BAR domains of srGAP1, srGAP2, and srGAP3 functionally distinct? Most previous reports and reviews have grouped the srGAP proteins into one functionally indistinct subfamily of the BAR-containing proteins; however, previous to the work in chapter 3, only a handful of reports looked into the functions of any of the proteins, and fewer focused on the F-BAR domains themselves. Furthermore, the only direct comparisons between the three had looked into mRNA localization throughout the CNS at

different developmental timepoints (Bacon et al., 2009) and the original paper suggesting that all three srGAP proteins bound the Robo receptor (Wong et al., 2001). In chapter 3, I demonstrate that the three F-BAR domains of the srGAP proteins are not functionally identical. The F-BAR of srGAP2 (F-BAR(2)) is a more potent filopodia inducer than F-BAR(1) or F-BAR(3) in non-neuronal cells; however, F-BAR(3) functions more similarly to F-BAR(2) in cortical neurons. F-BAR(1) seems to function to restrict membrane-deformation and protrusions. Moreover, this work demonstrates that the F-BARs of srGAP proteins can interact to more intricately regulate membrane deformation and cellular morphology.

1.9.3 Do alterations in the lipid composition of the plasma membrane regulate cellular function *in vivo*? PI(4,5)P₂, the most prominent phosphoinositide isoform in the plasma membrane, interacts directly with many members of the BAR superfamily of proteins, as well as the actin cytoskeleton and other actin-related proteins. In addition to its cytoskeletal scaffolding role, PI(4,5)P₂ acts as a second messenger in an abundance of cellular signaling pathways. Additionally, PI(4,5)P₂ regulates the activity of many ion channels, such as TRPV1, a key player in thermosensation of noxious temperatures. As discussed in chapter 4, we sought to reduce PI(4,5)P₂ in heat-sensing neurons *in vivo* using the rapamycin-induced dimerization system in order to reduce pain sensitization and chronic pain. Although we successfully adapted and expressed the rapamycin-induced PI(4,5)P₂ depletion system *in vivo*, we were unable to induce translocation. Chapter 4 illuminates some of the challenges and obstacles that arose along the way.

Overall, this work provides novel insights into the ways that physical and molecular manipulations of the plasma membrane alter cellular function.

1.9 Figures and legends

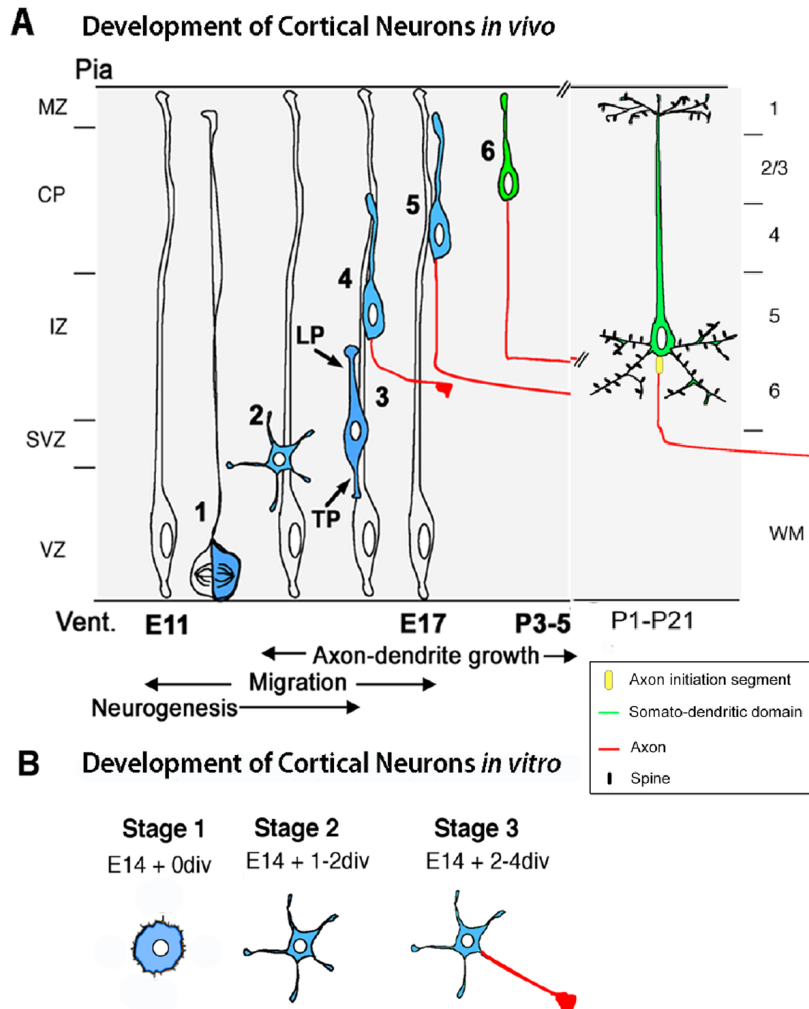


Figure 1.1. Cortical neuron development in vivo and in vitro

A) Radial glial cells divide asymmetrically (1) to produce a daughter radial glial cell (RGC) and a multipolar neuronal precursor cell that explores its surroundings looking for a path to migrate (2). This multipolar cell then polarizes, with a leading process towards the pial surface and a trailing process towards the ventricle (3). This cell attaches to a RGC (4) and migrates to the cortical plate, while extending its trailing process (5). Once the migrating neurons reach their target, they detach from the RGC and form an apical dendrite from its previous leading process (6) that will go on to mature into a highly arborized dendritic tree with dendritic spines. **B)** Dissociated cortical progenitors *in vitro* proceed through specific morphological transitions. Stage 1 neurons are flat cells with filopodia and lamellipodia protrusions. Stage 2 neurons have extended short, immature neurites. At stage 3, one neurite is molecularly distinct and has extended beyond the other neurites, specifying the axon. (Modified from Barnes and Polleux, 2009, *Annu Rev Neurosci*).

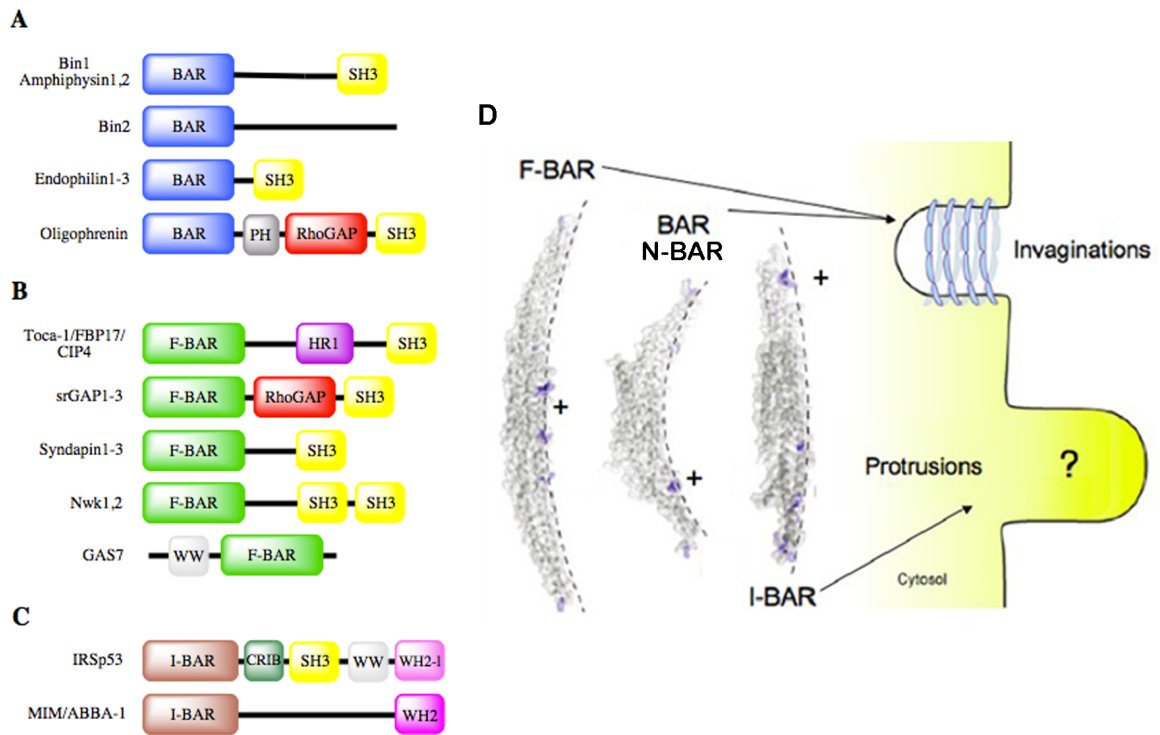


Figure 1.2. BAR superfamily proteins

(A-C) Domain organization of members of the Bin/Amphiphysin/Rvs (BAR) domain-containing superfamily of proteins. **A)** The founding subgroup, the BAR-containing proteins. **B)** Select members of the F-BAR domain-containing subgroup. F-BARs are elongated FCH-BAR domain that share similar sequence and helical domain secondary structure with BAR domains. **C)** Members of the inverse BAR (I-BAR) subfamily. In addition to BAR domains, many domains are common amongs the BAR domain-containing members, such as RhoGAP domains and SH3 domains. Many of these common additional domains aid in cytoskeletal rearrangement or protein-protein binding. Membrane-binding domains: BAR, F-BAR, I-BAR, and pleckstrin homology (PH). Small Rho GTPase binding domains: RhoGAP and HR1, and Cdc42/Rac1 Interactive Binding (CRIB). Domains that aid in protein-protein interaction: src homology 3 (SH3), WW (2 highly-conserved tryptophan residues), Wiscott-Aldrich syndrome homology 2 (WH2), and WH2-like (WH2-I). **D)** Crystallized dimers of F-BAR and BAR/N-BAR dimers are banana-shaped structures with positive amino acids (+) located on their concave surfaces. Inverse BAR (I-BAR) dimers are less curved, with phospholipid-binding positive amino acids on their convex surface. F-BAR and BAR/N-BAR domains oligomerize and bind membrane via electrostatic charge from the concave surface. These end to end oligomers form in a corkscrew fashion, invaginating membrane into the cell. Conversely, I-BAR domains protrude membrane, inducing filopodia-like structures. The mechanism for I-BAR-induced protrusions is currently unknown. (**Fig 1.2D** is modified from Scita et al., 2008, with permission from *Trends Cell Biol*)

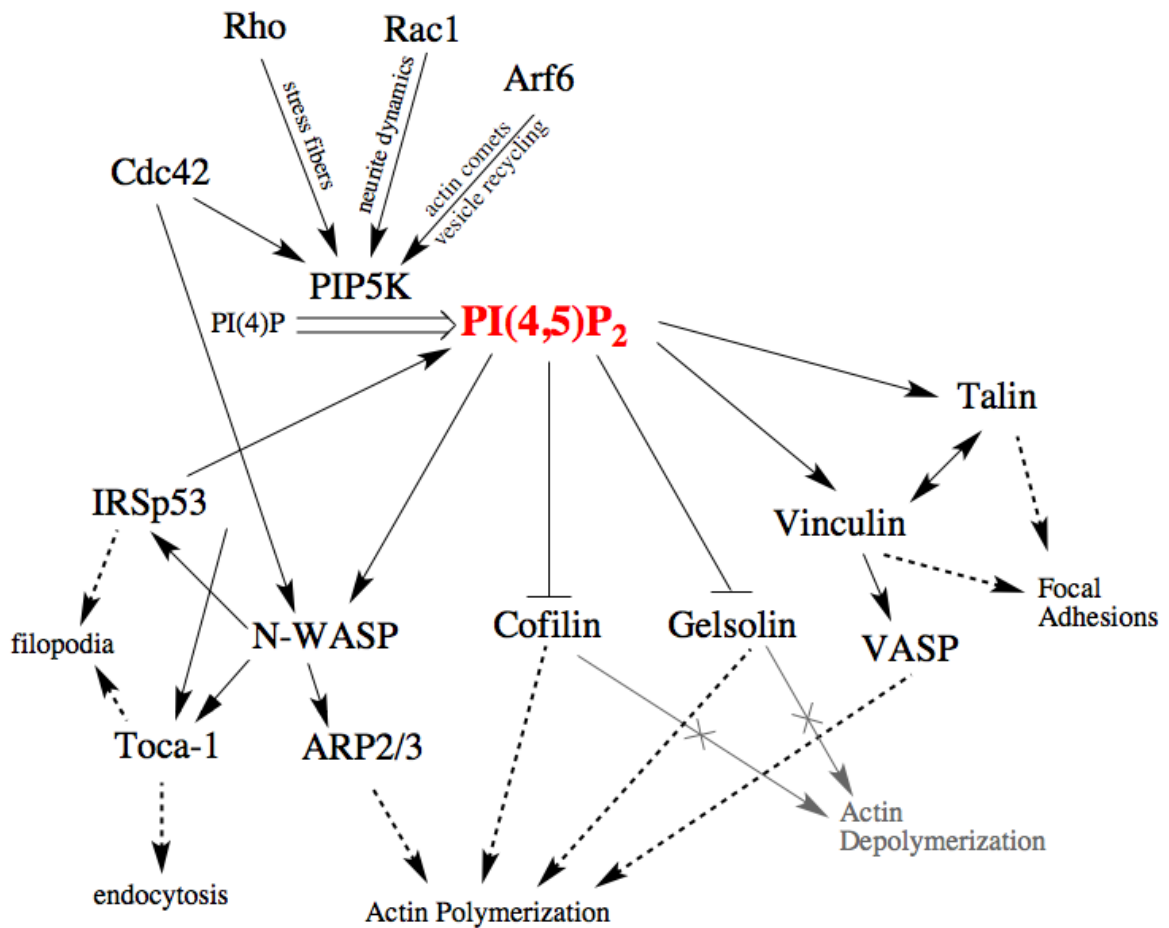


Figure 1.3. PI(4,5)P₂-mediated actin regulation through actin-related proteins

Small GTPases activate and mediate localization of the PI(4,5)P₂ producing kinase family PIP5Ks. High levels of PI(4,5)P₂ lead to actin polymerization through activation of actin polymerizing proteins, and inhibition of actin depolymerizing proteins. See text in section 1.5 for additional details.

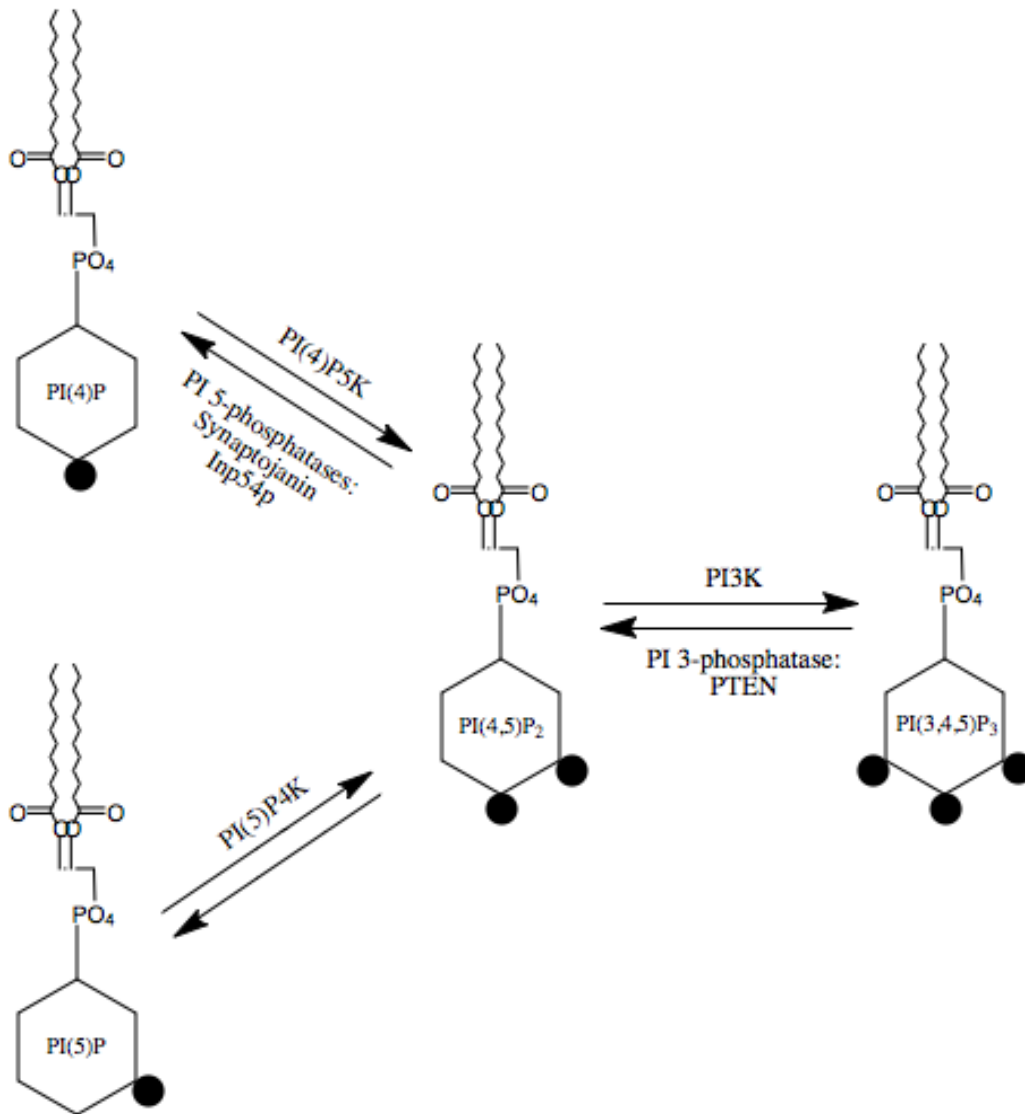


Figure 1.4. PI(4,5)P₂ metabolism

Interconversion between phosphoinositide species occurs with the addition and removal of phosphates (black circles) to certain positions of the inositol ring headgroup of the lipid by specific kinases and phosphatases, respectively. PI(4)P5K adds a phosphate group to the 5 position of PI(4)P to create PI(4,5)P₂, which can be reversed by PI 5-phosphatases such as the mammalian Synaptojanin or the yeast Inp54p. PI(4,5)P₂ can also be formed by the addition of a phosphate to the 4th position of the inositol ring by PI(5)P4K. There is currently no identified enzyme to reduce PI(4,5)P₂ to PI(5)P; however, bacterial IpgD can cause this reduction, resulting in decreased membrane-cytoskeletal adhesion. Formation of PI(4,5)P₂ can also occur in the opposite direction, from the removal of the 3-position phosphate of PI(3,4,5)P₃. Likewise, PI(4,5)P₂ can be converted to PI(3,4,5)P₃ with the addition of a phosphate to position 3 with PI3K. These kinases and phosphatases must remain in balance in order for proper lipid signaling.

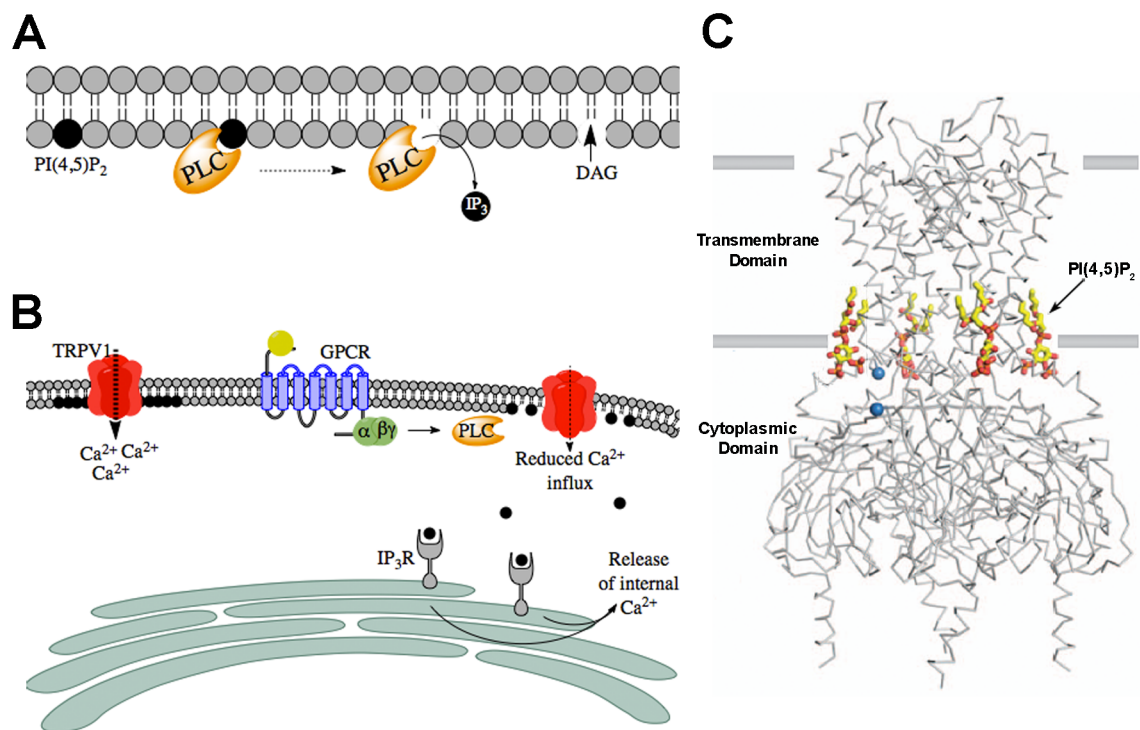


Figure 1.5. PI(4,5)P₂ signaling and ion channel regulation

A-B PI(4,5)P₂ (signified by lipid with black ball) is cleaved by phospholipase C (PLC) into inositol triphosphate (IP₃) and DAG. DAG remains at the membrane to activate protein kinase C (PKC), and IP₃ goes on to stimulate the IP₃ receptor (IP₃R) in the endoplasmic reticulum (seafoam green structure) and release intracellular calcium stores. **B**) When PI(4,5)P₂ is abundant at the plasma membrane, ion channels like TRPV1 (red channel) allow influx of ions. This channel current is inhibited by the reduction of PI(4,5)P₂ due to PLC activity. PLC activation can occur through G-protein (green α and $\beta\gamma$ subunits) activation due to activation of a G-protein coupled receptor (GPCR, blue channel) by a ligand (yellow circle) like adenosine, or through Ca²⁺ binding. **C**) The proposed mechanism for PI(4,5)P₂ ion channel regulation is due to conformational changes that occur between PI(4,5)P₂-bound and -unbound states. The inward rectifying potassium channel, Kir2.2, was crystallized in the presence of PI(4,5)P₂. Each of the 4 channel subunits bound to one molecule of PI(4,5)P₂, with the hydrophobic acyl chains binding to the transmembrane domain and the phosphorylated head group binding to cytoplasmic domain of the subunit. The conformational change induced by PI(4,5)P₂ binding is proposed to open the channel pore to allow ions to flow through. (**Fig. 1.5C** is modified from Hansen et al. (2011), with permission from *Nature*.)

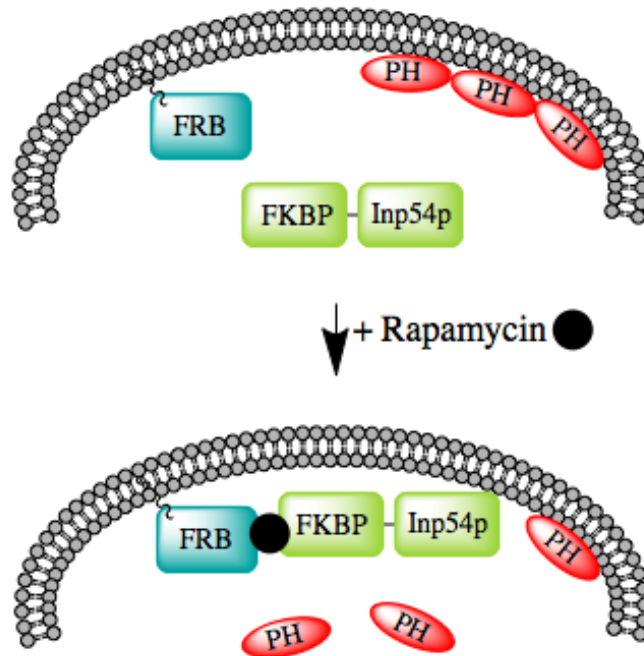


Figure 1.6. Schematic of rapamycin-induced depletion of PI(4,5)P₂ from the plasma membrane

Prior to rapamycin treatment, the FRB domain of mTOR is tagged to the plasma membrane with the membrane-targeting motif of GAP43, and the FKBP-Inp54p fusion protein is cytoplasmically localized. The PH domain of PLC δ 1 acts as a biosensor, and binds PI(4,5)P₂ in the plasma membrane. After rapamycin treatment, the FKBP domain dimerizes with the FRB domain, translocating the FKBP-Inp54p fusion protein to the plasma membrane, where the Inp54p phosphatase reduces PI(4,5)P₂ to PI(4)P, releasing the PH domain to the cytoplasm.

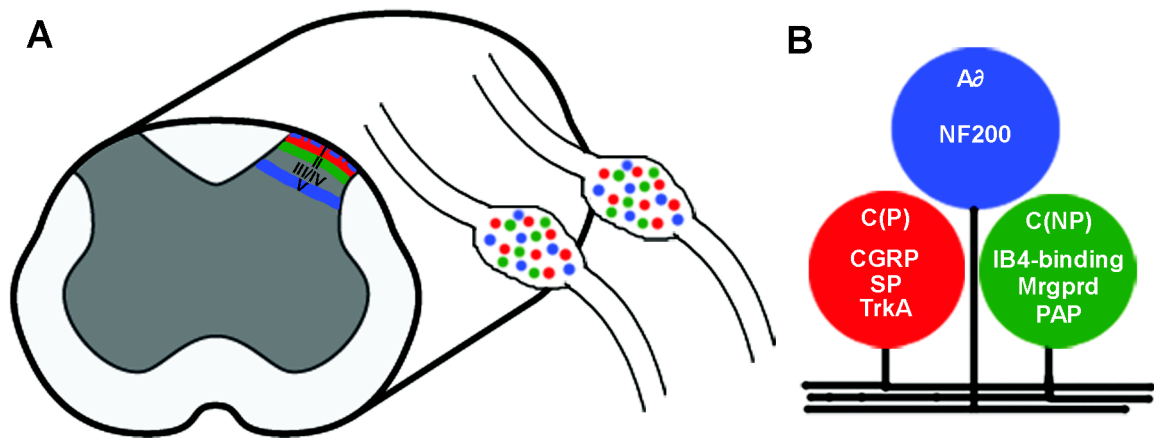


Figure 1.7. Subtypes of nociceptive neurons in the DRG

A) Dorsal root ganglia (DRG) contain multiple neuronal subtypes that project to different areas of the dorsal horn in the spinal cord. A δ fibers (blue) are lightly myelinated, high threshold neurons that synapse onto laminae I and IV of the dorsal horn. C-fibers are small, unmyelinated nociceptive neurons. C-fibers can be divided into peptidergic (C(P) in red) and non-peptidergic (C(NP) in green) neurons. C(P) neurons project to lamina I, while C(NP) neurons synapse in lamina II. **B)** Nociceptive neurons can be distinguished by size and molecular markers. A δ fibers are medium diameter neurons that express neurofilament 200 (NF200). C(P) neurons can be distinguished from C(NP) neurons by the expression of calcitonin gene related peptide (CGRP), substance P (SP), and the NGF receptor tyrosine receptor kinase A (TrkA), whereas C(NP) neurons bind isolectin-B4 (IB4), the GPCR Mrgprd, and the ectonucleotidase prostatic acid phosphatase (PAP). Many of these markers show partial overlap between subtypes.

CHAPTER 2

The F-BAR Domain of srGAP2 Induces Membrane Protrusions Required for Neuronal Migration and Morphogenesis¹

2.1 INTRODUCTION

During brain development, neural progenitor proliferation, neuronal migration, and differentiation require considerable changes in cell shape involving coordinated cytoskeletal and membrane remodeling (Ayala et al., 2007; Luo, 2002). Neuronal migration involves the coordinated extension and adhesion of the leading process (LP) along the radial glial scaffold with the forward translocation of the nucleus, which requires regulation of centrosome and microtubule dynamics by proteins such as Lis1, Doublecortin, and Nudel among others (Ayala et al., 2007; Higginbotham and Gleeson, 2007; Lambert de Rouvroit and Goffinet, 2001). However, little is known about the molecular mechanisms underlying membrane dynamics during neuronal migration and morphogenesis.

The basis of neurite initiation, outgrowth, and branching is rooted in the ability of the actin and microtubule cytoskeleton to undergo dynamic changes (Gupton and Gertler, 2007; Luo, 2002; Mattila and Lappalainen, 2008). Filopodia have been shown to play a role in neurite initiation (Dent et al., 2007; Kwiatkowski et al., 2007), growth cone dynamics (Burnette et al., 2007; Gallo and Letourneau, 2004), neurite outgrowth (Luo, 2002), and

¹ Sabrice Guerrier, Jaeda Coutinho-Budd, Takayuki Sassa, Aurelie Gresset, Nicole Vincent Jordan, Keng Chen, Wei-lin Jin, Adam Frost, and Franck Polleux (2009) srGAP2 regulates neuronal migration and morphogenesis through the ability of its F-BAR domain to induce membrane protrusions. *Cell* 138, 990-1004.

I have obtained the rights to include this work in my thesis. My contribution focused on the structure/function analysis of srGAP2 in COS7 cells and dissociated neurons, as well as biochemical analysis (Figures 2.3, 2.4, 2.S1, 2.S4, 2.S5, 2.S7, 2.S12, and 2.S13). I worked closely with the first author throughout my involvement with the project, contributed to scientific discussion, and assisted with layout and proofreading of the manuscript.

branching (Dent et al., 2004; Gallo and Letourneau, 1998). Downregulation of the actin anti-cappers ENA/VASP proteins, which are potent inducers of filopodia, resulted in failed neurite initiation and also in defects in cortical lamination (Kwiatkowski et al., 2007), suggesting a functional relationship between filopodia formation, neurite initiation, and neuronal migration.

Classically, filopodia formation is thought to be primarily dependent on proteins that regulate actin polymerization at the barbed end of actin filaments and proteins bundling F-actin (Gupton and Gertler, 2007). Interestingly, the BAR superfamily member IRSp53 has been shown to induce filopodia through membrane deformation independently of its F-actin bundling activity (Lim et al., 2008; Mattila et al., 2007; Saarikangas et al., 2009). The BAR domain superfamily contains three main groups: (1) the Bin/Amphiphysin/Rvs (BAR) domain subfamily (Itoh and De Camilli, 2006), (2) the Fes-Cip4 homology BAR (also called F-BAR or EFC) domain subfamily (Itoh et al., 2005; Tsujita et al., 2006; reviewed in Frost et al., 2009), and (3) the I-BAR subfamily (reviewed in Scita et al., 2008). Structural analysis of three F-BAR domains demonstrated that these domains are elongated homodimers characterized by a shallow curvature formed by the antiparallel interaction of two α -helical coiled coils (Henne et al., 2007; Shimada et al., 2007). In addition to sharing the general fold and quaternary organization of the BAR domain superfamily, F-BAR domains share functional properties with “classical” BAR domains, most notably the ability to bind and deform membranes *in vitro* and in living cells (Frost et al., 2008; Itoh et al., 2005; Kakimoto et al., 2006; Shimada et al., 2007). However, to date, the *in vivo* functions of F-BAR domain-containing proteins are largely unknown (Frost et al., 2009).

Here we identify slit-robo GTPase activating protein (srGAP2) as a regulator of neuronal migration and morphogenesis through the unexpected ability of its N-terminal F-BAR domain to induce filopodia-like membrane protrusions resembling those induced by I-

BAR domains. Our results highlight the functional importance of proteins directly regulating membrane deformation for proper neuronal migration and axon-dendrite morphogenesis.

2.2 RESULTS

2.2.1 Expression of srGAP2 in the developing cortex

To begin our study of the role of srGAP2 in cortical development, we first examined its pattern of expression. srGAP1–3 have recently been reported to be expressed throughout the cortex during and after radial migration (Bacon et al., 2009; Mattar et al., 2004; Yao et al., 2008). Our analysis confirmed that srGAP2 mRNA is expressed throughout the developing cortex and is found both in proliferative zones (ventricular zone [VZ] and subventricular zone [SVZ]) at embryonic day 13 (E13) and E15 and in postmitotic regions (cortical plate [CP]) at E15 and postnatal day 1 (P1) (**Figure 1A**). In order to determine the pattern of srGAP2 protein expression, we used a polyclonal antibody raised against the C terminus of srGAP2 (**Figures 1B and 1C**; Yao et al., 2008). srGAP2 protein is expressed throughout cortical development culminating at P1 corresponding to the peak of neuronal migration in the cortex. Its expression is maintained at P15 and reduced, but still present, in adult cortex (**Figure 1C**).

Immunofluorescent staining for srGAP2 shows that it is ubiquitously expressed in the cortical wall (**Figure 1D**) being found both in Nestin-positive neuronal progenitors in the VZ (**Figures 1H–1J**) and MAP2-positive postmitotic neurons in the CP (**Figures 1E–1G**). At the subcellular level, endogenous srGAP2 is found at the cell periphery (**Figures 1K–1M**, arrows) and was often localized along F-actin-rich filopodia-like protrusions (arrowhead in **Figures 1K–1P**) in acutely dissociated E15 cortical neurons.

2.2.2 Full-length srGAP2 and its F-BAR domain induce filopodia formation

Overexpression of F-BAR domain-containing proteins such as FBP17 or CIP4 have been shown to cause membrane invagination and tubulation in cell lines (Itoh et al., 2005;

Tsujita et al., 2006). Surprisingly, expression of srGAP2 did not induce any membrane invaginations, but instead induced filopodia formation (see **Figures S1D–S1F and S1P** available online). This effect requires its F-BAR domain since deletion of the F-BAR domain (srGAP2^{ΔF-BAR}-EGFP) does not induce filopodia formation in COS7 cells (**Figures S1G–S1I and S1P**).

Interestingly, unlike the F-BAR domains of FBP17 and CIP4 (Itoh et al., 2005), expression of the F-BAR domain of srGAP2 did not inhibit endocytosis, as assessed using Alexa546-Transferrin uptake assay (**Figure S2**). Furthermore, expression of the isolated F-BAR domain fused to EGFP induced filopodia formation similar to full-length srGAP2 (**Figures S1J, S1K, and S1P**). Of note, the F-BAR domain is a potent membrane-targeting motif (**Figure S1J**). These data suggest that the F-BAR domain of srGAP2 is necessary and sufficient for membrane localization and the induction of filopodia-like membrane protrusions.

In order to distinguish the membrane-targeting function of the F-BAR domain from its membrane deformation activity, we identified a small truncation of the last C-terminal 49 amino acids (F-BAR^{Δ49}) (**Figure S3A** and Supplemental Experimental Procedures for details). Expression of F-BAR^{Δ49}-EGFP results in significant membrane targeting (**Figure S4**) but fails to induce filopodia in COS7 cells (**Figures S1M–S1P**). We do not currently know the structural basis for the inability of this truncation to elicit filopodia, but we can at least exclude two possibilities: (1) instability of the F-BAR^{Δ49} protein since it expresses at a level comparable to full-length srGAP2 or its F-BAR domain in cells (**Figure S5**) and (2) this truncation does not disrupt its dimerization properties since F-BAR^{Δ49} can dimerize with F-BAR or full-length srGAP2 (data not shown). Interestingly, these 49 amino acids reside in an extension specific to the srGAP subfamily ($\alpha 6-8$; **Figure S3A**) that is C-terminal to the minimal, predicted F-BAR domain (amino acids 1–358; Itoh et al., 2005) (**Figure S3B**). Indeed, we were unable to obtain stable protein expression of this minimal predicted F-BAR

domain (amino acids 1–358) in mammalian cells or bacteria (data not shown). Furthermore, as shown for other F-BAR domains (Frost et al., 2008; Itoh et al., 2005; Kakimoto et al., 2006; Shimada et al., 2007), srGAP2 forms a stable dimer in solution as assessed by light scattering assays (**Figure S3C**), and deletion of the Fes-Cip4 homology (FCH) domain (green box in **Figure S3A**), which represents a significant portion of the dimerization interface, abolishes the ability of srGAP2 to induce filopodia in COS7 cells (data not shown). Altogether, these data suggest that all eight predicted α -helices are likely to be required for formation of the functional F-BAR domain of srGAP2.

2.2.3 The F-BAR domain of srGAP2 deforms membrane like an I-BAR domain

The ability of srGAP2 or its F-BAR domain to induce filopodia in COS7 cells is reminiscent of the activity of the structurally related I-BAR domain-containing proteins (Mattila et al., 2007; Millard et al., 2007; Saarikangas et al., 2009; Scita et al., 2008). Interestingly, F-actin depolymerization prevents the dynamics and formation of new filopodia, but does not affect the maintenance of pre-existing filopodia induced by the I-BAR domains of IRSp53 or MIM (Mattila et al., 2007). We found the same results for the F-BAR domain of srGAP2 (**Figures 2A–2C**), while cells treated with cytochalasin D were depleted of F-actin. Strikingly, this treatment had no effect on membrane localization of the F-BAR domain or on the maintenance of filopodia-like protrusions (**Figures 2D–2F**). F-BAR-induced filopodia were highly dynamic in COS7 cells (**Figures 2G–2J** and **Movie S1**). Treatment with cytochalasin D significantly impaired the extension and retraction of F-BAR-induced filopodia (**Figures 2K–2N** and **Movie S2**), suggesting that F-actin is required for the dynamics of these protrusions.

In order to directly test the membrane deformation properties of the F-BAR domain of srGAP2, we incubated purified F-BAR domain with preformed liposomes. As visualized by negative stain transmission electron microscopy, this did not result in liposome outward tubulation as has been reported for other F-BAR domains (see **Figure S5B**). Rather, the F-

BAR domain of srGAP2 induced an inward dimpling or “scalloping” of the liposome surface (**Figures 2O and 2P**), which is reminiscent of the activity of I-BAR domains in the same conditions (Suetsugu et al., 2006), suggesting that the F-BAR domain of srGAP2 can induce “inverse” membrane tubulation.

These results suggested the possibility that if the purified F-BAR domain of srGAP2 could be exposed to the inside surface of liposomes, then protrusive tubules would form (**Figure 2Q**). To test this hypothesis, mixtures of the F-BAR domain with intact, large unilamellar vesicles (LUVs) were briefly sonicated, which presumably resulted in transient pore formation in liposomes and introduction of the recombinant F-BAR inside LUVs. Following a wash, liposomes were fixed, negatively stained, and imaged using transmission electron microscopy. As predicted by the I-BAR model, this resulted in numerous long tubular extensions emerging from LUVs (**Figure 2R**), which is in stark contrast with control sonicated liposomes not incubated with recombinant protein (**Figure S6A**). Consistent with the dimensions of tubules induced by other members of the F-BAR and I-BAR families (Frost et al., 2008; Mattila et al., 2007), the srGAP2 F-BAR-induced tubules were $83 \text{ nm} \pm 15 \text{ nm}$ (average \pm SD, $n = 38$) in diameter. Importantly, at higher magnification, the tubules observed by negative staining electron microscopy after sonication do not have an obvious protein coat surrounding the liposomes (**Figure 2R**). This is in contrast with tubules induced by other F-BAR and BAR domains that coat the outer surface of the tubule (**Figure S6B**; Frost et al., 2008; Shimada et al., 2007). Together, these results suggest that unlike previously characterized F-BAR domains, the F-BAR domain of srGAP2 functions as an I-BAR domain (Mattila et al., 2007; Suetsugu et al., 2006).

2.2.4 srGAP2 regulates neurite formation and branching through the ability of its F-BAR domain to form filopodia

We next tested the function of srGAP2 in neuronal morphogenesis by designing short hairpin interfering RNA (shRNA) in order to acutely knock down srGAP2 expression

(**Figure 3A**). We found that srGAP2 knockdown in E15 cortical neurons led to a significant decrease in both axonal (**Figures 3C, 3D, and 3F**) and dendritic branching after 5 days in vitro (DIV) (**Figures 3G, 3H, and 3J**). Both of these effects were rescued by cotransfection of a shRNA-resistant form of srGAP2 (srGAP2*; **Figures 3B, 3E, 3F, 3I, and 3J**), demonstrating that this is not an off-target effect. The fact that srGAP2 knockdown reduced branching in cortical neurons, a process previously shown to require filopodia formation (Dent et al., 2004; Gallo and Letourneau, 1998), suggests that srGAP2 may promote neurite branching through its ability to induce filopodia in neurons.

To test this hypothesis, we performed a structure/function analysis using electroporation of E15 cortical progenitors with various srGAP2 constructs followed by dissociation and culture, which induces rapid differentiation. First, we restricted our analysis to stage 1 neurons (Dotti et al., 1988), when immature postmitotic neurons produce a significant number of filopodia-like protrusions (Dent et al., 2007; Kwiatkowski et al., 2007). Our analysis shows that expression of full-length srGAP2 induced a significant increase in filopodia-like protrusions in stage 1 cortical neurons compared to control EGFP (**Figures 4A–4C and 4F**). This effect requires the F-BAR domain since deletion of the F-BAR domain (srGAP2^{ΔF-BAR}) significantly reduced the ability of srGAP2 to induce filopodia in stage 1 neurons (**Figures 4C and 4F**). As in COS7 cells, expression of the F-BAR domain alone potently induces formation of F-actin-rich filopodia (**Figures 4D and 4F**). Again, the effect of the F-BAR domain requires its membrane deformation properties, and not simply its membrane targeting property since expression of F-BAR^{Δ49} does not induce filopodia in stage 1 cortical neurons (**Figures 4E and 4F**), and instead induces large lamellipodia (arrowhead in **Figure 4E**). These data suggest that srGAP2, through its F-BAR domain, induces filopodia in cortical neurons as shown in COS7 cells.

We then analyzed stage 2 neurons, i.e., prior to the emergence of a single axon (Dotti et al., 1988), in order to test if srGAP2 and its F-BAR domain were sufficient to

promote the transition between filopodia and elongating neurites defined by the presence of bundled microtubules (see also **Figure S7** for isolated β III-tubulin signal). Both full-length srGAP2 and the F-BAR domain significantly increased the total number of primary neurites emerging from the cell body (**Figures 4G–4K**) as well as the number of primary neurite branches (**Figure 4L**). Expression of srGAP2 ^{Δ F-BAR} as well as F-BAR ^{Δ 49} fails to increase primary neurite number and neurite branching compared to control (**Figures 4J–4L**).

2.2.5 Reduction of srGAP2 expression promotes neuronal migration

To determine the function of srGAP2 during cortical development, we introduced our shRNA constructs directed against srGAP2 (Dha2 and Dha5; **Figure 3A**) into radial glial progenitors at E15 using ex vivo cortical electroporation coupled with organotypic slice culture (Hand et al., 2005). Interestingly, after 3 days in culture, at a time point when few control shRNA electroporated neurons have already migrated (**Figures 5A, 5C, and 5D**), slices expressing srGAP2 shRNA showed a significant increase in the percentage of neurons that have reached the dense CP and a corresponding decreased percentage of neurons in the intermediate zone (IZ) (**Figures 5B–5D**), suggesting that reduction of srGAP2 expression accelerated radial migration. To test this directly, we used time-lapse confocal microscopy to visualize neurons coexpressing nuclear EGFP (to ease cell tracking) and control shRNA (**Figures 5E–5H and Movie S3**) or srGAP2 shRNA (**Figures 5E–5L and Movie S4**) in slice culture. We found that srGAP2 shRNA-expressing neurons migrated 25% faster than those expressing control shRNA (**Figure 5M**), suggesting that reduction of srGAP2 increased the actual rate of cell translocation.

Excessive LP branching in migrating cortical neurons can inhibit neuronal migration (Gupta et al., 2003; Ohshima et al., 2007). Indeed, the LP of srGAP2 knockdown neurons in layers 5/6 was significantly less branched compared to control shRNA neurons (**Figures 5N–5P**). These data suggest that srGAP2 may negatively regulate the rate of radial migration by promoting LP branching and dynamics.

2.2.6 The F-BAR domain is necessary and sufficient for srGAP2-mediated inhibition of radial migration

We hypothesized that overexpression of srGAP2 or its F-BAR domain should be sufficient to block migration by increasing filopodia formation and LP dynamics. Indeed, overexpression of srGAP2 severely inhibited radial migration compared to control EGFP-expressing slices electroporated at E15 and cultured for 5 DIV (**Figures 6E–6H**). We quantified radial migration by determining the ratio of neurons in the dense CP (where pyramidal neurons complete migration) and in the IZ, where they initiate radial migration (see **Figure S8** for definition of cytoarchitecture). This CP/IZ ratio (**Figure 6U**) is significantly decreased by srGAP2 overexpression (**Figures 6E–6H**) when compared to control EGFP-expressing neurons (**Figures 6A–6D**), demonstrating that srGAP2 overexpression inhibits neuronal migration. Expression of srGAP2^{ΔF-BAR} did not significantly reduce the CP/IZ ratio compared to EGFP control (**Figures 6I–6L and 6U**) and is significantly different from the ratio measured by srGAP2 overexpression (**Figure 6U**), suggesting that the F-BAR domain is partially required for srGAP2's ability to inhibit migration. Moreover, expression of the F-BAR domain alone was sufficient to reduce neuronal migration to the same extent as srGAP2 while expression of F-BAR^{Δ49} had no effect on the ability of neurons to migrate (**Figures 6M–6U**), suggesting that the ability of the F-BAR domain to induce filopodia is required for the ability of srGAP2 to inhibit neuronal migration.

2.2.7 srGAP2 inhibits migration by increasing leading process dynamics and branching

The accumulation of neurons expressing srGAP2 or its F-BAR domain in the IZ suggested that the neurons might be partially blocked in the multipolar to unipolar transition (Noctor et al., 2004). Indeed quantification of the percentage of multipolar cells (cells displaying three or more neurites) in the IZ of slices electroporated with srGAP2 or the F-

BAR domain revealed a significant increase in the percentage of neurons with multiple processes emerging from the cell body compared to control (**Figure 6V**). This is consistent with the ability of srGAP2 to induce filopodia and neurite initiation/branching in dissociated neurons (see **Figure 4**).

Our time-lapse confocal microscopy analysis shows that control neurons in the IZ form a stable LP upon initiating radial migration (green arrowheads in **Figure 6W** and **Movie S5**) and undergo efficient cell body translocation (green arrows in **Figure 6W** and **Movie S5**). In contrast, neurons overexpressing srGAP2 or the F-BAR domain alone do not undergo cell body translocation (red arrows in **Figures 6X and 6Y** and **Movies S6 and S7**), and instead form multiple processes that are highly dynamic and unstable (red arrowheads in **Figures 6X and 6Y** and **Movies S6 and S7**). The plasma membrane of these cells appears highly dynamic showing large, transient protrusions (green arrowheads in **Figure 6X**). While many neurons accumulate in the IZ, some did manage to translocate into layers 5/6 (**Figures 6E–6H and 6M–6P**), where expression of srGAP2 or its F-BAR domain significantly increases LP branching compared to EGFP control (**Figure 6Z and Figures 7A–7C**). Together, these data suggest that srGAP2 increases neurite initiation and branching through the ability of its F-BAR domain to induce filopodia, which in turn negatively regulates neuronal migration.

Finally, to ensure that the ability of srGAP2 expression to inhibit migration was not due to an indirect effect of srGAP2 expression on progenitor cell cycle exit, we designed a vector allowing us to express srGAP2 in early postmitotic neurons using the 2.2 kB NeuroD promoter (**Figure S9A**). NeuroD is a bHLH transcription factor and a direct transcriptional target of Ngn2 (Hand et al., 2005; Heng et al., 2008), thereby inducing cDNA expression in intermediate progenitors and early postmitotic neurons in the subventricular zones and IZ (**Figures S10E–S10H**) but not by Nestin⁺ radial glial progenitors in the VZ as obtained by the chicken β -actin promoter (**Figures S10A–S10D**). Furthermore, the level of protein

expression in neurons obtained with this promoter is significantly lower than using the chicken β -actin promoter (data not shown; Heng et al., 2008). Expression of srGAP2 using this NeuroD promoter significantly reduced the number of cells reaching the CP compared to control (Figures S9B–S9J).

2.2.8 srGAP2 partially requires its RhoGAP and SH3 Domains to inhibit migration

We next wanted to determine the contributions of the RhoGAP and SH3 domains to srGAP2 function in neuronal migration and morphogenesis. In order to determine the substrate specificity of the GAP domain of srGAP2, we purified its GAP domain as a GST fusion (**Figure S11A**). We then performed fluorescencebased GTP hydrolysis assays (**Figure S11B**; Shutes and Der, 2006). The GAP domain of srGAP2 increased the rate of GTP hydrolysis on Rac1, but had no effect on RhoA or Cdc42 (**Figure S11B**) or RhoG (data not shown). In addition, full-length srGAP2 strongly interacted with activated Rac1 (Rac1^{Q61L}) but only weakly interacted with activated Cdc42^{Q61L} (**Figure S11C**) and activated RhoAQ63L (data not shown). These two independent approaches demonstrate that the GAP domain of srGAP2 is specific for Rac1.

To determine the contribution of the Rac1-GAP domain on srGAP2's ability to regulate neuronal morphogenesis and migration, we engineered a catalytically inactive form of srGAP2 (srGAP2^{R527L}). Indeed this mutant was unable to accelerate GTP hydrolysis of Rac1 (**Figure S11D**). Expression of the “GAP-dead” srGAP2^{R527L} was as potent as srGAP2 at inducing filopodia-like membrane protrusions in stage 1 cortical neurons (compare **Figures S12B and S12C**; quantified in **Figure S12F**) and at promoting primary neurite initiation (**Figures S12H and S12I**; quantified in **Figure S12L**). While this mutation was competent to increase neurite initiation, there were significantly fewer (2-fold) srGAP2^{R527L}-expressing neurons at stage 2 when compared to srGAP2 (**Figure S13**). In addition, srGAP2^{R527L} displays a reduced ability to induce neurite branching when

compared to srGAP2 (**Figure S12L**), suggesting that the Rac1-GAP activity of srGAP2 might participate in its function in neurite branching.

We tested the contribution of the Rac1-GAP activity of srGAP2 in its ability to inhibit neuronal migration by expressing srGAP2^{R527L} in E15 cortical progenitors. This significantly inhibited migration compared to control EGFP (**Figures S14A–S14D, S14I–S14L, and S14U**) although not as potently as full-length srGAP2 (**Figures S14E–S14H and S14U**), suggesting that the Rac1-GAP activity of srGAP2 contributes to its ability to inhibit migration. In addition, similarly to srGAP2, expression of srGAP2^{R527L} increased the percentage of multipolar cells in the IZ (**Figure S14V**) and increased LP branching of radially migrating neurons in layer 5/6 (**Figures S14X and 6Z**). These data suggest that the Rac1-GAP activity may act to modulate protrusion formation induced by the F-BAR domain of srGAP2, but is not absolutely required to induce filopodia-like membrane protrusions and inhibit neuronal migration.

To test the contribution of the SH3 domain of srGAP2, we engineered a mutant to a conserved tryptophan residue (srGAP2^{W765A}), which was shown to be required for the ability of the SH3 domain of srGAP1 to bind to Robo1 and for the SH3 domain of srGAP3 to bind to WAVE-1 (Wong et al., 2001; Li et al., 2006; Soderling et al., 2002). Expression of srGAP2^{W765A}, unlike the expression of full-length srGAP2 or its F-BAR domain, did not efficiently induce filopodia-like membrane protrusions in stage 1 cortical neurons (**Figures S12D and S12F**) and had a significantly decreased ability to induce primary neurite branching compared to full-length srGAP2 (**Figures S12J and S12L**). Expression of srGAP2^{W765A} increased primary neurite initiation, but showed a significantly reduced percentage (2-fold) of neurons transitioning from stage 1 to stage 2 compared to srGAP2 (**Figure S13**), suggesting that all functional domains of srGAP2 are required for its ability to promote the transition from a filopodia to an elongating neurite.

Interestingly, expression of srGAP2^{W765A} had no effect on cortical neuron migration (**Figures S14M–S14P and S14U**), although there was a slight increase in cells with multipolar morphology in the IZ compared to EGFP (**Figure S14V**). The lack of effect of srGAP2^{W765A} overexpression on the CP/IZ ratio prompted us to use time-lapse microscopy to observe LP dynamics in radially migrating neurons. This analysis revealed that migrating neurons expressing srGAP2^{W765A} did not display increased LP branching, but instead had a single, stable LP (red arrowheads in **Figure S14W and Movie S8**) and translocated efficiently (green arrowheads in **Figure S14W and Movie S8**), which is strikingly different from neurons overexpressing full-length srGAP2 (**Figure 6X**). Moreover, analysis of neurons in layer 5/6 showed no significant increase in LP branching as demonstrated with other constructs containing an F-BAR domain (**Figures 6, 7E, and S14X**).

The fact that srGAP2^{W765A} showed weak filopodia formation compared to full-length srGAP2, and no increase in neurite branching suggested that the F-BAR domain might be inhibited in srGAP2^{W765A}. By analogy to the mode of activation of other RhoGAP and RhoGEF proteins (Eberth et al., 2009; Mitin et al., 2007; Yohe et al., 2007), we hypothesized that srGAP2 might normally be in an autoinhibited conformation through structural interaction between the N-terminal F-BAR domain and the C-terminal region (including the SH3 domain) that is released upon effector binding to its SH3 domain (see model in **Figure 7G**).

To test this model, we generated a C-terminal deletion of srGAP2 (srGAP2^{ΔC-term}), which deletes the entire C-terminal portion starting from the SH3 domain to the C-terminal end. Expression of srGAP2^{ΔC-term} potently induced filopodia formation in stage 1 neurons (**Figures S12E and S12F**) and neurite outgrowth and branching in stage 2 neurons (**Figures S12K and S12L**). In sharp contrast to srGAP2^{W765A}, expression of srGAP2^{ΔC-term} potently inhibited migration (**Figures S14Q– S14U**) resulting in increased multipolar cells in the IZ (**Figure S14V**) as well as increased LP branching of migrating neurons in layer 5/6

similarly to other F-BAR-containing constructs but unlike srGAP2^{W765A} (Figures S14X and 7F).

2.3 DISCUSSION

2.3.1 srGAP2 is a novel F-BAR domain-containing protein

It is well established that cytoskeletal dynamics produce forces to generate plasma membrane protrusions and invaginations; however, recent evidence suggests that many membrane-associated proteins directly sculpt and deform biological membranes (Doherty and McMahon, 2008). Here we report that srGAP2 regulates neuronal migration as well as neurite initiation and branching through the ability of its F-BAR domain to deform membranes and form filopodia-like membrane protrusions. This is a surprising finding since F-BAR domains have been mostly characterized for their ability to induce membrane tubulation and invaginations (Frost et al., 2008; Habermann, 2004; Henne et al., 2007; Itoh and De Camilli, 2006; Peter et al., 2004; Shimada et al., 2007). F-BAR domains are composed of a series of α -helices forming a strong dimerization motif, which allow the homodimers to adopt a quaternary “banana-like” structure (Frost et al., 2008; Henne et al., 2007; Peter et al., 2004; Shimada et al., 2007). One possibility for how srGAP2’s F-BAR domain may induce filopodia-like protrusions is by having a different curvature leading to a different surface distribution of positively charged residues than “canonical” F-BAR domains. Interestingly, I-BAR domains present in proteins such as IRSp53 or MIM induce filopodia, a property linked to the inherent curvature of the I-BAR homodimer and the presence of phospholipid-binding residues on the convex side of the homodimers (Lim et al., 2008; Mattila et al., 2007; Millard et al., 2007; Saarikangas et al., 2009).

We hypothesize that the homodimer formed by the F-BAR domain of srGAP2 displays a general quaternary structure and charge distribution comparable to I-BAR domains. While this can only be proven by structural information, we provide several lines

of evidence supporting an I-BAR like behavior: (a) the structural maintenance of filopodia induced by the F-BAR domain of srGAP2 is resistant to F-actin depolymerization, (b) overexpression of the F-BAR domain of srGAP2 does not inhibit endocytosis, and (c) the F-BAR domain of srGAP2 induces similar liposome deformations compared to IRSp53 (Suetsugu et al., 2006).

Interestingly, srGAP2 is not the only predicted F-BAR domain-containing protein inducing filopodia formation: Gas7 and PSTPIP2 (MAYP) have also been shown to induce filopodia in cell lines (Chitu et al., 2005; She et al., 2002). However, these proteins and more importantly their predicted F-BAR domains have not been directly tested for their ability to deform membranes. Our results suggest that the F-BAR domain subfamily could be functionally diverse and that this diversity might be due to subtle structural differences.

2.3.2 A role for srGAP2 during neuronal development

It was recently shown that filopodia were required for neurite initiation in cortical neurons (Dent et al., 2007). The absence of effect of srGAP2 knockdown on neurite initiation is likely due to the presence of many other proteins involved in filopodia formation, such as I-BAR-containing proteins such as IRSp53 or ABBA (Mattila and Lappalainen, 2008; Saarikangas et al., 2008) or other classes of proteins previously shown to promote filopodia formation and neurite initiation through distinct mechanisms (Dent et al., 2007; Kwiatkowski et al., 2007).

The ability of srGAP2 to promote neurite initiation and branching appears to also be important for its regulation of migration (**Figure 7H**). Knockdown of srGAP2 increased the rate of migration and significantly reduced LP complexity and branching (**Figure 7H**). This could potentially explain the increase in the rate of cell migration, since in fibroblasts, reduction of the activity of proteins promoting filopodia formation, such as ENA/VASP proteins, increased lamellipodia persistence and increased cell speed (Bear et al., 2000, 2002). In addition, it was recently shown that loss of ENA/VASP proteins in cortical neurons

lead to a more superficial laminar position, which could be due to increased rate of migration (Goh et al., 2002; Kwiatkowski et al., 2007). Recent siRNA screens in cancer cell lines revealed that downregulation of the srGAP2 homologue srGAP3 also increased the rate of cell migration, suggesting that negative regulation of cell migration may be a conserved function of the srGAP family (Simpson et al., 2008).

2.3.3 Regulation of srGAP2: GAP and SH3 domains

The BAR superfamily of proteins are involved in a wide range of functions and this diversity arises from the different functional domains associated with BAR-like domain (Itoh and De Camilli, 2006). We demonstrate that srGAP2 is a Rac1-specific GAP (as previously shown for srGAP3) and recent work has highlighted the importance of Rac1 regulation in neuronal development (Govek et al., 2005). Mutation of the Rac1/Cdc42 GEF ARHGEF6 (also called Cool-2 or a-PIX) results in X-linked mental retardation, suggesting the importance of properly regulating Rac1 activity during neuronal development (Kutsche et al., 2000). Interestingly, the BAR domain-containing protein Oligophrenin-1 as well as the F-BAR-containing protein srGAP3 (also called mental retardation GAP or MEGAP) are both Rac1-GAPs that have been involved in severe forms of mental retardation (Billuart et al., 1998; Endris et al., 2002; Govek et al., 2004).

Rac1 has also been implicated in regulating radial migration and neurite outgrowth (Causeret et al., 2008; Govek et al., 2005; Kawauchi et al., 2003; Konno et al., 2005; Yoshizawa et al., 2005). Although not required, the GAP activity of srGAP2 might play a role in neurite formation in two ways: (1) local inactivation of Rac1 could result in increased Cdc42 activity, which could in turn activate pathways that promote bundled F-actin that are required for filopodia formation (Raftopoulou and Hall, 2004), and/or, (2) alternatively, Rac1 inactivation could lead to increased activation of RhoA (since Rac1 activation has been shown to inactivate RhoA [Nimnual et al., 2003]), which in turn could lead to the activation of the formin mDia2 and increased actin nucleation (**Figure 7G**).

A high percentage of F-BAR domain-containing proteins possess SH3 domains (Itoh and De Camilli, 2006), which bind to effectors ranging from regulators of endocytosis such as dynamin (Itoh and De Camilli, 2006) to regulators of actin polymerization (Aspenstrom et al., 2006; Chitu et al., 2005) such as WAVE1 (Soderling et al., 2002). The SH3 domain of srGAP2 has been shown to bind the Robo1 receptor (Wong et al., 2001) and has also been shown to bind N-WASP (Linkermann et al., 2009), but the functional relevance of these interactions has yet to be determined. Our results strongly suggest that srGAP2 is autoinhibited at resting state, which is a commonly accepted model of regulation of many RhoGEF and RhoGAP proteins (Rossman et al., 2005) and the BAR domain-containing proteins GRAF and Oligophrenin-1 (Eberth et al., 2009). Future experiments will test if this autoinhibition can be released by effector binding to the SH3 domain exposing the F-BAR domain to facilitate membrane protrusion (**Figure 7G**).

2.4 EXPERIMENTAL PROCEDURES

2.4.1 Animals

Mice were used according to a protocol approved by the Institutional Animal Care and Use Committee at the University of North Carolina-Chapel Hill and in accordance with National Institutes of Health guidelines. Time-pregnant females were maintained in a 12 hr light/dark cycle and obtained by overnight breeding with males of the same strain. Noon following breeding is considered as E0.5.

2.4.2 Protein purification

srGAP2 (amino acids 1–785) and F-BAR (amino acids 22–501) were cloned into pLIC vectors and expressed in *Escherichia coli* BL21 (DE3) cells. Proteins were then purified on a Ni²⁺ affinity column. Proteins were further purified by cation exchange chromatography, using a Source S column, and concentrated in 20 mM Tris buffer (pH 8), 150 mM NaCl, 1 mM DTT, and 5% glycerol. GAP (amino acids 502–676) and GAP^{R527L}

domain of srGAP2 was cloned into pGex-4T3 (Amersham). Recombinant GST fusion proteins were then purified using glutathione sepharose and resuspended in 20mMTris buffer (pH 8), 150 mM NaCl, 1 mM DTT, and 5% glycerol.

2.4.3 In vitro GAP assay

In vitro fluorescent-based GAP assay was performed as described previously (Shutes and Der, 2006).

2.4.4 Liposome preparation, liposome tubulation assays, and electron microscopy

Folch Fraction I Brain Lipid Extract from bovine brain (B1502) in chloroform was obtained from Sigma-Aldrich and used without further purification (see Supplemental Experimental Procedures for details; Itoh et al., 2005). The liposomes described above were first subjected to ten cycles of freeze-thaw, and then used immediately or stored in aliquots at -80° C. The liposomes were then equilibrated at RT for 1 hr before adding protein (either FBP17 F-BAR domain or srGAP2 F-BAR) at a lipid/protein ratio of 2:1 mass/mass and final concentrations of 0.2 mg/ml (lipid) and 0.1 mg/ml (protein). The tubulation reaction was incubated for 30 min at room temperature before negative staining, as described below. In order to introduce the recombinant purified F-BAR into the liposomes, 250 μ l of the tubulation reaction was subjected to 5 s of bath sonication at room temperature immediately after adding protein. After sonication, the sample was allowed to incubate for another 30 min before negative staining and processed for electron microscopy as described in the Supplemental Experimental Procedures (see also Frost et al., 2008).

2.4.5 Ex vivo Cortical electroporation and primary cortical neuron cultures

Mouse cortical progenitors were electroporated *ex vivo* at E15 as described previously (Hand et al., 2005). Following electroporation, cerebral hemispheres were either (1) dissected, enzymatically dissociated with papain, and plated on poly-L-lysine and Laminin-coated glass coverslips as described previously (Polleux and Ghosh, 2002); or (2)

sliced using a LEICA VT1000S vibratome and cultured organotypically as described previously (Hand et al., 2005; see Supplemental Experimental Procedures for details). Sequence alignments, shRNA and cDNA constructs and neuronal cultures, and confocal microscopy are detailed in the Supplemental Experimental Procedures.

2.5 SUPPLEMENTAL EXPERIMENTAL PROCEDURES

2.5.1 Sequence alignments

Sequence alignments for srGAPs were obtained using MUSCLE (Edgar, 2004). Human srGAP2 (gi|48427907|sp|O75044.2) Mouse srGAP2 (image:BC030547), Human srGAP1 (NP_065813.1), Mouse srGAP1 (NP_001074506.1), Human srGAP3 (NP_055665.1), Mouse srGAP3 (NP_536696.4), Xenopus srGAP (NP_001087899.1), *C. elegans* (NP_502179.1). Secondary structure was obtained for srGAP2 using hhpred (Soding et al., 2005) (<http://toolkit.tuebingen.mpg.de/hhpred>), Bioinfobank Metaserver (<http://meta.bioinfo.pl>) and PromaS3D (Pei et al., 2008) (<http://prodata.swmed.edu/promals3d/promals3d.php>). Structural alignments srGAP2 and F-BAR domains were obtained using hhpred (Soding et al., 2005), Bioinfobank Metaserver and PromaS3D (Pei et al., 2008). Mouse FBP17 (NP_062279.1), Mouse Syndapin1 (CAQ52060.1), Mouse FCHo2 (NP_766179.1), Mouse PSTPIP2 (CAJ18516.1), Mouse Fer (AAB18988.1).

2.5.2 shRNA design and validation

shRNA sequences were obtained from Dharmacon Dha2 Sense (5'- GAT CCA ATG GAC TAC TCT CGA AAC TTC AAG AGA GTT TCG AGA GTA GTC CAT TTC TTT TTT GGA AA-3') Dha2 Antisense (AGC TTT TCC AAA AAA GAA ATG GAC TAC TCT CGA AAC TCT CTT GAA GTT TCG AGA GTA GTC CAT TG) and Dha5 Sense (5'- GAT CCG CTA TCT GCT GAA TTA AAT CTT CAA GAG AGA TTT AAT TCA GCA GAT AGG ATT TTT TGG AAA-3') Dha5 Anti-sense (AGC TTT TCC AAA AAA TCC TAT CTG CTG AAT

TAA ATC TCT CTT GAA GAT TTA ATT CAG CAG ATA GCG). These constructs were cloned into pSilencer 2.1 (ambion). These shRNA were subsequently cotransfected with srGAP2-EGFP into COS7 cells ((shRNA 1.5µg) and srGAP2-EGFP (.5µg)). Lysates were collected 48hrs. After transfection and level of knockdown was determined by western blot using rabbit anti-GFP (Molecular Probes).

2.5.3 Constructs

All constructs were cloned into pCIG2 vector (Hand et al., 2005), which contains a (cDNA)-IRESEGFP under the control of a CMV-enhancer/chicken-β-actin promoter. srGAP2 (IMAGE clone# BC030457) was first mutagenized using Quickchange (Stratagene) to repair a point mutation at position 596 to avoid premature stop in transcription. srGAP2 was then subcloned into pEGFP-N1 (Clontech). The entire srGAP2-EGFP cassette was then subcloned into pCIG2 replacing the IRES-EGFP resulting in pCIG2::srGAP2-EGFP. srGAP2 was also cloned into pNeuroD-EGFP vector. All subsequent constructs were cloned similarly. F-BAR (aa1-501), srGAP2^{ΔF-BAR} (aa502-1045), srGAP2^{ΔFCH} (aa121-1045), srGAP2^{R527L}, srGAP2^{W765A}, srGAP2^{ΔCterm}, and srGAP2* (dha5 shRNA resistant, base pairs mutation T898C, A900G, and C904T) were generated by mutagenesis using Quickchange (Stratagene). F-BAR^{Δ49} was generated by fusing amino acids (1-452) of human srGAP2 (accession number NM_015326) to the c-terminus of clone BC112927. This clone is a partial human duplication of the F-BAR of srGAP2 present in Chromosome 1p12 and encoding only the first nine exons (out of twenty-two in the original full length human srGAP2 (Sassa and Polleux, unpublished results). The first nine exons present in the 1p12 duplication encode for the F-BAR with the last 49 amino acids of the C-terminus are deleted, hence the name F-BAR^{Δ49} due to a splicing defect (Sassa and Polleux, unpublished results). This splicing defect also results in the addition of seven additional amino acids to the deleted C-terminus that are not normally present in the F-BAR of srGAP2, as they arise from intronic sequence.

2.5.4 COS7 cell culture, transfections, staining and filopodia measurements

COS7 cells were cultured in DMEM + 10%FBS 2mM L-glutamine and penicillin/streptomycin. For transfections, cells were plated in 6 well dishes and lipofectamine 2000 (4 μ l) was mixed with 2 μ g of DNA in Opti-mem and added to cells for 3hrs. After 3hrs, serum-free media was replaced with DMEM + 10%FBS and cells were cultured for 24hrs. After 24hrs, cells were trypsanized and replated on polyL-lysine coated coverslips and cultured for an additional 24hrs. Cells were then fixed using 4% paraformaldehyde. Cells were then washed 3 times in PBS, then blocked/permeablized in 0.3% triton-X 100 in PBS + 5% BSA (PBS-T) for 20 minutes. Cells were then incubated with alexa-546 phalloidin (1:200) in PBS-T overnight. Finally, cells were then washed 3 times in PBS-T and mounted.

To determine filopodia number, cells were imaged using LEICA TCS SL confocal microscope, 63x/1.4NA oil immersion objective. 2x zoomed images were taken of representative cells from each construct. Images were then imported to NIH ImageJ. Using the segmented line tool, a perimeter was drawn around the cells. The presence of filopodia was determined by counting the number of consecutive pixels on the line drawn around the cell perimeter and normalized by dividing the total number of filopodia by the cell perimeter (filopodia/microns). For cytochalasin D treatments, COS7 cells were transfected with F-BAR-EGFP and cultured for 48 hrs. Cells were then treated with 400 μ M cytochalasin D for 30 minutes. To observe the presence of F-actin, cells were fixed and stained with phalloidin. To observe dynamics, control, untreated cells were imaged for 10 minutes (picture taken every 10 seconds) and cytochalasin D treated cells were imaged for 27 minutes (picture taken every minute).

For transferrin uptake assay, COS7 cells were serum starved for one hour at 4 degrees in the presence of alexa-647 transferrin. Cells were then warmed to 37 degrees to allow uptake of transferrin and fixed and treated as described above.

2.5.5 *Ex vivo* Cortical electroporation and primary cultures

Mouse cortical progenitors were electroporated *ex vivo* at embryonic day (E) E15 as described (Hand et al., 2005). Briefly, cDNA constructs in overexpression experiments (1 µg/µl) were injected into the lateral ventricle of each embryo and electroporated using an ECM 830 electroporator (BTX) with four 100 ms pulses separated by 100 ms intervals at 25V. Following electroporation, cerebral cortices were dissected and enzymatically dissociated as described previously (Polleux and Ghosh, 2002).

1.25x10⁵ cells were plated onto glass coverslips coated with poly-L-lysine and laminin and cultured in serum-free media (Basal Medium Eagle containing both B27 and N2 supplements, L-Glutamine and Penicillin/Streptomycin) and fixed in 4% paraformaldehyde for immunohistochemistry. For shRNA rescue experiments in dissociation a mixture (shRNA 1.5 µg/µl) and srGAP2-EGFP* (0.5 µg/µl) was injected into lateral ventricle. For slice cultures, embryonic brains were electroporated and dissected as described above. The brains were then embedded in 3% low temperature gelling agarose and 250 µm-thick vibratome sections were cut using a LEICA VT1000S vibratome and placed on poly-Lysine/ laminin coated transwell inserts and cultured organotypically using an air interface protocol (Polleux and Ghosh, 2002). shRNA expressing slices were cultured for 3 days *in vitro* and cDNA expressing sections were cultured for 5 days *in vitro*.

2.5.6 Time lapse confocal microscopy of cortical sections

Using a Leica TCS-SL confocal microscope (mounted on a DM-IRE2 inverted microscope stand) and equipped with a X-Y motorized Märzhäuser stage, time-lapse confocal microscopy was performed by imaging multiple Z-stacks at pre-selected positions on a given set of electroporated slices as described previously (Hand et al, 2005). Slices were cultured on confocal inserts (Millipore, 5mm height) and imaged using a long distance 20x/0.4 NA objective. For shRNA expressing sections, pictures were taken at a frequency

of 1 picture every 12 minutes for 4hrs. In the case of srGAP2 overexpression experiments, sections were imaged every 16 minutes for a maximum of 10hrs 24 minutes.

2.5.7 Dissociated cortical neuron culture

Cultured neurons and brain sections were stained as described previously (Ghosh and Polleux 2002). The following antibodies were used chicken anti-GFP (Upstate), mouse anti-Tuj1 (β -III tubulin) (Sigma), mouse anti-nestin (BD Bioscience), mouse anti-MAP2 (a/b isoforms; AP20 Sigma), rabbit anti-srGAP2 (gift of Gong Ju, Shanghai JiaoTong University; (Yao et al., 2008)), and F-actin was labeled using alexa-546 phalloidin (Sigma). All images were captured using a LEICA TCS SL confocal microscope. For staining of endogenous srGAP2 in acutely dissociated neurons, cells were fixed in 4% paraformaldehyde for 30 minutes. The cells were then washed with PBS three times. They were then permeabilized with .05% triton-x 100 for 20 minutes and washed again in PBS. They were then incubated in blocking buffer (5% bovine serum albumin (BSA) in PBS) for 30 minutes and incubated with srGAP2-A2 antibody (1:200 in .2% BSA in PBS) overnight. For F-actin staining, phalloidin was added at 1:200. Cells were subsequently washed in 0.2% BSA in PBS and the appropriate Alexaconjugated secondary antibodies (Molecular Probes 1:2000) for 30 minutes. Cells were then washed in PBS and slides were mounted.

2.5.8 Quantification of neuron migration and neurite branching

For shRNA treated slices, the extent of cell migration was analyzed as described previously (Hand et al., 2005). In cDNA expressing sections, migration was assayed to different ways: (1) high magnification pictures were taken of the cortical plate and IZ and we quantified the ratio of cells/ μm^2 CP/ cells/ μm^2 in the IZ; (2) For branching measurements, high magnification images were obtained of neurons migrating in layer 5/6 in various conditions. Number of branches protruding from the leading process were counted. For cell speed measurements in shRNA treated slices, nuclei position was tracked manually during each frame using NIH ImageJ. Cell speed was calculated using Microsoft

Excel and speed was reported in micron/hr. Neurite branching was quantified using NIH ImageJ.

2.5.9 In situ hybridization

In situ hybridization was performed as previously described (Mattar et al., 2004).

2.5.10 Liposome preparation

Folch Fraction I Brain Lipid Extract from bovine brain (B1502) in chloroform was obtained from Sigma-Aldrich (St. Louis, MO) and used without further purification. 10 mg of total lipid were added to a glass vial and dried at room temperature under streaming argon while vortexing in order to form a thin lipid film around the tube surface. The lipids were re-dissolved in absolute hexane, dried under argon again while vortexing, and then dessicated *in vacuo* for >2 hours to remove the last traces of chloroform. The dried lipid film was then pre-hydrated at RT with water-saturated N₂ for 2 minutes until the film became transparent. Buffer (50 mM KCl/10 mM HEPES/1 mM DTT, pH 7.4) was added to the hydrated lipid film to a final lipid concentration of 2 mg/ml. The vial was sealed under argon and incubated at RT for 2 h, and then gently rocked overnight to disperse the lipids into solution.

2.5.11 Electron microscopy

Continuous carbon-coated Cu-grids were glow discharged in room air according to standard protocols. 4 μ l of sample were added and allowed to sit for ~10 seconds before being blotted onto filter paper. The grid surface was then immediately stained with freshly prepared (<15 minutes) 0.8% uranyl formate. Images were acquired using a Philips Tecnai F12 microscope operating at 120 kV using nominal magnifications of 29-50,000x, and defocus values of -15,000 to -22,000 Å. Images were recorded on a Gatan 1K CCD. Image analyses, including tubule diameter measurements, were performed with NIH ImageJ.

2.6 FIGURES AND LEGENDS

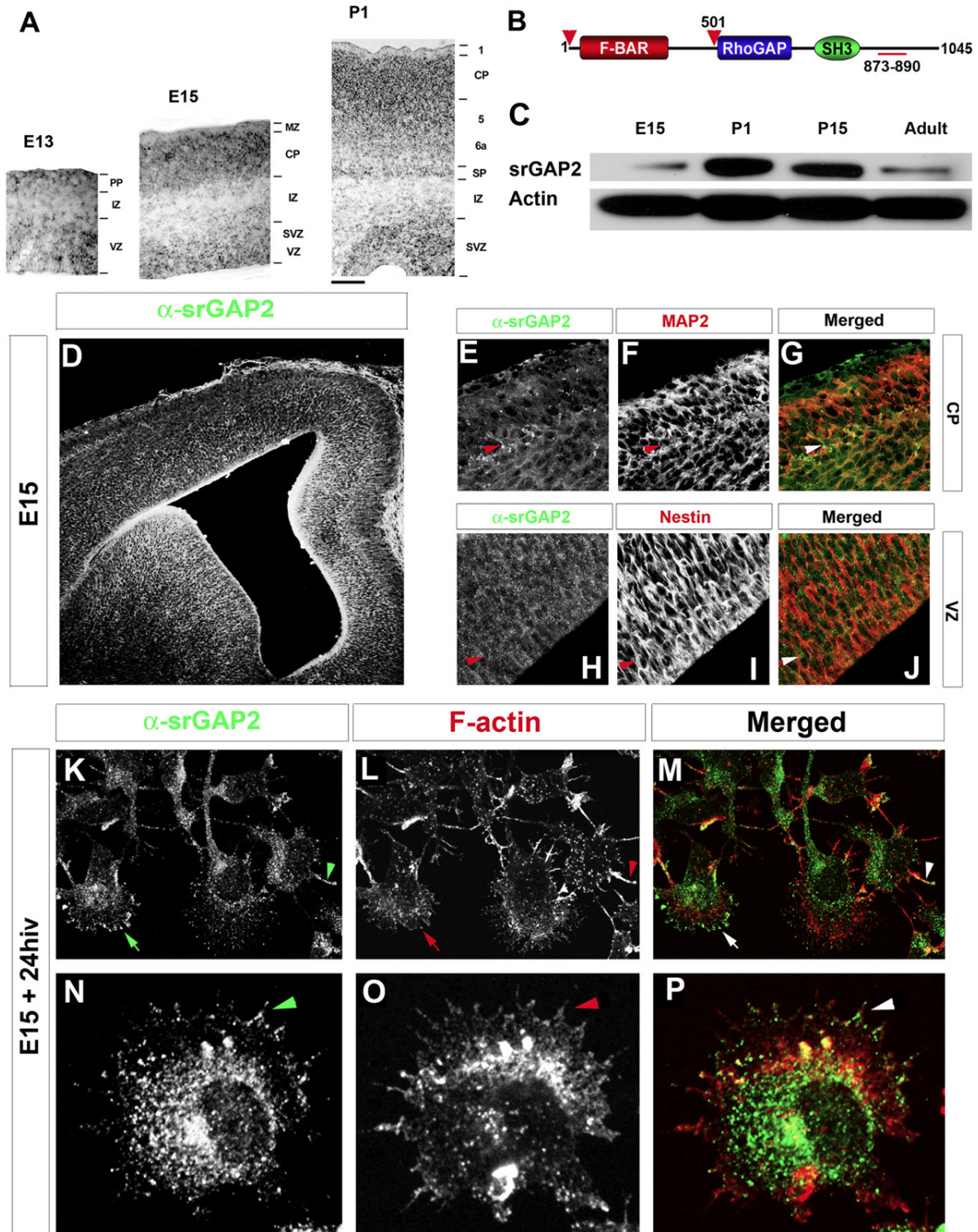


Figure 2.1. srGAP2 is expressed in neuronal progenitors and postmitotic neurons and localizes to sites of membrane protrusion

(A) In situ hybridization for srGAP2 in developing cortex at E13, E15, and P1. (B) Domain organization of srGAP2, which contains an F-BAR domain, a RhoGAP, and a SH3 domain from N- to C-terminal ends (1–1045 amino acids, predicted molecular weight of 118 kDa). The red bar indicates the localization of the antigen (A2; amino acids 873–890) used to affinity purify the srGAP2-specific polyclonal antibody to the C terminus of srGAP2. (C)

Western blot for srGAP2 protein levels during cortical development at the indicated time points (E15, P1, P15, and Adult) obtained by SDS-PAGE and immunoblotting with A2-rabbit polyclonal antibody. **(D–J)** Immunofluorescence staining of srGAP2 protein expression on fixed coronal sections of E15 mouse cortex. srGAP2 protein colocalizes (arrowheads) with MAP2 (postmitotic neuron marker) in the CP **(D–F)** and also colocalizes with Nestin (arrowheads) (neuronal precursor marker) in the VZ **(G–I)**. **(K–P)** Immunofluorescence staining of srGAP2 protein in early dissociated cortical neuron cultures (E15 + 24 hr in vitro [hiv]). srGAP2 protein is found close to the plasma membrane of immature cortical neurons (arrow in **K–M**) and to F-actin-rich filopodia (stained with Alexa546-phalloidin; arrowheads in **K–P**).

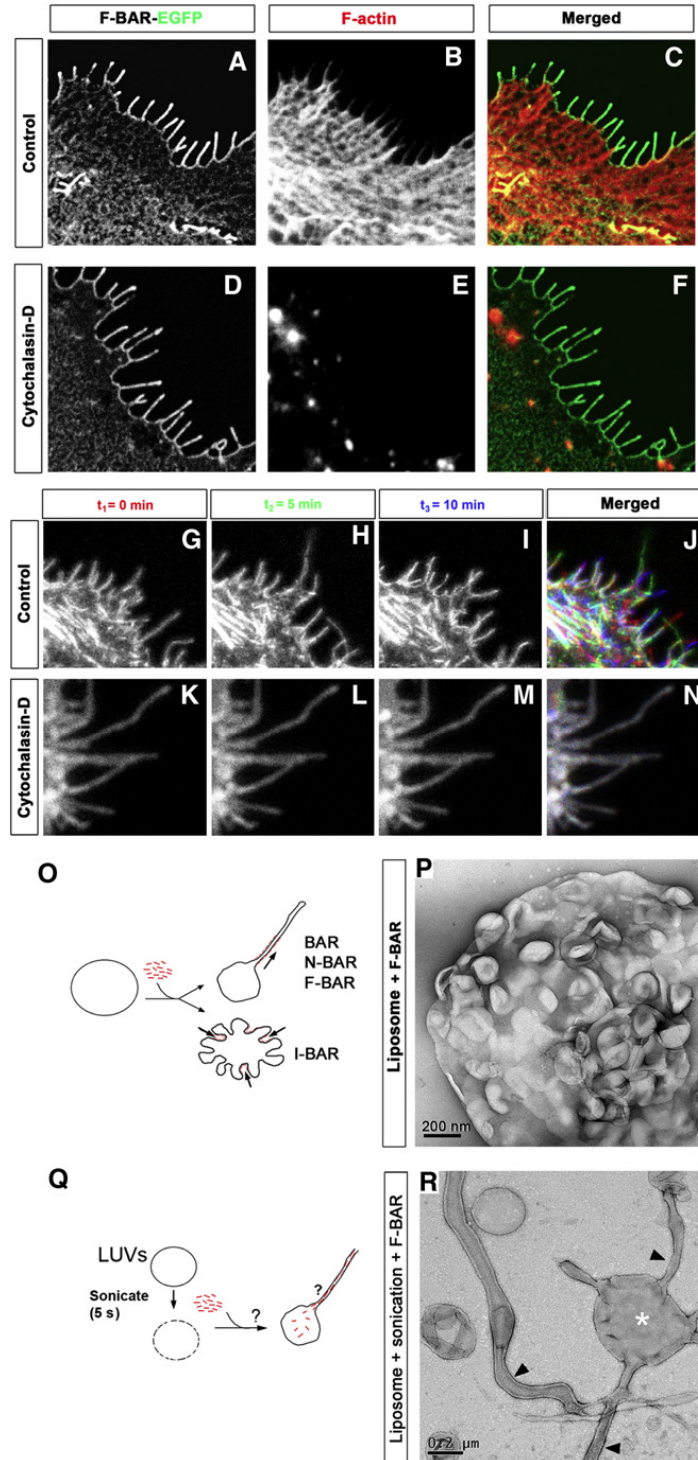


Figure 2.2 F-BAR-induced filopodia required F-Actin for their dynamic formation but not for their structural maintenance

(A–C) COS7 cell expressing the F-BAR-EGFP fusion protein not treated with cytochalasin D (control). Note the cortical localization of the F-BAR domain and the numerous F-actin-rich filopodia (phalloidin in B and C). (D–F) COS7 cell expressing the F-BAR-EGFP fusion protein incubated with 400 mM cytochalasin D for 30 min. Note that the complete loss of F-

actin (phalloidin) (**E**) had no effect on the localization of the F-BAR domain or on the structure of the F-BAR-mediated protrusions. (**G–J**) Time series showing the dynamics of F-BAR-EGFP-induced filopodia in COS7 cells. Time 0, 5, and 10 min are pseudocolored in red, green, and blue, respectively. Note that there is little colocalization of filopodia at the cell periphery (**J**). This is in stark contrast to COS7 cells expressing F-BAR-EGFP treated with cytochalasin D (30 min) (**K–N**), where the protrusions remain static and do not grow or retract for the same period of time shown in control cells. (**O**) Schema depicting tubulation assay in (**P**). (**P**) F-BAR domain of srGAP2 added to preformed liposomes. Note the inward dimpling or “scalping” of the liposome surface. (**Q**) Schema depicting tubulation assay in (**R**) where F-BAR domain of srGAP2 was added to liposomes after extrusion. This results in a fraction of the F-BAR domain resident inside the liposome. Note the formation of tubule protrusion from the liposome. (**R**) High magnification of liposome/F-BAR mixture after sonication. Note the absence of striations or an obvious protein coat on the lipid tubule, a hallmark of canonical F-BAR tubulation. These tubules are $83 \text{ nm} \pm 15 \text{ nm}$ (average \pm SD, $n = 38$) after being partially flattened by the negative staining procedure.

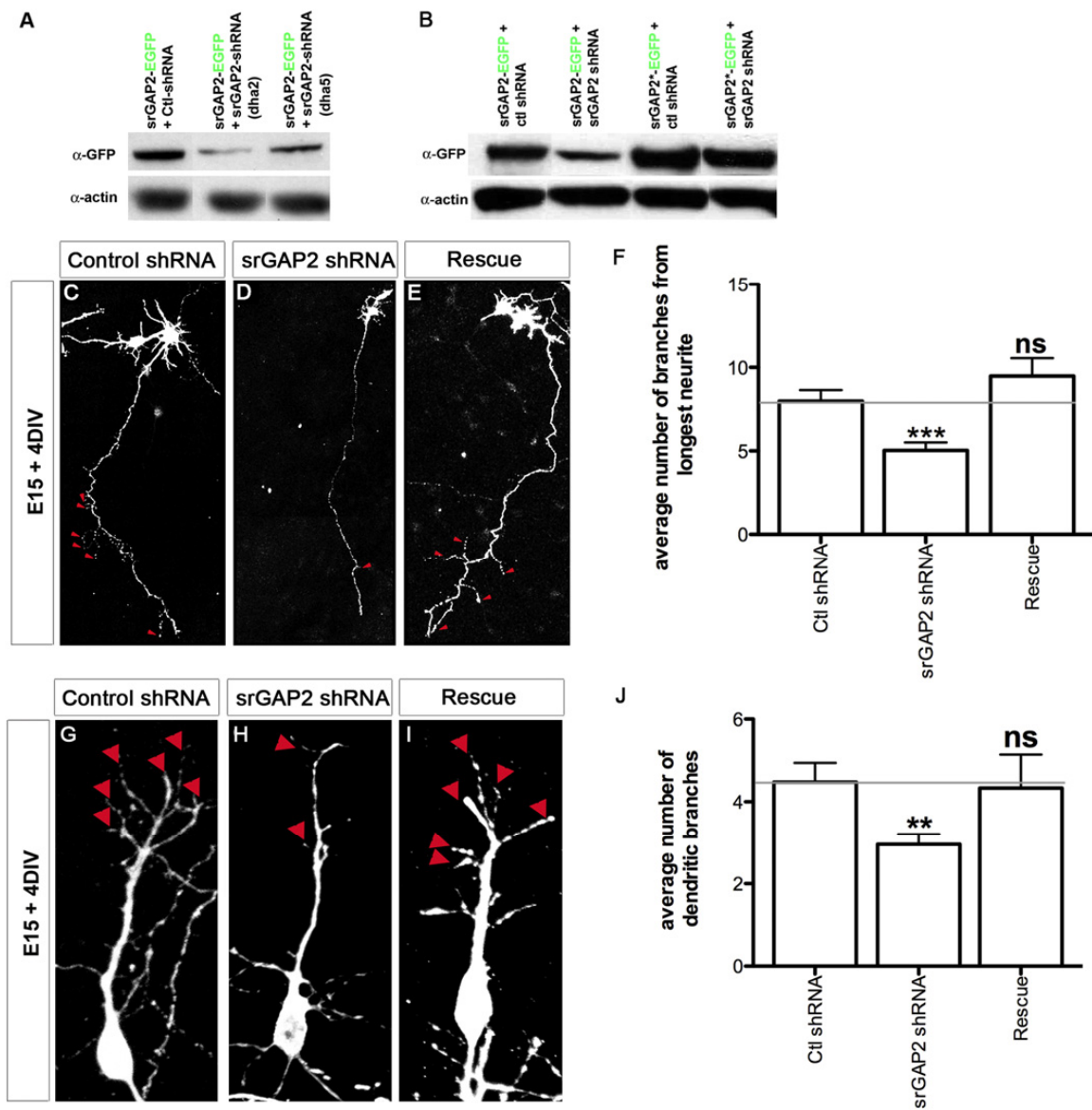


Figure 2.3. Knockdown of srGAP2 in cortical neurons reduces axonal and dendritic branching

(A) Western blot probed with anti-GFP and anti-actin antibodies from COS7 cells cotransfected with either control shRNA plus srGAP2-EGFP (lane 1), srGAP2 shRNA plus srGAP2-EGFP (Dha2, lane 2), or srGAP2 shRNA plus srGAP2-EGFP (Dha5, lane 3). (B) Western blot probed with anti-GFP and anti-actin antibodies from COS7 cells cotransfected with either control shRNA plus srGAP2-EGFP (lane 1), srGAP2 shRNA plus srGAP2-EGFP (lane 2), a mutated form of srGAP2*-EGFP (resistant to srGAP2 shRNA) plus control shRNA (lane 3), or srGAP2*-EGFP plus srGAP2 shRNA (lane 4). srGAP2 shRNA significantly knocks down srGAP2 expression compared to control shRNA, which can be rescued by expression of srGAP2*-EGFP (compare lanes 3 and 4). (C–E and G–I) E15 dissociated cortical neurons were cultured for 5 days after *ex vivo* cortical electroporation (EVCE) with control shRNA, srGAP2 shRNA, or srGAP2 shRNA + srGAP2*-EGFP. Control

shRNA-transfected neurons display frequent primary branches from the axon (arrowheads in **B**) and the primary dendrite (arrowheads in **F**). Both effects were markedly reduced in srGAP2 shRNA-transfected neurons (**D** and **H**) and rescued by cotransfection of srGAP2 shRNA with srGAP2*-EGFP (**E** and **I**). (**F**) Quantification of the number of branches from the longest neurite (axon) as shown in (**C**)–(**E**). (**J**) Quantification of the number of primary dendritic branches as shown in (**G**)–(**I**). Control shRNA, n = 42 cells; srGAP2 shRNA, n = 95; srGAP2*-EGFP + srGAP2 shRNA, n = 39. Cells were taken from three independent experiments and analyzed blind to the treatment. Mann-Whitney Test: *p < 0.05; **p < 0.01; ***p < 0.001.

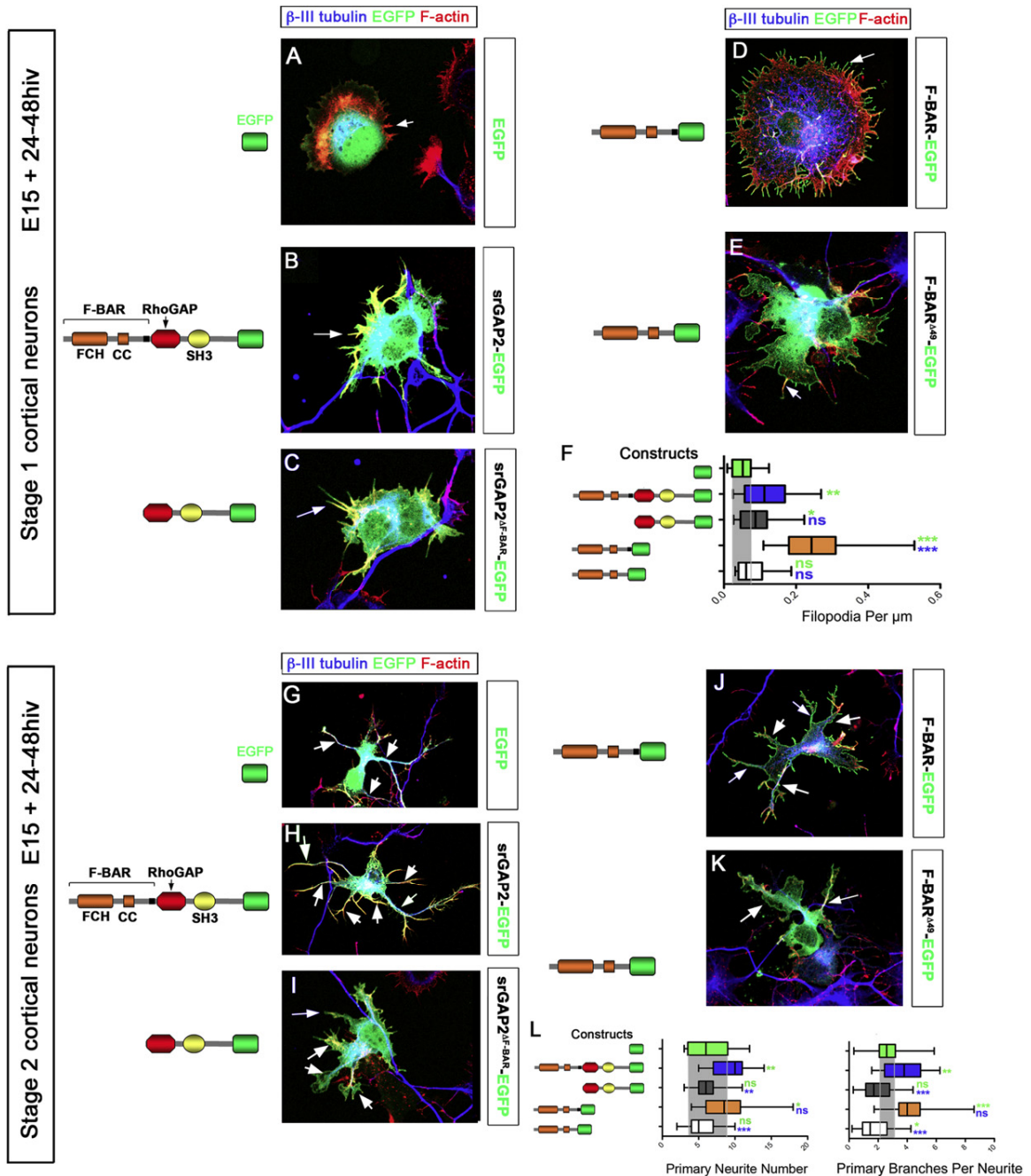


Figure 2.4. srGAP2 promotes filopodia formation and neurite outgrowth in an F-BAR-dependent manner

(A–E) Stage 1 cortical neurons expressing various srGAP2 constructs. All cells are stained with neuron-specific β III-tubulin (blue) to reveal presence of microtubules (see also Figure S7) and phalloidin (red) to visualize F-actin. (F) Quantification of filopodia normalized per cell perimeter in all conditions. EGFP, $n = 20$ cells; srGAP2-EGFP, $n = 21$; srGAP2^{ΔF-BAR}-EGFP, $n = 20$; F-BAR-EGFP, $n = 20$; F-BAR^{Δ49}-EGFP, $n = 20$. Cells were taken from three independent experiments and analyzed blind to the treatment. (G–K) Stage 2 cortical neurons expressing various srGAP2 constructs. All cells are stained with β III-tubulin (blue) and phalloidin (red) as in panels (A)–(F). Arrows point to primary neurites. (L)

Quantification of neurite number normalized per cell perimeter in all conditions and primary branch number per neurite. Note srGAP2 and F-BAR are potent inducers of neurite outgrowth while srGAP2^{ΔF-BAR} and F-BAR^{Δ49} are not. Mann-Whitney test: *p < 0.05; **p < 0.01; ***p < 0.001. Green stars indicates comparison to EGFP and blue stars indicates comparison to srGAP2-EGFP.

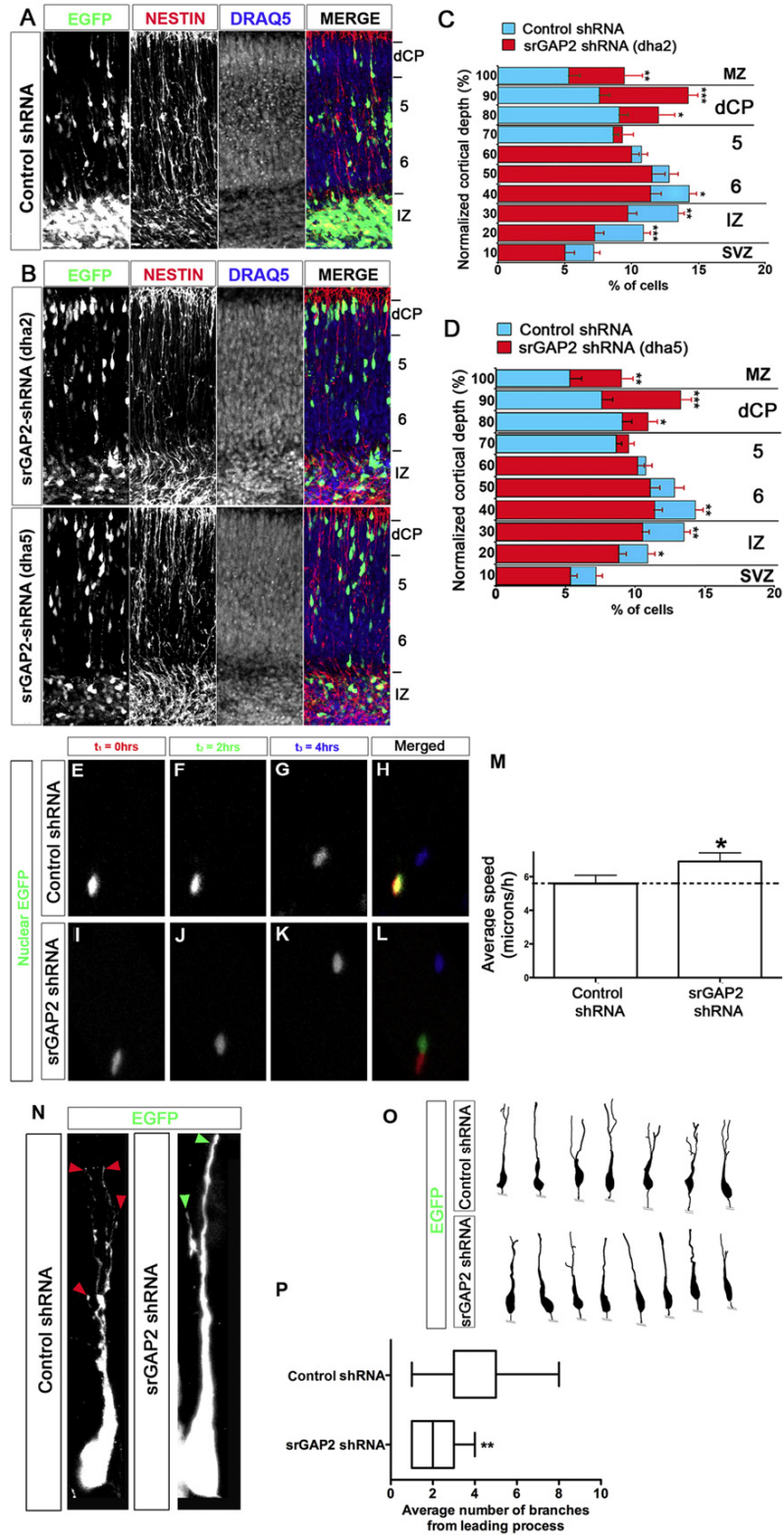


Figure 2.5. Knockdown of srGAP2 promotes neuronal migration and reduces LP branching

(A) E15 cortical slices cultured for 3 days after electroporation with EGFP + control shRNA. Slices were stained with anti-Nestin antibody revealing radial glial scaffold and Draq5 to illustrate cytoarchitecture. **(B)** E15 cortical slices cultured for 3 days after electroporation with EGFP + Dha2 (**B**, top panel) or Dha5 (**B**, lower panel). Slices were stained with anti-Nestin antibody, revealing radial glial scaffold and Draq5 to illustrate cytoarchitecture. **(C and D)** Quantification of cell distribution for slices expressing control shRNA (blue bars) and two independent srGAP2 shRNA (red in **C** and **D** for dha2 and dha5, respectively). **(E–L)** E15 cortical slices cultured for 2 days *ex vivo* after electroporation with nuclear EGFP (3NLS) along with control shRNA (**E–H**) or srGAP2 shRNA (**I–L**) were imaged using time-lapse confocal microscopy. Neurons transfected with srGAP2 shRNA undergo faster translocation within 4 hr (**I–L**; and no colocalization in **L**) than control shRNA-transfected neurons. **(M)** Quantification of effects of srGAP2 knockdown on cell speed. Neurons with reduced level of srGAP2 (shRNA) migrated approximately 25% faster (6.91 mm/hr compared to 5.59 mm/hr) compared to control shRNA-transfected neurons. Control shRNA, n = 95 cells; srGAP2 shRNA, n = 84. Cells were taken from three independent experiments. Mann-Whitney test: *p < 0.05; **p < 0.01; ***p < 0.001. **(N–O)** High magnification images (**N**) and reconstructions (**O**) of control shRNA (left panel) or srGAP2 shRNA (right panel) expressing neurons in layers 5/6. Arrowheads point to LP tips. **(P)** Quantification of the LP branch number in control shRNA or srGAP2 shRNA expressing neurons. Control shRNA, n = 19 cells; srGAP2 shRNA, n = 17 cells. Cells were taken from three independent experiments. Mann-Whitney test: *p < 0.05; **p < 0.01; ***p < 0.001.

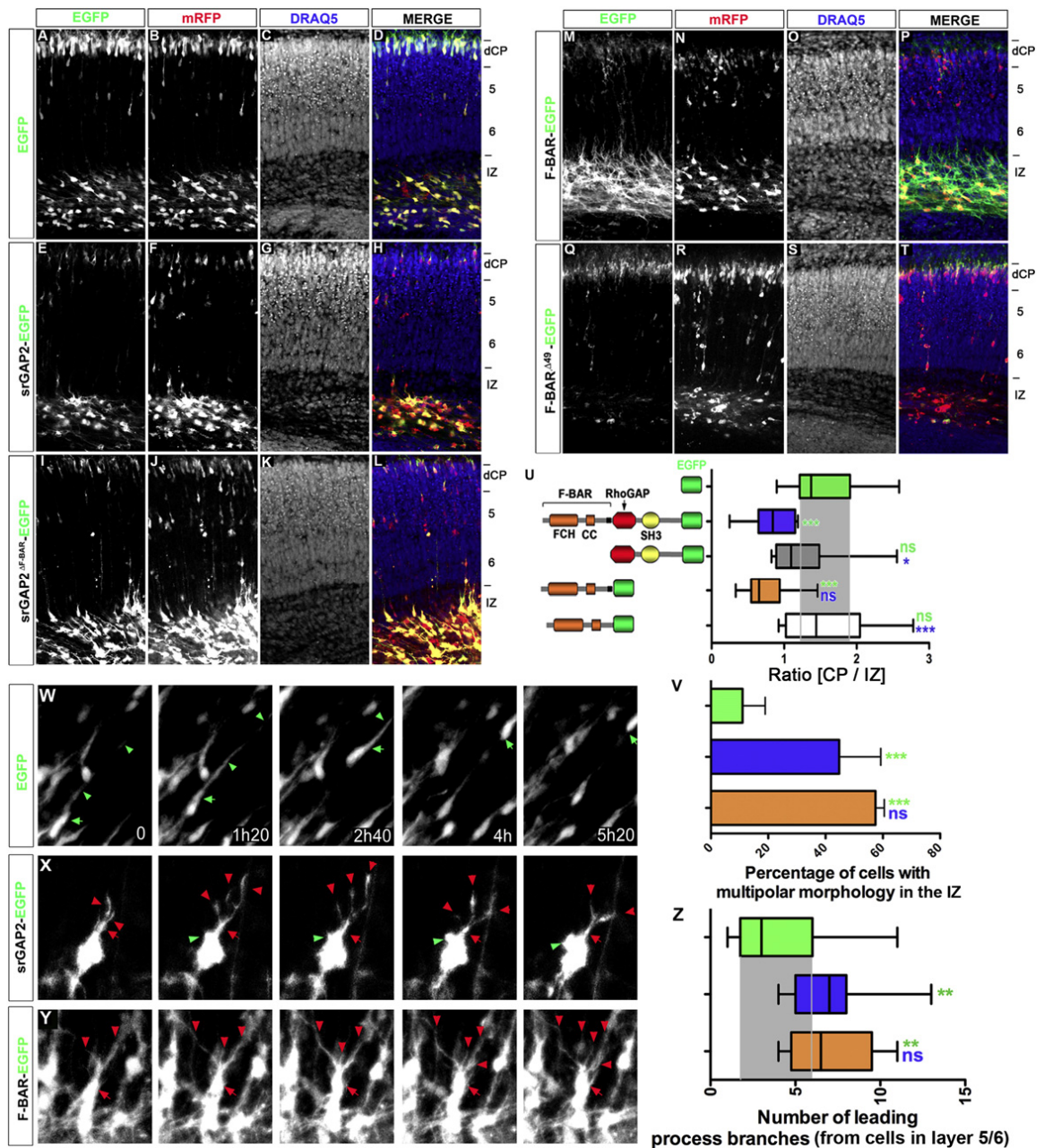


Figure 2.6. srGAP2-mediated inhibition of migration requires F-BAR-mediated membrane deformation

(A–T) E15 cortical slices cultured for 5 days after coelectroporation of monomeric red fluorescence protein (mRFP for cytoplasmic filing) together with EGFP (**A–D**), full-length srGAP2-EGFP (**E–H**), srGAP2^{ΔF-BAR}-EGFP (**I–L**), F-BAR-EGFP (**M–P**), and F-BAR^{Δ49}-EGFP fusion proteins (**Q–T**). **(U)** Quantification of CP/IZ ratio. EGFP, n = 13 slices; srGAP2-EGFP, n = 14 slices; srGAP2^{ΔF-BAR}-EGFP, n = 8 slices; F-BAR-EGFP, n = 10 slices; F-BAR^{Δ49}-EGFP, n = 6 slice. Slices were taken from four different experiments and CP/IZ ratio was analyzed using Mann-Whitney test: *p < 0.05; **p < 0.01; ***p < 0.001. Green stars indicate comparison to EGFP and blue stars indicate comparison to srGAP2-EGFP. **(V)** Quantification of percentage of cells with multipolar morphology in EGFP,

srGAP2-EGFP, or F-BAR-EGFP transfected slices. Multipolar cells were defined as cells possessing three or more processes. EGFP, n = 66 cells; srGAP2-EGFP, n = 42; F-BAR-EGFP, n = 57. Cells were taken from three different experiments and analyzed using Fisher's exact test: *p < 0.05; **p < 0.01; ***p < 0.001. **(W–Y)** Individual frames using time-lapse confocal microscopy of E15 cortical slices cultured for 3 days after electroporation with EGFP, srGAP2-EGFP, or F-BAR-EGFP (cotransfected with Venus plasmid). Arrows indicate LP and arrowheads indicate the cell body. **(Z)** Quantification of LP branch number from cells expressing EGFP, srGAP2-EGFP, or F-BAR-EGFP in layer 5/6. EGFP, n = 17 cells; srGAP2-EGFP, n = 21 cells; F-BAR-EGFP, n = 9 cells. Cells were taken from three independent slices. Mann-Whitney test: *p < 0.05; **p < 0.01; ***p < 0.001. Green stars indicate comparison to EGFP and blue stars indicate comparison to srGAP2-EGFP.

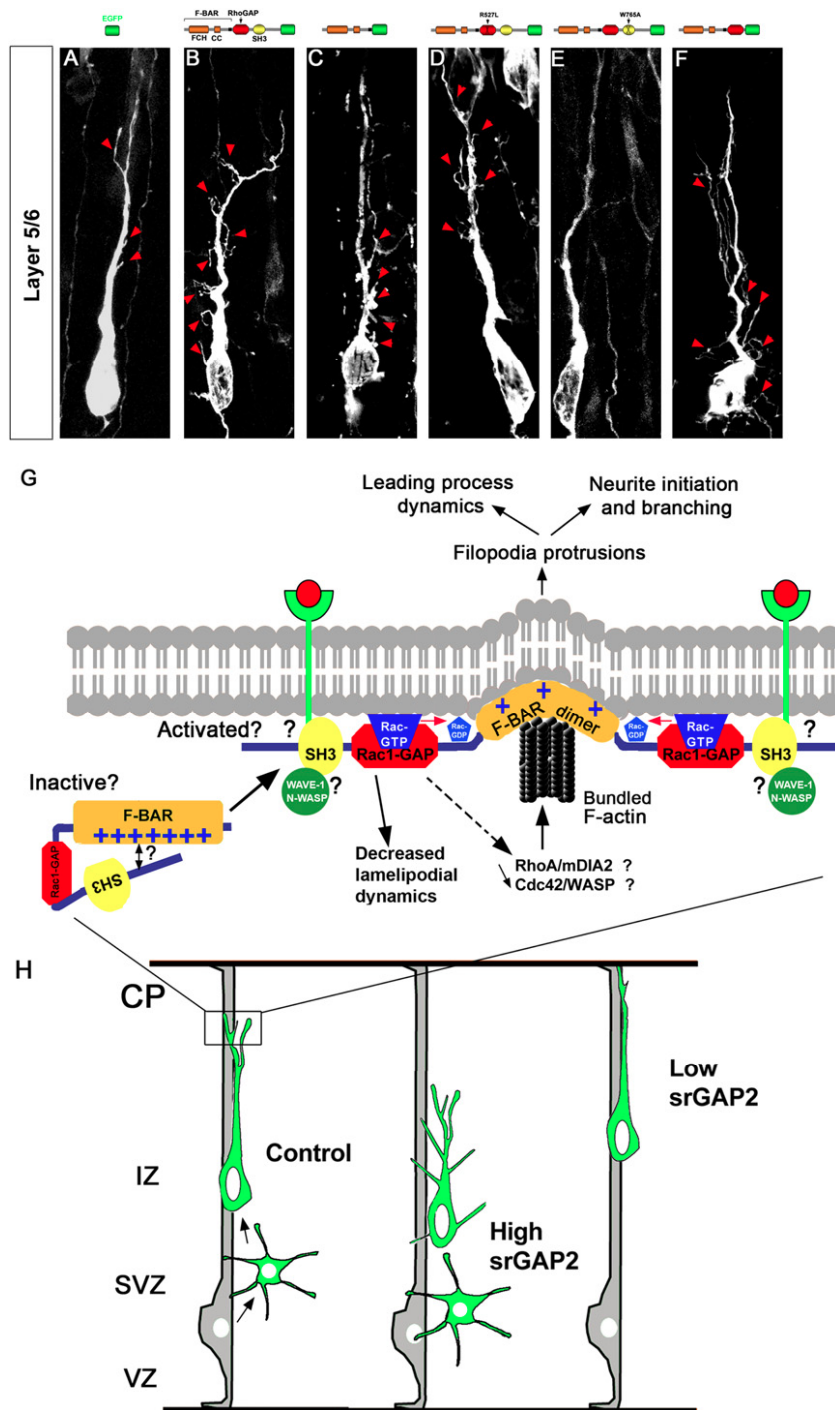


Figure 2.7. Model for srGAP2-regulated membrane protrusion in neuronal migration (A–F) Representative images of optically isolated neurons translocating radially through layer 5/6 following electroporation at E15 (+5 DIV) with indicated srGAP2 constructs containing an F-BAR domain. **(G and H)** Hypothetical model of the molecular mechanisms underlying srGAP2 function in membrane protrusion during neuronal migration and morphogenesis **(G)**. Summary of srGAP2 effects on neuronal migration and morphogenesis during cortical development **(H)**. See text for details.

SUPPLEMENTARY FIGURES AND LEGENDS

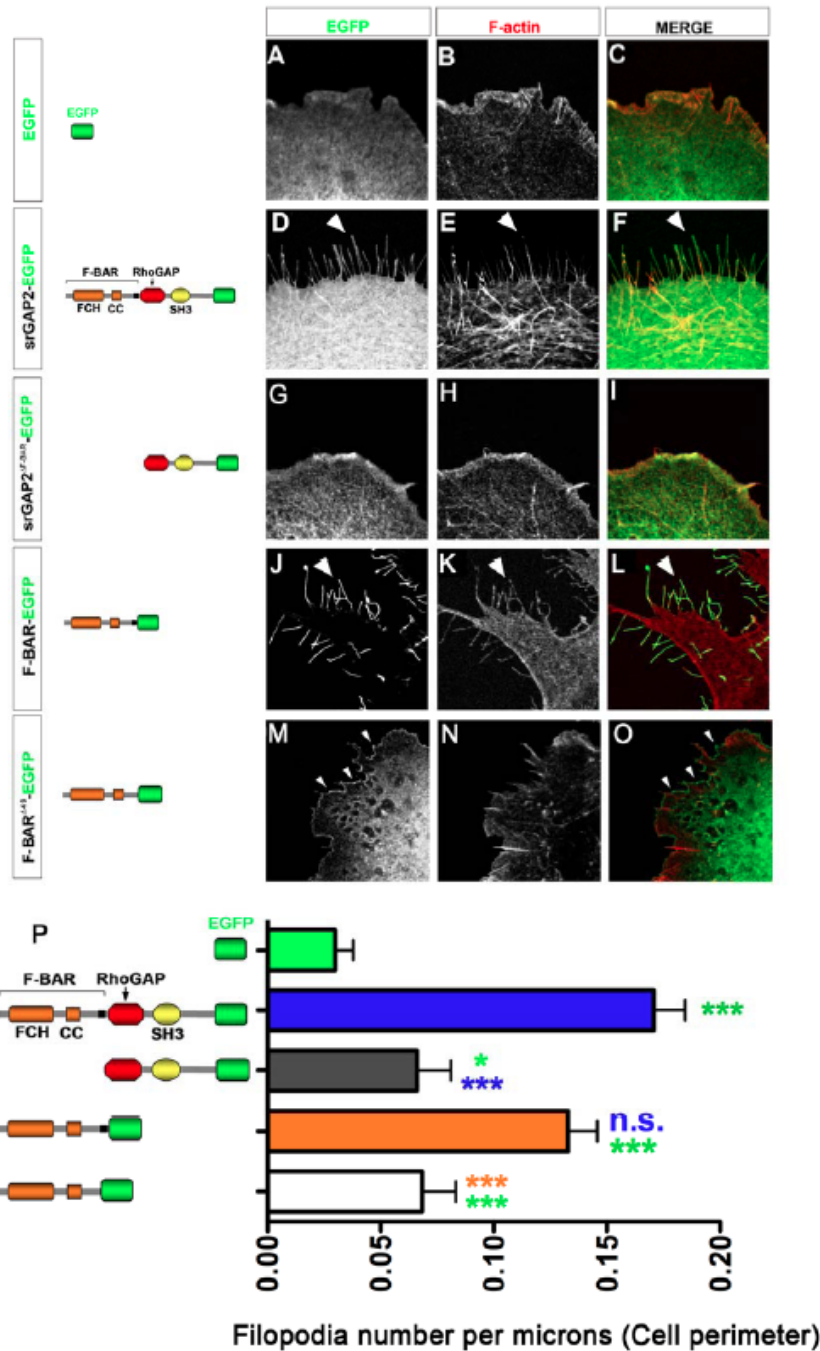


Figure 2.S1. srGAP2 induces filopodia formation in a F-BAR-dependent manner in COS7 cells

(A-C) COS7 cell expressing EGFP counter stained with phalloidin for F-actin (red). **(D-F)** COS7 cell expressing srGAP2-EGFP fusion protein for F-actin-rich filopodia (arrowheads in **D-F**). **(G-I)** Expression of srGAP2^{ΔF-BAR}-EGFP fusion protein does not promote filopodia formation. **(J-L)** Expression of the F-BAR-EGFP fusion protein is sufficient to promote filopodia formation in COS7 cells. Note the significant increase in

membrane targeting to the extreme periphery of the cell (**J-L**) and induces the formation of long F-actin rich protrusions (**J-L**) like full-length srGAP2. Thus expression of the F-BAR domain of srGAP2 is sufficient to induce filopodia. Moreover this activity is not simply dependent on localization to the plasma membrane since expression F-BAR^{Δ49}-EGFP (**M-O**), which localized nicely to the plasma membrane, did not cause a significant increase in filopodia. (**P**) Quantification of the effects described in **A-O**. (EGFP, n=41 cells; srGAP2-EGFP, n=52 cells; srGAP2^{ΔF-BAR}-EGFP, n=21 cells; F-BAR-EGFP, n=21 cells; F-BAR^{Δ49}-EGFP, n= 15 cells. Cells were taken from 3 independent experiments and analyzed using Mann-Whitney Test * p<0.05, ** p<0.01, *** p<0.001. Green color indicates comparison to EGFP and blue color indicates comparison to srGAP2-EGFP and orange indicated comparison to F-BAR-EGFP).

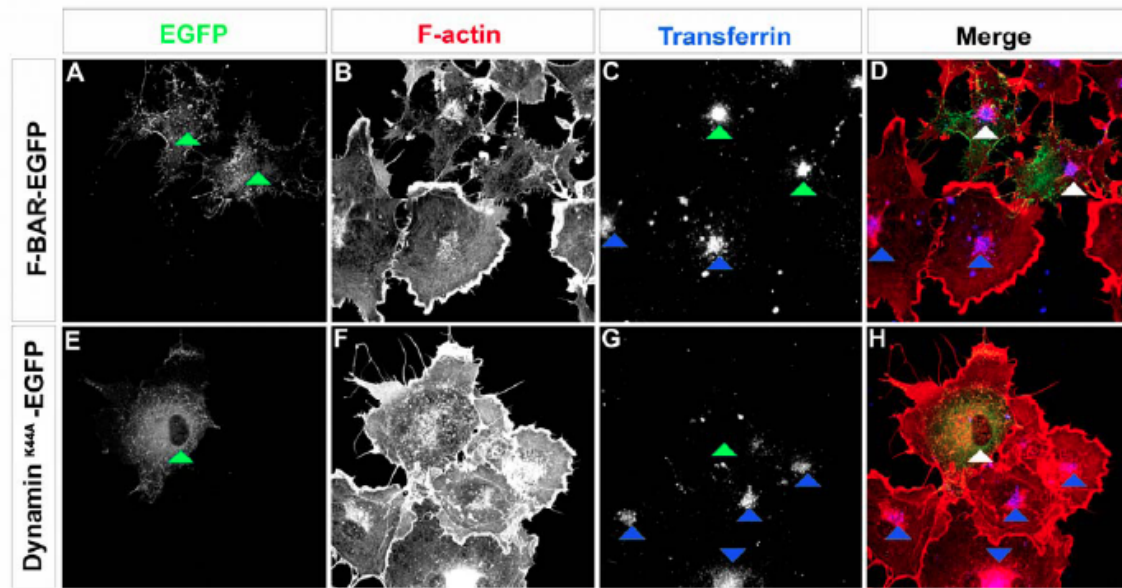
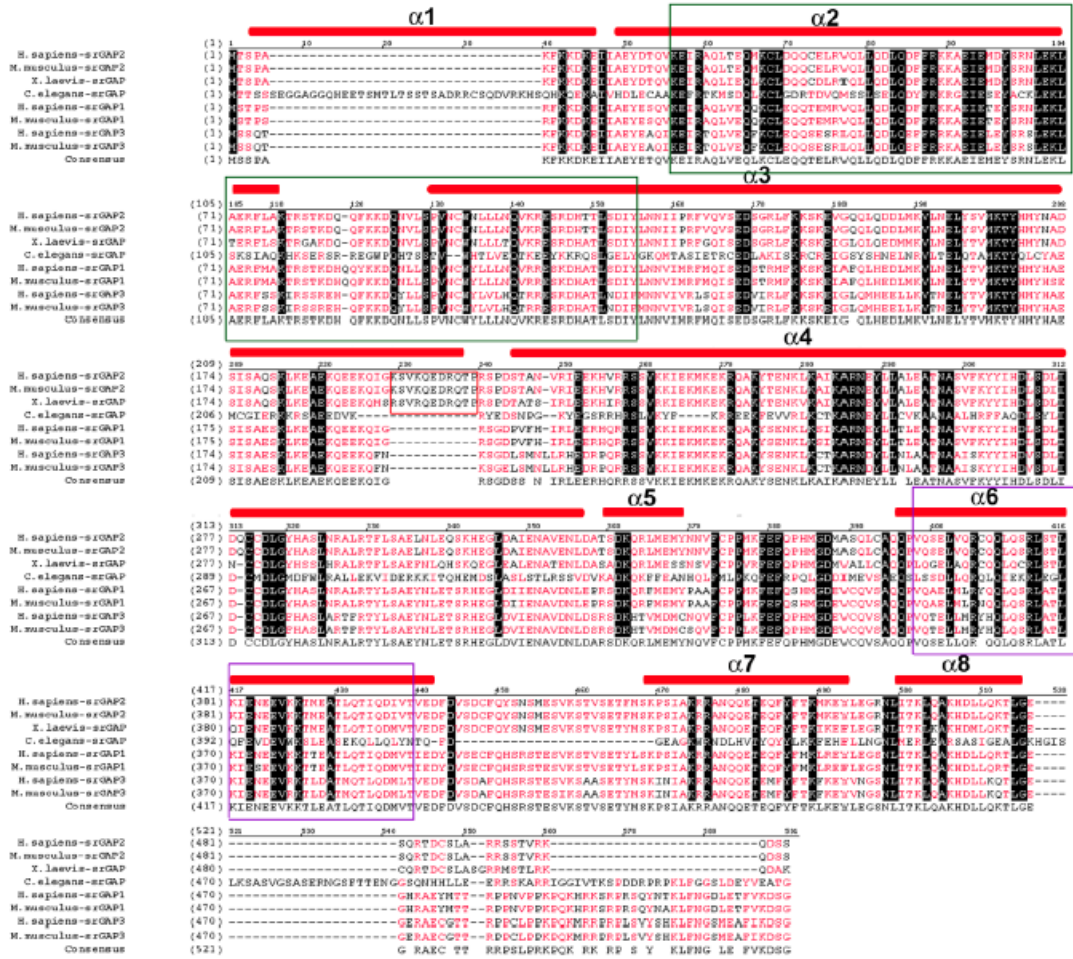


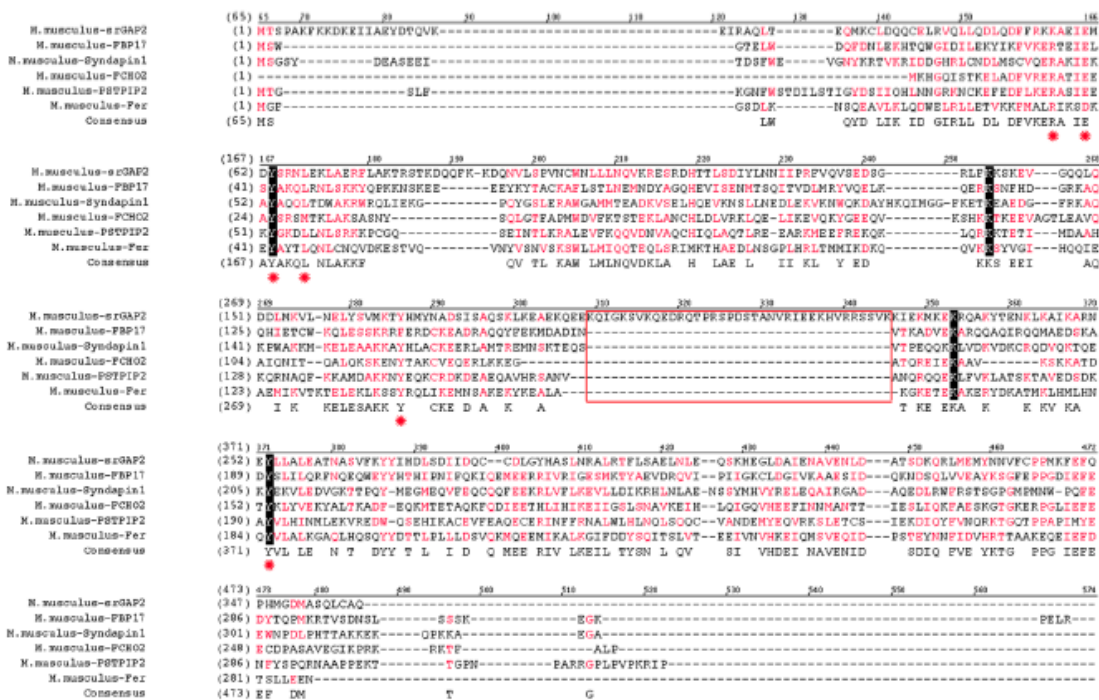
Figure 2.S2. Expression of the F-BAR domain of srGAP2 in COS7 cells does not inhibit endocytosis

(**A-D**) COS7 cells expressing the F-BAR-EGFP fusion protein were incubated with Alexa 647-conjugated transferrin then fixed and permeabilized and stained with Alexa546-phalloidin to label F-actin (**B**). This transferrin-uptake assay reveals no significant difference in the level of endocytosis between F-BAR-EGFP-expressing cells (white arrowheads in **D**) and untransfected cells (blue arrowheads in **D**). (**E-H**) COS7 cells expressing Dynamin2^{K44A}-EGFP (dominant negative) were used as a positive control for inhibition of endocytosis as these cells were unable to endocytose transferrin (white arrowheads in **H**).

A



B



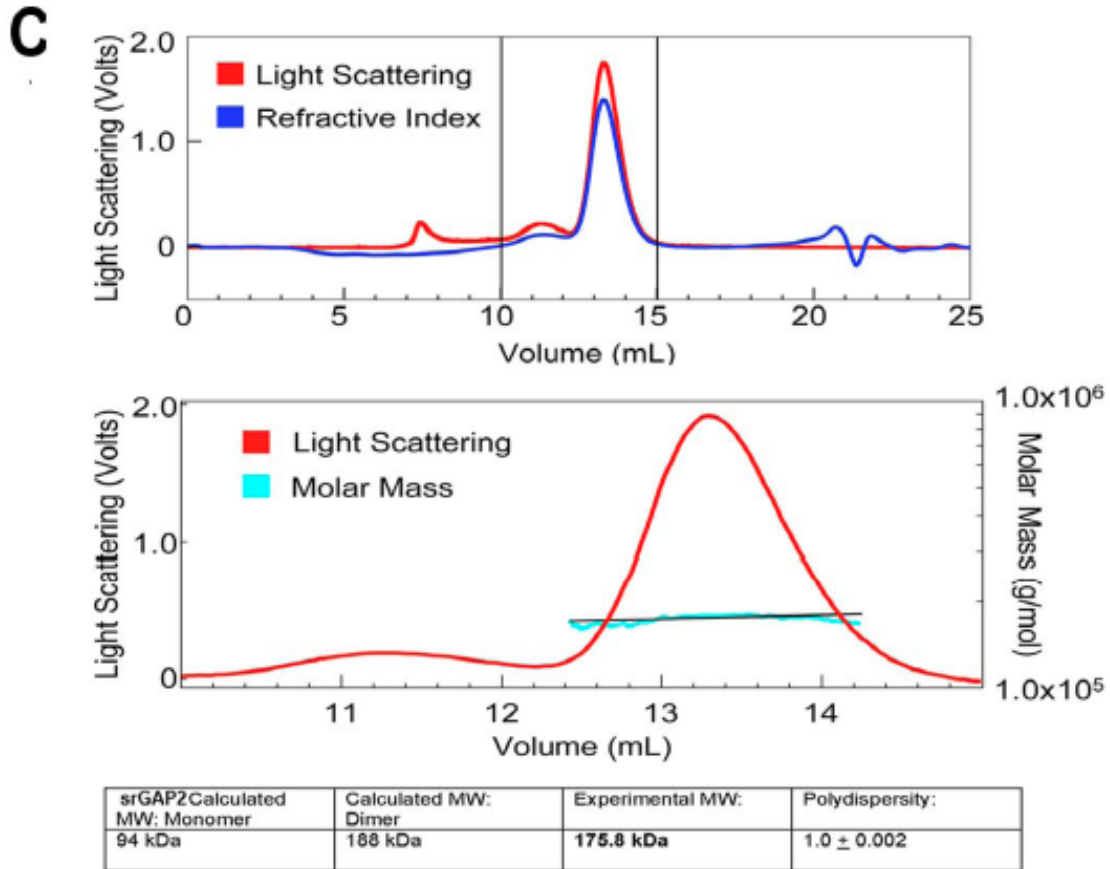


Figure 2.S3. Structural alignment of the predicted F-BAR domain of srGAP2

(A) Sequence alignment of the srGAP family of molecules from various species. Residues labeled in white on black background are identical. Red residues represent groups of conserved amino acids. srGAP2-specific insertion is boxed in red. Predicted alpha-helices are depicted as red bars (secondary structure prediction was obtained using hhpred (Soding et al., 2005) (<http://toolkit.tuebingen.mpg.de/hhpred>) and Bioinfobank metaserver (<http://meta.bioinfo.pl>). The FBAR domain is defined by the alpha helices 2-4. However, three additional alpha-helices are predicted C-terminal of the 'minimal' F-BAR domain and precede the GAP domain. (B) Structural alignment of mouse srGAP2 with representative mouse F-BAR domains was performed using Promals3D (Pei et al., 2008) (<http://prodata.swmed.edu/promals3d/promals3d.php>) and hhpred. Residues colored white on black background are identical between sequences. Red residues represent conserved groups of amino acids. Red stars depict amino acids shown to reside at the dimer interface. Green boxes represent FCH domain as defined by SMART (<http://smart.emblheidelberg.de/>). Purple boxes represent predicted coiled coil. Red box identifies srGAP specific insertion. (C) Top panel: purified full-length srGAP2 protein (aa 1-786 containing F-BAR, GAP and SH3 domains) (300 µg) was loaded onto a Superose 6 column and separated by size exclusion chromatography. Lower panel: expanded view of the light scattering curve (red) in brackets, with the predicted molar mass depicted in cyan. The molecular weight of srGAP2 in solution was determined to be 175.8 kDa by fitting the molar mass curve to a linear function using Astra software.

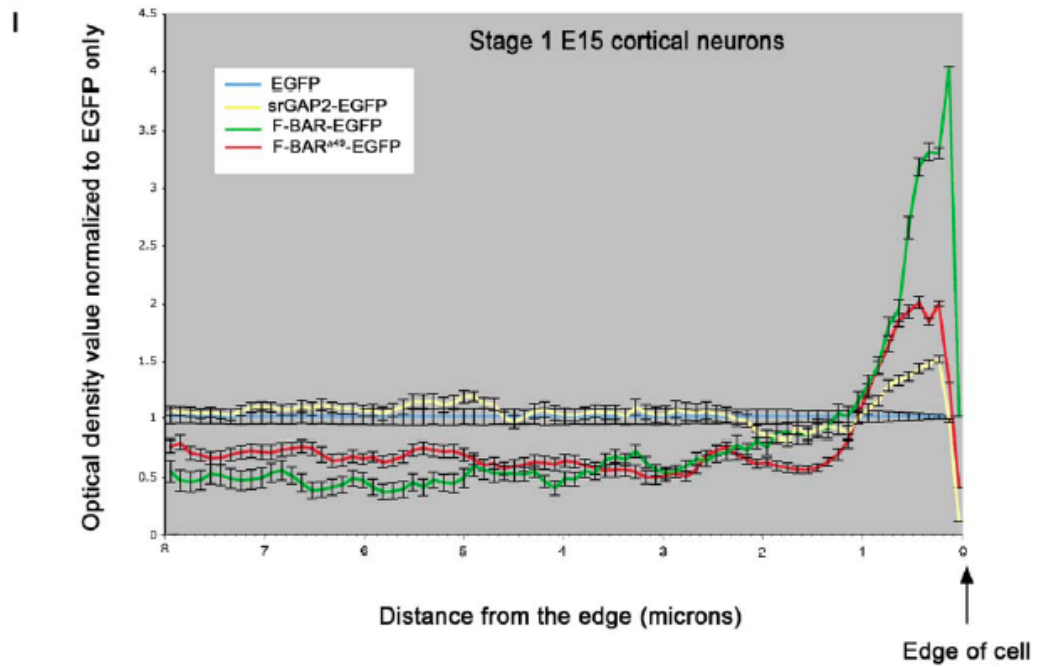
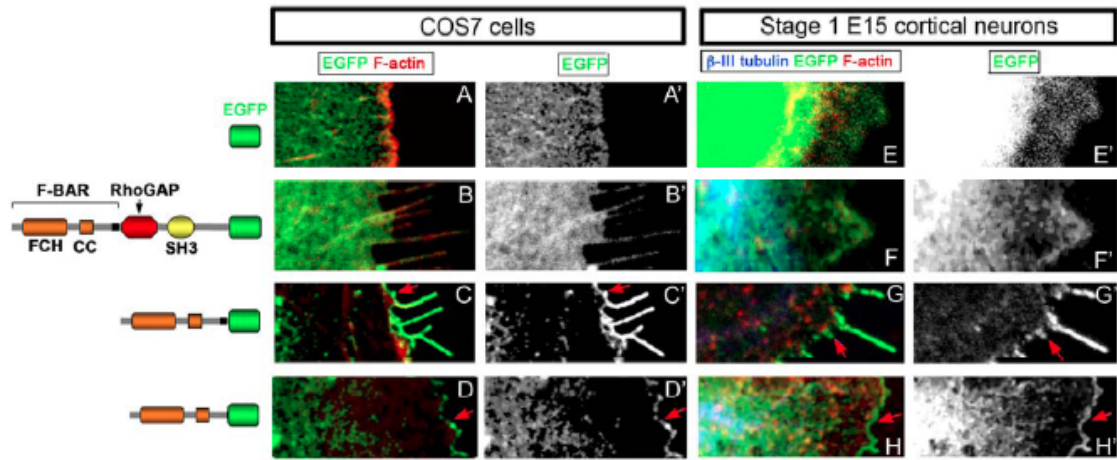


Figure 2.S4. Localization of srGAP2-EGFP, F-BAR-EGFP and F-BAR^{Δ49}-EGFP fusion proteins in COS7 cells (A-D') and stage 1 E15 cortical neurons (E-H'); see text for detail). Note that in both cell types, the F-BAR-EGFP and the F-BAR^{Δ49}-EGFP are enriched at the plasma membrane (red arrows). (I) Histogram of the optical density of EGFP signal for the four constructs examined as a function of distance from the edge of Stage 1 cortical neurons. The optical density for each EGFP fusion protein is normalized to the signal obtained for EGFP only, in order to normalize for variation of cytoplasmic volume.

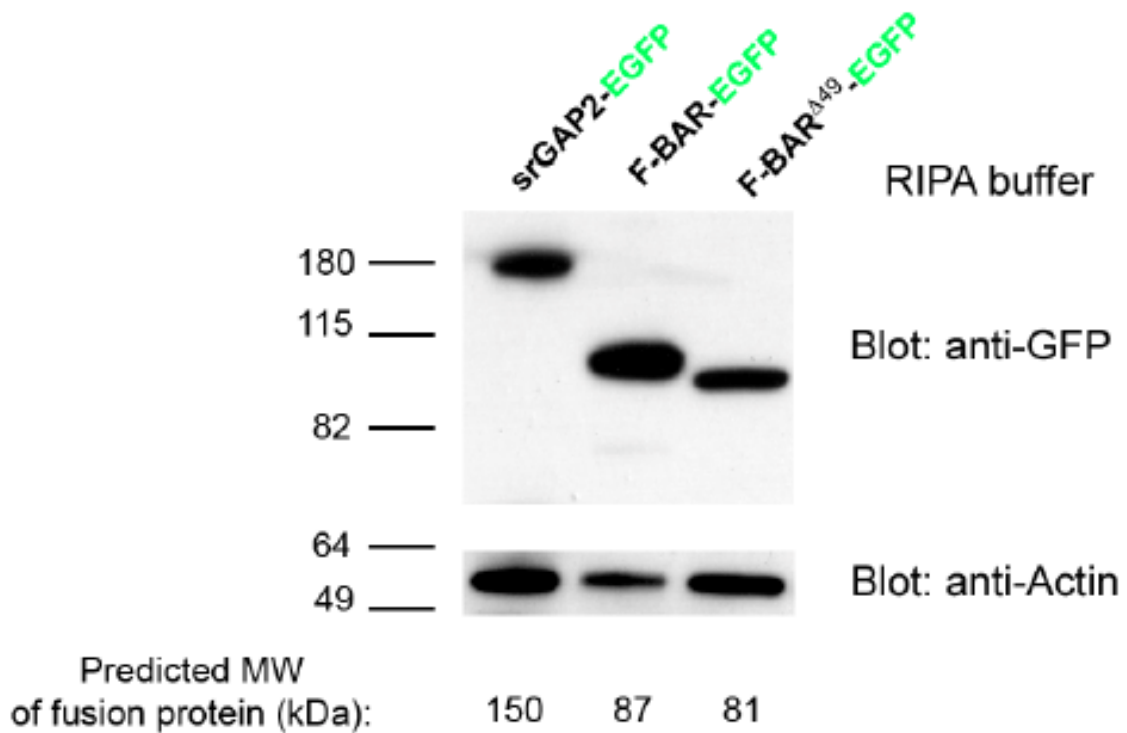


Figure 2.S5. Proper expression of srGAP2-EGFP, F-BAR-EGFP and F-BAR^{Δ49}-EGFP fusion proteins in COS7 cells

COS7 cells were transfected with the indicated constructs and lysed at 48h after transfection following a dual lysis procedure: co-immunoprecipitation buffer was made up of 50mM Tris-Cl (pH 7.4), 15mM EGTA, 100mM NaCl, 0.1% Triton-X, and then protease inhibitor, DTT (1mM), and PMSF (1mM). The insoluble portion of that (including the triton-insoluble protein fraction associated with membrane) was then subjected to a modified RIPA buffer: 50 mM Tris pH 7.4, 0.5% Na Deoxycholate, 0.2% SDS, 1 mM EDTA, 150mM NaCl, plus PMSF (1mM) and protease inhibitors. Proteins from the modified RIPA buffer soluble fraction were then separated by SDS-PAGE and blots were probed with anti-EGFP antibody (upper blot) or anti-actin antibody (lower blot). Note that each of these three constructs are expressed as a band at the expected molecular weight (indicated below the actin blot) although on this type of pre-casted gradient gels, proteins tend to migrate at a higher apparent MW.

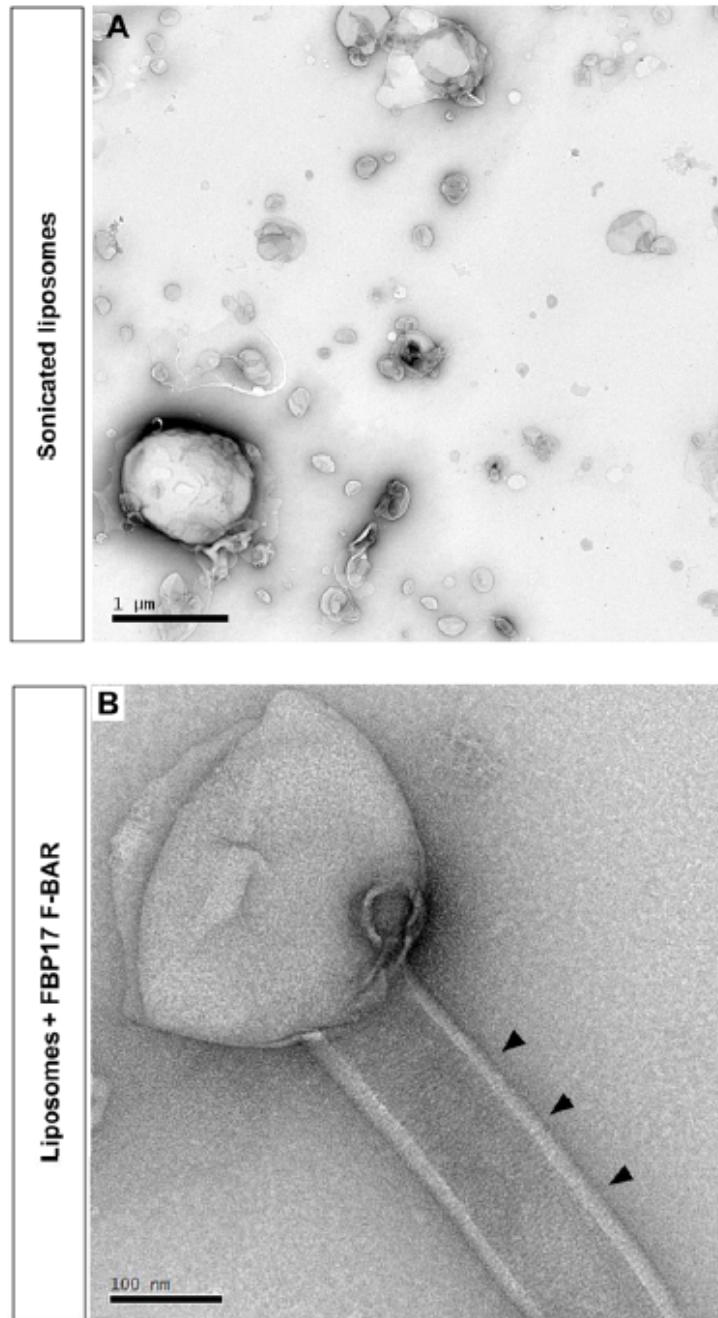


Figure 2.S6. Control FBP17 F-BAR tubulates liposome

(A) Normal morphology of control liposomes following sonication but without incubation with any recombinant protein. (B) The recombinant purified F-BAR domain of FBP17 incubated with preformed liposomes induces long tubulation (arrowheads).

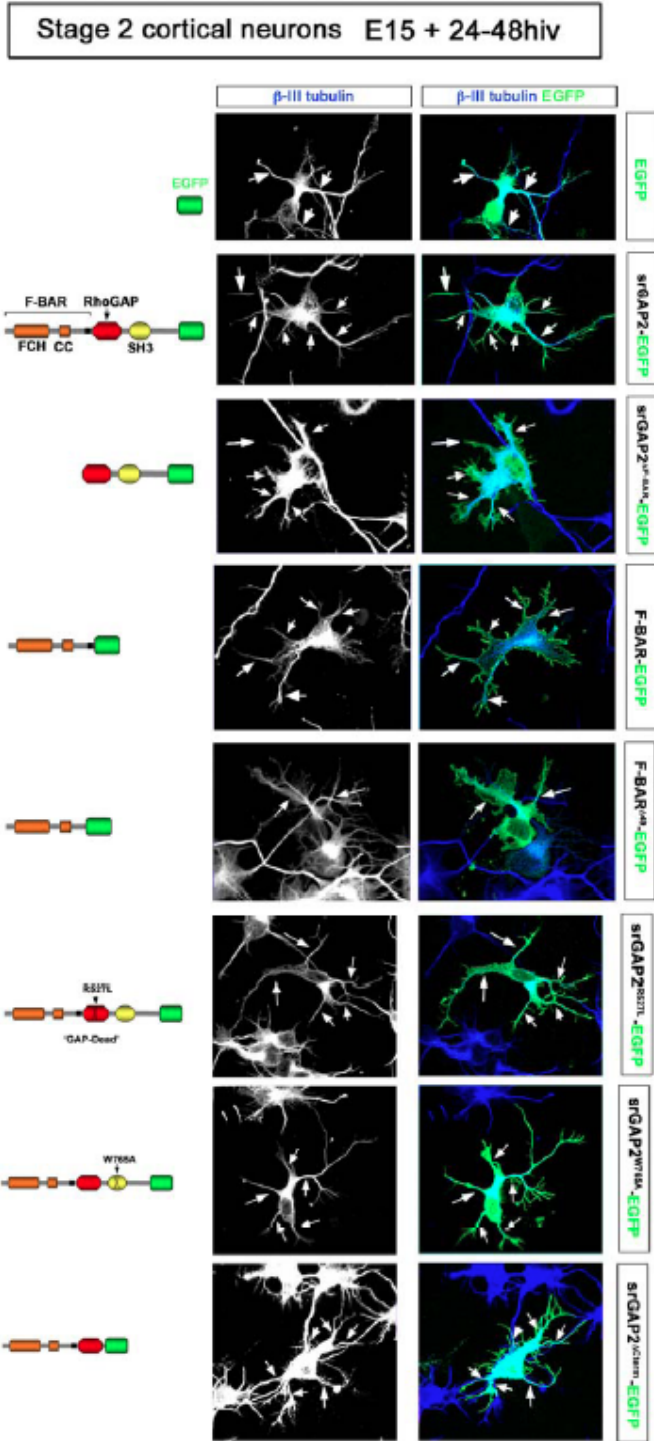


Figure 2.S7. Neurites induced by different srGAP2 constructs contain microtubules
 Compilation of all the images shown for Stage 2 E15 cortical neurons in Figure 4 and Suppl. Figure 12 showing the β III-tubulin signal (left panel) and the corresponding merged image with EGFP. The arrows indicate the presence of microtubules in all the neurites that were counted as 'primary' neurites emerging from the cell body.

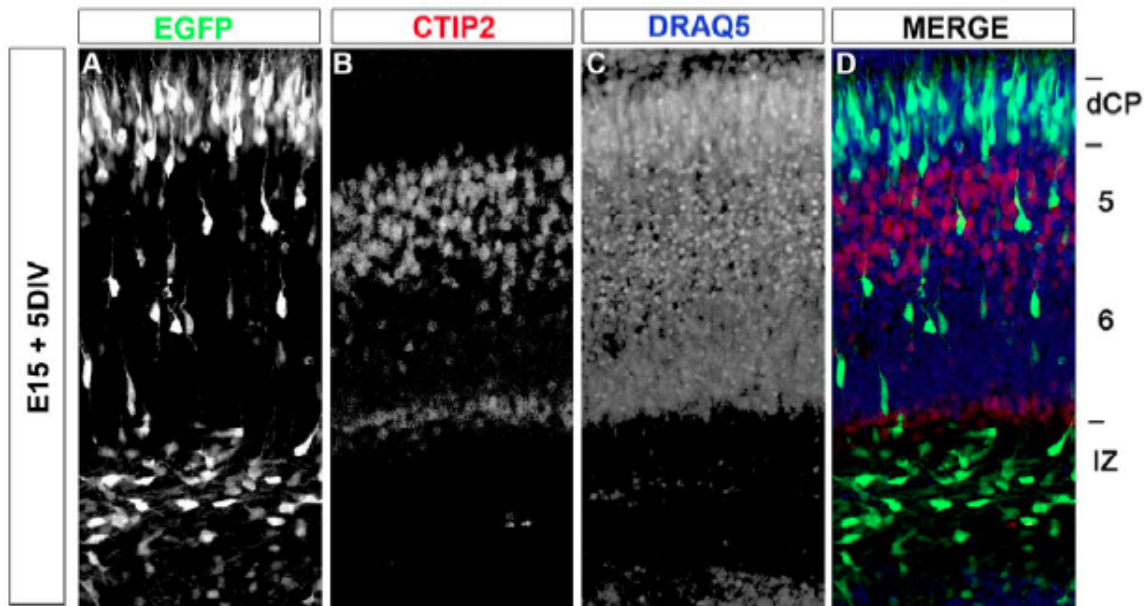


Figure 2.S8. Definition of layers in slices following dorsal electroporation and organotypic culture

(A-D) E15 cortical slices cultured for 5 days after electroporation with EGFP were fixed and stained with CTIP2 (layer 5/6 marker) as well as Draq 5 in order to reveal the cytoarchitecture. We use this laminar definition throughout the paper: dense Cortical Plate (dCP) defined as the densely packed, most immature neurons that migrated to the top of the cortical plate below the cell sparse marginal zone (MZ) and above CTIP2+ layer 5 neurons. The intermediate zone is defined by the low packing density visualized by Draq5 located under layer 5/6 and which contains neurons initiating radial migration.

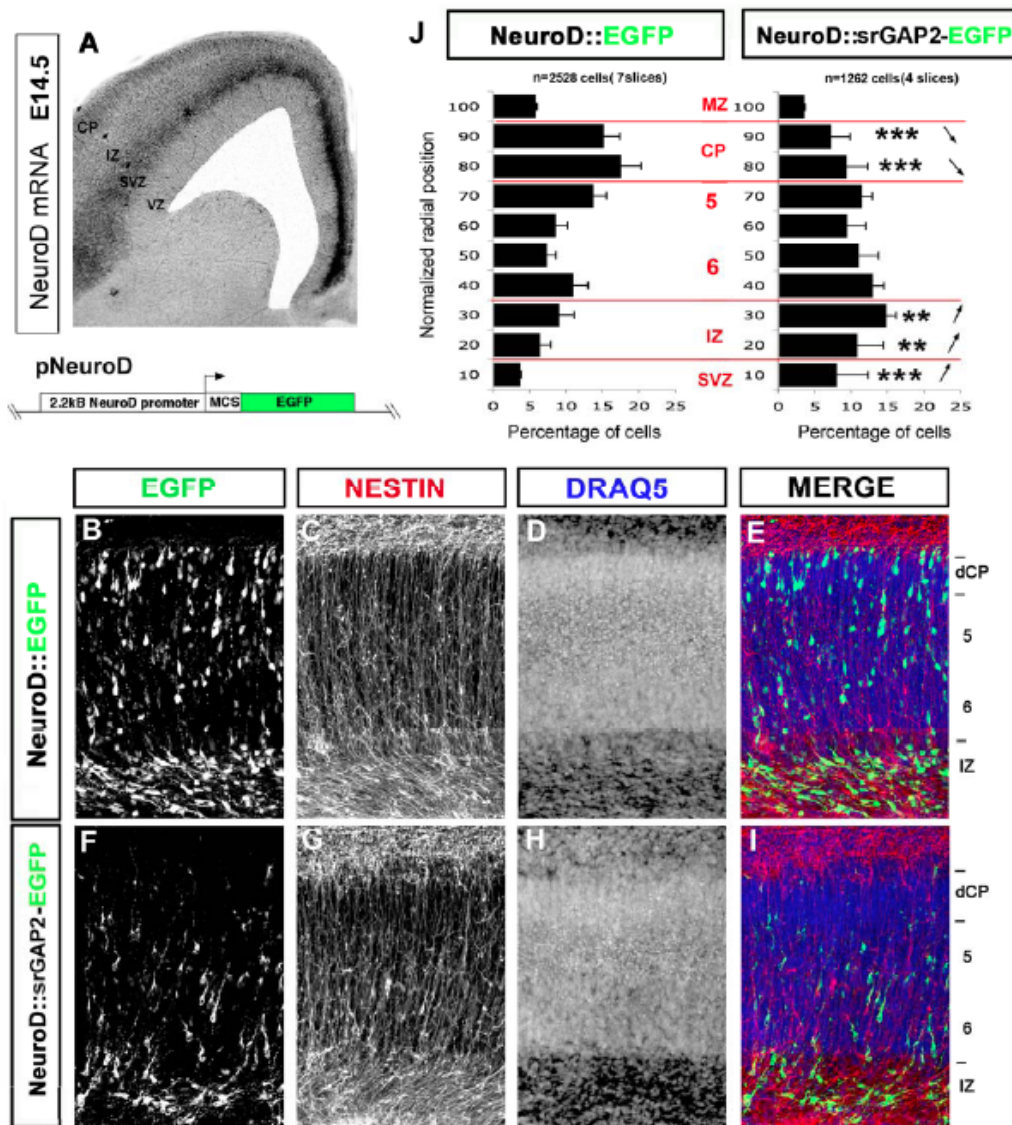


Figure 2.S9. Expression of srGAP2 in post mitotic neurons inhibits radial migration
(A) In situ hybridization of *NeuroD* mRNA in the developing neocortex of an E15 mouse embryo. *NeuroD* is expressed at the SVZ/IZ border but not in the VZ. Schematic representation of the construct used to express EGFP-fusion proteins under the control of the 2.2kB promoter region of *NeuroD*, which drives cDNA expression exclusively in post-mitotic neurons. **(B-I)** E15 cortical slice cultured for 5 days after transfection with pNeuroD-EGFP or pNeuroD-srGAP2-EGFP. EGFP expressing neurons migrate nicely to the cortical plate **(B-E)**. In contrast, srGAP2-EGFP expressing neurons migrate poorly to the cortical plate **(F-I)**. Slices were stained with anti-*nestin* to reveal the radial glial scaffold and *Draq5* to illustrate the cytoarchitecture. **(J)** Quantification of **B-G** showing that a greater proportion of neurons reach the cortical plate in control (EGFP transfected) conditions than in srGAP2 transfected neurons (note decrease proportion of cells in CP and increase proportion in IZ (denoted by arrows) when compared to control). (EGFP n= 7 slices and srGAP2 n= 5 slice).

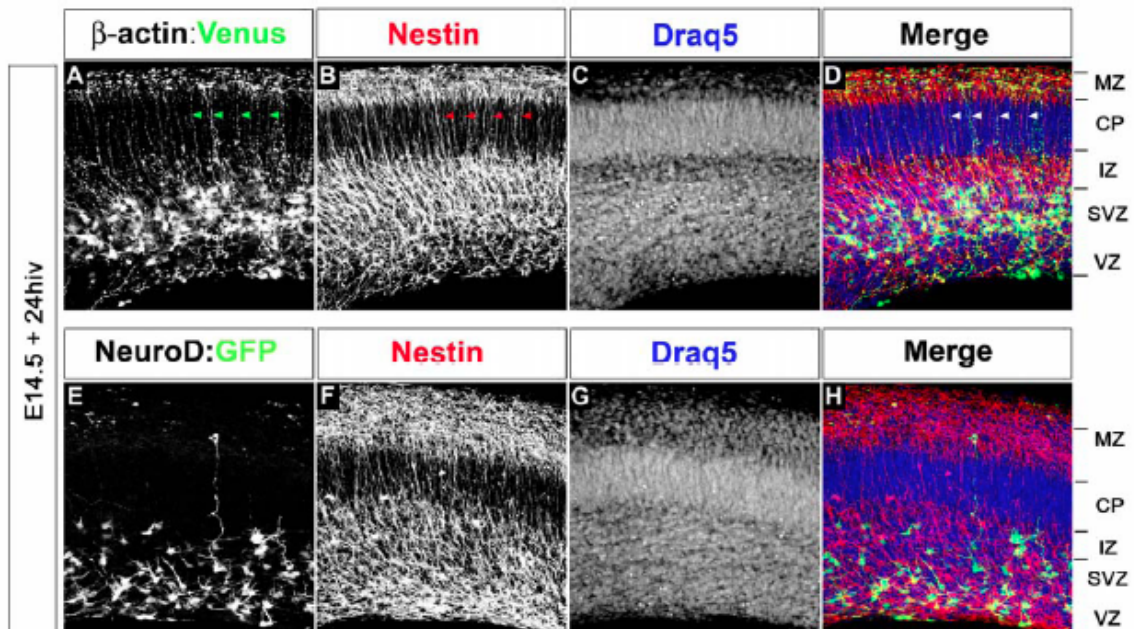


Figure 2.S10. 2.2kD NeuroD promoter drives gene expression in non-radial glial intermediate progenitors 24 hours after electroporation

(A-D) E15 cortices were electroporated chicken-β-actin driven Venus construct sliced and cultured for 24 hrs. After 24 hrs venus positive cells were also positive for anti-nestin (radial glia marker, green arrow heads in **A**, red arrowheads in **B** and white arrow heads in **D**). Also note the long radial glial like morphology of cells. (F-H) In contrast NeuroD drive EGFP expression in non-radial glial intermediate progenitors that are Nestin-negative, supporting the idea that the NeuroD promoter drives expression in intermediate progenitors and early postmitotic neurons in the SVZ/IZ but not in radial glial progenitors in the VZ.

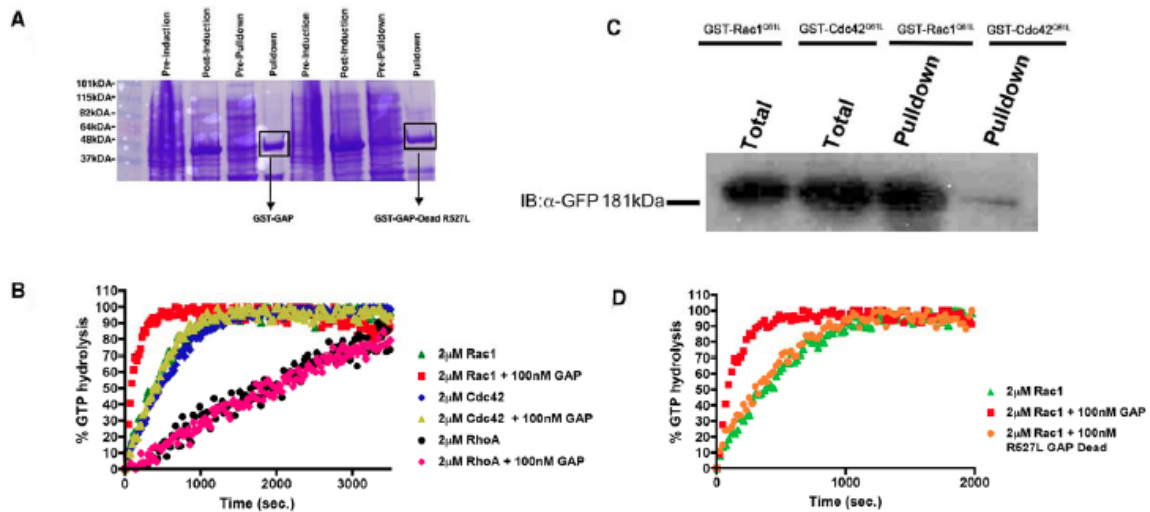


Figure 2.S11. The RhoGAP domain of srGAP2 is specific for Rac1

(A) GST-purification of the wild-type GAP and GAP^{R527L} forms of the RhoGAP domain of srGAP2. Coumassie-stained gel showing the yield recombinant proteins obtained before and after induction (lanes 1-2 and 5-6) in bacteria as well as before and after glutathione-elution of GST-GAP (lanes 3-4) and GST-GAP^{R527L} (lanes 7-8). The boxed areas correspond to the purified recombinant proteins used for the subsequent GTP hydrolysis assays in panel B-C. (B) Fluorescent-based GTP hydrolysis assay as a function of time (seconds) for 2 μ M purified Rac1, Cdc42, RhoA in the presence or absence of 100 nM of the recombinant GAP-domain of srGAP2. Note that the GAP domain of srGAP2 only accelerates the rate of GTP hydrolysis of Rac1 but not Cdc42 or RhoA. (C) Same as B except that 2 μ M purified Rac1 is incubated alone or in the presence of 100 nM of recombinant wild-type GAP domain or GAP^{R527L}. Note that this point mutation abolishes the accelerating effect of the GAP domain on Rac1 GTP hydrolysis. (D) GST pull-down of srGAP2-EGFP from COS7 cells using constitutively active forms of Rac1 (Rac1^{Q61L}) or Cdc42 (Cdc42^{Q61L}). GST-Rac1^{Q61L} pulls down significantly higher amounts of srGAP2 compared to GST-Cdc42^{Q61L} confirming that this is a Rac1-specific GAP.

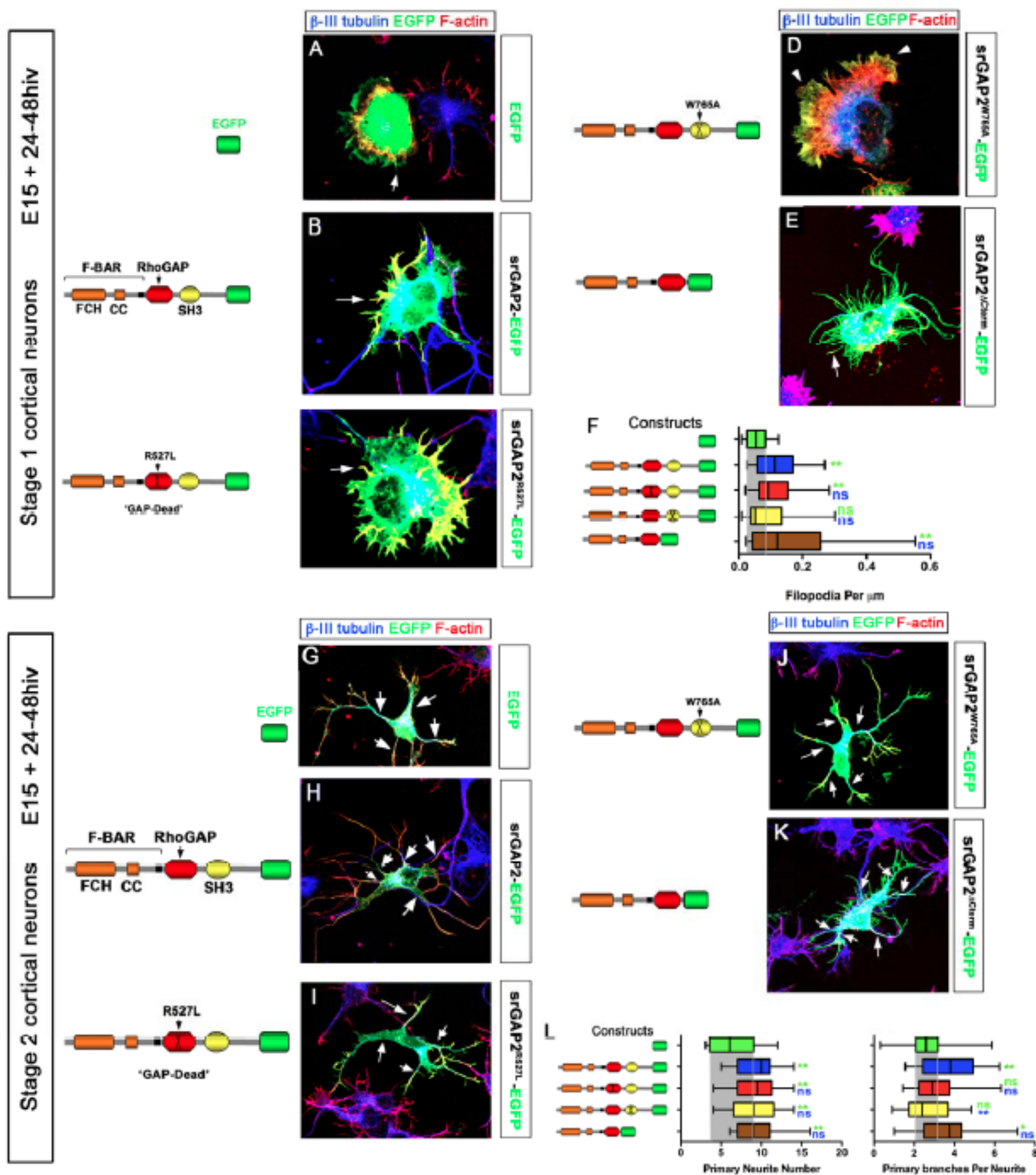


Figure 2.S12. The GAP and SH3 domains participate in srGAP2's ability to promote filopodia formation in neurons

(A-E) Stage 1 cortical neurons expressing various srGAP2 constructs. All cells are stained with β -III tubulin to indicate that it is a neuron and phalloidin to visualize F-actin. Control stage 1 neurons (EGFP (A)) normally display filopodia at cell periphery. However expression of srGAP2-EGFP (B) significantly increased the number of filopodia. Mutation of the GAP domain (srGAP2^{R527L}-EGFP (B)) did not appear to affect the ability of srGAP2 to make filopodia but did appear to increase lamellapodia formation. The SH3 domain mutant (srGAP2^{W765A}-EGFP (D)) completely abrogated srGAPs ability to induce filopodia formation while deletion of the c-terminus (E) (including the SH3 domain, srGAP2 ^{Δ Cterm}-EGFP) was able to induce filopodia. (F) Quantification of A-E. (EGFP n= 20 cells; srGAP2-EGFP n= 21

cells; srGAP2^{R527L}-EGFP n= 21 cells; srGAP2^{W765A}-EGFP n= 21 cells; srGAP2^{ΔCterm}-EGFP n=20 cells. Cells were taken from 3 different experiments and analyzed using Mann-Whitney Test * p<0.05; ** p<.001; *** p<0.001. Green color indicates comparison to EGFP and blue color indicates comparison to srGAP2-EGFP). (**G-K**) Stage 2 cortical neurons expressing various srGAP2 constructs. All cells are stained with β-III tubulin to indicate that it is a neuron and phalloidin to visualize F-actin. As shown previously expression of srGAP2 (**H**) caused increase neurites initiation and branching compared to EGFP (**G**) expressing neurons at stage 2. Expression of srGAP2^{R527L}-EGFP (**I**); srGAP2^{W765A}-EGFP (**J**); and srGAP2^{ΔCterm}-EGFP (**K**) all caused increased neurite initiation. While, srGAP2^{ΔCterm}-EGFP expression caused significant increases in neurite branching (**K**), srGAP2^{W765A}-EGFP expression (**I**) had no effect. Expression of srGAP2^{R527L}-EGFP did cause an increase in neurite branching, but not as significant as srGAP2. (**L**) Quantification of **G-K**. (EGFP n= 20 cells; srGAP2-EGFP n= 21 cells; srGAP2^{R527L}-EGFP n= 22 cells; srGAP2^{W765A}-EGFP n= 21 cells; srGAP2^{ΔCterm}-EGFP n=23 cells. Cells were taken from 3 independent experiments and analyzed using Mann-Whitney Test * p<0.05; ** p<.001; *** p<0.001).

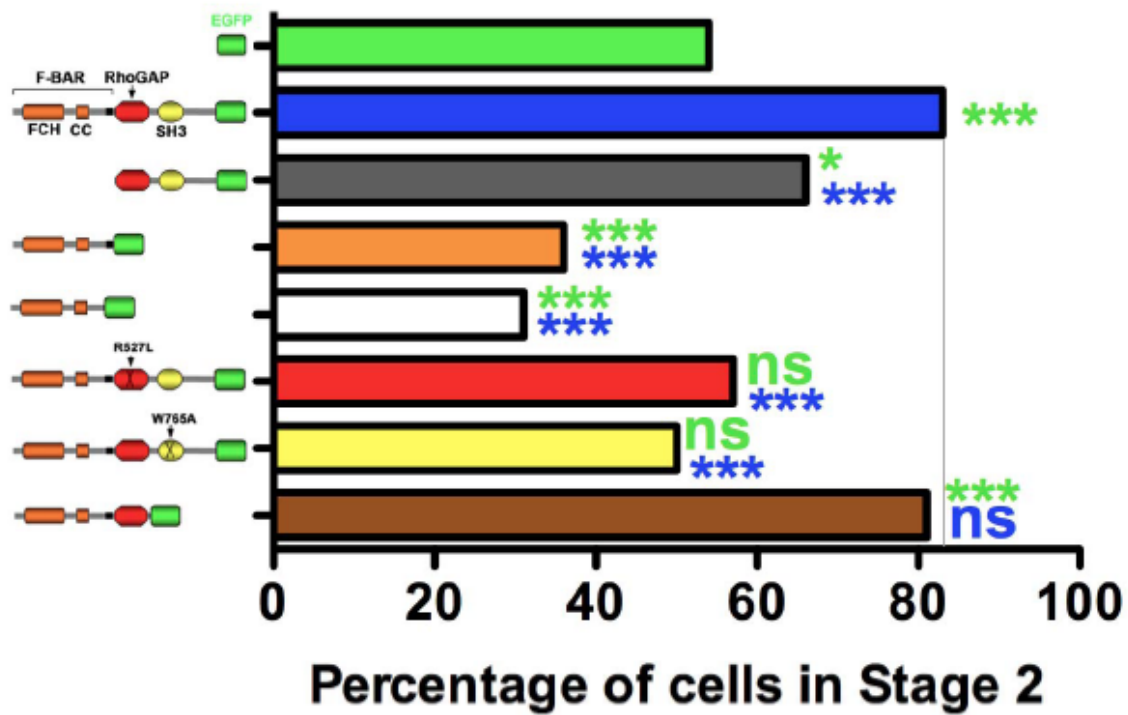


Figure 2.S13. srGAP2 expressing cells accumulate in Stage 2
 Analysis of the percentage of cells that accumulate at Stage 2 after transfection of various srGAP2 constructs. (n>80 neurons in each conditions).

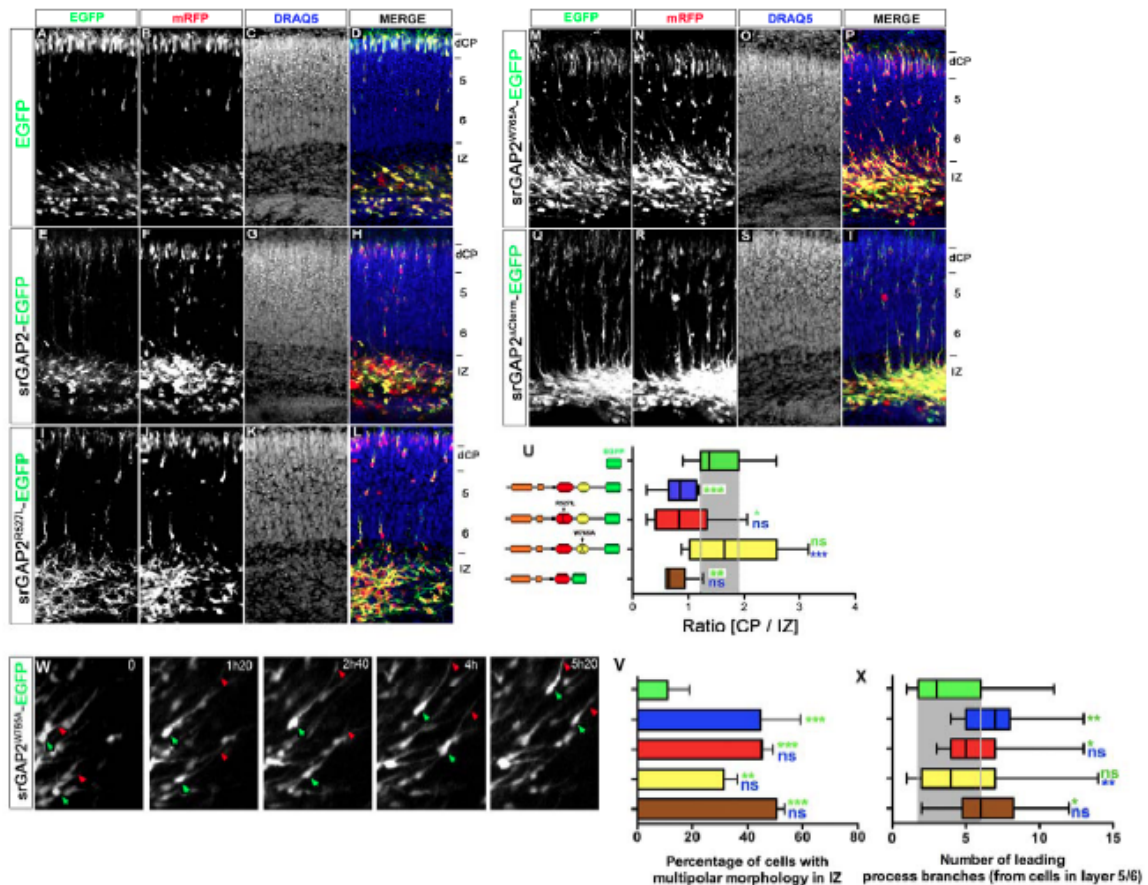


Figure 2.S14. The GAP and SH3 domains participate in srGAP2's ability to inhibit migration

(A-T) E15 cortical slices cultured for 5 days after electroporation with various srGAP2 constructs and mRFP. Slices were stained with DraQ5 in order to demonstrate cytoarchitecture. As shown previously srGAP2 expressing neurons migrate very poorly to the cortical plate (E-H) Impairment of the GAP activity of srGAP2 (srGAP2^{R527L}) inhibits migration albeit not to the degree of full-length srGAP2 (I-L). Moreover, mutation of the SH3 domain (srGAP2^{W765A}) (M-P) had no effect on the ability of neurons to migrate, in that it does not inhibit migration like full-length srGAP2. However, expression of the c-terminal deletion of srGAP2 (srGAP2^{ΔCterm}-EGFP) does impair migration (Q-T). (U) Quantification of effects displayed in A-L. (EGFP, n= 13 slices; srGAP2-EGFP n= 14 slices; srGAP2^{R527L}-EGFP n= 11 slices; srGAP2^{W765A}-EGFP n= 8 slices; srGAP2^{ΔCterm}-EGFP n= 6 slices. Slices were taken from 4 independent experiments and analyzed using Mann-Whitney Test * p<0.05; ** p<.001; *** p<0.001. Green color indicates comparison to EGFP and blue color indicates comparison to srGAP2-EGFP). (V) Quantification of percentage of cells with multipolar morphology in EGFP, srGAP2, or F-BAR transfected slices. Multipolar cells were defined as cells possessing > 3 processes. (EGFP n= 66 cells; srGAP2-EGFP n= 42 cells; srGAP2^{R527L}-EGFP n= 47 cells; srGAP2^{W765A}-EGFP n= 52 cells; srGAP2^{ΔCterm}-EGFP n= 50 cells. Cells were taken from 3 independent experiments and analyzed using Mann-Whitney Test * p<0.05; ** p<.001; *** p<0.001. Green color indicates comparison to EGFP and blue color indicates comparison to srGAP2-EGFP). (W) Time-series of E15 cortical slices cultured for 3 days after electroporation with srGAP2^{W765A}-EGFP (coelectroporated with

venus plasmid). These neurons showed a unipolar morphology with a single unbranched leading process (red arrowhead) and translocated very efficiently (green arrowhead). (X) Quantification of leading process branching from cells expressing EGFP, srGAP2-EGFP, srGAP2^{R527L}-EGFP, srGAP2^{W765A}-EGFP, or srGAP2^{ΔCterm}-EGFP in layer 5/6. (EGFP n= 17 cells; srGAP2-EGFP n= 21 cells; srGAP2^{R527L}-EGFP n= 18 cells; srGAP2^{W765A}-EGFP n= 26 cells; srGAP2^{ΔCterm}-EGFP n= 18 cells. Cells were taken from 3 independent experiments and analyzed using Mann-Whitney Test * p<0.05; ** p<.001; *** p<0.001. Green color indicates comparison to EGFP and blue color indicates comparison to srGAP2-EGFP).

CHAPTER 3

The F-BAR domains from srGAP1, srGAP2, and srGAP3 differentially regulate membrane deformation¹

3.1 INTRODUCTION

The plasma membrane and actin cytoskeleton work in concert to create, maintain, and modify cell shape (Raucher et al., 2000; Sheetz and Dai, 1996). The coordination of plasma membrane deformation and actin polymerization is critical for cellular processes including chemotaxis, endocytosis, polarity and cytokinesis (Ford et al., 2002; Frost et al., 2007; Han et al., 2006; Janetopoulos et al., 2005; Martin-Belmont et al., 2007; Vallis et al., 1999). The actin cytoskeleton can be linked to the plasma membrane through a diverse array of actin-binding proteins that interact directly with phosphoinositides, frequently phosphatidylinositol 4,5-bisphosphate (PI(4,5)P₂), present in the inner leaflet of the plasma membrane, such as the Wiscott Aldrich Syndrome Protein (WASP)-family (Miki et al., 1996; Oikawa et al., 2004), Actin Depolymerizing Factor (ADF)/cofilins (Zhao et al., 2010), and the small Rho-like GTPases (Yoshida et al., 2009). Alternatively, this link to the actin cytoskeleton can occur through scaffolding proteins that contain specific phospholipid-binding motifs, such as Pleckstrin Homology (PH) domains found in proteins like Phospholipase C (PLC), Dynamin (Flesch et al., 2005; Harlan et al., 2004; Vallis et al.,

¹ Jaeda Coutinho-Budd, Vladimir Ghukasyan, Mark J. Zylka, and Franck Polleux (2012) The F-BAR domains from srGAP1, srGAP2, and srGAP3 differentially regulate membrane deformation. *J Cell Sci*, In press.

According to the Journal of Cell Science's rights and permissions policy, "authors may reproduce the article, in whole or in part, in any printed book (including a thesis) of which they are author, provided the original article is properly and fully attributed." My contribution to this work includes direct involvement in all figures, with the exception of supplemental Figure 4, which was put together by Franck Polleux. Vladimir Ghukasyan performed the FRAP imaging and data analysis in Figure 3.4.

1999), or Bin/Amphiphysin/Rvs (BAR) domain-containing proteins (reviewed in Itoh and De Camilli, 2006; Tsujita et al., 2006). Over the past decade, emerging evidence suggests that in many instances F-Actin dynamics must be coupled with the function of membrane-deforming proteins. This coupling plays an instructive role in the localization and the type of membrane deformations observed in cells, such as lamellipodia and filopodia protrusions during endocytosis or phagocytosis (Doherty and McMahon, 2008; Itoh and De Camilli, 2006; Martin-Belmont et al., 2007).

One of the largest families of membrane-deforming proteins is the BAR proteins superfamily. Proteins of the BAR superfamily are recognized for their ability to sense and/or generate membrane deformation (Doherty and McMahon, 2008). BAR domains are membrane-binding modules, consisting of a series of three to five alpha-helices, that form a large dimerization interface to create banana-shaped quaternary structures. These homodimeric BAR-domains bind cellular membranes through electrostatic charge interaction between their positively-charged amino acids (arginine and lysine) and negatively charged phospholipids, such as PI(4,5)P₂ and phosphatidylserine (PS) (Saarikangas et al., 2009). BAR domain-containing proteins often contain multiple other domains, including the actin-binding domain WH2, GTPase activating protein (GAP) and guanine nucleotide exchange factor (GEF) domains, and src homology 3 (SH3) domains, lending to the interplay between cellular membranes and the actin cytoskeleton. The BAR superfamily has been segregated into subfamilies, based on structural and functional data (Itoh and De Camilli, 2006). N-BAR domains, such as those found in Amphiphysin and Endophilin, contain a N-terminal amphipathic helix that inserts into the lipid bilayer, aiding in their membrane-deforming properties (Masuda et al., 2006; Peter et al., 2004). BAR domains induce membrane invaginations, and function in endocytosis. F-BAR domains were recognized more recently through secondary structure prediction of the congruence of a Fes-CIP4 Homology (FCH) domain and a coiled-coil domain in its C-terminal (Henne et

al., 2007; Itoh et al., 2005; Shimada et al., 2007; Tsujita et al., 2006). Recently, several structures of F-BAR domains were solved, revealing an elongated dimer with more shallow curvature than the BAR domains (Shimada et al., 2007; Wang et al., 2009; Yoshida et al., 2009). Like BAR proteins, F-BAR domain-containing proteins, such as Formin Binding Protein 17 (FBP17) and FCH only 1 and 2 (FCHo1/2) induce membrane invaginations and play a role in the endocytic process (reviewed in Doherty and McMahon, 2008). A third class called Inverse BAR (I-BAR) domain-containing proteins such as Insulin Receptor tyrosine kinase substrate p53 (IRSp53) and Missing-in-Metastasis (MIM) induce membrane protrusions instead of invaginations (Mattila et al., 2007; Suetsugu et al., 2006; Yamagishi et al., 2004). However, this simple structure/function dichotomy, that BAR/N-BAR/F-BAR domains induce membrane invagination and tubulation, while I-BAR domain induce filopodial protrusions, has been recently challenged by results showing that the predicted F-BAR domain of slit-robo GTPase Activation Protein 2 (srGAP2) (Guerrier et al., 2009) and syndapins (Dharmalingam et al., 2009) can induce filopodia-like membrane protrusion and, thereby, regulate neuronal morphogenesis.

srGAP2 is a member of the srGAP family of proteins, which consists of three other members: srGAP1, srGAP3 (WRP/Megap), and ArhGAP4 (which has been renamed srGAP4 based on its domain organization and homology with srGAP1-3; MGI:2159577). srGAP proteins all contain a predicted N-terminal F-BAR domain, a central Rho-GAP domain, and a C-terminal SH3 domain (Carlson et al., 2011; Wong et al., 2001). The family was named based on the fact that the C-terminal SH3 domain binds the intracellular domain of the Roundabout receptor (Robo), the receptor for the axon guidance cue, Slit (Wong et al., 2001). Although each family member contains a GAP domain, there are differences in GTPase hydrolysis activity between the proteins. The RhoGAP domain of srGAP1 has been shown to promote GTP hydrolysis of cdc42 and RhoA, depending on the concentration of Slit1 (Wong et al., 2001), while the GAP domains of srGAP2 and srGAP3

are both specific for Rac1 (Guerrier et al., 2009; Soderling et al., 2002), and ArhGAP4 can act on both cdc42 and Rac1 (Vogt et al., 2007). All four family members display spatially and temporally distinct patterns of expression in the central nervous systems (Bacon et al., 2009; Foletta et al., 2002), and have been shown to regulate cell migration and neuronal morphology in mammalian cells (Guerrier et al., 2009; Soderling et al., 2002; Vogt et al., 2007; Wong et al., 2001; Yang et al., 2006), a function that seems evolutionary conserved in invertebrates (Zaidel-Bar et al. 2010). srGAP3 has been implicated in a severe form of mental retardation, the 3p- syndrome, giving srGAP3 the alternate name of Mental-Disorder Associated GAP Protein (MEGAP) (Endris et al., 2002). srGAP2 has also recently been implicated in a severe neurodevelopmental syndrome causing early infantile epileptic encephalopathy and profound psychomotor delay (Saitou et al. 2011). These human genetic data strongly suggest that srGAP2 and srGAP3 play a critical role during human brain development.

We recently found that the function of SRGAP2 in both neuronal migration and morphogenesis is largely mediated through the ability of its F-BAR domain to induce filopodia (Guerrier et al., 2009). However, the functional properties of the predicted F-BAR domains of the remaining srGAP family members has yet to be determined; furthermore, the molecular mechanisms underlying their function during filopodia formation are only starting to be examined in detail (Carlson and Soderling, 2009).

In the present study, we focused our analysis on the function of the other F-BAR domains present in srGAP1, srGAP2, and srGAP3. Our results reveal a surprising degree of diversity in the ability of these three closely-related F-BAR domains to induce filopodia-like membrane protrusions in non-neuronal and neuronal cells. Our study provides novel insights into the molecular mechanisms underlying the membrane deformation properties of this subclass of F-BAR domains during cell morphogenesis.

3.2 RESULTS

3.2.1. The srGAP family of proteins, through their respective F-BAR domains, exhibit different abilities to induce filopodia in non-neuronal cells

Recently, the F-BAR domain of srGAP2 (F-BAR(2)) has been implicated in the regulation of neuronal migration and morphogenesis due to its ability to induce filopodia and neurite branching (Guerrier et al., 2009). srGAP2 is one of four srGAP family proteins, although ArhGAP4/srGAP4 diverges in sequence from the rest of the family (**Fig. 3.S1A,B**); therefore, we restricted our analysis to the F-BAR domains of srGAP1, srGAP2, and srGAP3. While the F-BAR domains of srGAP1, srGAP2, and srGAP3 share approximately 85% amino-acid identity (**Fig. 3.S1C-D**), the molecular properties of the F-BAR domains of srGAP1 (F-BAR(1)) and srGAP3 (F-BAR(3)) are still poorly understood. To first compare the functions of these closely-related proteins, we transfected plasmids expressing full-length srGAPs, or their respective F-BAR domains fused in their C-terminal end to enhanced green fluorescent protein (EGFP) into COS7 cells (**Fig. 3.1A-H''**). Full-length srGAP1 (**Fig. 3.1B-B'',I,J**) and srGAP3 (**Fig. 3.1D-D'',I,J**) induce more filopodia than EGFP alone (**Fig. 3.1A-A'',I,J**), but are both significantly less potent than full-length srGAP2 (**Fig. 3.1C-C'',I,J**). A similar trend is found with expression of each respective F-BAR domain (**Fig. 3.1E-G''**). Therefore, both srGAP2 and its F-BAR(2) domain are more potent at inducing filopodia than srGAP3 and srGAP1, or their F-BAR domains (**Fig. 3.1I,J**) respectively. Additionally, both srGAP2 and F-BAR(2) induced significantly longer filopodia than the other srGAP family members or their F-BAR domains (**Fig. 3.1K**). There is no significant difference in filopodia number or length between each srGAP proteins and their respective F-BAR domain. These data illustrate that despite such closely related sequences, the members of the srGAP family of proteins are functionally distinct with regard to their ability to induce filopodia.

3.2.2 srGAP proteins can interact through their F-BAR domains

It has previously been shown that BAR, N-BAR, F-BAR and I-BAR domains homodimerize to form curved structures necessary for membrane deformation and tubulation (Henne et al., 2007; Shimada et al., 2007; Wang et al., 2009; Frost et al., 2008). We have previously shown using biochemical and biophysical approaches that the F-BAR domain of srGAP2 forms homodimers (Guerrier et al., 2009). Based on their high degree of conservation, we hypothesized that the F-BAR domains of the srGAP family proteins have the ability to heterodimerize, in addition to homodimerize. To test for interaction between F-BAR domains, combinations of myc-tagged and GFP-tagged srGAPs were co-transfected into COS7 cells and immunoprecipitated with a GFP antibody (**Fig. 3.2A**). Western blots were probed for myc, revealing interactions between all three paired combinations of full-length srGAP proteins. This interaction occurred through the respective F-BAR domains, and not through indirect interaction through SH3 domain binding, as indicated by co-immunoprecipitation of RFP-tagged F-BAR(2) with GFP-tagged F-BAR1/3 (**Fig. 3.2B**). This result suggests that all three F-BAR domains are structurally conserved and are capable of heterodimerization or oligomerization.

3.2.3 The F-BAR domains of different srGAP proteins localize to distinct regions of filopodia

In order to test for cooperative function of these three different F-BAR domains, GFP-tagged F-BAR(1) or F-BAR(3) were co-transfected into COS7 cells along with mRFP-tagged F-BAR(2) (**Fig. 3.3A-C''**). Surprisingly, co-expression of either F-BAR(1) (**Fig. 3.3A-A''**) or F-BAR(3) (**Fig. 3.3C-C''**) with F-BAR(2) exhibited a synergistic effect towards filopodia induction when compared to equivalent expression of F-BAR(2)-GFP and F-BAR(2)-mRFP (**Fig. 3.3B-B''**; quantified in **Fig. 3.3D**). Live-imaging of co-transfected COS7 cells revealed differences in filopodial dynamics with different F-BAR combinations: filopodia containing GFP- and RFP-tagged F-BAR(2) or the combination of F-BAR(2)-RFP and F-BAR(3)-GFP extend faster than filopodia containing F-BAR(2)-RFP and F-BAR(1)-

GFP (**Fig. 3.3E**).

We noticed that when co-expressed, these F-BARs domains showed distinct distribution along the filopodia. In order to quantify F-BAR distribution within the filopodia of COS7 cells, a line was drawn from the base to the tip of the filopodia to measure the fluorescence intensity of both the GFP- and mRFP-tagged signals. This quantification reveals significant differences in F-BAR distribution into the filopodia (**Fig. 3.3F-H**, quantified in **Fig. 3.3I**). In both instances F-BAR(2) extended to the tip of the filopodia, while the expression of F-BAR(1) or F-BAR(3) strongly decreased before reaching the tip. These results suggest (i) that the F-BAR domains of srGAP1-3 display synergistic effects towards filopodia induction and filopodia growth, and (ii) that these three F-BAR domains have distinct intra-filopodial localization when co-expressed. These data, combined with the interaction data, further suggest that the three F-BAR domains can form distinct complexes inside a filopodium to intricately regulate the induction and maintenance of membrane protrusions.

3.2.4 Molecular dynamics of the F-BAR Domains of srGAP1-3

Canonical F-BAR domain homodimers can form end-to-end oligomers that adopt a 'coiled' quaternary structure, which interacts with the plasma membrane (Shimada et al., 2007). These 'coils' are also stabilized by interactions between the sides of the F-BAR homodimers occurring between adjacent turns of the 'coil' in proteins such as FBP17 (Frost et al., 2008). The exact structural mechanism underlying I-BAR-mediated membrane tubulation in filopodia is currently unknown, but has been shown to require the ability of I-BAR domains to interact with the negatively-charged lipids via the convex surface, as well as insertion of an amphipathic helix into the inner leaflet of the plasma membrane (Saarikangas et al., 2009). Additionally, the I-BAR domains of IRSp53 (Millard et al., 2005), IRTKS (Millard et al., 2007), and MIM (Lee et al., 2007) have been suggested to directly bind actin. We hypothesized that part of the functional differences observed between the

ability of the three srGAP F-BAR domains to induce filopodia might be due to differences in their subcellular trafficking properties along the plasma membrane or the actin cytoskeleton, which can be assessed by quantifying their molecular dynamics using fluorescence recovery after photobleaching (FRAP).

Following photobleaching, the fluorescence recovery (F_R) plateaus at a certain percentage of the initial fluorescence, which represents the fraction of the protein that is mobile (mobile fraction). We also measured the time required to recover 50% of the fluorescence of the mobile fraction ($t_{1/2}$), which indicates the speed of the mobile fraction (i.e. how quickly F-BAR domains assemble and traffic along the plasma membrane). We made three types of comparisons for both F_R and $t_{1/2}$: (1) comparing all three F-BAR domains and the PH domain of PLC δ 1, (2) comparing the molecular dynamics of these domains in filopodia versus along the plasma membrane, and (3) comparing the molecular dynamics of these domains in control cells versus cells treated with cytochalasin-D in order to induce F-actin depolymerization.

These quantitative analyses reveal that F-BAR(2) displays a significantly higher mobile fraction, and shorter $t_{1/2}$ than F-BAR(1), in filopodia (**Fig. 3.4B-C**) and at the plasma membrane (**Fig. 3.4D-E**) while F-BAR(3) displays commonalities to both of the other F-BAR domains, depending on the context. In filopodia, the mobile fraction of F-BAR(3) matches that of F-BAR(2) in untreated cells, whereas the mobile fraction of F-BAR(3) matches that of F-BAR(1) at the peripheral membrane; however, depolymerization of the actin cytoskeleton with cytochalasin-D reduces the mobile fraction coefficient of F-BAR(3) to that of F-BAR(1) in filopodia, and raises the mobile fraction coefficient of F-BAR(3) at the membrane. Additionally, these experiments revealed that the speed of F-BAR mobility relies on an intact F-actin cytoskeleton, since depolymerization of F-Actin by cytochalasin-D treatment significantly increased $t_{1/2}$ for all three F-BAR domains, both in filopodia and at the plasma membrane (**Fig. 3.4C,E**). Given the direct interaction of actin with the plasma

membrane (Raucher et al., 2000), it is possible that the effects of cytochalasin-D treatment on F-BAR domain mobility at the membrane are due to indirect effects on lipid diffusion rates. To rule out this possibility, we performed the same FRAP experiments with the PH domain of PLC δ 1, which specifically binds PI(4,5)P $_2$. This analysis revealed two interesting differences in the molecular dynamics of F-BAR and PH domains. First, the PH domain displays significantly faster molecular dynamics (both increased mobile fraction and decreased $t_{1/2}$). Second, Cytochalasin-D-mediated actin depolymerization did not affect the mobile fraction coefficient or $t_{1/2}$ of the PH domain either inside filopodia or at the plasma membrane (**Fig. 3.4**). These results reveal two important new features regarding the molecular dynamics of these F-BAR domains in filopodia: (i) the molecular dynamics correlate well with the efficiency of each F-BAR domain to induce filopodia (i.e. F-BAR(2)>F-BAR(3)>F-BAR(1)), and (ii) the rate of intracellular mobility of the F-BAR domains is partially-dependent on F-actin.

3.2.5 Lipid specificity varies between the F-BARs of srGAP proteins

All BAR-like domains, including F-BAR and I-BAR domains, bind to the plasma membrane through electrostatic interactions to negatively charged phospholipids, such as PI(4,5)P $_2$ (Itoh et al., 2005; Mattila et al., 2007; Peter et al., 2004; Saarikangas et al., 2009), and/or the presence of an amphipatic helix (wedge loop) directly inserting into the phospholipid bilayer (Saarikangas et al., 2009; Wang et al., 2009). Membrane-binding proteins can be removed from the membrane in a variety of ways, such as exposure to salt solutions (e.g. weaker interactions can be disrupted by lower salt concentrations). Different lipids compositions can also be separated using different detergent solutions (London and Brown, 2000). Western blots of lysates expressing F-BAR(1), F-BAR(2), and F-BAR(3) reveal different affinity for triton-insoluble lipids and proteins. To test this, cells were lysed in a two-step process, first with a low-stringency triton-X-containing buffer, then the supernatant was removed, and the insoluble pellet was subjected to a higher-stringency

modified RIPA buffer and sonicated. Molecular components of the triton-insoluble fraction contain lipids found in lipid rafts, which are highly enriched for cholesterol and sphingolipids (London and Brown, 2000), as well as phosphatidylethanolamine (PE), phosphatidylcholine (PC), phosphatidylserine (PS), and phosphatidylinositol (PI) (Rouquette-Jazdanian et al., 2002). F-BAR(1) and F-BAR(3) have a 32-fold and 7.4-fold higher affinity for the triton-insoluble fraction, respectively, while F-BAR(2) is reduced to 0.6-fold that found in the triton-soluble fraction (**Fig. 3.5A**).

Recently, Carlson et al. (2011) reported that F-BAR(3) relies on PI(4,5)P₂ for its membrane-binding. Membrane localization was reduced with the coexpression of the PI(4,5)P₂-specific 5-phosphatase, Inp54p; however, constitutive Inp54p expression has been shown to negatively effect cell morphology and health, causing cell rounding and a loss of protrusions (Raucher et al., 2000). Although recombinant F-BAR(2) domain binds PI(4,5)P₂, it also binds several negatively-charged phosphoinositides, as well as PS (**Fig. 3.5B** and **Suppl. Fig 3.3**).

Given the high degree of homology between F-BAR(2) and F-BAR(3), and that PI(4,5)P₂ is the most abundant form of phosphorylated PI at the plasma membrane of many mammalian cells (Mitchell et al., 1986; Tran et al., 1993), we next tested if PI(4,5)P₂ is required for the maintenance of F-BAR localization to the plasma membrane in situ by employing an acute, rapamycin-inducible method of depleting PI(4,5)P₂ from the membrane (Varnai et al., 2006). This method allows for temporal control of PI(4,5)P₂ depletion and can avoid some of the consequences of constitutive PI(4,5)P₂ depletion (Raucher et al., 2000). Briefly, addition of rapamycin induces binding of the membrane-targeted FKBP-rapamycin-binding (FRB) domain to the FK506 binding protein (FKBP) domain, thereby recruiting Venus-FKBP-Inp54p, a PI(4,5)P₂-specific 5-phosphatase, to the plasma membrane where it dephosphorylates PI(4,5)P₂ into PI(4)P (Varnai et al., 2006) (**Fig. 3.5C-U**). Prior to rapamycin treatment, the FRB domain (**Fig. 3.5D,J,P**) and PH domain of PLD δ 1 (**Fig.**

3.5F), F-BAR(2) (**Fig. 3.5L**), and F-BAR(3) (**Fig. 3.5R**) are localized to the plasma membrane, while the FKBP12-Inp54p fusion (**Fig. 3.5E,K,Q**) is in the cytoplasm. Upon rapamycin treatment, the FKBP12 domain binds the FRB domain, translocating the phosphatase to the membrane (**Fig. 3.5H,N,T**). The depletion of PI(4,5)P₂ results in the translocation of the PI(4,5)P₂ binding partner, the PH domain of PLC δ 1, from the plasma membrane to the cytoplasm (**Fig. 3.5I**); however, PI(4,5)P₂ depletion is not enough to remove F-BAR(2) from the plasma membrane (**Fig. 3.5O**), as it remains bound after rapamycin treatment. In contrast, F-BAR(3) is significantly reduced at the plasma membrane following rapamycin treatment (**Fig. 3.5U**). These results strongly argue that F-BAR(2) and F-BAR(3) display different requirement for PI(4,5)P₂ for their membrane localization, and in particular, that F-BAR(2) relies on other negatively-charged phosphoinositides or other mechanisms for its membrane localization.

3.2.6 F-BAR(1) constrains cellular protrusions in cortical neurons, whereas F-BAR(2) and F-BAR(3) induce protrusions

We have previously shown that the activation of full-length srGAP2 varies between COS7 cells and cortical neurons (Guerrier et al., 2009); therefore, we wanted to compare the activities of these three F-BAR domains in cortical neurons. Mouse embryos were harvested and subjected to ex utero electroporation following injection of plasmid DNA into the lateral ventricles at Embryonic day 15.5 (E15.5) (described in Hand et al., 2005). Dorsal telencephalic progenitors were immediately dissociated, plated. At 24 hours in vitro (24 hiv), these immature neurons display high levels of lamellipodial and filopodial dynamics (Stage 1), processes that precede and are required for neurite initiation (Guerrier et al., 2009; Dent et al., 2007). The activities of the F-BAR domains of srGAPs diverge between COS7 cells and primary cortical neurons, most strikingly for srGAP1. Neurons electroporated with each of the three F-BAR domains contain more filopodia than control GFP-containing neurons (**Fig. 3.6A-D**, quantified in **3.6E**); however, F-BAR(1) localizes

very distinctly to areas of the plasma membrane that lack protrusions (arrowhead in **Fig. 3.6B**), whereas F-BAR(2) and F-BAR(3) localize to sites of filopodial and lamellipodial protrusions (**Fig. 3.6C,D**). Quantification reveals that areas of the plasma membrane where F-BAR(1) is found contains significantly less filopodia than areas of the plasma membrane that lack F-BAR(1), and vice versa for F-BAR(2) and F-BAR(3) (**Fig. 3.6F**). The trend is the same for F-BAR(1) and F-BAR(2) in lamellipodial protrusions, but reversed for F-BAR(3) (**Fig. 3.6G**).

To confirm these static analyses, we performed time-lapse confocal imaging of GFP-tagged F-BARs co-electroporated with F-Actin probe (LifeAct-mRFP_{pruby}; Riedl et al., 2008) into E15.5 cortical neuronal progenitors, then plated and cultured the neurons for 24hiv (**Fig. 3.7**). As we hypothesized, F-BAR(1) inhibits membrane protrusions and/or stabilizes plasma membrane. Strikingly, in neurons expressing F-BAR(1)-EGFP, filopodia-like F-actin-rich protrusions were only observed where F-BAR(1) is not present (**Fig. 3.7B-F**). F-BAR(2) coats the majority of the membrane, and induces the extension and retraction of neuronal F-actin rich filopodia (**Fig. 3.7J-R**); however, little to no ruffling activity occurred in the presence of F-BAR(2)-coated membrane. F-BAR(3) appears to have an intermediate phenotype between F-BAR(1) and F-BAR(2) in neurons. It induces a comparable number of filopodia to F-BAR(2), yet as seen for F-BAR(1), it is more often found in areas that do not contain lamellipodia (**Fig. 3.5D-F**). Analysis of membrane dynamics reveals both filopodia protrusions and ruffling activity coinciding with F-BAR(3) (**Fig. 3.7S-AA**). Taken together, these results demonstrate that in immature cortical neurons, F-BAR(1) restricts membrane protrusions and dynamics, while F-BAR(2) and F-BAR(3) domains induce filopodia protrusions through their membrane-deformation properties.

3.3 DISCUSSION

The functional characterization of BAR domain-containing proteins has expanded

quite rapidly over the past few years. Recently, Guerrier et al. (2009) found that the F-BAR domain of srGAP2 shares the functional properties of I-BAR domain activity, such as those contained in IRSp53 and Missing in Metastasis (MIM) (Mattila et al., 2007; Millard et al., 2007; Saarikangas et al., 2009) by inducing membrane protrusions, rather than making invaginations as observed with canonical F-BAR proteins (Frost et al., 2007; Itoh et al., 2005). Recent reports (Carlson et al., 2011) and reviews (Heath and Insall, 2008) describing the subclasses of F-BAR domain-containing proteins categorize srGAP family members into one functionally uniform subgroup; however, our work demonstrates discrete roles and intricate differences between each srGAP family members.

While the F-BAR domains of the srGAP family are all able to induce filopodia-like membrane protrusions to a greater extent than in control conditions, the degree to which these three domains induce such structures greatly varies. F-BAR(2) is much more potent at inducing protrusions than either F-BAR(1) or F-BAR(3) in COS7 cells, and F-BAR(1) actively restricts protrusive activity in cortical neurons. It is interesting to note that COS7 cells do not express endogenous srGAP1/2/3 proteins (**Fig. 3.S1E**), while cortical neurons express all three srGAP proteins in various combinations throughout development *in vitro* and *in vivo* (**Fig. 3.S1G**, Bacon et al., 2009). Bacon et al. (2009) demonstrated that srGAP3 mRNA appears to be the most highly expressed among srGAPs in the cortex at early developmental time points, followed closely by srGAP2, whereas srGAP1 is not significantly expressed until postnatal ages. We find similar expression levels in dissociated cortical neurons (**Fig. 3.S1G**). Interestingly, srGAP2 protein increases within a few days in culture, whereas srGAP3 remains relatively stable. However, immunohistochemical analysis of srGAP2 and srGAP3 in cortical neurons reveals no distinguishable difference in endogenous subcellular localization, with both proteins producing punctate staining throughout the cell body and protrusions (data not shown; Guerrier et al., 2009; Endris et al., 2011). Our data argue that the F-BAR domain expression may interact with

endogenous forms of these srGAP proteins, possibly explaining the different effects of these proteins when expressed in COS7 cells vs. cortical neurons. Given the high expression of endogenous srGAP3 in cortical neurons, this interaction could particularly explain the differences seen with F-BAR(3). In addition to differential expression of srGAP proteins between COS7 cells and neurons, cortical neurons display extensive filopodia dynamics during neurite initiation (Dent et al., 2007) as well as during spine formation (Yoshihara et al., 2009), whereas COS7 cells rarely display spontaneous filopodia formation (**Fig. 3.1A-A''**). These differences in native cytoskeleton composition and dynamics, as well as variance of membrane and cytoskeletal-related proteins, might also help to explain the differences we observed between F-BAR activities in these two cell types.

Recent analysis of srGAP3 (also called WAVE-1 Related Protein, WRP, and MEGAP) has shown that its F-BAR domain is involved in filopodia induction preceding spine morphogenesis (Carlson et al., 2011). However, the authors suggested that the F-BAR domain of srGAP3 is targeted to the plasma membrane through its ability to bind to PI(4,5)P₂ and PI(3,4,5)P₃. Our analysis shows a strikingly different pattern of phospholipid binding for the F-BAR domain of srGAP2, which seems to bind very broadly to negatively charged phospholipids, including six out of seven existing phosphoinositides, as well as phosphatidyl-serine (PS). In their analysis of the binding of F-BAR(3) to the membrane, Carlson et al. (2011) used a constitutively active PI(4,5)P₂ phosphatase, Inp54p, to reduce PI(4,5)P₂ levels at the plasma membrane; however, constitutive Inp54p expression leads to changes in cell shape due to PI(4,5)P₂-mediated alterations in the actin cytoskeleton from reduced interaction between the actin network and the plasma membrane (Raucher et al., 2000). Given the close interaction of many BAR-containing proteins with the cytoskeleton as well as with the plasma membrane, we wanted to look at the effects of acute PI(4,5)P₂ depletion on F-BAR membrane-binding. Our results demonstrate that acute depletion of

PI(4,5)P₂ has no effect on the targeting of F-BAR(2) to the plasma membrane, however it does affect F-BAR(3) localization. We did not find co-expression alone to be effective enough to reduce localization of F-BAR(3) (data not shown); however, the difference between the ability to induce translocation upon acute, inducible PI(4,5)P₂ depletion is clearly compatible with the lack of binding specificity of F-BAR(2) to PI(4,5)P₂, and suggests that the F-BAR domain of srGAP2 could bind to the plasma membrane through other negatively charged phospholipids, including PS. An interesting possibility exists that these proteins need the electrostatic charge interaction primarily for initial binding, and subsequently localization occurs through hydrophobic interaction such as the insertion of an amphipathic helix seen in N-BAR (Itoh and Camilli, 2006) and I-BAR domains (Saarikangas et al., 2009). While the F-BAR domain of srGAP3 does translocate after PI(4,5)P₂ depletion, the effect is less specific and more variable than with the PH domain of PLC δ 1. This variation, as well as the lack of translocation with F-BAR(2), could be accounted for by the broad lipid specificity, a physical insertion into the plasma membrane, or both.

Alternatively, F-BARs of the srGAP family could be tuned to differentially bind to a specific range of membrane curvature found at the plasma membrane, as previously shown for other BAR and F-BAR domains (Frost et al., 2007; Zhao et al., 2011). This could further explain the differential localization between the srGAP F-BAR domains within filopodial protrusions, where curvature varies along the base, neck, and tip of a filopodium. The molecular mechanisms underlying the differences in phospholipid-binding specificity between F-BAR(2) and F-BAR(3) are currently unknown, but might involve differences in electrostatic positive charge distribution (lysine and arginine residues) at the surface of these two F-BAR dimers; however, the structures of these F-BAR domains have yet to be solved, therefore, further experiments will be necessary to identify the precise molecular basis for these differences.

The molecular basis for self-assembly of this class of F-BAR domains is currently

unknown, however shorter F-BAR domains present in proteins such as FBP17, have been shown to interact through both 'end-to-end' interactions as well as 'side-to-side' interactions of individual dimers. These oligomers form a corkscrew-like helix that binds and tubulates membranes (Frost et al., 2008; Shimada et al., 2007; Wang et al., 2009). Based on combinations of in vitro cryo-EM, structural and bio-informatics modeling analysis, it was found that F-BAR and I-BAR proteins are able to form molecular assemblies inducing specific membrane topologies, ranging from membrane tubules to shallow membrane curvature (Frost et al., 2008; Wang et al., 2009), and even to planar membrane sheets (Pykäläinen et al., 2011). However, the mechanisms underlying F-BAR domain assembly in cells and the way they control membrane deformation and dynamics is currently unknown, and warrants further investigation. Our data show for the first time that the F-BAR domains of srGAP proteins display differential function and dynamics in both cell lines and primary neurons. These F-BAR domains display different lipid binding properties, as well as a clear F-actin-dependence for their intracellular mobility (**Fig. 3.S4**). Our data raises the possibility that F-BAR(1) and F-BAR(3), which have lower mobile fraction coefficients than F-BAR(2) in various conditions, could have a stronger association with the plasma membrane, and therefore aid in membrane stabilization, as opposed to membrane deformation. Our time-lapse data in neurons supports this hypothesis by revealing reduced membrane protrusions where F-BAR(1) is present at the plasma membrane, as well as reduced filopodial dynamics in transfected COS7 cells. Our results also point to the fact that the F-BAR domains of three srGAP proteins are able to interact and possibly heterodimerize, and that these three F-BAR domains act synergistically towards filopodia formation (**Figs 3.2, 3.3, 3.S4**). Overall, our results point to the unique function of the srGAP family of proteins, through their F-BAR domains, in inducing and regulating filopodia-like protrusions in neuronal and non-neuronal cells due to their ability to control membrane deformation.

3.4 MATERIALS AND METHODS

3.4.1 Plasmid constructs and sequence alignments

All srGAP constructs were cloned into a modified pCIG2 vector (Guerrier et al., 2009) with the IRES removed for GFP-, RFP-, or Myc-tagged C-terminal fusions. Lifeact-pRuby was subcloned from EGFP-N1 into the modified pCIG2 construct, using XhoI/NotI cut sites. srGAP constructs contain the following proteins and F-BAR truncations: human fulllength srGAP1(NP_065813.1), srGAP2(NP_056141.2), srGAP3(NP_001028289.1), or F-BAR truncations F-BAR(1) (AA 1-516), F-BAR(2) (AA 1-501), F-BAR(3) (AA 1-492). Constructs for rapamycin-induced PI(4,5)P₂ depletion, with the exception of F-BAR(2)-RFP and F-BAR(3)-RFP described above, were obtained from Tamas Balla (NICHD, Bethesda, MD USA) and Tobias Meyer (Stanford, Stanford, CA USA) and cloned into pcDNA3.1 by Sam Snider (Zylka Lab, UNC-Chapel Hill, NC USA). Protein phylogenetic tree prediction was created using GeneBee TreeTop (<http://www.genebee.msu.su/>). Amino acid conservation percentage determined by NCBI Blast tool. Sequence alignment was created using MultAlign (Corpet, 1988).

3.4.2 Cell culture

COS7 and HEK293 cells were plated onto poly-d-lysine (Sigma P0899) and maintained in Delbucco's Modified Eagle's Medium (DMEM, Sigma D6046) supplemented with 10% FBS (Foundation 900-108) and 1x Penicillin-Streptomycin (Pen/Strep, Gibco 15070-063). Cell culture transfections were performed twenty-four hours post plating, using Lipofectamine 2000 (Invitrogen 11668) according to manufacturer's instructions. Fixed cells were treated with 4% paraformaldehyde for 20 minutes, washed in PBS, permeabilized in 0.05% triton-X-100 in PBS, washed, and then blocked in 5% BSA (Sigma A6003) for 20 minutes. COS7 cells were then incubated with primary antibody [(anti-myc antibody 1:500, Cell Signaling 2276), (anti-GFP antibody 1:1000, Aves GFP-1020) or (anti-RFP antibody 1:1000, Invitrogen R10367)] in PBS with 0.2% BSA and 10% Normal Goat Serum overnight

at 4°C. Cells were washed in PBS and incubated with secondary antibody [(goat anti-chicken Alexafluor-488 (1:1000, Invitrogen A11039), goat anti-rabbit Alexafluor-546 (1:1000, Invitrogen A11035), Alexafluor-546 phalloidin (1:200, Invitrogen A22283), Alexafluor-647 phalloidin (1:200, Invitrogen A22287), or DRAQ5 (1:10000, Fisher NC9165029)] for two hours at room temperature. Finally, cells were then washed in PBS and mounted with Biomedica Mounting Media (Fisher NC9034735).

Primary neuronal cultures were plated onto poly-d-lysine/laminin (Sigma L2020) and maintained for 24 hours in Neurobasal-A (Invitrogen 10888-022) supplemented with 1x Pen/Strep, L-glutamine (Gibco 25030-081), 1x B-27 (Gibco 17504044), and N2 (Gemini 400-163). Cortical neurons were transfected prior to dissociation via ex vivo electroporation at E15.5, according to Hand et al., (2005). Neurons were fixed for 10 min at 24 hours after plating, using a 1% glutaraldehyde solution in PHEM buffer (pH 6.9; 60 mM PIPES, 25mM HEPES, 10 mM EGTA, and 2 mM MgCl₂) to preserve cytoskeletal integrity (Kaeck et al., 1997). The rest of the staining protocol is the same as used for COS7 cells, with the primary antibodies anti-GFP (Invitrogen A11122) and anti-Tubulin (Covance MMS-435P-100), and secondary antibodies goat anti-rabbit Alexafluor-488 (Invitrogen 11034), Alexafluor-546 phalloidin, and goat anti-mouse Alexafluor-647 (Invitrogen A21235).

To determine filopodia number, fixed cells were imaged using LEICA TCS SL confocal microscope, 63x/1.4NA oil immersion objective. 2x zoomed images were taken of representative cells from each construct. Images were then imported to NIH ImageJ. Using the line tool, a perimeter was drawn around the cells. The presence of filopodia was determined by counting the number of consecutive pixels on the line drawn around the cell perimeter and normalized by dividing the total number of filopodia by the cell perimeter (filopodia/microns). Protein extension into filopodia was determined using NIH ImageJ software to draw a line from the base to the tip of the filopodium, and measure fluorescence intensity of each fluorescence channel.

3.4.3 Live cell imaging

Live cell imaging of COS7 cells, HEK293 cells, and neuronal cultures were imaged using Leica TCS confocal microscope with either 20x objective, or 63x/1.4NA oil immersion objective, with 37 °C stage warmer. COS7 cells were imaged in their culture media at 12 second intervals. The path of filopodial tips was traced over time using NIH ImageJ software to obtain quantification of filopodial dynamics ($\mu\text{m}/\text{min}$). Culture media was removed from HEK cells prior to imaging, and replaced with 37°C Hank's Balanced Salt Solution (HBSS, Gibco 14025) supplemented with 0.24% HEPES (Fisher BP310), 0.2% dextrose (Fisher D16), and 0.1% BSA (Sigma A6003). Images were taken before and after 1 μM rapamycin (Calbiochem 553212) in supplemented HBSS solution was added to the cells. Membrane to cytoplasm ratio in pre- and post-ramapycin-treated cells was measured in HEK cells expressing all three constructs, using NIH ImageJ software. Neuronal cultures were imaged in their culture media, at 12-second intervals.

Live cell imaging for FRAP experiments was performed with a PLAPO 60x/1.42 objective (Olympus, Inc.) on an Olympus FV1000 confocal microscope, equipped with a plastic cage incubator (Presicion Plastics, Inc., MA, USA) maintained at 37 °C with 5% CO₂ and 60% humidity to prevent media evaporation. To measure fast fluorescence dynamics in single filopodia images of 256x256 pixels were taken at 36x zoom with pixel dwell time of 2 μs . A rectangular shape bleach area of a fixed width ($\sim 0.4 \mu\text{m}$) was drawn across the filopodia or a membrane region, 20 prebleach frames acquired with a 488 excitation laser (multiline Argon laser) attenuated to 0.7% to minimize photobleaching of the sample, followed by 300 ms bleaching with the same laser operated at full power. The recovery was then measured at the speed of $\sim 0.5 \text{ s}/\text{frame}$ with the 488 laser, operated at the same 0.7% transmission as for the prebleaching acquisition. For cytochalasin-D treatments, COS7 cells were transfected with F-BAR constructs and cultured for 48 hrs. Cells were then treated with 200 μM cytochalasin D (Sigma C2873) for 1 hour prior to

imaging. To observe the presence of F-actin, cells were fixed post-imaging and stained with phalloidin as previously stated. Fluorescence intensity curve from FRAP imaging was then analyzed with the Igor Pro 6.12A (Wavemetrics, Inc.) using the K_FRAPcalc v9 procedure developed by Dr. Kota Miura (EMBL).

3.4.4 Biochemistry

Western blots were run from COS7 cells transfected with either tagged F-BAR, or full-length srGAP constructs, treated with Ripa Buffer (50 mM Tris, pH 7.4, 1% Triton-X-100, 0.25% Sodium Deoxycholate, 0.1% SDS, 1 mM EDTA, 150 mM NaCl, 1x Complete Protease Inhibitor Cocktail (1x, Roche), 1mM PMSF) 24 hours post transfection. Lysates were run through 4-12% NuPage gels (Invitrogen NP0321) and transferred to PVDF membrane (Amersham RPN303F), which was then blocked with 5% dry milk (Carnation) in TBS-T. Primary [(anti-srGAP1 1:1000, Abcam ab57504), (anti-srGAP2 A2 and anti-srGAP3 A1 1:1000, gifts from Wei-Lin Jin lab, Univ. Shanghai), (anti-GFP 1:1000, Invitrogen A11122), and (anti-Actin 1:5000, Millipore MAB 1501)], and secondary antibodies [(donkey anti-rabbit IRDye 800, Li-cor Biosciences 926-32213) or (donkey anti-mouse IRDye 680, Licor Biosciences 926-32222)] were incubated in 3% dry milk in TBS-T.

Co-immunoprecipitations were obtained from double-transfected cells, treated with co-immunoprecipitation buffer (50mM Tris-Cl pH 7.4, 15 mM EGTA, 100 mM NaCl, 0.1% Triton-X 100, protease inhibitor, 1 mM DTT, and 1mM PMSF) 24 hours after transfection. Incubations and washes were performed in the same buffer. 10% of lysis volume was collected prior to antibody incubations for input controls. The rest of the co-immunoprecipitation lysis was subjected to the immunoprecipitation antibody [(1 µg anti-GFP, Invitrogen A11122, or 1 µg anti-IgG control antibody)] bound to protein A/G beads (Santa Cruz 2003), washed, and dissociated with SDS Loading Buffer at 95°C. The two-step lysis buffer to analyze triton-soluble and triton-insoluble fractions were first subjected to the co-immunoprecipitation buffer described above. The lysates were then centrifuged

at 15000 rpm for 20 minutes. The supernatant was removed and used for the triton-soluble fraction. The insoluble pellet was then subjected to a modified RIPA buffer (50 mM Tris pH 7.4, 0.5% Na Deoxycholate, 0.2% SDS, 1 mM EDTA, 150mM NaCl, 1mM PMSF, and 1x protease inhibitor), sonicated briefly, and spun at 15000 rpm for 10 minutes. The supernatant was removed and used for the triton-insoluble fraction. Western blots were run as described before, using anti-GFP, anti-RFP, or anti-Myc primary antibodies, and anti-mouse and anti-rabbit antibodies described above. Western blots were imaged on the LI-COR Odyssey Infrared Imaging System.

Immobilized lipids were spotted onto PIP Strip membranes (Molecular Probes P23750) and treated according to manufacturer's instructions. Briefly, the PIP Strip membrane was blocked with 3% BSA/TBS-T (Sigma A6003), incubated with 0.5 µg/ml purified F-BAR(2) (AA 1-480, purified by Holger Sondermann's lab, Cornell University, Ithaca, NY, USA) in 3% BSA/TBS-T for 1 hour at room temperature, washed in TBS-T, incubated with primary antibody (anti-srGAP2 A1 1:1000, gift from Wei Lin Jin, Shanghai Univ., China), washed in TBS-T, incubated with secondary antibody (goat anti-rabbit IRDye800), washed, and developed using the LI-COR Odyssey Infrared Imaging System.

3.5 FIGURE LEGENDS

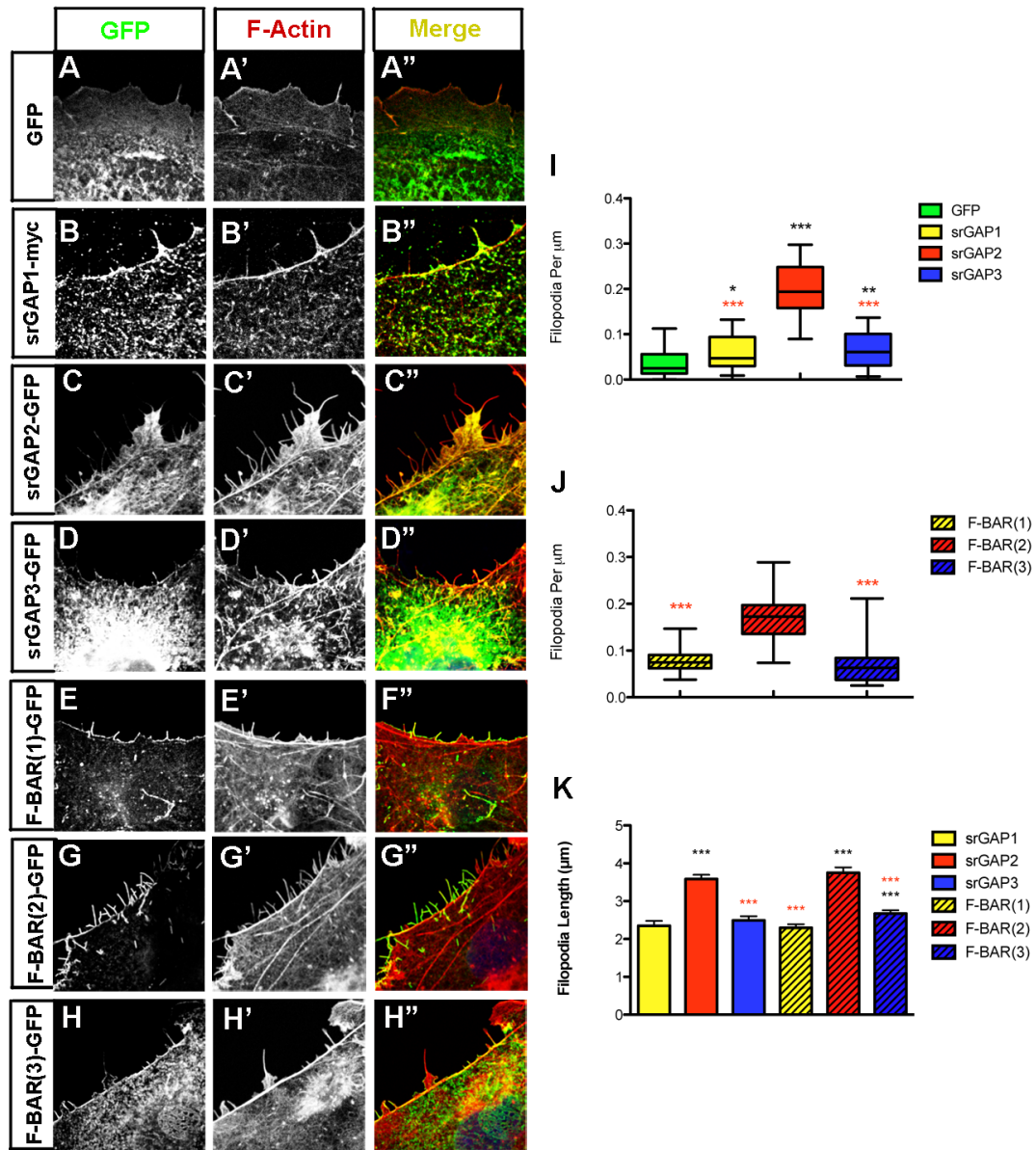


Figure 3.1. srGAP2 induces significantly more filopodia than srGAP1 or srGAP3. (A-H'') COS7 cells expressing EGFP only (A'A''), EGFP-tagged full-length srGAP1 (B-B''), srGAP2 (C-C'') or srGAP3 (D-D''), or their respective F-BAR domains (E-H'') were counterstained with phalloidin for F-actin (A'-H') in red. (I-J). Quantification of the effects described in A-H'' (n>25 cells). (K) srGAP2 and its F-BAR domain (F-BAR(2)) induce significantly longer filopodia than full-length srGAP1, srGAP3, or their respective F-BAR domains (n>200 filopodia; p<0.0001). Quantifications were taken from at least three independent experiments and analyzed using non-parametric Mann-Whitney Test. Black asterisks indicate comparison to EGFP and red asterisks indicate comparison to srGAP2-EGFP or F-BAR(2)-EGFP.

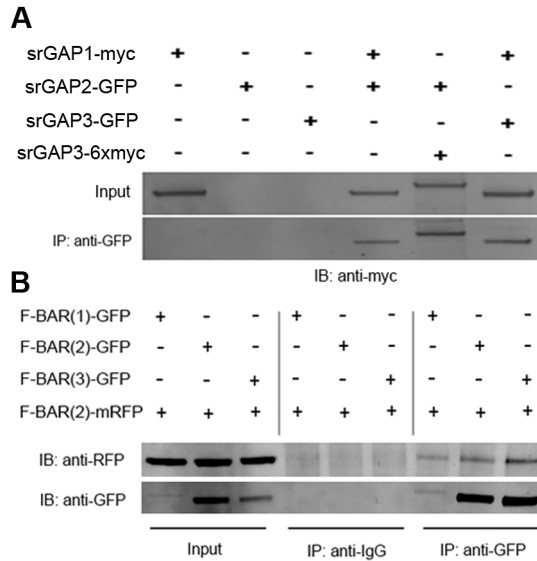
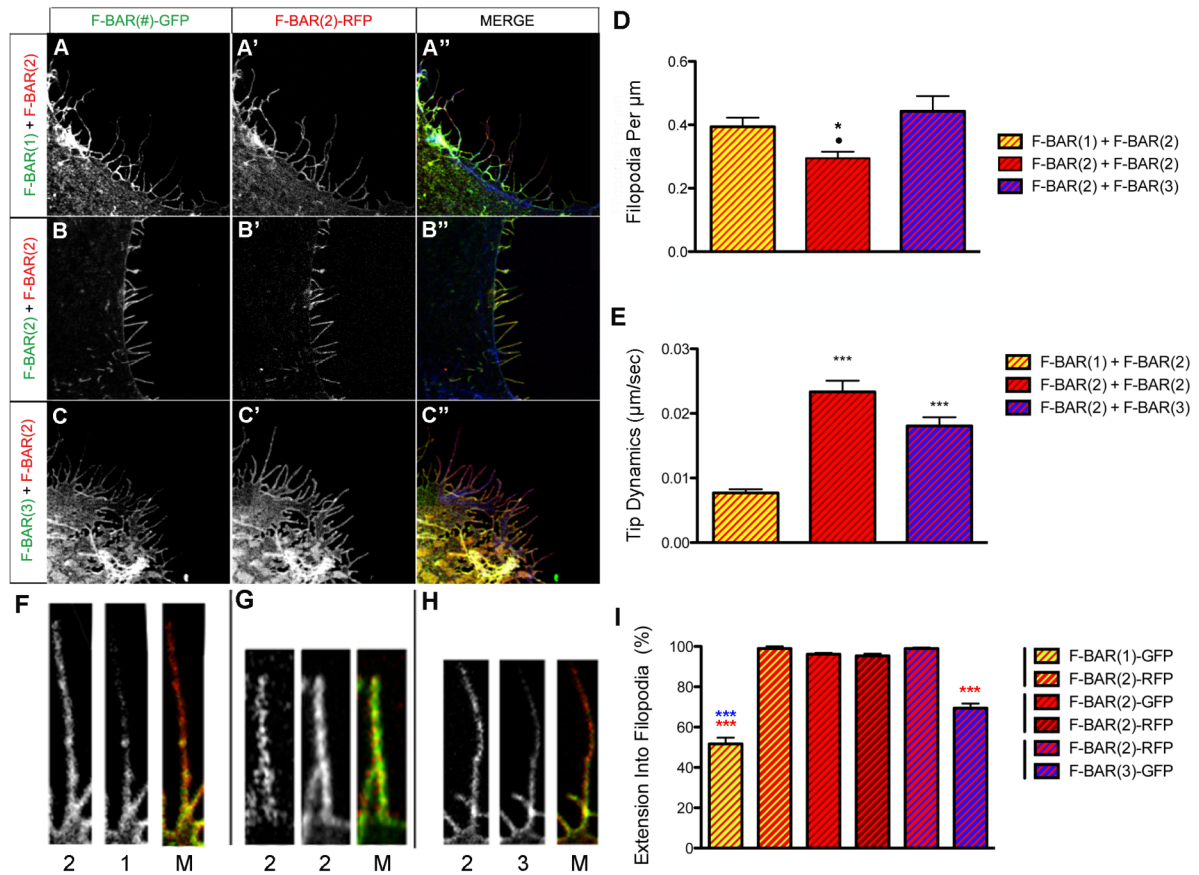


Figure 3.2. srGAP proteins interact through their F-BAR domains.

(A) Combinations of EGFP- and myc-tagged full-length srGAP proteins were co-expressed in COS7 cells, immunoprecipiated (IP) with anti-GFP, and immunoblotted (IB) with anti-myc. Single-transfected control lysates demonstrate the specificity of the rabbit anti-EGFP and mouse anti-myc antibodies. Every combination of the three srGAP proteins was able to co-immunoprecipitate. (B) EGFP-tagged F-BARs(1-3) were co-expressed with mRFP-tagged F-BAR(2) in COS7 cells. Cells lysates were incubated and immunoprecipitated with either rabbit anti-IgG control antibody or rabbit anti-EGFP antibody, and immunoblotted for either rabbit anti-RFP antibody or mouse anti-GFP antibody. All three EGFP-tagged F-BAR domains co-immunoprecipitated with F-BAR(2)-mRFP.



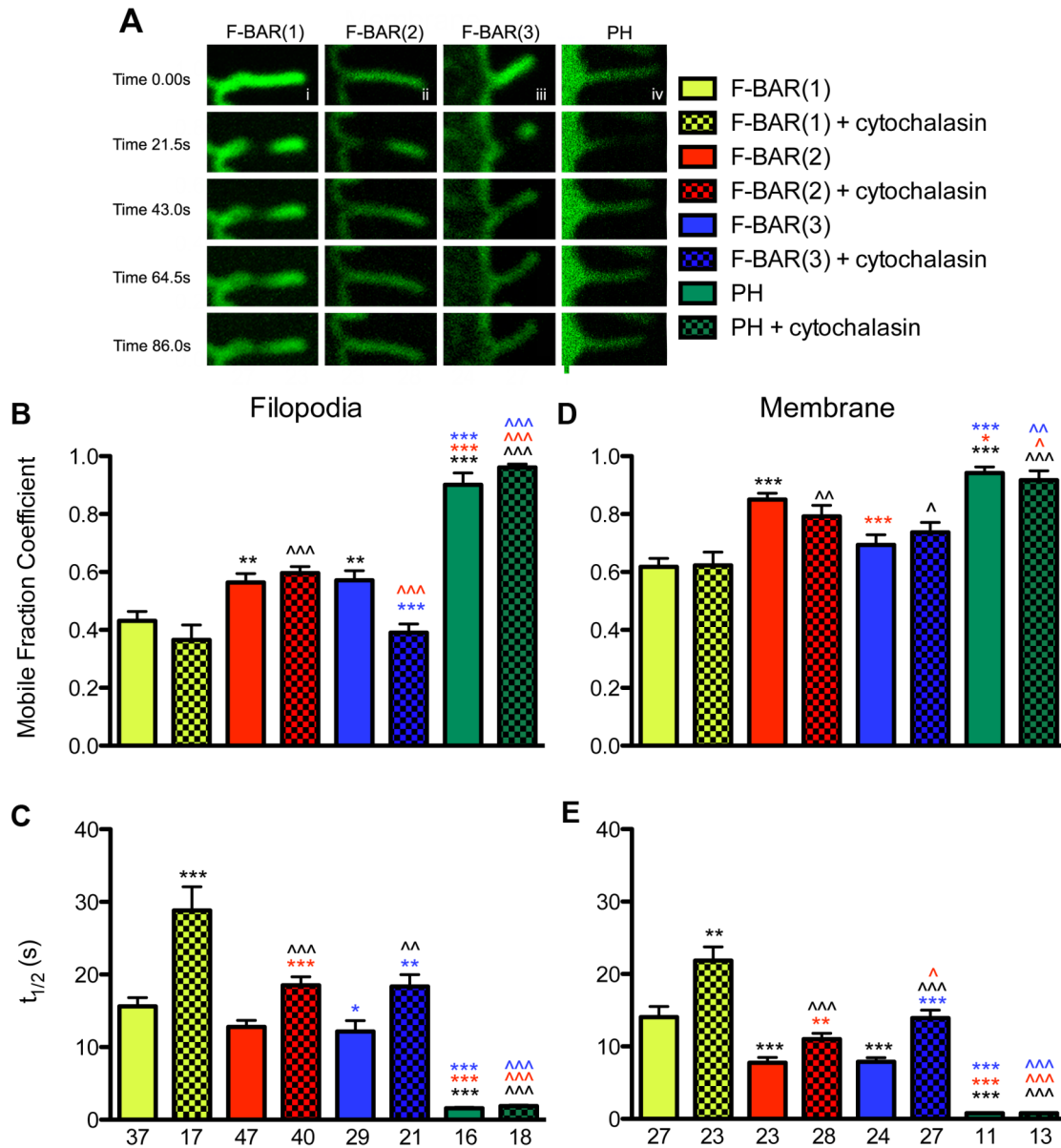


Figure 3.4. The three F-BAR domains of srGAP proteins differ in their subcellular molecular dynamics.

(A) FRAP analysis of EGFP-tagged F-BAR(1) (i), F-BAR(2) (ii), F-BAR(3) (iii), and PH domain of PLC δ 1 (iv) in filopodia protrusions. The same analyses were performed at the peripheral membrane of the cell. (B-E) Quantification of the mobile fraction coefficient (B,D) and half-time of recovery ($t_{1/2}$; C,E) in filopodial protrusions (B-C) and at the peripheral plasma membrane (D-E). Cells were either imaged as untreated controls, or treated with cytochalasin-D for depolymerization of the actin cytoskeleton. Significance compared to untreated controls are marked by asterisks (*), and significance to cytochalasin-treated samples is marked with a caret (^). Significance is color-coded with black for F-BAR(1), red for F-BAR(2), and blue for F-BAR(3). n for each condition is marked below the bottom graph for filopodial and membrane, and is the same for mobile fraction and $t_{1/2}$ at each location. $^*/\wedge p < 0.05$, $^{**}/\wedge\wedge p < 0.005$, $^{***}/\wedge\wedge\wedge p < 0.0005$

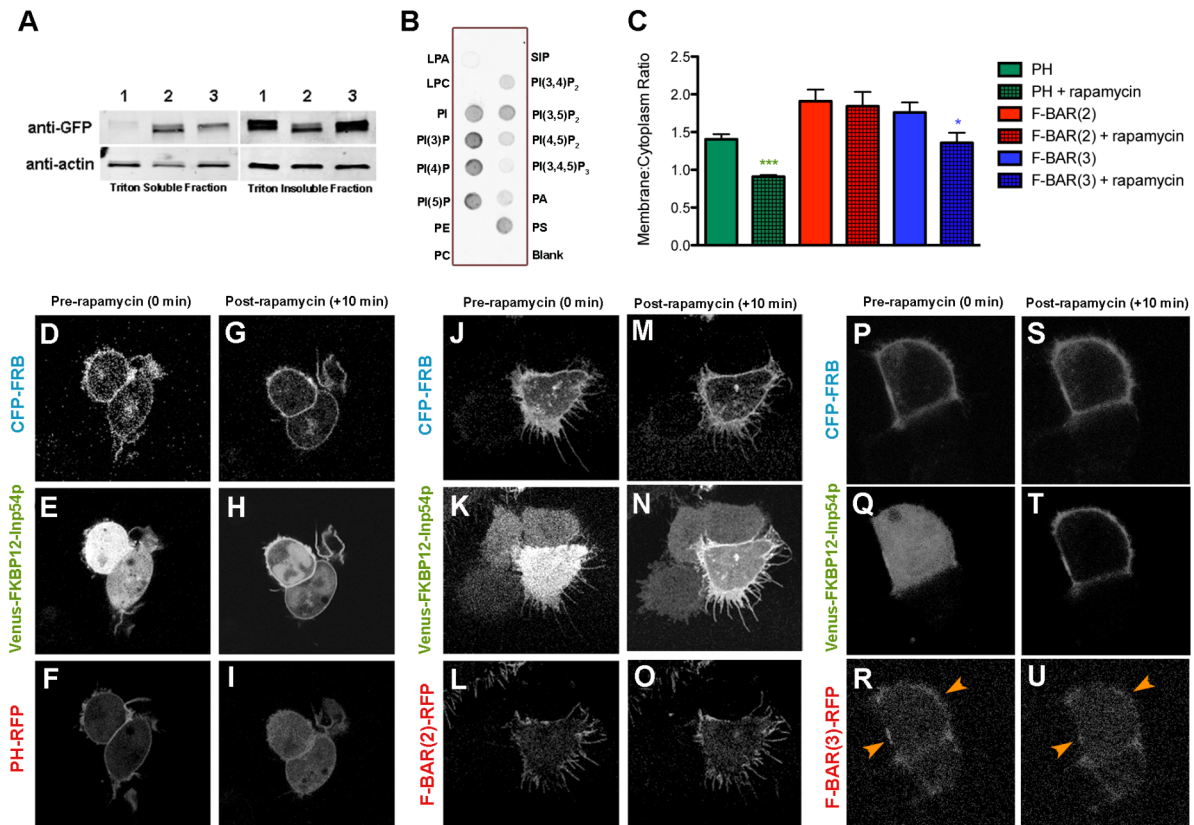


Figure 3.5. F-BAR(2) binds multiple negatively-charged phospholipids

(A) Western blot depicting F-BARs found in two separate fractions, a triton-soluble and triton-insoluble. F-BAR(1) is 32-fold higher expressed in the triton-insoluble fraction, while F-BAR(2) is slightly reduced in this fraction (0.6-fold), and F-BAR(3) is more highly expressed in the insoluble fraction (7.4-fold). (B) Binding of F-BAR(2) to immobilized phospholipids on nitrocellulose membrane (PIP Strip, Molecular Probes). Membrane was incubated with recombinant F-BAR(2) (amino acids 1-480) and subsequently immunoblotted with an antibody to srGAP2. LPA, lysophosphatidic acid; LPC, lysophosphatidylcholine; PE, phosphatidylethanolamine; PC, phosphatidylcholine; SIP, sphingosine 1-phosphate; PA, phosphatidic acid; PS, phosphatidylserine. (C) Quantification of pixel intensity of membrane to cytoplasmic localization pre- and post-rapamycin treatment (n=15-16). (D-U) Representative images of HEK293 cells triple-transfected with CFP-FRB, Venus-FKBP12-Inp54p, and RFP-PH domain of PLC β 1 (D-I), F-BAR(2)-RFP (J-O), or F-BAR(3)-RFP (P-U) both pre- (C-E, I-K, P-R) and post-rapamycin treatment (F-H, L-N, S-U). Asterisks demonstrate difference between pre- and post-rapamycin membrane to cytoplasmic ratios of the same condition. *p<0.05, ***p<0.001

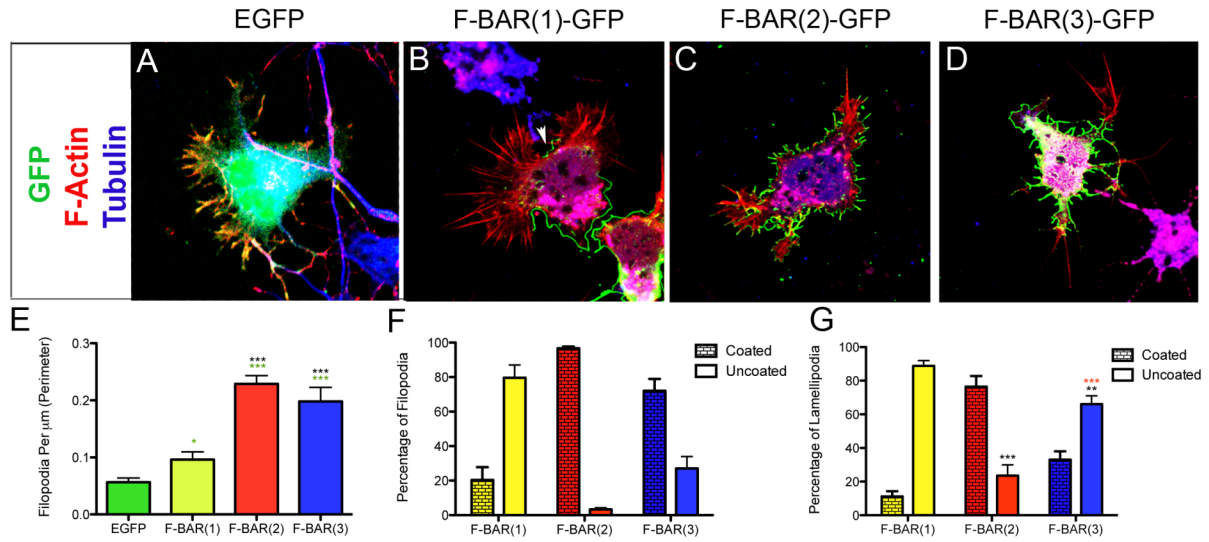


Figure 3.6. F-BAR domains of srGAP proteins differ in their ability to induce filopodia in cortical neurons.

(A-D) E15.5 cortical neurons expressing EGFP (A) or EGFP-tagged F-BAR(1) (B), F-BAR(2) (C), or F-BAR(3) (D) were cultured for 24hours in vitro (hiv) after ex vivo electroporation, fixed and stained with F-Actin marker phalloidin (red) . (E) Cells with any of the three F-BARs contain more filopodia than GFP alone, though F-BAR(2) and F-BAR(3) induce significantly more filopodia than F-BAR(1). (F-G) Quantifications of the percentage of plasma membrane in filopodia (F) or lamellipodia (G) that is coated or uncoated with F-BAR protein. Quantifications were performed on at least three independent cultures and analyzed using Mann-Whitney Test (** p<0.01, *** p<0.001; n>20 neurons). Black asterisks illustrate comparison against F-BAR(1), while red asterisks indicate difference from F-BAR(2).

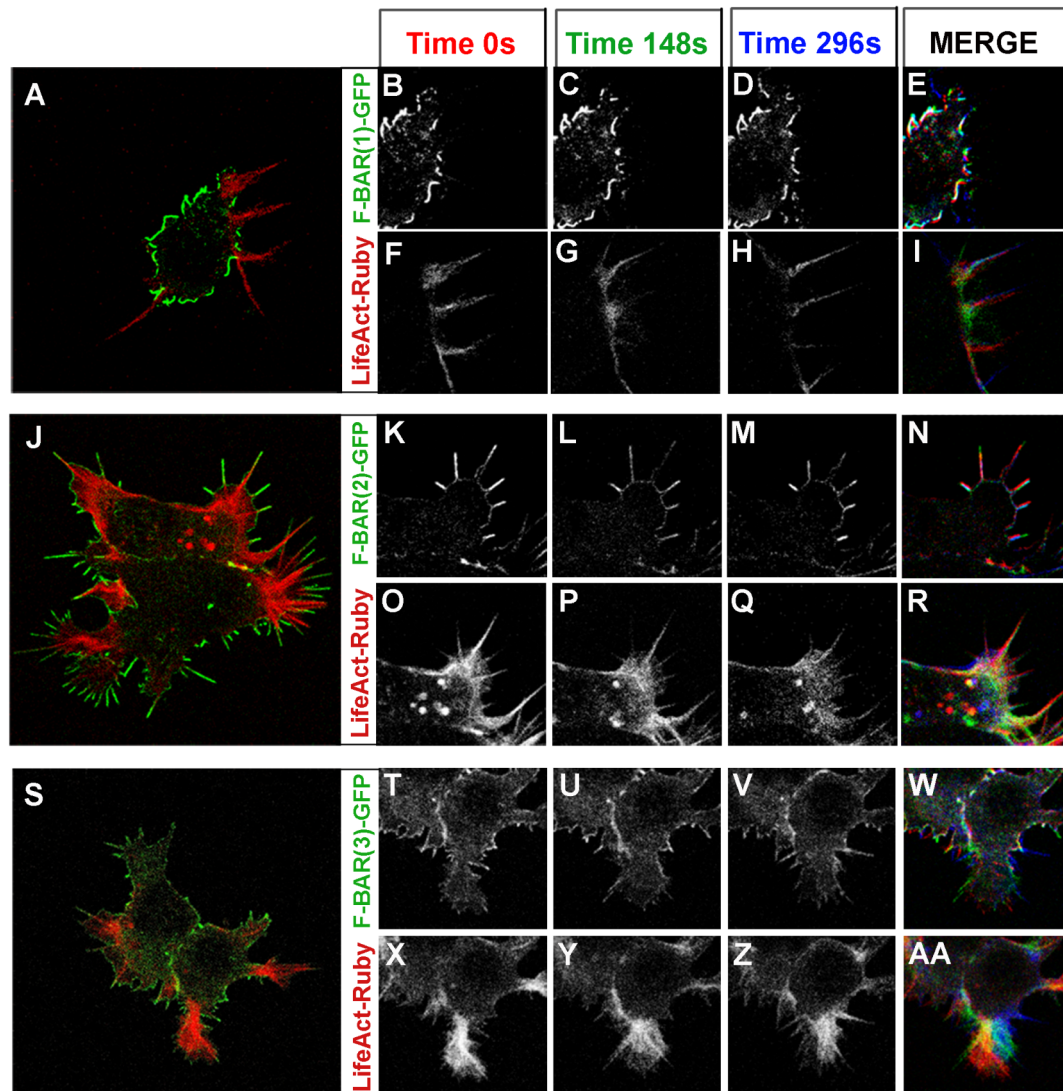


Figure 3.7. Real-time imaging of membrane and F-Actin dynamics induced by F-BAR domains in cortical neurons

E15.5 cortical neurons expressing the F-Actin probe LifeAct-mRFPruby (red) and GFP-tagged F-BAR(1) (A-I), F-BAR(2) (J-R), or F-BAR(3) (S-AA) following ex vivo electroporation and 24h in dissociated culture. GFP and mRuby channels are shown separately for ease of visualization (see also MovieS1-3). Images from time series taken at 0, 148, and 296 seconds are pseudocolored in red, green, and blue, respectively. White overlay in merge panel indicates limited spatial dynamics throughout the movie. (A) Whole-cell image of F-BAR(1)-EGFP- and LifeAct-mRFPruby-co-expressing cortical neuron. (B-I) F-BAR(1)-coated membrane shows little to no spatial dynamics (B-E); however, dynamic neuritic protrusions can be visualized with LifeAct-mRFPruby at sites of ‘breaks’ in F-BAR(1)-GFP coated plasma membrane (F-I). (J) Whole-cell image of F-BAR(2)-EGFP and LifeAct-mRFPruby co-expressing neuron. (K-R) F-BAR(2)-coated membrane displays rapid extension and retraction of filopodia protrusions (K-N), although F-Actin dynamics are largely confined to the area within the F-BAR(2)-coated membrane (O-R). (S) Whole-cell image of F-BAR(3)-EGFP and LifeAct-mRFPruby co-expressing cortical neuron. (T-AA) F-BAR(3)-GFP-coated membrane presents numerous sites of filopodia-like membrane dynamics (arrowhead in T-AA).

3.6 SUPPLEMENTARY FIGURE LEGENDS

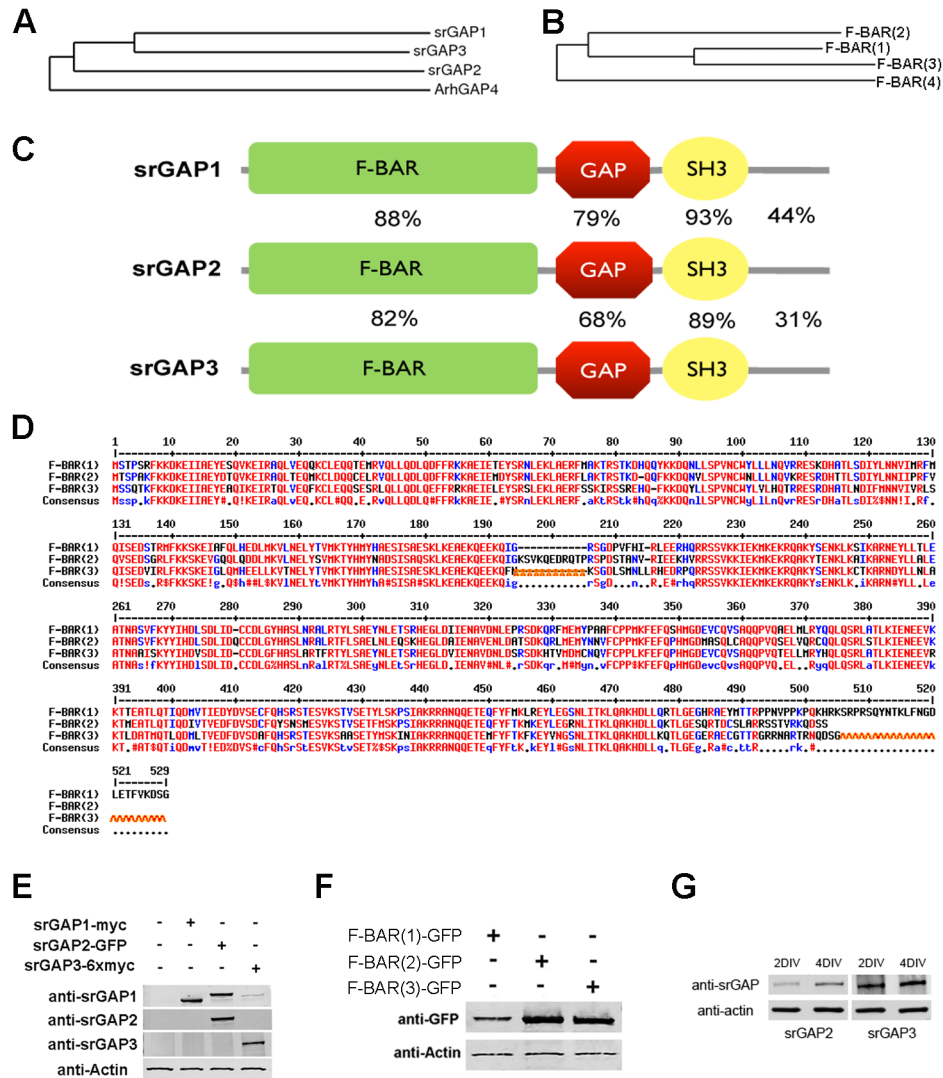


Figure 3.S1. Conservation and alignments of the srGAP family of proteins

(A-B) Phylogenetic tree illustrating the evolutionary conservation of human full-length srGAP1 (*NP_065813.1*), srGAP2 (*NP_056141.2*), srGAP3 (*NP_001028289.1*), and srGAP4/ArhGAP4 (*NP_001158213.1*) (A), and F-BAR(1) (AA 1-516), F-BAR(2) (AA 1-501), F-BAR(3) (AA 1-492), and F-BAR(4) (AA 1-557). (B). (C) Domain structure of human full-length srGAP1, srGAP2, and srGAP3. Percentages indicate conserved amino acids in the sequence of each domain of srGAP1 and srGAP3, compared to the same domain in srGAP2. (D) Sequence alignment of F-BARs (1-3). Red asterisks point out a sequence specific insertion (AA 197-207) in srGAP2, and red carets denote an insertion (AA493-516) in srGAP1. (E-F) Expression of srGAP1-myc, srGAP-GFP, and srGAP3-6xmyc fusion proteins (E) and F-BAR-GFP fusion proteins (F) to illustrate proper expression and detection of srGAP proteins. The commercially available anti-srGAP1 antibody recognizes all three full-length proteins, and therefore was not used for the remainder of the study. Untagged srGAP protein bands appear at the same molecular weight in Western blot (data not shown). (G) srGAP2 levels in E15.5 cortical neurons cultured for 2 and 4 days in vitro.

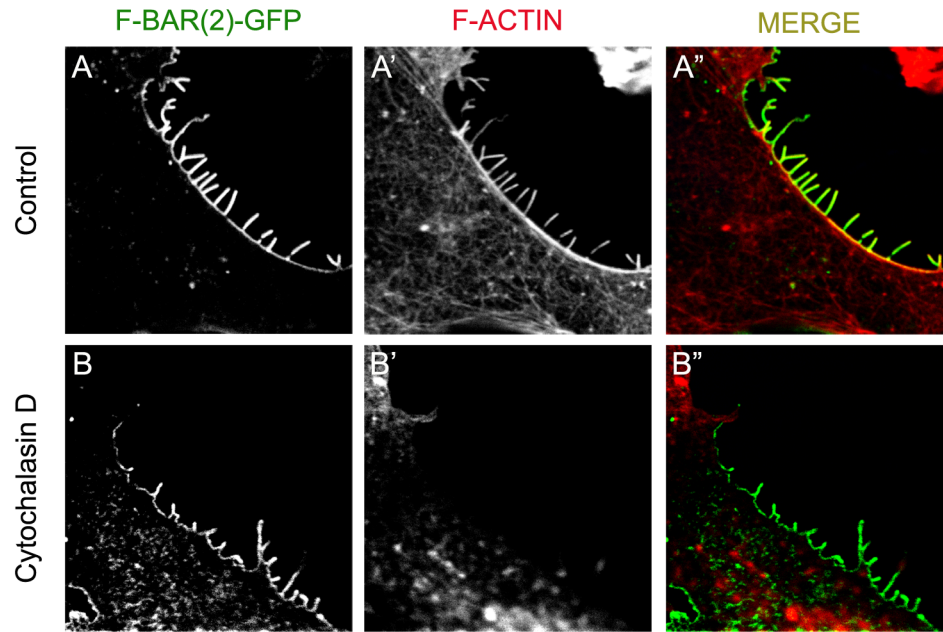


Figure 3.S2. The F-Actin network is disrupted after cytochalasin-D treatment. (A-A'') Control COS7 cell used for FRAP experiments. This cell, transfected with F-BAR(2), displays a normal, intact F-actin network when stained with phalloidin. (B-B'') Validation of F-actin depolymerization after cytochalasin-D treatment in a COS7 cell used in FRAP experiments.

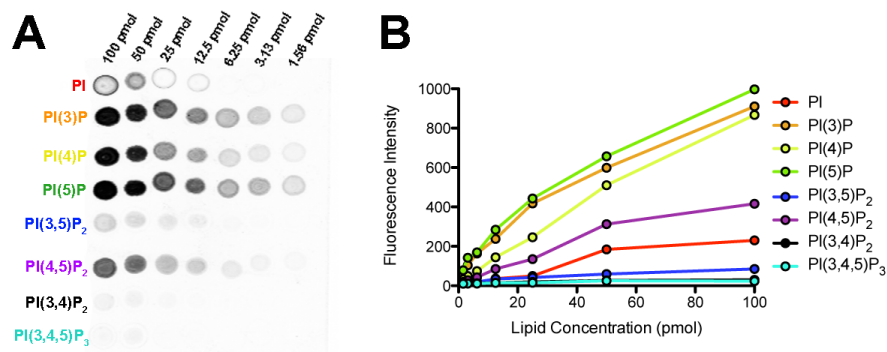


Figure 3.S3. Dose-dependent binding of F-BAR(2) to various phosphoinositides.

(A) PIP array showing lipid-binding specificity of recombinant F-BAR(2) for different concentrations of phosphorylated phosphatidylinositol (PI). **(B)** Quantification reveals that F-BAR(2) strongly binds to singly-phosphorylated species of PI, has intermediate association with PI(4,5)P₂ and PI, and low affinity for PI(3,5)P₂, PI(3,4)P₂, and PI(3,4,5)P₂

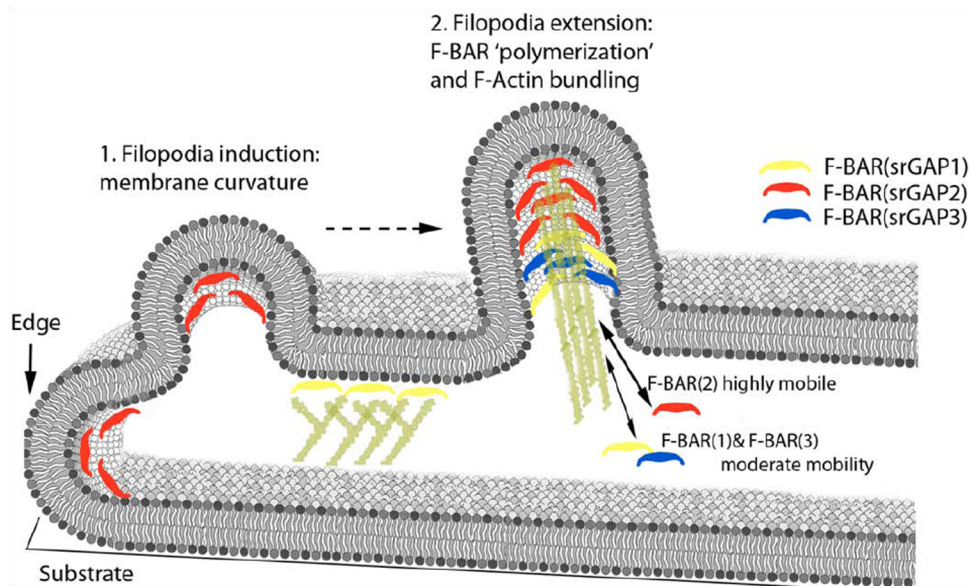


Figure 3.S4. Model of the functional properties of the F-BAR domains of three srGAP family members.
See text for details.

CHAPTER 4

Rapamycin-induced depletion of PI(4,5)P₂ is effective in cell lines, but not in dorsal root ganglia neurons *in vitro* or *in vivo*¹

4.1 INTRODUCTION

Transgenic and knockout mice are useful models for studying the role of genes and proteins *in vivo*; however, constitutive alterations can often lead to off-target effects, as many transgenic lines are embryonic or postnatal lethal (Volpicelli-Daley et al., 2010; Kühn and Schwenk, 2002). Conditional transgenic and knockout mice have overcome a lot of these problems by targeting the genetic alterations to specific regions or developmental timepoints (Kühn and Schwenk, 2002); however, conditional genetic manipulations rely on relatively slow changes in transcription.

Pharmacological manipulation in cellular signaling is faster than genetic alterations, yet often leads to many off-target effects due to non-selective activation of entire signaling pathways. One approach that has been growing in popularity is to take advantage of the dimerization-inducing activity of the natural product, rapamycin. Rapamycin induces the dimerization of two naturally occurring protein domains: the FKBP domain of FKBP12, and the FRB domain of mTOR (Crabtree and Screiber, 1996). Tagging a protein of interest to one of these domains allows for precise spatial and temporal control of cellular signaling

¹ Jaeda C. Coutinho-Budd, Sam B. Snider, Brendan J. Fitzpatrick, Mark J. Zylka. (2012) Rapamycin-induced depletion of PI(4,5)P₂ is effective in cell lines, but not in dorsal root ganglia neurons *in vitro* or *in vivo*. In preparation.

My direct contribution to this work includes everything in Figures 4.1 through 4.5, and indirectly to Figure 4.6. I did not clone the constructs into pcDNA3.1(+) (Sam Snider), design or construct the knockin mice (Sam Snider and Mark Zylka), nor test the mice in behavioral paradigms (Brendan Fitzpatrick).

when the two proteins are co-expressed in the same cell and treated with rapamycin. For example, this system has been used to activate cell surface receptors to control cell growth (Jin et al., 2000) or induce cell death (Spencer et al., 1996), regulate protein localization to alter lipid composition of cellular membranes (Suh et al., 2006; Várnai et al., 2006), traffic proteins to the nucleus (Xu et al., 2010), or induce GPCR signaling (Putyrski et al., 2011). Given that these two rapamycin-binding domains exist endogenously, rapamycin treatment can have off-target effects, such as lung toxicity (Chhajed et al., 2000) and teratogenicity (Hentges et al., 2001), which are unrelated to the dimerization of the exogenous fusion proteins of interest. Fortunately, there are FRB domain mutations that have minimal interaction with rapamycin, and instead interact with rapamycin analogs (rapalogs) that do not affect the endogenous mTOR pathway (Liberles et al. 1997; Stankunas et al., 2003; Bayle et al., 2006).

These proteins have been used to design a system for the depletion of phosphatidylinositol (4-5)-bisphosphate (PI(4,5)P₂) from the plasma membrane within 10-20 seconds of rapamycin treatment (**Fig. 4.1A**; Suh et al., 2006; Várnai et al., 2006). PI(4,5)P₂ acts as second messenger in a variety of signaling pathways (Berridge and Irvine, 1984; Majerus et al., 1990; McLaughlin et al., 2002), as well as an important modulator of many ion channels (Suh and Hille, 2008). So far, dimerization-induced depletion of PI(4,5)P₂ has only been utilized *in vitro*; however, the use of this system *in vivo* could shed light on how alterations in PI(4,5)P₂ effect animal physiology and behavior as a whole.

PI(4,5)P₂ is a modulator of the heat-sensing ion channel, Transient Receptor Potential Vanilloid 1 (TRPV1), having both inhibitory and activating effects depending on the concentration of PI(4,5)P₂ and the TRPV1 agonist, capsaicin (Lukacs et al., 2007; Rohacs, et al., 2008). Recently, Sowa et al. (2010) found that increased PI(4,5)P₂ in the dorsal root ganglia (DRG) *in vivo* leads to enhanced thermosensation, while reduced PI(4,5)P₂ attenuates thermosensation. Since this previous study used an indirect approach

to reduce PI(4,5)P₂, we sought to use rapamycin-induced depletion of PI(4,5)P₂ *in vivo* to directly test whether PI(4,5)P₂ reduction can attenuate thermal hyperalgesia.

In the present study, we adapted the rapamycin-induced PI(4,5)P₂ depletion system for use *in vivo* by generating two knockin mice. The first knockin mouse contains Inp54p, a yeast PI(4,5)P₂-specific 5-phosphatase, fused to the FKBP domain and venus fluorescent protein, expressed in the cytoplasm of a subset of heat-sensing DRG neurons. The second ubiquitously expresses a CFP-tagged FRB domain tethered to the plasma membrane. To avoid possible complications of rapamycin in the endogenous system, we used one of the FRB mutants, FRB^{PLF}, that interacts with the rapalog, C20-marap (Bayle et al., 2006). When these mice are crossed, both components of the rapamycin-induced PI(4,5)P₂ system are expressed in heat-sensing neurons. However, here we report that we are unable to induce translocation of the FKBP-fused phosphatase to the plasma membrane upon rapamycin treatment in these DRG neurons *in vivo*.

4.2 RESULTS

4.2.1 Rapamycin-induced dimerization is an effective tool for studying biological processes in cell lines

Rapamycin-induced translocation is an elegant tool that utilizes the dimerization of FRB and FKBP domains in order to promote the translocation of one protein to the location of the other. Typically, one of these proteins is targeted to a specific cellular location or compartment, and the free protein undergoes translocation. This technique has been used in a variety of studies to allow for precise temporal control of biological manipulations, from G-protein sequestration (Putyrski et al., 2011) to depletion of PI(4,5)P₂ from the plasma membrane (Varnai et al., 2006; Suh et al., 2006).

Time-sensitive PI(4,5)P₂ depletion is one of the most common examples of this biological tool. Commonly, the FRB domain is tagged to the plasma membrane, and a

PI(4,5)P₂-specific phosphatase domain is fused to the FKBP domain and localized to the cytoplasm prior to rapamycin treatment. Administration of rapamycin promotes dimerization of the FRB and FKBP domains, translocating a P(4,5)P₂-specific phosphatase, to the plasma membrane where it rapidly hydrolyzes PI(4,5)P₂. To visualize PI(4,5)P₂ reduction at the plasma membrane, a fluorescently-tagged PH domain of PLC δ 1 is expressed simultaneously, acting as a PI(4,5)P₂ biosensor. When PI(4,5)P₂ levels are high in the plasma membrane, the PH domain localizes to the plasma membrane. After depletion by the phosphatase, the PH domain no longer has substrate to bind, and is therefore released into the cytoplasm (**Fig. 4.1A**). We wanted to take advantage of the ability to deplete PI(4,5)P₂ to study its role in nociceptive signaling *in vivo*; however, in order to implement this system in mouse models, we needed to ensure that our knockin protein constructs expressed and functioned as previously reported. Our constructs recapitulated the results of other studies: prior to rapamycin application, the CFP-tagged FRB^{PLF} domain localized to the plasma membrane with the membrane-binding motif of GAP43 (**Fig. 4.1B-i, 1C**), the Venus-tagged FKBP domain fused to the yeast PI(4,5)P₂-specific phosphatase, Inp54p, successfully expressed in the cytoplasm (**Fig. 4.1B-ii, 1C**), and the PH domain of PLC δ 1 bound to the PI(4,5)P₂-rich plasma membrane (**Fig. 4.1B-iii, 1C**). After rapamycin, there is no change in membrane localization of the FRB^{PLF} domain (**Fig. 4.1B-iv, 1C**), but the Inp54p phosphatase translocated to the plasma membrane (**Fig. 4.1B-v, 1C**), where it successfully depleted PI(4,5)P₂ and caused the translocation of the PH domain to the cytoplasm (**Fig. 4.1B-vi, 1C**). We found these constructs work as expected to deplete PI(4,5)P₂ in a number of cell lines, including in HEK293 cells (Fig. 1B), Rat1 Fibroblasts, Hela Cells, and COS7 cells (data not shown).

4.2.2 Construction of two mouse lines to study rapamycin-induced PI(4,5)P₂ depletion in thermal sensitivity in vivo

To adapt this system for use *in vivo*, we engineered two separate knockin mouse

lines, each expressing half of the translocation machinery. Dorsal root ganglia (DRG) are comprised of genetically distinct subtypes of nociceptive neurons that respond to different stimuli, such as thermal (CGRP+ neurons) or mechanical (MrgD/IB4+ neurons) pain (Cavanaugh et al., 2009; Wang and Zylka, 2009). The discrete genetic identities allow for specific manipulation of individual pain circuits *in vivo*. To test the hypothesis that PI(4,5)P₂ depletion attenuates thermal sensitivity, we targeted the Venus-FKBP-Inp54p construct to CGRP-expressing neurons. Heterozygous and homozygous CGRP-Inp54p mice are viable and capable of producing offspring. Using immunohistochemistry, we found that the venus-FKBP-Inp54p protein was successfully targeted to CGRP-expressing neurons, colocalizing with 87.9% of neurons stained with an anti-CGRP antibody (**Fig. 4.2A**). In contrast, Venus expression was found in 3.7% of an alternative subset of small nociceptive neurons, marked by binding of Isolectin B4 (IB4)-binding neurons (**Fig. 4.2B**), consistent with the limited overlap between CGRP and IB4 markers.

The Rosa26 locus ubiquitously drives expression in all cell types (Stirling et al., 2005), including DRG. This locus was used to express the CFP-tagged FRB^{PLF} domain at the plasma membrane, using the double palmitoylated membrane-targeting motif of GAP43. This knockin also uses the CAG promoter to drive expression, rather than the endogenous Rosa26 promoter alone. As expected, the anti-GFP antibody staining revealed expression of the CFP-tagged FRB^{PLF} domain at the plasma membrane of approximately 99% of DRG neurons (**Fig. 4.2C**). As with the CGRP-Inp54p mice, the Rosa-FRB^{PLF} heterozygous and homozygous mice are viable and successful breeders.

4.2.3 Injection of rapamycin does not induce translocation of Venus-FKBP-Inp54p from the cytoplasm to the plasma membrane in DRG neurons

Rapamycin has been administered *in vivo* in animal models, and has been shown to have antinociceptive effects (Xu et al., 2011, Géranton et al., 2009). Moreover, these properties have been attributed to a direct effect on DRG neurons when administered

intrathecally (Géranton et al., 2009). Rosa-FRB^{PLF}/CGRP-Inp54p or CGRP-Inp54p heterozygous mice received two rounds of two rapamycin injections, one intrathecal (IT) injection and one intraperitoneal (IP) injection, to ensure that the DRG could be reached from both central and peripheral sources. All mice tested received the rapamycin injections; however, mice lacking the FRB^{PLF} domain at the plasma membrane (CGRP-Inp54p heterozygotes) were used as no-translocation controls (**Fig 4.3A**). Injection of rapamycin did not induce obvious translocation of Venus-FKBP-Inp54p from the cytoplasm to the plasma membrane in double heterozygous mice (**Fig. 4.3B**). There is no significant difference between membrane to cytoplasmic ratio of venus-FKBP-Inp54p in either the control or double heterozygous mice post-rapamycin injection (**Fig. 4.3C**). Treatment of these neurons with rapamycin in dissociated culture also failed to induced translocation (data not shown).

4.2.4 Expression of Inp54p in CGRP+ neurons leads to basal depletion of PI(4,5)P₂ in cultured DRG neurons

The 5-ptase domain of Inp54p is expected to be constitutively active (Nebl et al., 2000). Although the venus-FKBP-Inp54p protein is expressed in the cytoplasm, it is not specifically excluded from the plasma membrane, and therefore can likely interact with, and hydrolyze, PI(4,5)P₂ without rapamycin-induced translocation. To test this hypothesis, we examined basal levels of PI(4,5)P₂ in dissociated neurons of CGRP-Inp54p neurons. Given that phosphoinositide concentrations vary with cell type (Insall and Weiner, 2001), we wanted to ensure that we focused on CGRP+ neurons in both the venus-FKBP-Inp54p and control conditions. We therefore utilized another mouse line constructed in the lab, which expresses farnesylated EGFP in CGRP+ neurons (McCoy et al., manuscript submitted, 2012).

Comparison of PI(4,5)P₂ levels using an anti-PI(4,5)P₂ antibody revealed a reduction in PI(4,5)P₂ in the plasma membrane for CGRP-Inp54p neurons compared to

CGRP-GFP controls (**Fig. 4.4A**, quantified in **Fig. 4.4B**). This led to the hypothesis that PI(4,5)P₂-regulated signaling would be reduced in these mice as well. Many studies have shown that activity of the noxious heat-sensing channel, TRPV1, is modulated by the levels of PI(4,5)P₂ at the plasma membrane (Sowa et al., 2010, Lusaks et al., 2007; Rohacs et al., 2008). Using calcium mobility as a readout for ligand-evoked response, we treated both sets of neurons with the TRPV1 agonist, capsaicin. As expected from the reduced levels of PI(4,5)P₂ at the plasma membrane of CGRP-Inp54p neurons, capsaicin-evoked neuronal response is reduced in CGRP-Inp54p neurons compared to CGRP-GFP controls (**Fig. 4.4C**).

To determine if the diminished capsaicin-evoked signaling was due to PI(4,5)P₂ reduction, we sought to replenish PI(4,5)P₂ levels in dissociated neurons prior to imaging. Pre-incubation with PI(4,5)P₂ did not rescue signaling in CGRP-Inp54p neurons compared to CGRP-Inp54p neurons treated with carrier alone (**Fig. 4.5A**). In contrast, PI(4,5)P₂ add-back significantly decreased signaling. The decreased signaling and inability to rescue cell signaling with PI(4,5)P₂ could, therefore, be due to deleterious effects on cell health. One consequence of chronic PI(4,5)P₂ depletion is the activation of cleaved caspase-3 (Azuma et al., 2000), a marker of apoptosis. We found that in cultured neurons, Venus-FKBP-Inp54p-expressing neurons had a higher prevalence of cleaved caspase-3 staining, compared to farnesylated GFP-expressing neurons (**Fig. 4.5B**), with 1.1% of neurons expressing cleaved caspase-3 expression in CGRP-GFP neurons (n=44), and 10% in CGRP-Inp54p neurons (n=42). When cultured with NGF to increase CGRP expression, and therefore knockin protein expression, this percentage increased to 38.9% in Venus-FKBP-Inp54p-expressing neurons (n=64), but was unchanged in CGRP-GFP control neurons (n=46). However, expression of cleaved caspase-3 was not the same *in vivo* (**Fig. 4.5C**). DRG sections from perfused animals revealed 9 out of 182 neurons with overlap of cleaved caspase-3 expression in CGRP-GFP neurons, and only 2 out of 282 in CGRP-

Inp54p neurons. This result suggested that *in vivo* data might be more telling than results from dissociated neurons.

4.2.5 Expression of Inp54p in CGRP+ neurons does not affect behavior *in vivo*

To directly assess whether the expression of venus-FKBP-Inp54p in CGRP neurons would elicit a behavioral phenotype *in vivo*, we probed CGRP-Inp54p heterozygous mice and wildtype littermates for thermal and mechanical sensitivity. Mice were tested for baseline responses, injected with complete Freund's adjuvant (CFA) into the left hind paw to inflame and sensitize the paw, and then tested for nociceptive response on subsequent days. CGRP+ neurons are partially responsible for thermal sensation (Salmon et al., 1999; Zhang et al., 2001), so we would expect to see a difference in thermal sensitivity, while mechanical sensitivity should remain at wildtype levels. There was no difference between genotypes in the paw size after CFA injection (**Fig. 4.6A**). Moreover, CGRP-Inp54p responses to both mechanical (**Fig. 4.6B**) and thermal (**Fig. 4.6C**) pain stimuli matched those of wildtype controls before or after CFA sensitization. These results confirm that even if the venus-FKBP-Inp54p construct does reduce PI(4,5)P₂ *in vivo* prior to rapamycin treatment, it is not enough to cause a behavioral response. It will therefore be necessary to test double heterozygous mice injected with rapamycin, and repeat with the same behavioral assays to assess whether rapamycin can enhance PI(4,5)P₂ depletion enough to cause reduction in thermosensitivity.

4.3 DISCUSSION

We have successfully constructed viable transgenic mice that express the components for rapamycin-inducible PI(4,5)P₂ depletion *in vivo*. Each mouse expresses its respective knockin protein in the correctly targeted neurons; however, the rapamycin-induction machinery proteins fail to function as intended. We cannot visualize rapamycin-induced translocation *in vivo*, and although we see effects related to PI(4,5)P₂ depletion in cultured dissociated DRG neurons, these effects do not appear to recapitulate the *in vivo*

environment.

In working with cell line transfection of the FRB, FKBP-Inp54p, and PH constructs, it became apparent that the ratio between the three proteins varied highly between cells. Cells that lacked enough of one component, or had too much of another, failed to undergo rapamycin-induced translocation. In an attempt to configure the chemically induced dimerization system for use in a wider variety of organelles, since many of the previously used rapamycin-induced dimerization experiments have focused targeting proteins to the plasma membrane (Spencer et al., 1996; Jin et al., 2000; Putyrski et al., 2011; Suh et al., 2006; Várnai et al., 2006) or endosomes (Fili et al., 2006), Komatsu et al. (2010) found that slight alterations in these protein ratios would change the extent and effectiveness of translocation. While troubleshooting these experiments, the authors found that each organelle varied slightly in its preferred expression ratio necessary to induce proper translocation. Many times, protein stability was one of the key factors for lack of effectiveness, and proteins had to be reconstructed in order to optimize this factor.

The FRB domain mutation used in our Rosa-FRB mouse consists of three point mutations: K2095P, T2098L, and W2101F. The W2101F mutation is necessary for interaction with the rapalog, C20-marap (Bayle et al., 2006), and the T2098L mutation is responsible for protein destabilization (Stankunas et al., 2003; Stankunas et al., 2007). Moreover, this destabilization is extended to proteins fused to the FRB^{PLF} mutant, such as fluorescently-tagged FRB^{PLF}. This destabilization is reversed within 24 hours of rapamycin treatment, as the FKBP-FRB^{PLF} complex stabilizes the FRB^{PLF} protein. Two possibilities arise from this: a) degradation of CFP-FRB^{PLF} interrupts the FRB to FKBP ratio, inhibiting translocation, or b) translocation is possible 24 hours after rapamycin or rapalog treatment. However, this is not the only factor that might interfere with venus-FKBP-Inp54p translocation in our system. FKBP12 has been shown to depalmitoylate H-Ras at the plasma membrane (Ahearn et al., 2011). The membrane-targeting motif of GAP43 used to

anchor FRB^{PLF} to the plasma membrane in our mice consists of two palmitoylated cysteines (Cys3 and Cys4). It is possible that the FKBP domain of FKBP12 tagged to our transgenic protein is basally depalmitoylating the CFP-tagged FRB^{PLF} domain throughout gestation and the life of the animal, thereby downregulating its expression at the plasma membrane and disrupting the proper translocation ratio. Additionally, we have shown that the Inp54p knockin protein has the ability to reduce PI(4,5)P₂ levels without rapamycin-induced translocation in cultured DRG neurons (**Fig. 4.4A-B**). Heo et al. (2006) demonstrated that palmitoylation motifs are partially dependent on PI(4,5)P₂ for membrane binding. The authors also show a dependence on PI(3,4,5)P₂ for proper palmyitoyl-targeting, and we do not know the effect of constitutive Inp54p expression on PI(3,4,5)P₂ levels in our CGRP-Inp54p knockin mice. It is possible that due to a combination of any or all of these factors, the ratio of FRB^{PLF} to FKBP is unsuitable for translocation.

Few reports of *in vivo* application of this chemically-induced dimerization system exist. The only transgenic study of rapamycin-induced dimerization *in vivo* come from Stankunas et al. (2003), and in this case they merely focused on dimerization to induce the stabilization of cytoplasmically localized FRB^{PLF}-fusion proteins to cytoplasmically localized FKBP12. One study successfully used a similar system for transgenic mice *in vivo* (Karpova et al., 2005), but the authors used a rapamycin-independent FKBP-homodimerization system, obtained from Clontech. Furthermore, all experiments involving FKBP-FRB dimerization were carried out with short-term electroporation. It is possible that rapamycin-induced heterodimerization is not suitable for *in vivo* function.

Overexpression of Inp54p in neurons is not trivial (personal experience; Angela Mabb, personal communication, 2011), and when finally expressed can cause toxic side effects (Scott Soderling, personal communication, 2011). Its constitutive activation in cell lines can lead to loss of cell adhesion, membrane blebbing, and ultimately cell death (Raucher et al., 2000; Azuma et al. 2000). It is possible that the reason we see increased

apoptosis in CGRP-Inp54p neurons in culture is that the long-term expression of Inp54p compromises neuronal health, which is aggravated further in the dissociation and culture process. It is likely that we do not see markers of cell death in sectioned DRG because of environmental factors that compensate for the increased cell stress in the intact animal. However, few studies have successfully reported the use of the rapamycin-induced Inp54p translocation to deplete PI(4,5)P₂ in neurons. Further studies from one of the original groups to describe this rapamycin-induced PI(4,5)P₂ depletion (Suh et al., 2006) have focused the effect of PI(4,5)P₂ depletion on high-voltage calcium channels, Ca_v1.2 and Ca_v1.3. Suh et al. (2010) show that diC₈-PIP₂, a synthetic PI(4,5)P₂, can rescue calcium current suppression after PI(4,5)P₂ depletion in sympathetic neurons. Interestingly, they only report use of the rapamycin-induced Inp54p-mediated depletion of PI(4,5)P₂ in cell lines. In contrast, they use a voltage-activated 5-phosphatase to deplete PI(4,5)P₂ in neurons. To my knowledge, only one study has used this rapamycin-inducible Inp54p method to deplete PI(4,5)P₂ in neurons. Chen et al. (2011) show that GRK5, a G-protein couple receptor kinase, promotes the bundling of F-actin in a PI(4,5)P₂-dependent manner. They arrive at this conclusion by transfecting GRK5, the membrane-associated Lyn-FRB, and CFP-Inp54p or its phosphatase-dead mutation, into cultured hippocampal neurons. After rapamycin treatment, there is reduced filopodial motility in neurons transfected with Inp54p, but not its phosphatase-dead counterpart; however, they do not show translocation, nor do they demonstrate these conditions prior to rapamycin treatment. It is possible that there is reduced motility due to expression of the wildtype Inp54p alone. An alternative explanation for the difference between our system and that used by Chen et al. (2011), besides the short-term transfection versus lifetime expression, is the use of central hippocampal neurons versus our focus on peripheral DRG neurons. There are known differences between central and peripheral neurons, such as the ability to regenerate after injury (Fenrich and Gordon, 2004). It is possible that certain molecular mechanisms allow

for the use of rapamycin-induced translocation in neurons of the central nervous system. Taken together, it seems that current limitations prevent the application of rapamycin-induced PI(4,5)P₂ depletion *in vivo*; however, future studies might reveal the molecular mechanisms necessary to make this possible.

4.4 MATERIALS AND METHODS

All procedures and behavioral experiments involving vertebrate animals were approved by the Institutional Animal Care and Use Committee at the University of North Carolina at Chapel Hill.

4.4.1 DNA plasmid constructs

Constructs for rapamycin-induced PI(4,5)P₂ depletion in HEK293 cells were obtained from Ken Mackie (University of Indiana), Tamas Balla (NICHD, Bethesda, MD USA) and Tobias Meyer (Stanford, Stanford, CA USA). The RFP-tagged PH domain of rat PLC δ 1 was a kind gift from Ken Mackie. The CFP-tagged FRB domain was tethered to the plasma membrane using the first 20 amino acids of the human GAP43, as described in Várnai et al. (2006), was obtained from Tamas Balla, and subcloned cloned into pcDNA3.1(+). The FKBP-Inp54p PI(4,5)P₂ phosphatase construct was donated by Tobias Meyer, subcloned into pcDNA3.1(+), and modified with a venus fluorescent protein tag.

4.4.2 Cell culture and live-imaging

HEK293 cells were grown on glass bottom cell culture dishes (MatTek; P35G-0-10-C) in Dulbecco's Modified Eagle Medium (DMEM, Sigma) supplemented with 10% fetal bovine serum, 100 U/ml penicillin, and 100 μ g/ml streptomycin. Cells were transfected with 4 μ l Lipofectamine 2000 (Invitrogen) and 1 μ g total DNA per culture dish in Opti-MEM (Gibco) for two hours, at which point media was replaced with the supplemented DMEM. After 16-24 hours, supplemented DMEM was replaced with Hank's Balanced Salt Solution (HBSS Gibco 14025, supplemented with 9 mM HEPES, 11 mM D-glucose, 0.1% fatty-acid

free BSA, pH 7.3) warmed to 37° C. After baseline imaging, HBSS was replaced with HBSS containing 1 µM rapamycin (Calbiochem). Each plate was imaged on a Leica TCS confocal microscope using a 40x objective, and maintained at 37° C throughout the imaging session using a heated stage attachment. Cells were treated for 10 minutes, at which point a final post-rapamycin image was taken. Membrane to cytoplasm ratio in pre- and post-rapamycin-treated cells was measured in cells expressing all three constructs, using NIH ImageJ software.

4.4.3 Generation of FRB^{PLF}-CFP and Venus-FKBP-Inp54p knockin mice

The GAP43-FRB^{PLF}-CFP construct containing three point mutations of the FRB domain (K2095P, T2098L, and W2101F) was subcloned into the Rosa26 targeting construct. This insert was placed under the control of the CAG promoter, and the entire CAG-GAP43-FRB^{PLF}-CFP insert was followed by a self-excising neomycin resistance cassette (ACN, Bunting et al., 1999). CGRP targeting was accomplished by recombineering of Calca targeting arms from a C57BL/6-derived bacterial artificial chromosome (BAC; RP24-136021). The start codon, located in exon 2, is common to CGRP α and calcitonin and was replaced with an *Ascl* site to facilitate cloning. The Venus-FKBP-Inp54p construct described above was subcloned into this CGRP targeting construct, without an external promoter, but with the ACN cassette. Successful targeting of embryonic stem cells (E14) by homologous recombination was identified with Southern blot hybridization, using probes that flanked the 5' and 3' arms of the targeting constructs, as well as an internal neomycin probe. Chimeric mice were produced by blastocyst injection, and mated to C57BL/6 mice to establish the line. CGRP-GFP mice were generated as described in McCoy et al. (Submitted, February 2012), and used as controls.

Transgenic mice were identified by PCR amplification of genomic DNA with specific primers. CGRP2 (5' CAGCTCCCTGGCTTTCATCTGC), CGRP (5' AAATGTCGGGGAGTCACAGGC), and EGFP2 (5' CCGTAGGTCAGGGTGGTCACGAGG)

were used to evaluate wildtype and/or knockin bands for CGRP knockin mice. Internal CFP primers (5' CGATGAGATGTGGCATGAAGG and 5' CCGTCGTCCTTGAAGAAGATGG) were used to detect the presence of the Rosa-FRB^{PLF}-CFP knockin allele.

4.4.4 Neuronal dissociation and imaging

Male CGRP-Inp54p, Rosa-FRB^{PLF}/CGRP-Inp54p, and CGRP-GFP control mice (3-4 weeks old) were decapitated without anesthesia, the DRG were dissected into 4° C Hank's Balanced Salt Solution (HBSS; Gibco, 14175-095), and dissociated using collagenase (1 mg/mL; Worthington, CLS1) and dispase (5 mg/mL; Gibco, 17105-041) dissolved in HBSS. Neurons were plated in Neurobasal-A medium (Invitrogen, 10888022), supplemented with B-27 Supplement (Gibco, 17504-044), L-glutamine (Gibco, 25030-081), and penicillin-streptomycin (Gibco, 15140-122). In some cases, 50 ng/ml nerve growth factor (NGF) was added to the plating media to enhance CGRP expression. The neurons were plated onto coverslips coated with 0.1 mg/mL poly-D-lysine (Sigma P0899) and 5 µg/mL laminin (Sigma, L2020).

Rapamycin treatment and imaging for dissociated neuronal cultures was carried out identically to the imaging procedures described for HEK293 cells above. For calcium imaging, neurons (24 hours *in vitro*) were washed with assay buffer (HBSS Gibco 14025, supplemented with 9 mM HEPES, 11 mM D-glucose, 0.1% fatty-acid free BSA, pH 7.3) and incubated for 1 h with 2 µM Fura2-AM (Invitrogen, F1221) with 0.2% pluronic (Invitrogen P3000-MP) in assay buffer in the dark at room temperature. The neurons were then washed with assay buffer and allowed to equilibrate at room temperature for 30 minutes prior to imaging. After a 120 seconds baseline perfusion of assay buffer, 1 µM capsaicin was washed onto the neurons for 30 seconds, at which point HBSS perfusion resumed to wash off the agonist, followed by treatment of 100 µM KCl to distinguish neurons from other cell types present. PI(4,5)P₂ rescue was prepared according to manufacturer instructions

(Echelon Bioscience Inc.), and performed by pre-incubating 10 μ M carrier and 10 μ M PI(4,5)P₂, or 10 μ M carrier alone, for 15 minutes prior to calcium imaging. Images were acquired on a Nikon Eclipse Ti microscope (Nikon, Melville, NY). Venus+ neurons were identified by 500 ms exposure with a FITC filter.

4.4.5 Immunohistochemistry

Male mice 4-6 weeks were injected intraperitoneally with pentobarbital, and perfused with 4% PFA in 0.1 M phosphate buffer, pH 7.4. Lumbar DRG (L2-L6) were dissected and post-fixed for 2 hours in 4% PFA. The DRG were subsequently cryoprotected in 30% sucrose, 0.1 M phosphate buffer, pH 7.3 at 4° C for 24 h, frozen in OCT TissueTek, cryosectioned at 20 μ m, mounted on Superfrost Plus slides, and stored at -20° C until use.

Tissue was rehydrated and washed in PBS to remove OCT embedding compound, permeabilized and blocked in TBS-Tx (0.05 M Tris, 2.7% NaCl, 0.3% Triton-X 100, pH 7.6) containing 10% normal goat serum (NGS) for 1 hr at room temperature. Sections were incubated overnight at 4° C with primary antibodies in TBS-Tx/10%NGS, washed, incubated at room temperature for 2 hours with secondary antibodies in TBS-Tx/10%NGS, washed, and mounted with Fluorogel (Biomedex). Primary antibodies used were chicken anti-GFP (1:500; Aves Labs, GFP-1020), rabbit anti-CGRP (1:750; Peninsula, T-4032), mouse anti-NeuN (1:200, Millipore), and rabbit anti-cleaved caspase-3 (1:200, Cell Signaling) in TBS-Tx/10% NGS. Secondary antibodies include goat anti-chicken Alexafluor 488 (1:2000, Invitrogen), goat anti-Rabbit Alexafluor 633 (1:2000, Invitrogen), and goat anti-mouse Alexafluor 633 (1:2000, Invitrogen).

Dissociated neuronal cultures were prepared as described above, and fixed at 24 hours *in vitro* with 4% PFA warmed to 37° C for 30 min. Neurons were washed with TBS to remove fixative, and then stained according to the Echelon PIP staining protocol (Echelon Bioscience Inc.). Briefly, cells were blocked with TBS containing 10% NGS for 30 min at

37° C, then incubated with primary antibodies (biotinylated mouse anti-PI(4,5)P₂ (1:100, Echelon Bioscience Inc) and chicken anti-GFP (1:500, Aves Labs), diluted in TBS) at 37° C for 1 hour, washed with TBS containing 1% NGS, incubated in secondary antibody (Streptavidin AlexaFluor 647 (1:2000, Invitrogen) and goat anti-chicken Alexafluor 488 (1:2000, Invitrogen)) for 1 hr at 37° C, washed in TBS, and mounted with Fluorogel.

4.4.6 Drug administration

Mice that were either heterozygous for both Rosa-FRB^{PLF} and CGRP-Inp54p, or CGRP-Inp54p heterozygous alone, received four injections of rapamycin. All mice received two sets of two injections: one intrathecal injection of 1 nmol rapamycin per 5 µl, and one intraperitoneal injection of 5 µg/g. Each pair of injections was administered two hours apart. Mice were perfused and dissected, as described above, 30 minutes after the second round of injections.

4.4.7 Behavior

Male 3- to 4-month-old CGRP-Inp54p^{+/-} and WT littermate mice were acclimated to the testing apparatuses and experimenter for 2 days prior to testing. The experimenter was blind to genotype throughout the experiment. Baseline thermal and mechanical sensitivity were tested using a Hargreaves and Von Frey apparatuses, respectively, prior to intraplantar injection with complete Freund's adjuvant (CFA) into the left hindpaw, and behavioral testing on subsequent days, as described previously (Zylka et al., 2008).

4.5 FIGURES AND LEGENDS

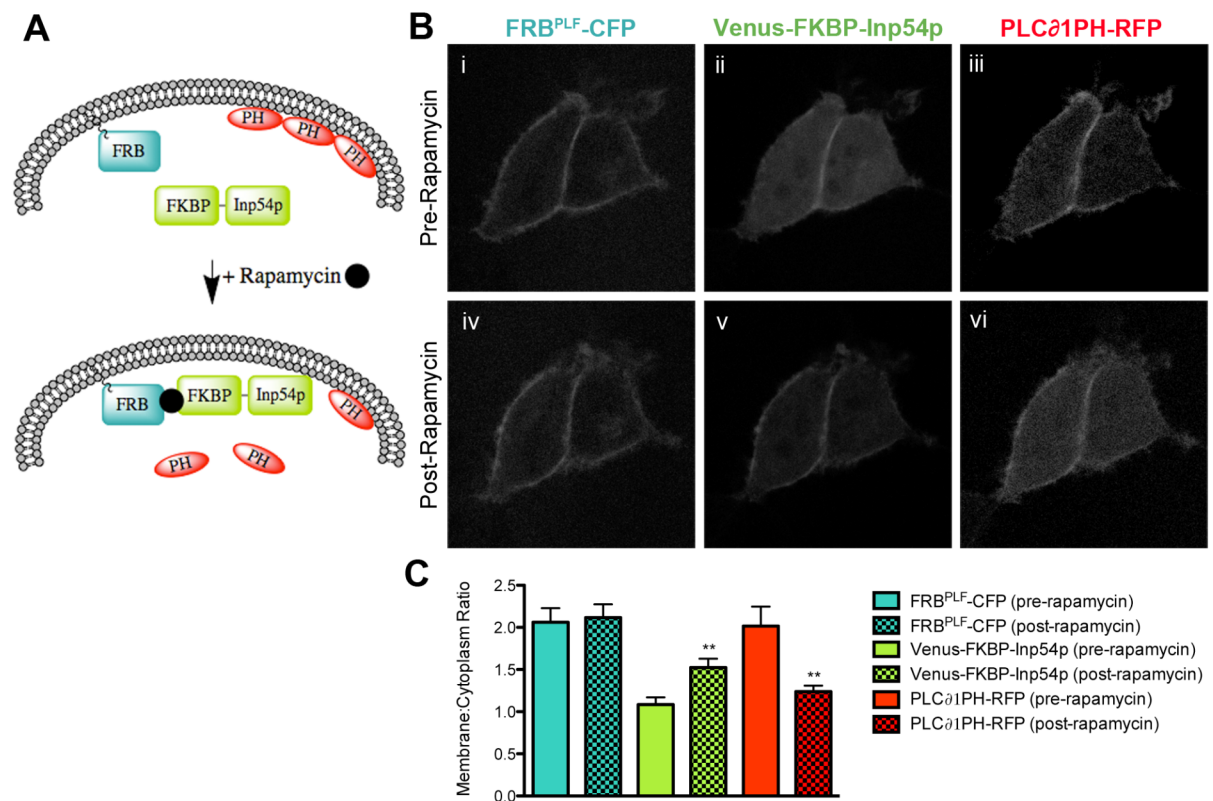


Figure 4.1. Rapamycin-induced translocation effectively allows for PI(4,5)P₂ reduction in HEK293 cells.

A) Schematic of rapamycin-induced translocation components and mechanism. Prior to rapamycin treatment, the CFP-fused FRB^{PLF} domain of mTOR is tagged to the plasma membrane with the membrane-targeting motif of GAP43, and the venus-tagged FKBP-Inp54p fusion protein is cytoplasmically localized. The PH domain of PLC δ 1 acts as a biosensor, and binds PI(4,5)P₂ in the plasma membrane. After rapamycin treatment, the FKBP domain dimerizes with the FRB^{PLF} domain, translocating the FKBP-Inp54p fusion protein to the plasma membrane, where the Inp54p phosphatase hydrolyzes PI(4,5)P₂, releasing the PH domain to the cytoplasm. **B)** Expression in HEK293 cells reveals that before rapamycin treatment, the FRB^{PLF}-CFP protein (i), Venus-FKBP-Inp54p fusion (ii), and the RFP-tagged PH domain of PLC δ 1 (iii) are properly localized. Application of rapamycin causes translocation of the venus-FKBP-Inp54p protein to the plasma membrane (v), where the proximity of the yeast phosphatase, Inp54p, hydrolyzes PI(4,5)P₂, causing a release of the PH domain (vi) to plasma membrane. **C)** Quantification of translocation in HEK293 cells. **p>0.005 compared to pre-rapamycin condition, n=20 cells.

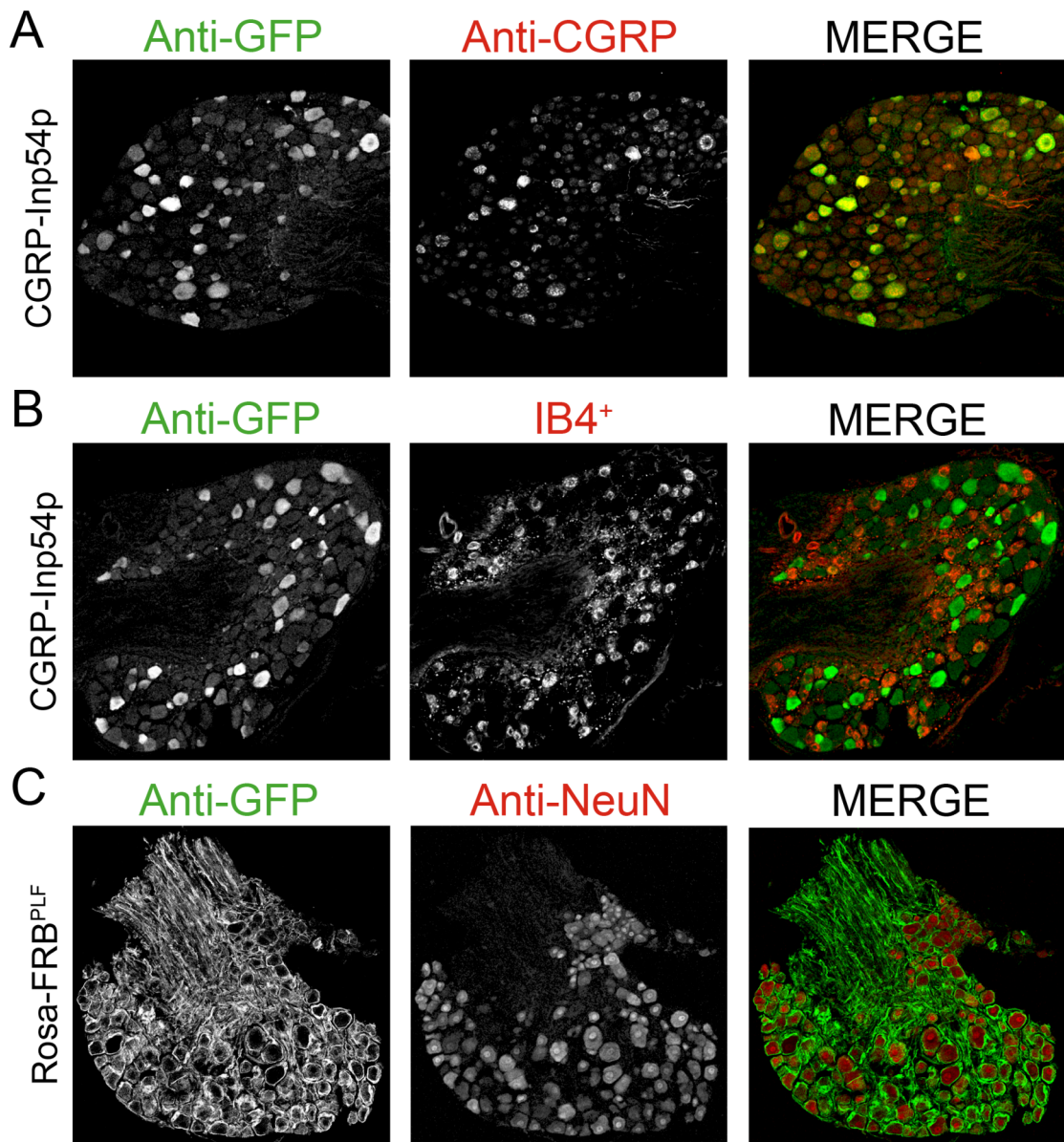


Figure 4.2. Both knockin mouse lines express the correct protein in the appropriate DRG neurons.

A-B) Venus-FKBP-Inp54p shares 87.9% colocalization with anti-CGRP staining in sectioned DRG, but only 3.7% overlap with IB4⁺ neurons (B). The Venus-FKBP-Inp54p is confined to cell bodies, with little staining in processes. **C)** FRB^{PLF}-CFP is expressed at the plasma membrane of 99% of neurons in the DRG. FRB^{PLF}-CFP expression is excluded from the cytoplasm, and is strong throughout the neuronal processes. n>500 neurons counted from 5 DRG sections from two animals per condition.

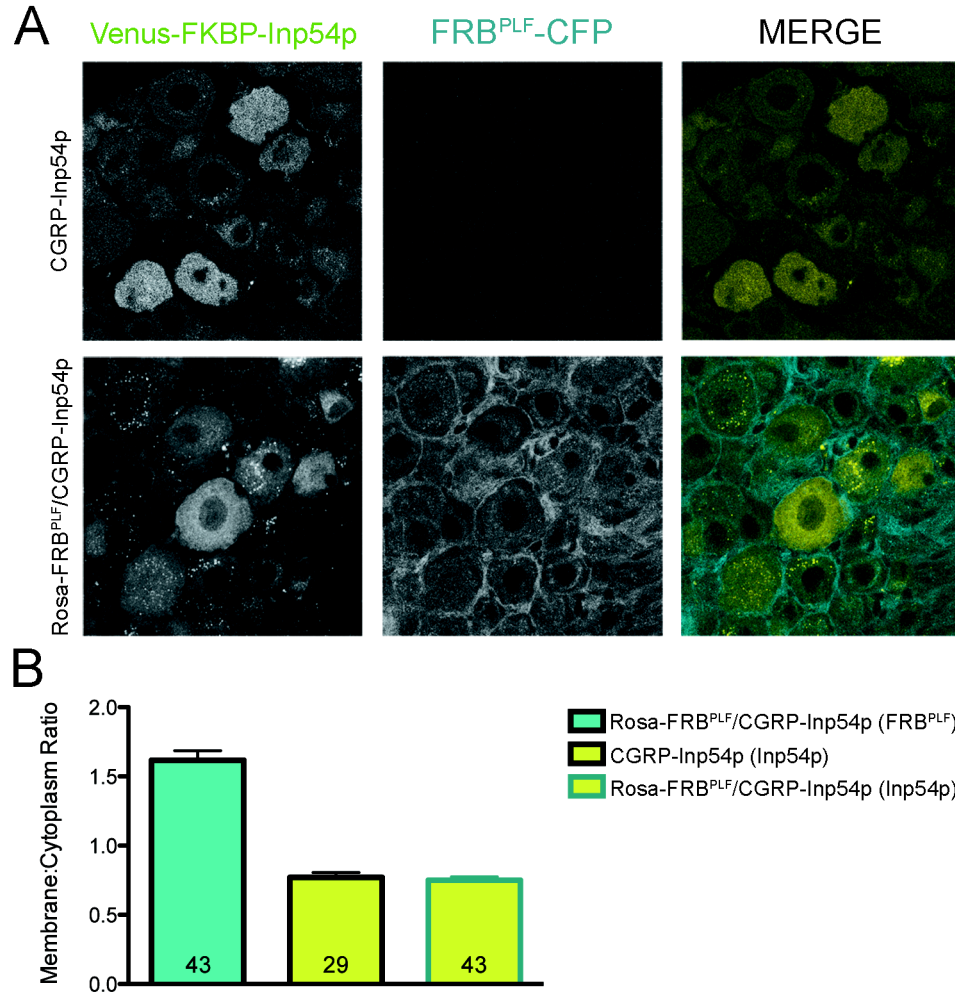


Figure 4.3. Rapamycin does not induce translocation in double heterozygotic mice *in vivo*.

A) DRG section from a CGRP-Inp54p heterozygous mouse injected with rapamycin (top), and a Rosa-FRB^{PLF}/CGRP-Inp54p double heterozygous mouse injected with rapamycin (bottom). Both mice received two rounds of IP (5 µg/g) and IT (1 nmol/5 µl) injections, 2 hours apart, and were sacrificed after the second round of injections. **B)** Quantification of translocation. There is no difference in the membrane to cytoplasmic ratio of Venus-FKBP-Inp54p in FRB^{PLF}-expressing neurons compared to neurons lacking FRB^{PLF}-expression. FRB^{PLF} domain ratio is included to demonstrate membrane localization. n=neurons per condition, included in bar graph.

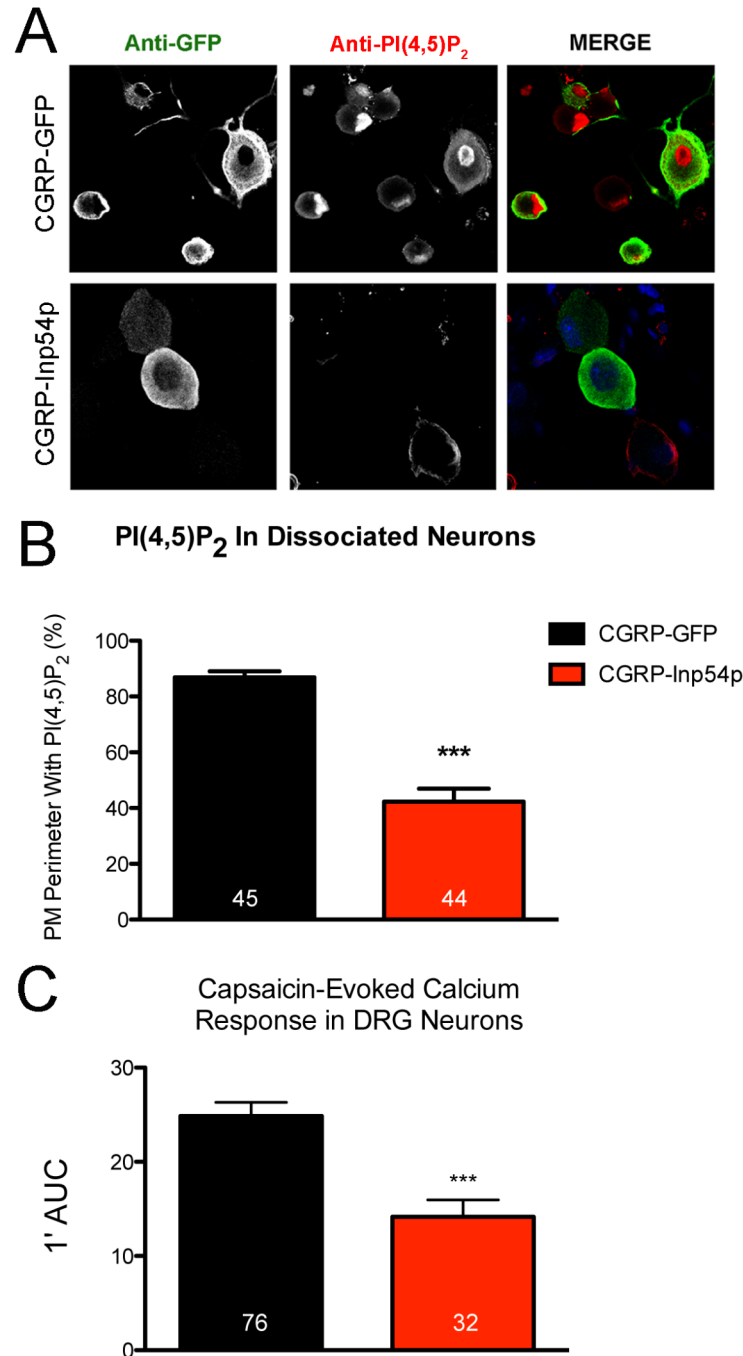


Figure 4.4. PI(4,5)P₂ is depleted in CGRP-Inp54p knockin neurons.

A) Anti-PI(4,5)P₂ staining is reduced in venus-FKBP-Inp54p-expressing neurons compared to CGRP-GFP control neurons. **B)** Quantification of PI(4,5)P₂ antibody staining reveals that, on average, PI(4,5)P₂ levels are reduced by approximately 50% in CGRP-Inp54p dissociated neurons compared to neurons from CGRP-GFP control mice. **C)** Quantification of 2' area under the curve (AUC) of a calcium trace of 1 μM capsaicin-treated dissociated neurons reveals decreased calcium signaling in CGRP-Inp54p neurons compared to CGRP-GFP controls. n = number of neurons, depicted as white numbers in each bar of B and C). ***p<0.0001

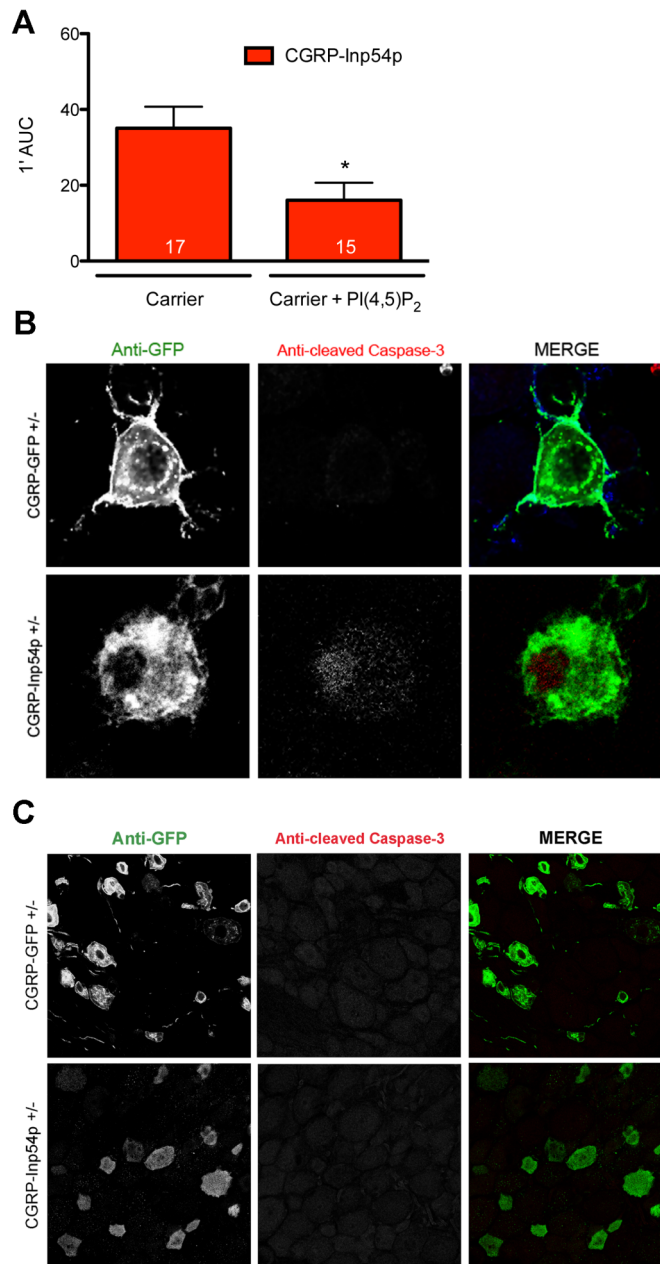


Figure 4.5. PI(4,5)P₂ add-back does not rescue deficits in calcium signaling in CGRP-Inp54p neurons. Deficits in calcium signaling are most likely due to poor cell health *in vitro*.

A) Addition of 10 μ M PI(4,5)P₂ does not rescue capsaicin-evoked calcium imaging in dissociated CGRP-Inp54p neurons, but in fact, decreases it compared to control treatment with carrier alone. n = number of neurons, depicted as white numbers in bar graph. * $p < 0.05$. **B)** Anti-cleaved caspase-3 staining, a marker for apoptosis, reveals higher expression in CGRP-Inp54p dissociated neurons compared to CGRP-GFP controls. **C)** However, this difference is not found in DRG sections from perfused animals, suggesting that cell health is not compromised in these neurons *in vivo*.

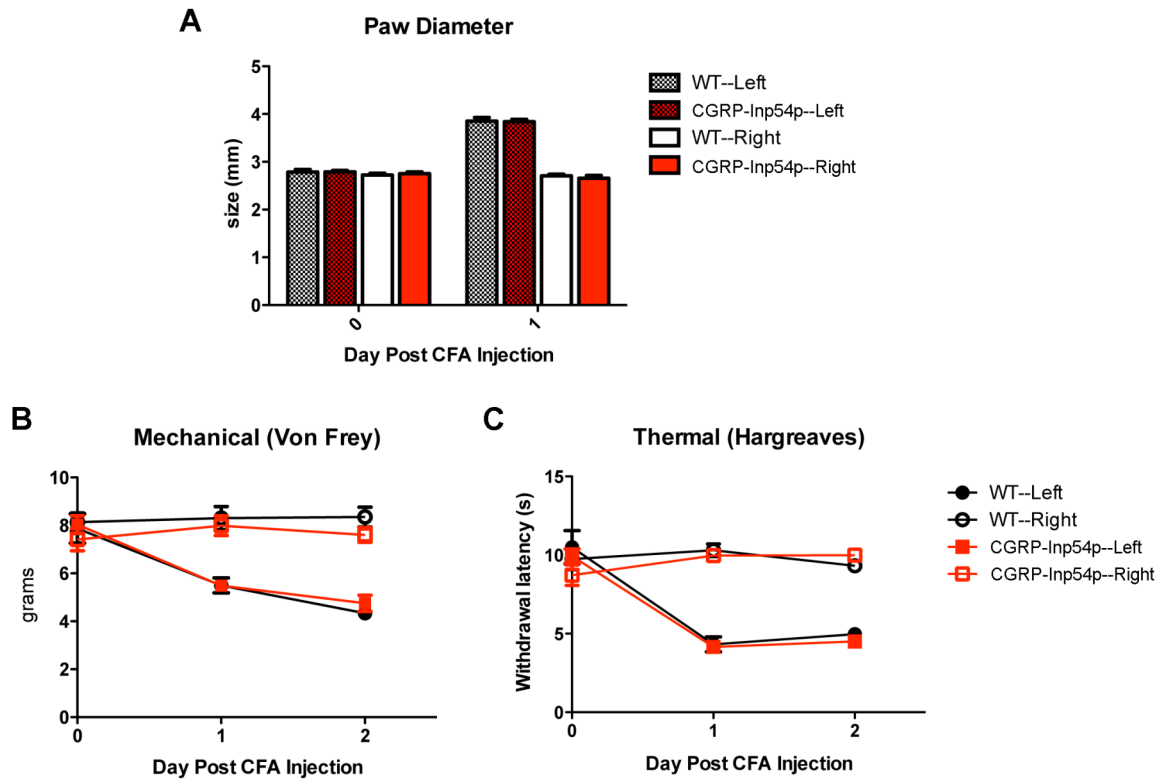


Figure 4.6. Expression of Venus-FKBP-Inp54p in heat-sensing CGRP neurons is not sufficient for reduced thermal sensitivity *in vivo*.

A) CGRP-Inp54p mice show normal inflammatory response to intraplantar injection of CFA. **B-C)** There is no statistical difference in response between CGRP-Inp54p mice and wildtype littermates in response to thermal (B) or mechanical (C) stimuli before or after CFA sensitization. n = 12 mice per genotype.

CHAPTER 5

DISCUSSION

5.1 Summary of findings

Overall, this work focused on how alterations to the plasma membrane result in functional changes to the cell as a whole. These alterations included both physical perturbations with membrane-deforming BAR domains for the srGAP family (chapters 2 and 3), and compositional changes by chemically-inducing the depletion of the phospholipid, PI(4,5)P₂ (chapter 4). This work emphasizes the importance of proper regulation of the plasma membrane to maintain a functional cell.

Chapter 2 focused on the functional consequences of altered plasma membrane curvature during cortical neuron development. Overexpression of srGAP2 in cortical neurons induced filopodia-like membrane protrusions, leading to a greater number of neurites, as well as enhanced neurite branching. These phenotypes were reduced in neurons lacking srGAP2. In fact, any srGAP2 construct containing a full-length F-BAR domain (not srGAP2^{ΔF-BAR} or F-BAR^{Δ49}) was sufficient to enhance neurite number. Additionally, there was an inverse relationship between filopodia/branching and neuronal migration. Neurons expressing exogenous srGAP2 showed inhibited migration, while shRNA-knockdown of srGAP2 resulted in increased migration. Interestingly, a point mutation rendering the SH3 domain incapable of binding other proteins was sufficient to reduce neurite branching and neuronal migration, while the complete lack of the C-terminus of srGAP2 (including the SH3 domain) restored the ability to inhibit neurite branching and cortical migration. These seemingly contradictory results suggested a model of

autoinhibitory regulation of full-length srGAP2, wherein srGAP2 exists in a closed conformation until the binding of its SH3 domain to another protein. This SH3-mediated binding could interfere with the intramolecular binding of srGAP2, which would induce a conformational change the protein and allow its F-BAR domain to dimerize, bind membrane, and induce membrane protrusions. Overall, this work illustrated that the protrusion-inducing activity and functional effects were phenocopied by the F-BAR domain alone, suggesting that the F-BAR domain of srGAP2 serves as the driving force behind srGAP2 function.

The work presented in chapter 3 further explored F-BAR domains of the srGAP family by investigating the similarities and differences in membrane-binding and curvature-induction between the F-BAR domains of srGAP1, srGAP2, and srGAP3 (F-BAR(1), F-BAR(2), and F-BAR(3), respectively). Most reviews and reports had previously grouped the three srGAP proteins into one functionally indistinct family. The work in chapter 3 demonstrated that the srGAP2 more potently induced filopodia-like membrane protrusions in non-neuronal cells than srGAP1 or srGAP3. Moreover, the protrusion formation of the three F-BAR domains mimicked their full-length counterparts; therefore, we restricted our investigation to the F-BAR domains alone, and delved into their functional and molecular differences of these srGAP family F-BAR domains. As previously described in chapter 2, F-BAR(2) potently induces filopodia-like protrusions. Alternatively, F-BAR(1) and F-BAR(3) are much less effective at producing filopodia-like membrane protrusions in non-neuronal cells; however the function of F-BAR(3) was more similar to F-BAR(2) in cortical neurons. In contrast, F-BAR(1) seemed to restrict membrane dynamics and, therefore, inhibit the induction of filopodia-like protrusions. Moreover, this work revealed that these F-BAR domains are capable of interacting, suggesting a collaboration among the three srGAP proteins in the regulation of membrane curvature.

Chapter 4 deviates from membrane curvature in order to study the effect of altering

the lipid composition of the plasma membrane on cellular signaling. The work presented in chapter 4 describes the attempt to deplete PI(4,5)P₂ from the plasma membrane of pain-sensing neurons using rapamycin-induced dimerization *in vivo*, and puts forth some of the challenges encountered in doing so. Rapamycin-induced PI(4,5)P₂ depletion worked well in transfected cell lines (**Fig. 3.5** and **Fig. 4.1**), however, our attempt to implement this system *in vivo* was not successful. While mice expressing the dimerization machinery were viable, there was no translocation of the FKBP-fused PI(4,5)P₂ phosphatase, Inp54p, upon rapamycin treatment. There are a number of possible explanations for the hindrance of the adaptation of this approach *in vivo*, many of which are discussed in chapter 4.

5.2 srGAP2 in neuronal morphology

srGAP2 was the first F-BAR containing protein to show direct involvement in neuronal morphogenesis and migration. Since the publication of the work in chapter 2, much more evidence for the role of membrane deformation in neuronal morphology has surfaced. Syndapin I has been linked to neurite outgrowth in the hippocampus; however, in contrast to the results of our work with srGAP2, the SH3 domain of syndapin I was found to be most important for its activity (Dharmalingam et al., 2009). Interestingly, the authors put forth that its F-BAR domain merely serves as a way to target the SH3 domain to the plasma membrane, as membrane-targeted SH3 domain phenocopied the neurite induction seen with the full-length protein. Unlike srGAP2, this activity was not directly due to membrane deformation of the F-BAR domain, but rather the ability of syndapin I to bind and activate N-WASP. Another F-BAR protein, Toca-1, has been implicated in neurite development through its ability to bind N-WASP as well (Kakimoto et al., 2006). FBP17 has been shown to induce spine formation, and while the authors showed that the ability to bind the plasma membrane was necessary for spine formation, they did not show whether this activity could be induced by its F-BAR domain alone. These data suggest that while many F-BAR

domain-containing proteins play a role in neurite development, it is not necessarily a direct result of membrane deformation. Recently, srGAP3 has been shown to play a role in spine formation, due to the activity of its F-BAR domain (Carlson et al., 2011). The F-BAR domain of srGAP3 was shown to be important for early spinogenesis, and could compensate for loss of srGAP3. Interestingly, knockdown of srGAP3 resulted in reduction of mature mushroom-like spines, and an increase in immature filopodia-like spines. A complete loss of srGAP3 in homozygous null animals resulted in reduced spine density in both cortical and hippocampal neurons. The Polleux lab has also found that knockdown of srGAP2 led to an increase in immature, filopodia-like protrusions (Charrier et al., *Cell*, In Press); however, in contrast to srGAP3, knockdown of srGAP2 increases spine density. These results highlight the need to delve further into the mechanisms that regulate differences between the srGAP family proteins.

5.2.1 Regulation of srGAP2 autoinhibition

Perhaps the most intriguing, unanswered question raised from the work in chapter 2 is: how is srGAP2 autoinhibition regulated? The model in chapter 2 (**Fig. 2.7**) proposed a mechanism of srGAP2 activation in which the protein is kept in an autoinhibitory state until its SH3 domain binds another protein, thereby opening the protein and allowing its F-BAR domain to dimerize and induce filopodia-like protrusions. This model of activation could account for how the seemingly ubiquitous expression of srGAP2 within the cell could still lead to precisely located activity. The question remains, however, what are the upstream activators of srGAP2?

The srGAP family was originally founded as a novel group of Rho GAP proteins that bind Robo, the membrane-bound receptor for the secreted chemorepulsive cue, Slit. Slit proteins are known to induce axon branching (Wang et al., 1999) and inhibit neuronal migration (Wu et al., 1999), making this protein a likely candidate to regulate srGAP2 activity. Other known binding partners that could act as candidates to unlock srGAP2

activity include WASP and WASP interacting protein (WIP), which have been shown to bind srGAP2 in T cells (Linkermann et al., 2009), formin-like 1 (FMNL1, Mason et al., 2010), and the actin associated scaffolding protein Palladin (Okada et al., 2011). It is known that a similar mechanism occurs with Syndapin I, as the crystal structure of full-length syndapin I shows the SH3 domain binding to the F-BAR domain (Rao et al., 2010), so it is likely to be a recurring mechanism throughout the BAR family proteins. Interestingly, while it is likely that similar regulation occurs with other srGAP proteins, activation might occur from different proteins. We have found that srGAP3 binds dynamin 2, while srGAP2 does not (data not shown). Even with similar protein domain structure, and even similar function, the proteins might be regulated by different proteins, and therefore be activated and take effect in separate cellular locations.

What are possible intramolecular interactions responsible for autoinhibition of srGAP2? One candidate for the mechanism of this autoinhibition is a cluster of negatively charged amino acids that flank the SH3 domain: amino acids number 725, 726, and 727 (D, D, and E, respectively). These negatively charged residues might interact with the positive charges in the F-BAR domain, keeping the protein closed and inactive. Additionally, identical negative charges before the SH3 domain of two canonical F-BAR-containing proteins, FBP17 and Toca-1, have been shown to regulate the activity of both proteins (Takano et al., 2008). A second potential C-terminal site for intramolecular binding is the C-terminal coiled-coil (CC) domain. CC domains have previously been implicated in autoinhibition. The CC domains of Myotonic dystrophy kinase-related Cdc42-binding kinase (MRCK) interact with the N-terminal kinase domain, thereby blocking dimerization and causing autoinhibition (Tan et al., 2001). The C-terminal CC domain of srGAP2 could interact with the N-terminal CC domain of the F-BAR, to block dimerization and lead to autoinhibition. It remains to be determined whether specific interactions are necessary to disrupt srGAP2 autoinhibition, or whether any binding partner that can interfere with

intramolecular binding is suitable to unlock srGAP2 autoinhibition to expose the F-BAR for activation.

5.3 Functional differences between F-BARs of the srGAP protein family

While the work discussed in chapter 3 demonstrated functional differences between the F-BAR domains of srGAP family proteins, there is still a lot of work to be done regarding the molecular mechanisms responsible for these differences. Some of these mechanisms were briefly touched upon in this work, as in differences between lipid-binding specificity, however these open more questions for the field. Furthermore, although this work provides interesting insight into the differences between the filopodia-inducing activities and regulation of membrane dynamics of these F-BAR domains, the full-length proteins most likely introduce further discrepancies in function of the srGAP proteins.

Chapter 3 shows that there is different lipid-binding specificity between F-BAR(2) and F-BAR(3), specifically in regards to PI(4,5)P₂ and PS. The best way to address the differences in lipid-binding specificity is to use purified with purified lipids of known composition. In collaboration with Holger Sondermann's lab, we attempted the purification of F-BARs 1-3 to elucidate the differences in lipid-binding specific for the work in chapter 3; however, due to technical difficulties, they were unable to purify these F-BARs within our timeframe. Elucidating the differences in lipid-specificity between these F-BAR domains could help to explain the differences in localization, and therefore partially explain differences in function between the three proteins. As shown in chapter 3, F-BAR(3) is more dependent on PI(4,5)P₂ than F-BAR(2). PI(4,5)P₂ is thought to exist in clusters within the plasma membrane, similar to lipid rafts, rather than evenly distributed around the plasma membrane (Johnson et al., 2008). Furthermore, these clustered pools of PI(4,5)P₂ are thought to relate strongly to cell morphology and PI(4,5)P₂ signaling. Binding of F-BAR(3) to these clusters of concentrated PI(4,5)P₂ pools could serve to localize srGAP3 to

different areas of the plasma membrane than srGAP2, presumably resulting in different protein-protein interactions as well. Additionally, local lipid composition can affect membrane curvature (Janmey and Kannunen, 2006), which could result in different binding and localization of the F-BAR domains of the srGAP protein family.

The results regarding the differences in F-BAR localization within filopodia are quite interesting, specifically that F-BAR(2) extends throughout the length of the filopodium, while F-BAR(1) and F-BAR(3) stop prematurely (**Fig. 3.3**). These results lead to the hypothesis that three F-BAR domains could have specificity for different degrees of membrane curvature. The question of whether BAR domain proteins can sense curvature, as well as function in membrane-deformation, has been long debated within the field. If these F-BAR domains are able to sense membrane curvature and bind to different degrees of curvature, this could account for functional differences between the srGAP proteins. The tip of a filopodium is a highly-curved, concave structure with relation to the cytoplasmic surface of the cell, whereas the membrane along the filopodial shaft is much less curved. In contrast, the membrane connecting the base of the filopodium to the peripheral membrane of the cell is convex from the perspective of cytoplasmic proteins. If the degree of membrane curvature plays a role in the binding of F-BAR domains of the srGAP family proteins to the plasma membrane, then this would account for differential localization between the three proteins. It is especially interesting to note that the F-BAR of srGAP2 was shown to bind single-phosphorylated forms of PI more strongly than PI(4,5)P₂ when assessed with PIP strips and PIP arrays, yet this F-BAR strongly localizes to the plasma membrane where these single-phosphorylated PI concentrations are low. This suggests that more than lipid composition is responsible for F-BAR localization, and membrane curvature might be a key suspect. One way to test this hypothesis would be to form liposomes of different sizes by forcing purified lipids through porous gradients of varying sizes. Larger liposomes have more shallow curvature, and smaller liposomes have more extreme curvature. These

liposomes could then be mixed purified F-BAR domains or full-length srGAP proteins to assess the curvature-specificity range of each protein. Furthermore, these liposomes could be made from different lipid compositions to assess the combination of lipid specificity and curvature binding. Unfortunately, as discussed previously, we currently do not have the purified proteins to test.

Our data also revealed that these proteins can interact. While we do not currently know whether this occurs through direct binding (possibly through heterodimerization) or indirect binding through other proteins, the interaction through formation of a membrane-deforming complex made up of F-BAR domain-containing proteins with different functions is intriguing. This also raises the possibility that these proteins binding to other BAR domain-containing proteins, or other proteins that can affect membrane deformation, to intricately regulate membrane and cellular morphology.

5.4 Challenges to rapamycin-inducible PI(4,5)P₂ depletion *in vivo*

As discussed in Chapter 4, there are both documented and undocumented limitations to using this rapamycin-inducible translocation system to deplete PI(4,5)P₂ in neurons and *in vivo*. These complications might be additive when attempting to use this system in neurons *in vivo*. Section 5.4.1 further discusses these challenges, as well as puts forth ways to test and possibly overcome these obstacles.

5.4.1 Future directions with the current design

5.4.1i Behavioral assessment Rosa-FRB^{PLF}/CGRP-Inp54p double heterozygous mice.

Although we cannot visualize translocation of venus-FKBP-Inp54p in the double heterozygous mice after injection of rapamycin, it is possible that PI(4,5)P₂ is depleted upon sub-visual levels of translocation. Unfortunately, this cannot currently be measured directly with the two methods of PI(4,5)P₂ measurement that we use in the Zylka lab, namely anti-PI(4,5)P₂ antibody (Echelon Bioscience, Inc.) and PI(4,5)P₂ Mass Elisa (Echelon

Bioscience, Inc.), as these do not appear work in these mice *in vivo*. Although we have seen a reduction in PI(4,5)P₂ using the antibody with dissociated CGRP-Inp54p DRG neurons *in vitro* (**Fig. 4.4**), the antibody does not cleanly label the plasma membrane in DRG tissue (data not shown). Although troubleshooting this technique has led to better staining, it has not yet achieved a strong enough level of staining with a large enough dynamic range can be seen to confidently and positively assess PI(4,5)P₂ depletion. In contrast to the reduction of PI(4,5)P₂ seen *in vitro*, PI(4,5)P₂ mass elisa reveals no difference in PI(4,5)P₂ levels in lumbar DRG from CGRP-Inp54p mice compared to wildtype littermates (data not shown). Two possibilities for lack of difference arise: 1) there is no difference in resting PI(4,5)P₂ levels in CGRP-Inp54p neurons *in vivo*, and 2) any difference induced by Inp54p would be drowned out by the large percentage of CGRP/Inp54p-negative (~70%) neurons in the DRG. The original hypothesis for the use of rapamycin-inducible depletion of PI(4,5)P₂ by translocation of Inp54p from the cytoplasm to the membrane was that Inp54p could only induce its effect after translocation; however, *in vitro* results in neurons (**Fig. 4.4**) and non-neuronal cell lines (data not shown) suggests that there is some basal reduction of PI(4,5)P₂ by the cytoplasmic venus-FKBP-Inp54p. This is not too surprising, as expression of cytoplasmic proteins are not secluded from the plasma membrane, and therefore will be able to interact with, and reduce, PI(4,5)P₂ when the two interact. However, there could compensation that occurs *in vivo* to rescue this PI(4,5)P₂ depletion. In terms of the normal PI(4,5)P₂ levels assessed by mass elisa, the small reduction in PI(4,5)P₂ might be drowned out by the other 70% of neurons with wildtype levels of PI(4,5)P₂. Furthermore, this assay has a large amount of variation that could serve to drown out small changes in this 30% of neurons. Therefore, behavioral assessment might be the best way to assess translocation and PI(4,5)P₂ depletion *in vivo*.

Intrathecal (IT) injection of rapamycin has been shown to reduce persistent pain sensitivity in Sprague Dawley rats (Géranton et al, 2009; Xu et al., 2011); however, this

effect was most potent in myelinated sensory A-fiber DRG neurons, rather than unmyelinated nociceptive C-fibers (Géranton et al, 2009). These results demonstrate that 1) IT injection of rapamycin can reach and affect DRG neurons *in vivo*, and 2) rapamycin injection affects pain states, therefore the proper controls are crucial for rapamycin-induced depletion of PI(4,5)P₂ to assess pain behavior. Therefore, the last experiment to round out the current study of rapamycin-induced PI(4,5)P₂ depletion in pain sensitivity *in vivo*, will be to assess mechanical and thermal sensitivity (see section 4.4.5, **Fig. 4.6**) after rapamycin injection in Rosa-FRB^{PLF}/CGRP-Inp54p double heterozygous mice compared to CGRP-Inp54p littermate controls. The use of the single CGRP-Inp54p heterozygous mice will serve as controls for the alleviated pain resulting from rapamycin injection alone. Given the lack of visual translocation, we do not expect to see a difference after rapamycin injection; however, this is a critical experiment in assessing the feasibility of rapamycin-induced translocation of Inp54p, and subsequent reduction in PI(4,5)P₂ and related signaling *in vivo*.

5.4.1ii Stabilization of the FRB^{PLF} domain might be necessary for sufficient PI(4,5)P₂ depletion *in vivo*.

Studies by Stankunas et al. (2003, 2007) suggest that FRB domain containing the K2095P, T2098L, and W2101F mutations is not stabilized until after prolonged exposure to rapamycin, which causes stabilization through complex formation of FKBP-rapamycin-FRB. The authors found that stabilization of the FRB^{PLF}-GSK-3 β fusion started around 6 hours, but full stabilization did not occur until after approximately 24 hours of rapamycin treatment (Stankunas et al., 2003). It is therefore possible that any effects of rapamycin-induced translocation between the CFP-FRB^{PLF} and the venus-FKBP-Inp54p will not occur until the FRB domain is properly stabilized. This hypothesis can be tested by injecting rapamycin at 12 hour intervals for 24 hours (0, 12, and 24 hours), sacrificing the mice, and looking at membrane to cytoplasm ratios of venus-FKBP-Inp54p. Alternatively, this can be done *in vitro* to assess translocation after prolonged rapamycin treatment of dissociated neurons.

Additionally, this *in vitro* treatment will allow for assessment of PI(4,5)P₂ depletion over time using the anti-PI(4,5)P₂ antibody.

While we do see expression of CFP at the plasma membrane of Rosa-FRB^{PLF} heterozygous mice, expression is quite weak, especially for the fact that the protein is driven by the strong CAG promoter. Even if rapamycin treatment can further stabilize the FRB^{PLF} domain, the possibility remains, that destabilized FRB^{PLF} at the membrane is incapable of binding to cytoplasmic FKBP-Inp54p in sufficient quantities to cause adequate stabilization. Stankunas et al. (2003) expressed the GSK3 β -FRB^{PLF} fusion in the cytoplasm, and relied on rapamycin-induced binding to endogenous FKBP12 in the cytoplasm for stabilization. If stabilization needs to occur for proper translocation, this might be a catch-22 experiment. Results from cell lines would suggest that this is not the issue, but as I have shown, there are clearly differences between cell lines in culture, and neurons *in vivo*.

5.4.1iii The magic ratio problem

As discussed by Komatsu et al. (2010), different FRB- and FKBP-containing constructs require different expression ratios to induce translocation. These ratios can be altered by a number of factors, including domain order in the expression constructs, the organelle targeted for translocation, etc. It is possible that different cell types have their own magic ratios necessary for rapamycin-induced translocation. Using the constructs expressed in our mice in cell lines, it seemed as though the FRB domain might be the limiting factor in translocation. Unfortunately, the expression in the mouse is fixed, and levels cannot be adjusted much *in vivo*. However, it is possible to use a Rosa-FRB^{PLF} homozygous/CGRP-Inp54p heterozygous mouse to achieve a more optimal protein ratio for translocation. Again, translocation can be assessed in DRG sections after IT injection of rapamycin *in vivo*, or treatment of dissociated neurons *in vitro*. Alternatively, dissociated neurons can be transfected with an array of different ratios to assess if there is any ratio

that will work in these neurons.

5.4.1iv Rapamycin-induced depletion of PI(4,5)P₂ with Inp54p might not work in neurons

There is a tacit awareness regarding the fact that PI(4,5)P₂ depletion with Inp54p might not work in neurons. Personal communication with faculty and postdoctoral fellows who have attempted to use either the full rapamycin-induced PI(4,5)P₂ depletion system in neurons, or Inp54p constructs alone in neurons, have suggested that the system does not work in neurons. Furthermore, they suggested that neuron health is highly compromised after transfection with these constructs. Cytoplasmic Inp54p has been described as a constitutively active 5-phosphatase (Nebl et al., 2000), and chronic PI(4,5)P₂ depletion can lead to loss of cytoskeletal-membrane adhesion (Raucher et al., 2000), and activated apoptotic pathways, assessed by cleaved caspase-3 activation (Azuma et al., 2000; Mejillano et al., 2000). Accordingly, dissociated neurons from our mice expressing the venus-FKBP-Inp54p construct have elevated levels of cleaved caspase-3 compared to control neurons (**Fig. 4.5**). The only use of rapamycin-induced PI(4,5)P₂ depletion by translocation of Inp54p in neurons was by Chen et al. (2010). The authors showed that transfection of the membrane-tagged FRB domain and FKBP-Inp54p components into cultured hippocampal neurons, followed by rapamycin treatment, led to reduced filopodial dynamics. In contrast, rapamycin treatment did not change filopodial dynamics in hippocampal neurons transfected with the FRB domain and a phosphatase-dead mutant of Inp54p. However, the authors did not show both conditions prior to rapamycin treatment, nor did they visualize any translocation. It is possible that the effects were not due to translocation-induced depletion of PI(4,5)P₂, but rather due to leaky effects of expressing Inp54p in the neurons.

One approach to test this would be to dissociate DRG, and transfect the translocation component constructs into cells in culture. Transfection into dissociated DRG

would lead to the expression of these constructs in multiple cell types of the DRG, both neuronal and non-neuronal. After rapamycin treatment, we could assess the extent of translocation in all cell types. It is possible that other cell types could allow for rapamycin-induced translocation, or be able to better tolerate the expression of Inp54p. Therefore, no matter how extensively we troubleshoot Inp54p translocation in these mice, it is possible that we just cannot achieve PI(4,5)P₂ depletion, or even Inp54p-translocation, in neurons.

5.4.2 Alternative design and approach to rapamycin-inducible PI(4,5)P₂ depletion in vivo

If destabilization of the FRB^{PLF} domain is the cause of lack of translocation, an easy fix would be to redesign the Rosa-FRB mouse with a stable FRB construct. Stankunas et al. (2007) found that the T2098L mutation led to its destabilizing properties, whereas the W2101F mutation was responsible for its ability to bind the rapalog, C20-MaRap (Bayle et al., 2006). Therefore, the benefit of C20-MaRap can still be achieved without protein destabilization by using a FRB^{PTF} mutation. However, if the problem is that rapamycin-induced translocation does not work in neurons, this FRB mutation would not solve the problem.

An alternative approach would be to take advantage of the destabilizing properties of the FRB^{PLF} domain, and redesign the system to make translocation unnecessary. Expressing of a fusion protein that targets a FRB^{PLF}-destabilized 5-phosphatase to the plasma membrane would still allow for temporal control of PI(4,5)P₂ depletion upon treatment of rapamycin or C20-MaRap. In this case, there would be no need for expression of an FKBP construct, as rapamycin would induce stabilization with binding of endogenous FKBP12, as used by Stankunas et al. (2003). This would also overcome the magic ratio problem because there would be no need for translocation. Additionally, it could be possible to control the amount of destabilization, and therefore level of PI(4,5)P₂ depletion by stabilized Inp54p, by injecting different amounts of rapamycin. However, if

complete destabilization due to FRB^{PLF} fusion does not occur, this fusion would lead to a constitutively active Inp54p at the plasma membrane, which could lead to the same cell health problems discussed above. Alternative 5-phosphatases, such as Synaptojanin or mammalian Type IV 5-phosphatase, could possibly be more amenable for use in neurons than the yeast 5-phosphatase, Inp54p. Therefore, this design should be extensively tested and optimized in neurons before implementation *in vivo*.

REFERENCES

1. **Ahearn, I. M., Tsai, F. D., Court, H., Zhou, M., Jennings, B. C., Ahmed, M., Fehrenbacher, N., Linder, M. E. and Philips, M. R.** (2011). FKBP12 Binds to Acylated H-Ras and Promotes Depalmitoylation. *Mol Cell* **41**, 173-185.
2. **Allen, V., Swigart, P., Cheung, R., Cockcroft, S. and Katan, M.** (1997). Regulation of inositol lipid-specific phospholipase C-delta by changes in Ca²⁺ ion concentration. *Biochem J* **327**, 545-552.
3. **Arnold, S. J., Huang, G.-J., Cheung, A. F. P., Era, T., Nishikawa, S.-I., Bikoff, E. K., Molnar, Z., Robertson, E. J. and Groszer, M.** (2008). The T-box transcription factor Eomes/Tbr2 regulates neurogenesis in the cortical subventricular zone. *Genes & Dev* **22**, 2479-2484.
4. **Aspenstrom, P., Fransson, A. and Richnau, N.** (2006). Pombe Cdc15 homology proteins: regulators of membrane dynamics and the actin cytoskeleton. *Trends Biochem Sci* **31**, 670-679.
5. **Ayala, R., Shu, T. and Tsai, L. H.** (2007). Trekking across the brain: the journey of neuronal migration. *Cell* **128**, 29-43.
6. **Azuma, T., Koths, K., Flanagan, L. and Kwiatkowski, D.** (2000). Gelsolin in Complex with Phosphatidylinositol 4,5-Bisphosphate Inhibits Caspase-3 and -9 to Retard Apoptotic Progression. *J Biol Chem* **275**, 3761-3766.
7. **Bacon, C., Endris, V. and Rappold, G.** (2009). Dynamic expression of the Slit-Robo GTPase activating protein genes during development of the murine nervous system. *J Comp Neurol* **513**, 224-236.
8. **Barnes, A. P. and Polleux, F.** (2009). Establishment of axon-dendrite polarity in developing neurons. *Annu Rev Neurosci* **32**, 347-381.
9. **Bayle, J., Grimley, J., Stankunas, K., Gestwicki, J., Wandless, T. and Crabtree, G.** (2006). Rapamycin analogs with differential binding specificity permit orthogonal control of protein activity. *Chem Biol* **13**, 99-107.
10. **Bear, J. E., Loureiro, J. J., Libova, I., Fassler, R., Wehland, J. and Gertler, F. B.** (2000). Negative regulation of fibroblast motility by Ena/VASP proteins. *Cell* **101**, 717-728.
11. **Bear, J. E., Svitkina, T. M., Krause, M., Schafer, D. A., Loureiro, J. J., Strasser, G. A., Maly, I. V., Chaga, O. Y., Cooper, J. A., Borisy, G. G. et al.** (2002). Antagonism between Ena/VASP proteins and actin filament capping regulates fibroblast motility. *Cell* **109**, 509-521.
12. **Berridge, M. J.** (1983). Rapid accumulation of inositol trisphosphate reveals that agonists hydrolyse polyphosphoinositides instead of phosphatidylinositol. *Biochem J* **212**, 849-858.
13. **Berridge, M. J. and Irvine, R. F.** (1984). Inositol trisphosphate, a novel second

- messenger in cellular signal transduction. *Nature* **312**, 315-321.
14. **Biluart, P., Bienvenu, T., Ronce, N., Portes, V. d., Vinet, M. C., Zemni, R., Crolius, H. R., Carrie, A., Fauchereau, F., Cherry, M. et al.** (1998). Oligophrenin-1 encodes a rhoGAP protein involved in X-linked mental retardation. *Nature* **392**, 923-926.
 15. **Brauchi, S., Orta, G., Mascayano, C., Salazar, M., Raddatz, N., Urbina, H., Rosenmann, E., Gonzalez, F. and Latorre, R.** (2007). Dissection of the components for PIP2 activation and thermosensation in TRP channels. *Proc Natl Acad Sci* **104**, 10246-10251.
 16. **Bu, W., Chou, A. M., Lim, K. B., Sudhaharn, T. and Ahmed, S.** (2009). The Toca-1-N-WASP complex links filopodial formation to endocytosis. *J Biol Chem* **284**, 289-297.
 17. **Burnette, D. T., Schaefer, A. W., Ji, L., Danuser, G. and Forscher, P.** (2007). Filopodial actin bundles are not necessary for microtubule advance into the peripheral domain of Aplysia neuronal growth cones. *Nat Cell Biol* **9**, 1360-1369.
 18. **Carlson, B. and Soderling, S. H.** (2009). Mechanisms of cellular protrusions branch out. *Dev Cell* **17**, 307-309.
 19. **Carlson, B. R., Lloyd, K. E., Kruszewski, A., Kim, I. H., Rodriguiz, R. M., Heindel, C., Faytell, M., Dudek, S. M., Wetsel, W. C. and Soderling, S. H.** (2011). WRP/srGAP3 facilitates the initiation of spine development by an inverse F-BAR domain, and its loss impairs long-term memory. *J Neurosci* **31**, 2447-2460.
 20. **Caterina, M. J., Leffler, A., Malmberg, A. B., Martin, W. J., Trafton, J., Petersen-Zeit, K. R., Koltzenburg, M., Basbaum, A. I. and Julius, D.** (2000). Impaired nociception and pain sensation in mice lacking the capsaicin receptor. *Science* **288**, 306-313.
 21. **Causeret, F., Terao, M., Jacobs, T., Nishimura, Y. V., Yanagawa, Y., Obata, K., Hoshino, M. and Nikolic, M.** (2008). The p21-activated kinase is required for neuronal migration in the cerebral cortex. *Cereb Cortex* **19**, 861-875.
 22. **Cavanaugh, D. J., Lee, H., Lo, L., Shields, S. D., Zylka, M. J., Basbaum, A. I. and Anderson, D. J.** (2009). Distinct subsets of unmyelinated primary sensory fibers mediate behavioral responses to noxious thermal and mechanical stimuli. *Proc Natl Acad Sci* **106**, 9075-9080.
 23. **Charrier, C., Joshi, K., Coutinho-Budd, J., Kim, J.-E., Lambert, N., deMarchenaPowell, J., Jin, W.-L., Vanderhaeghen, P., Ghosh, A., Sassa, T. et al.** (2012). Inhibition of SRGAP2 function in dendritic spine maturation by its human-specific paralogs. *Cell In Press*.
 24. **Chen, Y., Wang, F., Long, H., Chen, Y., Wu, Z. and Ma, L.** (2011). GRK5 promotes F-actin bundling and targets bundles to membrane structures to control neuronal morphogenesis. *J Cell Biol* **194**, 905-920.

25. **Chen, Z. B., Zhang, H. Y., Zhao, J. H., Zhao, W., Zhao, D., Zheng, L. F., Zhang, X. F., Liao, X. P. and Yi, X. N.** (2012). Slit-Robo GTPase-Activating Proteins are Differentially Expressed in Murine Dorsal Root Ganglia: Modulation by Peripheral Nerve Injury. *Anat Rec Epub*.
26. **Chhajed, P. N., Dickenmann, M., Bubendorf, L., Mayr, M., Steiger, J. and Tamm, M.** (2006). Patterns of Pulmonary Complications Associated with Sirolimus. *Respiration* **73**, 367-374.
27. **Chitu, V., Pixley, F. J., Macaluso, F., Larson, D. R., Condeelis, J., Yeung, Y. G. and Stanley, E. R.** (2005). The PCH family member MAYP/PSTPIP2 directly regulates F-actin bundling and enhances filopodia formation and motility in macrophages. *Mol Biol Cell* **16**, 2947-2959.
28. **Chong, L. D., Traynor-Kaplan, A., Bokoch, G. M. and Schwartz, M. A.** (1994). The small GTP-binding protein Rho regulates a phosphatidylinositol 4-phosphate 5-kinase in mammalian cells. *Cell* **79**, 507-513.
29. **Chuang, H. H., Prescott, E. D., Kong, H., Shields, S., Jordt, S. E., Basbaum, A. I., Chao, M. V. and Julius, D.** (2001). Bradykinin and nerve growth factor release the capsaicin receptor from PtdIns(4,5)P₂-mediated inhibition. *Nature* **411**, 957-962.
30. **Corpet, F.** (1988). Multiple sequence alignment with hierarchical clustering. *Nucl Acids Res* **16**, 10881-10890.
31. **Crabtree, G. R. and Schreiber, S. L.** (1996). Three-part inventions: intracellular signaling and induced proximity. *Trends Biochem Sci* **21**, 418-422.
32. **Dent, E. W., Barnes, A. M., Tang, F. and Kalil, K.** (2004). Netrin-1 and semaphorin 3A promote or inhibit cortical axon branching, respectively, by reorganization of the cytoskeleton. *J Neurosci* **24**, 3002-3012.
33. **Dent, E. W., Kwiatkowski, A. V., Mebane, L. M., Philippar, U., Barzik, M., Rubinson, D. A., Gupton, S., Van Veen, J. E., Furman, C., Zhang, J. et al.** (2007). Filopodia are required for cortical neurite initiation. *Nat Cell Biol* **9**, 1347-1359.
34. **Dharmalingam, E., Haeckel, A., Pinyol, R., Schwintzer, L., Koch, D., Kessels, M. M. and Qualmann, B.** (2009). F-BAR proteins of the syndapin family shape the plasma membrane and are crucial for neuromorphogenesis. *J Neurosci* **29**, 13315-13327.
35. **Dingwall, C., Sharnick, S. V. and Laskey, R. A.** (1982). A polypeptide domain that specifies migration of nucleoplasmin into the nucleus. *Cell* **30**, 449-458.
36. **DiPaolo, G., Sankaranarayanan, S., Wenk, M. R., Daniell, L., Perucco, E., Caldarone, B. J., Flavell, R., Picciotto, M., Ryan, T., Cremona, O. et al.** (2002). Decreased synaptic vesicle recycling efficiency and cognitive deficits in amphiphysin 1 knockout mice. *Neuron* **33**, 789-804.
37. **Doherty, G. J. and McMahon, H. T.** (2008). Mediation, modulation, and consequences of membrane-cytoskeleton interactions. *Annu Rev Biophys* **37**, 65-95.

38. **Dotti, C. G., Sullivan, C. A. and Banker, G. A.** (1988). The establishment of polarity by hippocampal neurons in culture. *J Neurosci* **8**, 1454-1468.
39. **Eberth, A., Lundmark, R., Gremer, L., Dvorsky, R., Koessmeier, K. T., McMahon, H. T. and Ahmadian, M. R.** (2009). A BAR domain-mediated autoinhibitory mechanism for RhoGAPs of the GRAF family. *Biochem J* **417**, 371-377.
40. **Endris, V., Haussman, L., Buss, E., Bacon, C., Bartsch, D. and Rappold, G.** (2011). SrGAP3 interacts with lamellipodin at the cell membrane and regulates Rac-dependent cellular protrusions. *J Cell Sci* **124**, 3941-3955.
41. **Endris, V., Wogatzky, B., Leimer, U., Bartsch, D., Zatyka, M., Latif, F., Maher, E. R., Tariverdian, G., Kirsch, S., Karch, D. et al.** (2002). The novel Rho-GTPase activating gene MEGAP/ srGAP3 has a putative role in severe mental retardation. *Proc Natl Acad Sci U S A* **99**, 11754-11759.
42. **Fenrich, K. and Gordon, T.** (2004). Canadian Association of Neuroscience review: axonal regeneration in the peripheral and central nervous systems--current issues and advances. *Can J Neurol Sci* **31**, 142-156.
43. **Fili, N., Calleja, V., Woscholski, R., Parker, P. J. and Larijani, B.** (2006). Compartmental signal modulation: Endosomal phosphatidylinositol 3-phosphate controls endosome morphology and selective cargo sorting. *Proc Natl Acad Sci* **103**, 15473-15478.
44. **Flesch, F., Yu, J., Lemmon, M. and Burger, K.** (2005). Membrane activity of the phospholipase C-delta1 pleckstrin homology (PH) domain. *Biochem* **389**, 435-441.
45. **Foletta, V. C., Brown, F. D. and Young, W. S., 3rd.** (2002). Cloning of rat ARHGAP4/C1, a RhoGAP family member expressed in the nervous system that colocalizes with the Golgi complex and microtubules. *Brain Res Mol Brain Res* **107**, 65-79.
46. **Ford, M. G., Mills, I. G., Peter, B. J., Vallis, Y., Praefcke, G. J., Evans, P. R. and McMahon, H. T.** (2002). Curvature of clathrin-coated pits driven by epsin. *Nature* **419**, 361-366.
47. **Frost, A., De Camilli, P. and Unger, V. M.** (2007). F-BAR proteins join the BAR family fold. *Structure* **15**, 751-753.
48. **Frost, A., Perera, R., Roux, A., Spasov, K., Destaing, O., Egelman, E. H., De Camilli, P. and Unger, V. M.** (2008). Structural basis of membrane invagination by F-BAR domains. *Cell* **132**, 807-817.
49. **Frost, A., Unger, V. M. and Camilli, P. D.** (2009). The BAR domain superfamily: membrane-molding macromolecules. *Cell* **137**, 191-196.
50. **Funakoshi, Y., Hasegawa, H. and Kanaho, Y.** (2011). Regulation of PIP5K activity by Arf6 and its physiological significance. *J Cell Physiol* **226**, 888-895.

51. **Gallo, G. and Letourneau, P. C.** (1998). Localized sources of neurotrophins initiate axon collateral sprouting. *J Neurosci* **18**, 5403-5414.
52. **Gallo, G. and Letourneau, P. C.** (1998). Regulation of growth cone actin filaments by guidance cues. *J Neurobiol* **2004**, 92-102.
53. **Geranton, S. M., Jimenez-Diaz, L., Torsney, C., Tochiki, K. K., Stuart, S. A., Leith, J. L., Lumb, B. M. and Hunt, S. P.** (2009). A rapamycin-sensitive signaling pathway is essential for the full expression of persistent pain states. *J Neurosci* **29**, 15017-15027.
54. **Gilmore, A. P. and Burridge, K.** (1996). Regulation of vinculin binding to talin and actin by phosphatidyl-inositol-4-5-bisphosphate. *Nature* **381**, 531-535.
55. **Goh, K. L., Cepko, C. L. and Gertler, F. B.** (2002). Ena/VASP proteins regulate cortical neuronal positioning. *Curr Biol* **12**, 565-569.
56. **Govek, E. E., Newey, S. E., Akerman, C. J., Cross, J. R., Veken, L. V. d. and Aelst, L. V.** (2004). The X-linked mental retardation protein oligophrenin-1 is required for dendritic spine morphogenesis. *Nat Neurosci* **7**, 364-372.
57. **Govek, E. E., Newey, S. E. and Van Aelst, L.** (2005). The role of the Rho GTPases in neuronal development. *Genes Dev* **19**, 1-49.
58. **Guerrier, S., Coutinho-Budd, J., Sassa, T., Gresset, A., Jordan, N. V., Chen, K., Jin, W. L., Frost, A. and Polleux, F.** (2009). The F-BAR domain of srGAP2 induces membrane protrusions required for neuronal migration and morphogenesis. *Cell* **138**, 990-1004.
59. **Guo, S. and Bao, S.** (2010). srGAP2 arginine methylation regulates cell migration and cell spreading through promoting dimerization. *J Biol Chem* **285**, 35133-35141.
60. **Gupta, A., Sanada, K., Miyamoto, D. T., Rovelstad, S., Nadarajah, B., Pearlman, A. L., Brunstrom, J. and Tsai, L. H.** (2003). Layering defect in p35 deficiency is linked to improper neuronal-glia interaction in radial migration. *Nat Neurosci* **6**, 1284-1291.
61. **Gupta, A., Tsai, L. H. and Wynshaw-Boris, A.** (2002). Life is a journey: a genetic look at neocortical development. *Nat Rev Genet* **3**, 342-355.
62. **Gupton, S. L. and Gertler, F. B.** (2007). Filopodia: the fingers that do the walking. *Sci STKE* **2007**, re5.
63. **Habermann, B.** (2004). The BAR-domain family of proteins: a case of bending and binding? *EMBO Rep* **5**, 250-255.
64. **Hall, A.** (1994). Small GTP-binding proteins and the regulation of the actin cytoskeleton. *Annu Rev Cell Biol* **10**, 31-54.
65. **Halstead, J. R., Savaskan, N. E., vandenBout, I., VanHorck, F., Hajdo-Milasinovic, A., Snell, M., Keune, W. J., TenKlooster, J. P., Hordijk, P. L. and**

- Divecha, N.** (2010). Rac controls PIP5K localisation and PtdIns(4,5)P₂ synthesis, which modulates vinculin localisation and neurite dynamics. *J Cell Sci* **123**, 3535-3546.
66. **Han, J., Leeper, L., Rivero, F. and Chung, C.** (2006). Role of RacC for the regulation of WASP and phosphatidylinositol 3-kinase during chemotaxis of Dictyostelium. *J Biol Chem* **281**, 35224-25234.
67. **Hand, R., Bortone, D., Mattar, P., Nguyen, L., Heng, J. I., Guerrier, S., Boutt, E., Peters, E., Barnes, A. P., Parras, C. et al.** (2005). Phosphorylation of Neurogenin2 specifies the migration properties and the dendritic morphology of pyramidal neurons in the neocortex. *Neuron* **48**, 45-62.
68. **Hansen, S. B., Tao, X. and MacKinnon, R.** (2011). Structural basis of PIP2 activation of the classical inward rectifier K⁺ channel Kir2.2. *Nature* **477**, 495-498.
69. **Harlan, J., Hajduk, P., Yoon, H. and Fesik, S.** (1994). Pleckstrin homology domains bind to phosphatidylinositol-4,5-bisphosphate. *Nature* **371**, 168-170.
70. **Heath, R. and Insall, R.** (2008). F-BAR domains: multifunctional regulators of membrane curvature. *Biochem Biophys Acta* **1761**, 897-912.
71. **Heng, J. I., Nguyen, L., Castro, D. S., Zimmer, C., Wildner, H., Armant, O., Skowronska-Krawczyk, D., Bedogni, F., Matter, J. M., Hevner, R. et al.** (2008). Neurogenin 2 controls cortical neuron migration through regulation of Rnd2. *Nature*.
72. **Henne, W. M., Kent, H. M., Ford, M. G., Hegde, B. G., Daumke, O., Butler, P. J., Mittal, R., Langen, R., Evans, P. R. and McMahon, H. T.** (2007). Structure and analysis of FCHO2 F-BAR domain: a dimerizing and membrane recruitment module that effects membrane curvature. *Structure* **15**, 839-852.
73. **Hentges, K. E., Sirry, B., Gingeras, A.-C., Sarbassov, D., Sonenberg, N., Sabatini, D. and Peterson, A. S.** (2001). FRAP_mTOR is required for proliferation and patterning during embryonic development in the mouse. *Proc Natl Acad Sci* **98**, 13796-13801.
74. **Heo, W. D., Inoue, T., Park, W. S., Kim, M. L., Park, B. O., Wandless, T. J. and Meyer, T.** (2006). PI(3,4,5)P₃ and PI(4,5)P₂ Lipids Target Proteins with Polybasic Clusters to the Plasma Membrane. *Science* **314**, 1458-1461.
75. **Higginbotham, H. R. and Gleeson, J. G.** (2007). The centrosome in neuronal development. *Trends Neurosci* **30**, 276-283.
76. **Hilgemann, D. W. and Ball, R.** (1996). Regulation of cardiac Na⁺, Ca²⁺ exchange and KATP potassium channels by PIP₂. *Science* **273**, 956-959.
77. **Honda, A., Nogami, M., Yokozeki, T., Yamazaki, M., Nakamura, H., Watanabe, H., Kawamoto, K., Nakayama, K., Morris, A. J., Frohman, M. A. et al.** (1999). Phosphatidylinositol 4-phosphate 5-kinase alpha is a downstream effector of the small G protein ARF6 in membrane ruffle formation. *Cell* **99**, 521-532.

78. **Huang, F., Matthies, H., Speese, S., Smith, M. and Broadie, K.** (2004). Rolling blackout, a newly identified PIP2-DAG pathway lipase required for Drosophila phototransduction. *Nat Neurosci* **7**, 1070-1078.
79. **Huttelmaier, S., Mayboroda, O., Harbeck, B., Jarchau, T., Jockusch, B. M. and Rudiger, M.** (1998). The interaction of the cell-contact proteins VASP and vinculin is regulated by phosphatidylinositol-4,5-bisphosphate. *Curr Biol* **8**, 479-488.
80. **Insall, R. H. and Weiner, O. D.** (2001). PIP3, PIP2, and Cell Movement—Similar Messages, Different Meanings? *Dev Cell* **1**, 743-749.
81. **Itoh, T. and De Camilli, P.** (2006). BAR, F-BAR (EFC) and ENTH/ANTH domains in the regulation of membrane-cytosol interfaces and membrane curvature. *Biochim Biophys Acta* **1761**, 897-912.
82. **Itoh, T., Erdmann, K. S., Roux, A., Habermann, B., Werner, H. and De Camilli, P.** (2005). Dynamin and the actin cytoskeleton cooperatively regulate plasma membrane invagination by BAR and F-BAR proteins. *Dev Cell* **9**, 791-804.
83. **Janetopoulos, C., Borleis, J., Vazquez, F., Iijima, M. and Devreotes, P.** (2005). Temporal and spatial regulation of phosphoinositide signaling mediates cytokinesis. *Dev Cell* **8**, 467-477.
84. **Janmey, P. A. and Kinnunen, P. K.** (2006). Biophysical properties of lipids and dynamic membranes. *Trends Cell Biol* **16**, 538-546.
85. **Jin, L., Zeng, H., Chien, S., Otto, K., Richard, R. E., Emery, D. W. and Blau, A.** (2000). In vivo selection using a cell-growth switch. *Nature Gen* **26**, 64-66.
86. **Johnson, C. M., Chichilli, G. R. and Rodgers, W.** (2008). Compartmentalization of phosphatidylinositol 4,5-bisphosphate signaling evidenced using targeted phosphatases. *J Biol Chem* **283**, 29920-29928.
87. **Julius, D. and Basbaum, A. I.** (2001). Molecular mechanisms of nociception. *Nature* **413**, 203-210.
88. **Kaech, S., Fischer, M., Doll, T. and Matus, A.** (1997). Isoform specificity in the relationship of actin to dendritic spines. *J Neurosci* **17**, 9565-9572.
89. **Kakimoto, T., Katoh, H. and Negishi, M.** (2006). Regulation of neuronal morphology by Toca-1, an F-BAR/EFC protein that induces plasma membrane invagination. *J Biol Chem* **281**, 29042-29053.
90. **Karpova, A. Y., Tervo, D. G., Gray, N. W. and Svoboda, K.** (2005). Rapid and reversible chemical inactivation of synaptic transmission in genetically targeted neurons. *Neuron* **48**, 727-735.
91. **Kawauchi, T., Chihama, K., Nabeshima, Y. and Hoshino, M.** (2003). The in vivo roles of STEF/Tiam1, Rac1 and JNK in cortical neuronal migration. *EMBO J* **22**, 4190-4201.

92. **Kim, W., Chang, S., Daniell, L., Cremona, O., DiPaolo, G. and DeCamilli, P.** (2002). Delayed reentry of recycling vesicles into the fusion-competent synaptic vesicle pool in synaptojanin 1 knockout mice. *Proc Natl Acad Sci* **99**, 17143-17148.
93. **Kinoshita, M.** (2006). Diversity of septin scaffolds. *Curr Opin Cell Biol* **18**, 54-60.
94. **Klein, R. M., Ufret-Vincenty, C. A., Hua, L. and Gordon, S. E.** (2008). Determinants of Molecular Specificity in Phosphoinositide Regulation: PHOSPHATIDYLINOSITOL (4,5)-BISPHOSPHATE (PI(4,5)P₂) IS THE ENDOGENOUS LIPID REGULATING TRPV1. *J Biol Chem* **283**, 26208-26216.
95. **Koch, D., Spiwoks-Becker, I., Sabanov, V., Sinning, A., Dugladze, T., Stellmacher, A., Ahuja, R., Grimm, J., Schuler, S., Muller, A. et al.** (2011). Proper synaptic vesicle formation and neuronal network activity critically rely on syndapin I. *EMBO J* **30**, 4955-4969.
96. **Komatsu, T., Kukelyansky, I., McCaffery, J. M., Ueno, T., Varela, L. C. and Inoue, T.** (2010). Organelle-specific, rapid induction of molecular activities and membrane tethering. *Nat Methods* **7**, 206-208.
97. **Konno, D., Yoshimura, S., Hori, K., Maruoka, H. and Sobue, K.** (2005). Involvement of the phosphatidylinositol 3-kinase/rac1 and cdc42 pathways in radial migration of cortical neurons. *J Biol Chem* **280**, 5082-5088.
98. **Kuhn, R. and Schwenk, F.** (2002). Conditional Knockout Mice. *Methods in Mol Biol* **209**, 159-185.
99. **Kutsche, K., Yntema, H., Brandt, A., Jantke, I., Nothwang, H. G., Orth, U., Boavida, M. G., David, D., Chelly, J., Fryns, J. P. et al.** (2000). Mutations in ARHGEF6, encoding a guanine nucleotide exchange factor for Rho GTPases, in patients with X-linked mental retardation. *Nat Genet* **26**, 247-250.
100. **Kwiatkowski, A. V., Rubinson, D. A., Dent, E. W., Edward van Veen, J., Leslie, J. D., Zhang, J., Mebane, L. M., Philippar, U., Pinheiro, E. M., Burds, A. A. et al.** (2007). Ena/VASP Is Required for neuritogenesis in the developing cortex. *Neuron* **56**, 441-455.
101. **Lambert de Rouvroit, C. and Goffinet, A. M.** (2001). Neuronal migration. *Mech Dev* **105**, 47-56.
102. **Lee, S., Kerff, F., Chereau, D., Ferron, R., Klug, A. and Doinguez, R.** (2007). Structural basis for the actin-binding function of Missing-in-Metastasis. *Structure* **15**, 145-155.
103. **Li, X., Chen, Y., Liu, Y., Gao, J., Gao, F., Bartlam, M., Wu, J. Y. and Rao, Z.** (2006). Structural basis of Robo proline-rich motif recognition by the srGAP1 Src homology 3 domain in the Slit-Robo signaling pathway. *J Biol Chem* **281**, 28430-28437.
104. **Liberles, S. D., Diver, S. T., Austin, D. J. and Schreiber, S. L.** (1997). Inducible gene expression and protein translocation using nontoxic ligands identified by a mammalian three-hybrid screen. *Proc Natl Acad Sci* **94**, 7825-7830.

105. **Lim, K. B., Bu, W., Goh, W. I., Koh, E., Ong, S. H., Pawson, T., Sudhakaran, T. and Ahmed, S.** (2008). The Cdc42 effector IRSp53 generates filopodia by coupling membrane protrusion with actin dynamics. *J Biol Chem* **283**, 20454-20472.
106. **Linkermann, A., Gelhaus, C., Lettau, M., Qian, J., Kabelitz, D. and Janssen, O.** (2009). Identification of interaction partners for individual SH3 domains of Fas ligand associated members of the PCH protein family in T lymphocytes. *Biochim Biophys Acta* **1794**, 168-176.
107. **Liu, Y. and Bankaitis, V. A.** (2010). Phosphoinositide phosphatases in cell biology and disease. *Prog Lipid Res* **49**, 201-217.
108. **London, E. and Brown, D.** (2000). Insolubility of lipids in Triton X-100: physical origin and relationship to sphingolipid/cholesterol membrane domains (rafts). *Biochem Biophys Acta* **1508**, 182-195.
109. **Lopes, C. M., Zhang, H., Rohacs, T., Jin, T., Yang, J. and Logothetis, D. E.** (2002). Alterations in conserved Kir channel-PIP2 interactions underlie channelopathies. *Neuron* **34**, 933-944.
110. **Lowe, C. U., Terrey, M. and Mac, L. E.** (1952). Organic-aciduria, decreased renal ammonia production, hydrophthalmos, and mental retardation; a clinical entity. *AMA Am J Dis Child* **83**, 164-183.
111. **Lukacs, V., Thyagarajan, B., Varnai, P., Balla, A., Balla, T. and Rohacs, T.** (2007). Dual regulation of TRPV1 by phosphoinositides. *J Neurosci* **27**, 7070-7080.
112. **Luo, L.** (2002). Actin cytoskeleton regulation in neuronal morphogenesis and structural plasticity. *Annu Rev Cell Dev Biol* **18**, 601-635.
113. **Majerus, P. W., Ross, T. S., Cunningham, T. W., Caldwell, K. K., Jefferson, A. B. and Bansai, V. S.** (1990). Recent insights in phosphatidylinositol signaling. *Cell* **63**, 459-465.
114. **Martel, V., Racaud-Sultan, C., Dupe, S., Marie, C., Paulhe, F., Galmiche, A., Block, M. R. and Albiges-Rizo, C.** (2001). Conformation, localization, and integrin binding of talin depend on its interaction with phosphoinositides. *J Biol Chem* **276**, 21217-21227.
115. **Martin-Belmonte, F., Gassama, A., Datta, A., Yu, W., Rescher, U., Gerke, V. and Mostov, K.** (2007). PTEN-mediated apical segregation of phosphoinositides controls epithelial morphogenesis through Cdc42. *Cell* **128**, 383-397.
116. **Mason, F. M., Heimsath, E. G., Higgs, H. N. and Soderling, S. H.** (2011). Bi-modal regulation of a formin by srGAP2. *J Biol Chem* **286**, 6577-6586.
117. **Masuda, M., Takeda, S., Sone, M., Ohki, T., Mori, H., Kamioka, Y. and Mochizuki, N.** (2006). Endophilin BAR domain drives membrane curvature by two newly identified structure-based mechanisms. *EMBO J* **25**, 2889-2897.
118. **Mattar, P., Britz, O., Johannes, C., Nieto, M., Ma, L., Rebeyka, A., Klenin, N.,**

- Polleux, F., Guillemot, F. and Schuurmans, C.** (2004). A screen for downstream effectors of Neurogenin2 in the embryonic neocortex. *Dev Biol* **273**, 373-389.
119. **Mattila, P. K. and Lappalainen, P.** (2008). Filopodia: molecular architecture and cellular functions. *Nat Rev Mol Cell Biol* **9**, 446-454.
120. **Mattila, P. K., Pykalainen, A., Saarikangas, J., Paavilainen, V. O., Vihinen, H., Jokitalo, E. and Lappalainen, P.** (2007). Missing-in-metastasis and IRSp53 deform PI(4,5)P2-rich membranes by an inverse BAR domain-like mechanism. *J Cell Biol* **176**, 953-964.
121. **McCoy, E. S., Taylor-Blake, B. and Zylka, M. J.** (2012). CGRP α -expressing sensory neurons respond to stimuli that evoke sensations of pain and itch. *PloS One Submitted*.
122. **McLaughlin, S., Wang, J., Gambhir, A. and Murray, D.** (2002). PIP(2) and proteins; interactions, organization, and information flow. *Annu Rev Biophys Biomol Struct* **31**, 151-175.
123. **Mejillano, M., Yamamoto, M., Rozelle, A. L., Sun, H. Q., Wang, X. and Yin, H. L.** (2001). Regulation of apoptosis by phosphatidylinositol 4,5-bisphosphate inhibition of caspases, and caspase inactivation of phosphatidylinositol phosphate 5-kinases. *J Biol Chem* **276**, 1865-1872.
124. **Miki, H., Miura, K. and Takenawa, T.** (1996). N-WASP, a novel actin-depolymerizing protein, regulates the cortical cytoskeletal rearrangement in a PIP2-dependent manner downstream of tyrosine kinases. *EMBO J* **15**, 5326-5335.
125. **Millard, T. H., Bompard, G., Hueng, M. Y., Dafforn, T. R., Scott, D. J., Machesky, L. M. and Fütterer, K.** (2005). Structural basis of filopodia formation induced by the IRSp53/MIM homology domain of human IRSp53. *EMBO J* **24**, 240-250.
126. **Millard, T. H., Dawson, J. and Machesky, L. M.** (2007). Characterisation of IRTKS, a novel IRSp53/MIM family actin regulator with distinct filament bundling properties. *J Cell Sci* **120**, 1663-1672.
127. **Mitchell, K., Ferrell, J. and Huestis, W.** (1986). Separation of phosphoinositides and other phospholipids by two-dimensional thin-layer chromatography. *Anal Biochem* **158**, 447-453.
128. **Mitin, N., Betts, L., Yohe, M. E., Der, C. J., Sondek, J. and Rossman, K. L.** (2007). Release of autoinhibition of ASEF by APC leads to CDC42 activation and tumor suppression. *Nat Struct Mol Biol* **14**, 814-823.
129. **Molyneaux, B. J., Arlotta, P., Menezes, J. R. L. and Macklis, J. D.** (2007). Neuronal subtype specification in the cerebral cortex. *Nat Rev Neurosci* **8**, 427-437.
130. **Neascu, N. and Flonta, M.-L.** (2006). Classification of dorsal root ganglion neurons from newborn rat in organotypic cultures. *Romanian J Biophys* **16**, 77-91.
131. **Nebi, T., Oh, S. W. and Luna, E. J.** (2000). Membrane cytoskeleton: PIP2 pulls the

- strings. *Curr Biol* **10**, R351-R354.
132. **Neukomm, L. J., Frei, A. P., Cabello, J., Kinchen, J. M., Zaidel-Bar, R., Ma, Z., Haney, L. B., Hardin, J., Ravichandran, K. S., Moreno, S. et al.** (2011). Loss of the RhoGAP SRGP-1 promotes the clearance of dead and injured cells in *Caenorhabditis elegans*. *Nat Cell Biol* **13**, 79-86.
 133. **Ng, J. and Luo, L.** (2004). Rho GTPases regulate axon growth through convergent and divergent signaling pathways. *Neuron* **44**, 779-793.
 134. **Nimnual, A. S., Taylor, L. J. and Bar-Sagi, D.** (2003). Redox-dependent downregulation of Rho by Rac. *Nat Cell Biol* **5**, 236-241.
 135. **Noctor, S. C., Martinez-Cerdeno, V., Ivic, L. and Kriegstein, A. R.** (2004). Cortical neurons arise in symmetric and asymmetric division zones and migrate through specific phases. *Nat Neurosci* **7**, 136-144.
 136. **Ogawa, M., Miyata, T., Nakajima, K., Yagyu, K., Seike, M., Ikenaka, K., Yamamoto, H. and Mikoshiba, K.** (1995). The reeler gene-associated antigen on Cajal-Retzius neurons is a crucial molecule for laminar organization of cortical neurons. *Neuron* **14**, 899-912.
 137. **Ohshima, T., Hirasawa, M., Tabata, H., Mutoh, T., Adachi, T., Suzuki, H., Saruta, K., Iwasato, T., Itohara, S., Hashimoto, M. et al.** (2007). Cdk5 is required for multipolar-to-bipolar transition during radial neuronal migration and proper dendrite development of pyramidal neurons in the cerebral cortex. *Development* **134**, 2273-2282.
 138. **Oikawa, T., Yamaguchi, H., Itoh, T., Kato, M., Ijuin, T., Yamazaki, D., Suetsugu, S. and Takenawa, T.** (2004). PtdIns(3,4,5)P3 binding is necessary for WAVE2-induced formation of lamellipodia. *Nat Cell Biol* **6**, 420-426.
 139. **Ojala, P. J., Paavilainen, V. and Lappalainen, P.** (2001). Identification of yeast cofilin residues specific for actin monomer and PIP2 binding. *Biochemistry* **40**, 15562-15569.
 140. **Okada, H., Uezu, A., Mason, F. M., Soderblom, E. J., Moseley, M. A. and Soderling, S. H.** (2011). SH3 domain-based phototrapping in living cells reveals Rho family GAP signaling complexes. *Sci Signal* **4**, rs13.
 141. **Peter, B. J., Kent, H. M., Mills, I. G., Vallis, Y., Butler, P. J., Evans, P. R. and McMahon, H. T.** (2004). BAR domains as sensors of membrane curvature: the amphiphysin BAR structure. *Science* **303**, 495-499.
 142. **Polleux, F. and Ghosh, A.** (2002). The slice overlay assay: a versatile tool to study the influence of extracellular signals on neuronal development. *Sci STKE* **2002**, PL9.
 143. **Prescott, E. D. and Julius, D.** (2003). A modular PIP2 binding site as a determinant of capsaicin receptor sensitivity. *Science* **23**, 1284-1288.
 144. **Putyrski, M. and Schultz, C.** (2011). Switching Heterotrimeric G Protein Subunits

- with a Chemical Dimerizer. *Chem Biol* **18**, 1126-1133.
145. **Pykäläinen, A., Boczkowska, M., Zhao, H., Saarikangas, J., Rebowski, G., Jansen, M., Hakanen, J., Koskela, E., Peränen, J., Vihinen, H. et al.** (2011). Pinkbar is an epithelial-specific BAR domain protein that generates planar membrane structures. *Nat Struct Mol Biol* **Epub ahead of print**
 146. **Qualmann, B., Roos, J., DiGregorio, P. J. and Kelly, R. B.** (1999). Syndapin I, a synaptic dynamin-binding protein that associates with the neural Wiskott-Aldrich syndrome protein. *Mol Biol Cell* **10**, 501-513.
 147. **Quinones, G. A., Jin, J. and Oro, A. E.** (2010). I-BAR protein antagonism of endocytosis mediates directional sensing during guided cell migration. *J Cell Biol* **189**, 353-367.
 148. **Raftopoulou, M. and Hall, A.** (2004). Cell migration: Rho GTPases lead the way. *Dev Biol* **265**, 23-32.
 149. **Rao, Y., Ma, Q., Vahedi-Faridi, A., Sundborger, A., Pechstein, A., Puchkov, D., Luo, L., Shupliakov, O., Saenger, W. and Haucke, V.** (2010). Molecular basis for SH3 domain regulation of F-BAR-mediated membrane deformation. *Proc Natl Acad Sci U S A* **107**, 8213-8218.
 150. **Raucher, D., Stauffer, T., Chen, W., Shen, K., Guo, S., York, J., Sheetz, M. and Meyer, T.** (2000). Phosphatidylinositol 4,5-bisphosphate functions as a second messenger that regulates cytoskeleton-plasma membrane adhesion. *Cell* **100**, 221-228.
 151. **Rebecchi, M. J. and Pentylala, S. N.** (2000). Structure, function, and control of phosphoinositide-specific phospholipase C. *Physiol Rev* **80**, 1291-1335.
 152. **Riedl, J., Crevenna, A. H., Kessenbrock, K., Yu, J. H., Neukirchen, D., Bista, M., Bradke, F., Jenne, D., Holak, T. A., Werb, Z. et al.** (2008). Lifeact: a versatile marker to visualize F-actin. *Nat Methods* **5**, 605-607.
 153. **Rodal, A. A., Motola-Barnes, R. N. and Littleton, J. T.** (2008). Nervous wreck and Cdc42 cooperate to regulate endocytic actin assembly during synaptic growth. *J Neurosci* **28**, 8316-8325.
 154. **Rohacs, T., Thyagarajan, B. and Lukacs, V.** (2008). Phospholipase C mediated modulation of TRPV1 channels. *Mol Neurobiol* **37**, 153-163.
 155. **Rossman, K. L., Der, C. J. and Sondek, J.** (2005). GEF means go: turning on RHO GTPases with guanine nucleotide-exchange factors. *Nat Rev Mol Cell Biol* **6**, 167-180.
 156. **Rouquette-Jazdanian, A., Pelassy, C., Breitmayer, J.-P., Cousin, J.-L. and Aussenel, C.** (2002). Metabolic labeling of membrane microdomains/rafts in Jurkat cells indicates the presence of glycerophospholipids implicated in signal transduction by the CD3 T-cell receptor. *Biochem J* **363**, 645-655.

157. **Saarikangas, J., Hakanen, J., Mattila, P. K., Grumet, M., Salminen, M. and Lappalainen, P.** (2008). ABBA regulates plasma-membrane and actin dynamics to promote radial glia extension. *J Cell Sci* **121**, 1444-1454.
158. **Saarikangas, J., Zhao, H., Pykalainen, A., Laurinmaki, P., Mattila, P. K., Kinnunen, P. K., Butcher, S. J. and Lappalainen, P.** (2009). Molecular mechanisms of membrane deformation by I-BAR domain proteins. *Curr Biol* **19**, 95-107.
159. **Saengsawang, W., Mitok, K., Viesselmann, C., Pietila, L., Lombard, D. C., Corey, S. J. and Dent, E. W.** (2012). The F-BAR Protein CIP4 Inhibits Neurite Formation by Producing Lamellipodial Protrusions. *Curr Biol* **EPub**.
160. **Saitsu, H., Osaka, H., Sugiyama, S., Kurosawa, K., Mizuguchi, T., Nishiyama, K., Nishimura, A., Tsurusaki, Y., Doi, H., Miyake, N. et al.** (2011). Early infantile epileptic encephalopathy associated with the disrupted gene encoding Slit-Robo Rho GTPase activating protein 2 (SRGAP2). *Am J Med Genet A* **EPub**.
161. **Salmon, A. M., Damaj, I., Sekine, S., Picciotto, M. R., Marubio, L. M. and Changeux, J. P.** (1999). Modulation of morphine analgesia in alphaCGRP mutant mice. *Neuroreport* **10**, 849-854.
162. **Schuske, K. R., Richmond, J. E., Matthies, D. S., Davis, W. S., Runz, S., Rube, D. A., vanderBliet, A. M. and Jorgensen, E. M.** (2003). Endophilin is required for synaptic vesicle endocytosis by localizing synaptojanin. *Neuron* **40**, 749-762.
163. **Scita, G., Confalonieri, S., Lappalainen, P. and Suetsugu, S.** (2008). IRSp53: crossing the road of membrane and actin dynamics in the formation of membrane protrusions. *Trends Cell Biol* **18**, 52-60.
164. **She, B. R., Liou, G. G. and Lin-Chao, S.** (2002). Association of the growth-arrest-specific protein Gas7 with F-actin induces reorganization of microfilaments and promotes membrane outgrowth. *Exp Cell Res* **273**, 34-44.
165. **Sheetz, M. and Dai, J.** (1996). Modulation of membrane dynamics and cell motility by membrane tension. *Trends Cell Biol* **6**, 85-89.
166. **Shimada, A., Niwa, H., Tsujita, K., Suetsugu, S., Nitta, K., Hanawa-Suetsugu, K., Akasaka, R., Nishino, Y., Toyama, M., Chen, L. et al.** (2007). Curved EFC/F-BAR-domain dimers are joined end to end into a filament for membrane invagination in endocytosis. *Cell* **129**, 761-772.
167. **Shutes, A. and Der, C. J.** (2006). Real-time in vitro measurement of intrinsic and Ras GAP-mediated GTP hydrolysis. *Methods Enzymol* **407**, 9-22.
168. **Simpson, K. J., Selfors, L. M., Bui, J., Reynolds, A., Leake, D., Khvorova, A. and Brugge, J. S.** (2008). Identification of genes that regulate epithelial cell migration using an siRNA screening approach. *Nat Cell Biol*.
169. **Soares, J., Dippold, C., Wells, K., Franck, E., Kupfer, D. and Mallinger, A.** (2001). Increased platelet membrane phosphatidylinositol-4,5-bisphosphate in drug-

- free depressed bipolar patients. *Neurosci Letters* **299**, 150-152.
170. **Soares, J., Mallinger, A., Dippold, C., Wells, K. F., Frank, E. and Kupfer, D.** (2000). PIP2 is known to inhibit the product of a gene that has been shown to be linked to bipolar disorder in some individuals. *Psychopharm* **149**, 12-16.
 171. **Soderling, S. H., Binns, K. L., Wayman, G. A., Davee, S. M., Ong, S. H., Pawson, T. and Scott, J. D.** (2002). The WRP component of the WAVE-1 complex attenuates Rac-mediated signalling. *Nat Cell Biol* **4**, 970-975.
 172. **Soderling, S. H., Guire, E. S., Kaech, S., White, J., Zhang, F., Schutz, K., Langeberg, L. K., Banker, G., Raber, J. and Scott, J. D.** (2007). A WAVE-1 and WRP signaling complex regulates spine density, synaptic plasticity, and memory. *J Neurosci* **27**, 355-365.
 173. **Sowa, N., Street, S., Vihko, P. and Zylka, M.** (2010). Prostatic acid phosphatase reduces thermal sensitivity and chronic pain sensitization by depleting phosphatidylinositol 4,5-bisphosphate. *J Neurosci* **30**, 10282-10293.
 174. **Spencer, D. M., Belshaw, P. J., Chen, L., Ho, S. N., Randazzo, F., Crabtree, G. R. and Schreiber, S. L.** (1996). Functional analysis of Fas signaling in vivo using synthetic inducers of dimerization. *Curr Biol* **6**, 839-847.
 175. **Stankunas, K., Bayle, J. H., Gestwicki, J. E., Lin, Y. M., Wandless, T. J. and Crabtree, G. R.** (2003). Conditional protein alleles using knockin mice and a chemical inducer of dimerization. *Mol Cell* **12**, 1615-1624.
 176. **Stankunas, K., Bayle, J. H., Havranek, J. J., Wandless, T. J., Baker, D., Crabtree, G. R. and Gestwicki, J. E.** (2007). Rescue of degradation-prone mutants of the FK506-rapamycin binding (FRB) protein with chemical ligands. *Chembiochem* **8**, 1162-1169.
 177. **Stefan, C. J., Audhya, A. and Emr, S. D.** (2002). The yeast synaptojanin-like proteins control the cellular distribution of phosphatidylinositol (4,5)-bisphosphate. *Mol Biol Cell* **13**, 542-557.
 178. **Stirling, L. C., Forlani, G., Baker, M. D., Wood, J. N., Matthews, E. A., Dickenson, A. H. and Nassar, M. A.** (2005). Nociceptor-specific gene deletion using heterozygous NaV1.8-Cre recombinase mice. *Pain* **113**, 27-36.
 179. **Suetsugu, S., Murayama, K., Sakamoto, A., Hanawa-Suetsugu, K., Seto, A., Oikawa, T., Mishima, C., Shirouzu, M., Takenawa, T. and Yokoyama, S.** (2006). The RAC binding domain/IRSp53-MIM homology domain of IRSp53 induces RAC-dependent membrane deformation. *J Biol Chem* **281**, 35347-35358.
 180. **Suh, B.-C. and Hille, B.** (2005). Regulation of ion channels by phosphatidylinositol 4,5-bisphosphate. *Curr Opin Neurobio* **15**, 370-378.
 181. **Suh, B.-C. and Hille, B.** (2008). PIP2 is a necessary cofactor for ion channel function: how and why? *Annu Rev Biophys* **37**, 175-195.

182. **Suh, B.-C., Inoue, T., Meyer, T. and Hille, B.** (2006). Rapid chemically induced changes of PtdIns(4,5)P₂ gate KCNQ ion channels. *Science* **314**, 1454-1457.
183. **Suh, B.-C., Leal, K. and Hille, B.** (2010). Modulation of High-Voltage Activated Ca²⁺ Channels by Membrane Phosphatidylinositol 4,5-Bisphosphate. *Neuron* **67**, 224-238.
184. **Symons, M., Derry, J. M., Karlak, B., Jiang, S., Lemahieu, V., McCormick, F., Francke, U. and Abo, A.** (1996). Wiskott-Aldrich syndrome protein, a novel effector for the GTPase CDC42Hs, is implicated in actin polymerization. *Cell* **84**, 723-734.
185. **Takano, K., Toyooka, K. and Suetsugu, S.** (2008). EFC/F-BAR proteins and the N-WASP-WIP complex induce membrane curvature-dependent actin polymerization. *EMBO J* **27**, 2817-2828.
186. **Takei, K., Slepnev, V., Haucke, V. and DeCamilli, P.** (1999). Functional partnership between amphiphysin and dynamin in clathrin-mediated endocytosis. *Nat Cell Biol* **1**, 33-39.
187. **Tan, I., Seow, K., Lim, L. and Leung, T.** (2008). Intermolecular and intramolecular interactions regulate catalytic activity of myotonic dystrophy kinase-related Cdc42-binding kinase alpha. *Mol Cell Biol* **21**, 2767-2778.
188. **Threadgill, R., Bobb, K. and Ghosh, A.** (1997). Regulation of Dendritic Growth and Remodeling by Rho, Rac, and Cdc42. *Neuron* **19**, 625-634.
189. **Tran, D., Gascard, P., Berthon, B., Fukami, K., Takenawa, T., Giraud, F. and Claret, M.** (1993). Cellular distribution of polyphosphoinositides in rat hepatocytes. *Cell Signal* **5**, 565-581.
190. **Tsujita, K., Suetsugu, S., Sasaki, N., Furutani, M., Oikawa, T. and Takenawa, T.** (2006). Coordination between the actin cytoskeleton and membrane deformation by a novel membrane tubulation domain of PCH proteins is involved in endocytosis. *J Cell Biol* **172**, 269-279.
191. **Ufret-Vincenty, C. A., Klein, R. M., Hua, L., Angueyra, J. and Gordon, S. E.** (2011). Localization of the PIP₂ sensor of TRPV1 ion channels. *J Biol Chem* **286**, 9688-9698.
192. **Vallis, Y., Wigge, P., Marks, B., Evans, P. R. and McMahon, H. T.** (1999). Importance of the pleckstrin homology domain of dynamin in clathrin-mediated endocytosis. *Curr Biol* **9**, 257-260.
193. **Varnai, P., Thyagarajan, B., Rohacs, T. and Balla, T.** (2006). Rapidly inducible changes in phosphatidylinositol 4,5-bisphosphate levels influence multiple regulatory functions of the lipid in intact living cells. *J Cell Biol* **175**, 377-382.
194. **Vogt, D. L., Gray, C. D., Young, W. S., 3rd, Orellana, S. A. and Malouf, A. T.** (2007). ARHGAP4 is a novel RhoGAP that mediates inhibition of cell motility and axon outgrowth. *Mol Cell Neurosci* **36**, 332-342.

195. **Volpicelli-Daley, L. A., Lucast, L., Gong, L. W., Liu, L., Sasaki, J., Abrams, C. S., Kanaho, Y. and DeCamilli, P.** (2010). Phosphatidylinositol-4-phosphate 5-kinases and phosphatidylinositol 4,5-bisphosphate synthesis in the brain. *J Biol Chem* **285**, 28708-28714.
196. **Voronov, S. V., Frere, S. G., Giovedi, S., Pollina, E. A., Borel, C., Zhang, H., Schmidt, C., Akeson, E. C., Wenk, M. R., Cimasoni, L. et al.** (2008). Synaptojanin 1-linked phosphoinositide dyshomeostasis and cognitive deficits in mouse models of Down's syndrome. *Proc Natl Acad Sci* **105**, 9416-9420.
197. **Wakita, Y., Kakimoto, T., Katoh, H. and Negishi, M.** (2011). The F-BAR protein Rapostlin regulates dendritic spine formation in hippocampal neurons. *J Biol Chem* **286**, 32672-32683.
198. **Wang, H. and Zylka, M. J.** (2009). Mrgprd-expressing polymodal nociceptive neurons innervate most known classes of substantia gelatinosa neurons. *J Neurosci* **29**, 13202-13209.
199. **Wang, K. H., Brose, K., Arnott, D., Kidd, T., Goodman, C. S., Henzel, W. and Tessier-Lavigne, M.** (1999). Biochemical purification of a mammalian slit protein as a positive regulator of sensory axon elongation and branching. *Cell* **96**, 771-784.
200. **Wang, Q., Navarro, M. V., Peng, G., Molinelli, E., Goh, S. L., Judson, B. L., Rajashankar, K. R. and Sonderrmann, H.** (2009). Molecular mechanism of membrane constriction and tubulation mediated by the F-BAR protein Pacsin/Syndapin. *Proc Natl Acad Sci U S A* **106**, 12700-12705.
201. **Wang, Y., Lian, L., Golden, J. A., Morrissey, E. E. and Abrams, C. S.** (2007). PIP5Kly is required for cardiovascular and neuronal development. *Proc Nat Acad Sci* **2007**, 11748-11753.
202. **Weernink, P. A., Meletiadis, K., Hommeltenberg, S., Hinz, M., Ishihara, H., Schmidt, M. and Jakobs, K.** (2004). Activation of type I phosphatidylinositol 4-phosphate 5-kinase isoforms by the Rho GTPases, RhoA, Rac1, and Cdc42. *J Biol Chem* **279**, 7840-7849.
203. **Weernink, P. A. O., Schulte, P., Guo, Y., Wetzels, J., Amano, M., Kaibuchi, K., Haverland, S., Voss, M., Schmidt, M., Mayr, G. W. et al.** (2000). Stimulation of phosphatidylinositol-4-phosphate 5-kinase by Rho-kinase. *J Biol Chem* **275**, 10168-10174.
204. **Wiradjaja, F., Ooms, L. M., Whisstock, J. C., McColl, B., Helfenbaum, L., Sambrook, J. F., Gething, M. J. and Mitchell, C. A.** (2001). The yeast inositol polyphosphate 5-phosphatase Inp54p localizes to the endoplasmic reticulum via a C-terminal hydrophobic anchoring tail: regulation of secretion from the endoplasmic reticulum. *J Biol Chem* **276**, 7643-7653.
205. **Wong, K., Ren, X. R., Huang, Y. Z., Xie, Y., Liu, G., Saito, H., Tang, H., Wen, L., Brady-Kalnay, S. M., Mei, L. et al.** (2001). Signal transduction in neuronal migration: roles of GTPase activating proteins and the small GTPase Cdc42 in the Slit-Robo pathway. *Cell* **107**, 209-221.

206. **Wu, M., Huang, B., Graham, M., Raimondi, A., Heuser, J. E., Zhuang, X. and DeCamilli, P.** (2010). Coupling between clathrin-dependent endocytic budding and F-BAR-dependent tubulation in a cell-free system. *Nat Cell Biol* **12**, 902-908.
207. **Wu, W., Wong, K., Chen, J. H., Jiang, Z. H., Dupuis, S., Wu, J. Y. and Rao, Y.** (1999). Directional guidance of neuronal migration in the olfactory system by the secreted protein Slit. *Nature* **400**, 331-336.
208. **Xu, Q., Fitzsimmons, B., Steinauer, J., O'Neill, A., Newton, A. C., Hua, X.-Y. and Yaksh, T. L.** (2011). Spinal Phosphoinositide 3-Kinase–Akt–Mammalian Target of Rapamycin Signaling Cascades in Inflammation-Induced Hyperalgesia. *J Neurosci* **31**, 2114-2124.
209. **Xu, T., Johnson, C. A., Gestwicki, J. E. and Kumar, A.** (2010). Conditionally controlling nuclear trafficking in yeast by chemical-induced protein dimerization. *Nat Protocol* **5**, 1831-1843.
210. **Yamagishi, A., Masuda, M., Ohki, T., Onishi, H. and Mochizuki, N.** (2004). A novel actin bundling/filopodium-forming domain conserved in insulin receptor tyrosine kinase substrate p53 and missing in metastasis protein. *J Biol Chem* **279**, 14929-14936.
211. **Yamamoto, M., Hilgemann, D. H., Feng, S., Bito, H., Ishihara, H., Shibasaki, Y. and Yin, H. L.** (2001). Phosphatidylinositol 4,5-Bisphosphate Induces Actin Stress-Fiber Formation and Inhibits Membrane Ruffling in Cv1 Cells. *J Cell Biol* **152**, 867-876.
212. **Yang, C., Hoelzle, M., Disanza, A., Scita, G. and Svitkina, T.** (2009). Coordination of membrane and actin cytoskeleton dynamics during filopodia protrusion. *PLoS One* **4**, e5678.
213. **Yang, Y., Marcello, M., Endris, V., Saffrich, R., Fischer, R., Trendelenburg, M. F., Sprengel, R. and Rappold, G.** (2006). MEGAP impedes cell migration via regulating actin and microtubule dynamics and focal complex formation. *Exp Cell Res* **312**, 2379-2393.
214. **Yao, Q., Jin, W. L., Wang, Y. and Ju, G.** (2008). Regulated shuttling of Slit-Robo-GTPase activating proteins between nucleus and cytoplasm during brain development. *Cell Mol Neurobiol* **28**, 205-221.
215. **Yohe, M. E., Rossman, K. L., Gardner, O. S., Karnoub, A. E., Snyder, J. T., Gershburg, S., Graves, L. M., Der, C. J. and Sondek, J.** (2007). Auto-inhibition of the Dbl family protein Tim by an N-terminal helical motif. *J Biol Chem* **282**, 13813-13823.
216. **Yoshida, S., Bartolini, S. and Pellman, D.** (2009). Mechanisms for concentrating Rho1 during cytokinesis. *Genes Dev* **23**, 810-823.
217. **Yoshihara, Y., Roo, M. D. and Muller, D.** (2009). Dendritic spine formation and stabilization. *Curr Opin Neurobiol* **19**, 146-153.

218. **Yoshizawa, M., Kawauchi, T., Sone, M., Nishimura, Y. V., Terao, M., Chihama, K., Nabeshima, Y. and Hoshino, M.** (2005). Involvement of a Rac activator, P-Rex1, in neurotrophin-derived signaling and neuronal migration. *J Neurosci* **25**, 4406-4419.
219. **Yu, F. X., Sun, H. Q., Janmey, P. A. and Yin, H. L.** (1992). Identification of a polyphosphoinositide-binding sequence in an actin monomer-binding domain of gelsolin. *J Biol Chem* **267**, 14616-14621.
220. **Zaidel-Bar, R., Joyce, M. J., Lynch, A. M., Witte, K., Audhya, A. and Hardin, J.** (2010). The F-BAR domain of SRGP-1 facilitates cell-cell adhesion during *C. elegans* morphogenesis. *J Cell Biol* **15**, 761-769.
221. **Zhang, H., Craciun, L. C., Mirshahi, T., Rohacs, T., Lopes, C. M., Jin, T. and Logothetis, D. E.** (2003). PIP(2) activates KCNQ channels, and its hydrolysis underlies receptor-mediated inhibition of M currents. *Neuron* **37**, 963-975.
222. **Zhang, L., Hoff, A., Wimalawansa, S. J., Cote, G., Gagel, R. F. and Westlund, K. N.** (2001). Arthritic calcitonin/alpha calcitonin gene related peptide knockout mice have reduced nociceptive hypersensitivity. *Pain* **89**, 265-273.
223. **Zhao, H., Hakala, M. and Lappalainen, P.** (2010). ADF/cofilin binds phosphoinositides in a multivalent manner to act as a PIP(2)-density sensor. *Biophys J* **98**, 2327-2336.
224. **Zhao, H., Pykalainen, A. and Lappalainen, P.** (2011). I-BAR domain proteins: linking actin and plasma membrane dynamics. *Curr Opin Cell Biol* **23**, 14-21.